THE UNIVERSITY OF LIVERPOOL

"A Study of The Quadrupole Mass Spectrometer for Operation in Hostile Environments"

Thesis submitted in accordance with the requirements of the University of Liverpool for the degree of Doctor in Philosophy

by

Jin Man Yang

Department of Electrical
Engineering and Electronics

May, 1985

SYNOPSIS

The aim of the project described in this thesis was to develop an analytical measuring instrument for use as a residual gas analyser in industrial vacuum systems. The quadrupole mass spectrometer was chosen operating in a new and as yet not fully tested mode. In this novel mode, only a.c. voltages are applied to the rods and a special collection system using energy and spacial filtering is employed (so called the a.c. mode). This is in contrast to the normal mode, where a.c. and d.c. voltages are applied to the rods, and a simple plate or an electron multiplier collector is used.

This thesis describes a series of experiments to investigate the properties of the quadrupole mass filter in the a.c. mode when operating in hostile environments. To carry out this investigation a small vacuum furnace was built and charged with workshop swarf and viton gaskets. The sensitivity of a 50 mm quadrupole mass filter operating in the a.c. mode was observed to fall by 40% after 100 hours of operation at 10^{-3} mbar in the above gases. However, the relative sensitivity over the mass range 10-100 a.m.u. remained the same. In a separate set of experiments the relative sensitivity of an 85 mm quadrupole mass filter was examined in the a.c. mode. The ratio of singly to doubly charged ions for argon and krypton changed by 15% or less after 50 hours contamination. This is in complete contrast with that of the normal mode. In the

normal mode instability caused by even minor comtamination was always observed. There is shown in the thesis to be a theoretical basis for this difference. It was verified that heating the source to 200^{o}C and sweeping the ion energy to relatively high value for high mass successfully aided the development.

In addition, the use of a Nier type source, high pressure limitation, and multi-peaks were also investigated. The Nier source was found to provide an improved ion beam, enabling good resolution to be achieved. The high pressure limit of a quadrupole mass filter in the a.c. mode was found to be 10^{-4} mbar. The multi-peaks were shown to be a fundamental phenomenon which could be avoided when operating with normal ion energy. The resolution of a quadrupole mass filter in the a.c. mode was found to be proportional to the power 2.3 of the number of cycles ions spent in quadrupole field.

ACKNOWLEDGMENTS

I would like to thank my supervisor Professor J.H. Leck for his patient, thoughtful advice and assistance throughout this work.

I would also like to thank Mr. H.H.H. Watson of Culham Laboratory for collaborating with Professor J.H. Leck to make this project both possible and fruitful.

It is a pleasure to acknowledge the help given to me by the staff of the Instrument, Electronic, Mechanical, Vacuum, and Glass-blowing workshops, and by the friends in the Department.

I am grateful for the financial support afforded by a Co-operative award from the UKAEA, for the ORS award from the CVCP, and for the support from the Education Ministry of China.

Finally I would like to express my appreciation to Mr. W. E. Austin, Mr. M. Evans and Miss R. Knox for their helpful proof-reading.

Contents

List of figures

List of tables

Table 4.6.4. The changes in the relative sensitivity of an 85 mm quadrupole mass filter after 50 hours contamination.

Table 4.8.1 The sensitivity and resolution of the 50 mm quadrupole mass filter with the Nier source for different gases.

Table 4.8.2. Interference at low mass side of the argon peak for different operating frequencies.

Principal symbols

a	parameter in the Mathieu equation of ion motion depending on U.
A_o	constant in the solution of the Mathieu equation depending on the initial conditions.
A_n	weighting factor.
B_o	constant in the solution of the Mathieu equation depending on the initial conditions.
B	magnetic induction.
C_n	constant in the solution to the Mathieu equation of ion motion depending on "a" and "q".
D_b	inner diameter of the base plate of an ion source.
D_n	distance between adjacent nods in a beat form of ion trajectories.
e	electron charge.
E	electric field strength.
E_o	amplitude of the r.f. field in omegatron.
f	radio frequency.
I	current.
I_e	emission current.

I_t trap current in the Nier source.

I^+ ion current.

I_{40} current of ions M/e=40.

K constant.

L length of an analyser.

L_r mean free path at a reference pressure.

L_p mean free path at the pressure of P.

M ion mass.

ΔM peak width for a single peak, or distance between sister peaks for multi-peaks. (half peak height)

ΔM_o original peak width.

n an integer.

N number of cycles an ion spends in an r.f. field.

P pressure.

P_{H2} pressure of hydrogen.

P_o background pressure.

P_r reference pressure.

q parameter in the Mathieu equation of ion motion depending on "V".

r rod radius.

r_a radius of acceptance area of a quadrupole field.

r_c radial coordinate.

r_o half distance between opposite rods.

r_s radius of the shadow casted by the stop in front of a collector.

R resolution. (half peak height)

R_h rod housing radius.

R_{lim} limiting resolution.

R_m deflection radius.

R_o distance of the collector from the central axis in omegatron.

R_2 leakage resistance between lens 2 and ground.

S sensitivity of a QMF.

S_o original sensitivity.

ΔS change in sensitivity.

t,T time.

t_n time factor.

u universal coordinate in the Mathieu equation of ion motion.

U d.c. voltage.

U_b d.c. voltage on the box of the Nier source.

U_c d.c. voltage on the cage of the conventional source.

U_f d.c. voltage on the filament.

U_g d.c. voltage on the gate of the Nier source.

U_{ic} d.c. voltage on the inner collector.

U_1 d.c. voltage on the lens of the Nier source.

U_{11} d.c. voltage on lens 1 of the conventional source.

U_{12} d.c. voltage on lens 2 of the conventional source.

U_t d.c. voltage on the trap of the Nier source.

U_z d.c. voltage determinig the ion energy (eU_z).

ΔU a small bias d.c. potential on a rod.

v velocity of an ion.

V r.f. voltage on the rods. (peak to ground)

V_{ac} a specific r.f. voltage on the rods. (peak to ground)

V_o r.f. voltage at an operating point.(peak to ground)

V_{2m} r.f. voltage on lens 2 of the conventional source. (peak to ground)

X transverse coordinate.

X_1, X_2 capacitance.

Y transverse coordinate.

Z axial coordinate.

β parameter of the solution of the Mathieu equation.

ϵ construction tolerance.

θ angle between an operating line and the "q" axis.

ξ parameter representing time.

τ characteristic period of ion oscillation.

ψ angular coordinate.

ψ_0 initial angle.

ω angular frequency of an r.f. voltage.

ω_m angular frequency of an ion motion inside an omegatron.

φ electric potential in space.

φ_0 electric potential on a rod.

CHAPTER 1. Introduction

1.1. The aim of the project

The aim of the project is to develop a device for reliable use as a residual gas analyser in an industrial system. It should cover the pressure range from 10^{-8} to 10^{-3} mbar (a range up to 10^{-2} mbar would be desirable, but this is probably not realistic). A typical example of the application is in a vacuum furnace. The basic requirements for this and many other applications are the following.

(a) Simple to operate.

(b) Mass range up to 100 a.m.u., i.e. 2-100 a.m.u.

(c) Stable output even with operation in hostile environments.

(d) No mass discrimination (no change in relative sensitivity over a long period).

1.2. Design criteria

To meet the above requirements, a mass spectrometer is an obvious choice. When a mass spectrometer is used, ions are formed from the gas phase by electron impact and then separated by some form of mass filter. There are five main types of mass spectrometer to be considered.

(a) Magnetic deflection mass spectrometer.

(b) Quadrupole mass filter.

(c) Monopole mass spectrometer.

(d) Time of flight mass spectrometer.

(e) Omegatron.

All the above instruments will be reviewed briefly in the following sections. From this review a choice is made for the present application.

1.3. The Magnetic Deflection Mass Spectrometer

1/ 180° deflection instrument

The 180° magnetic deflection mass spectrometer was first introduced by Dempster (1/1) in 1918. This spectrometer is illustrated schematically in Fig.1.1. A singly charged ion produced in the ion source (1) is accelerated by a potential U. The kinetic energy of the ion is then given by

$$eU = Mv^2/2 \qquad (1\text{-}1)$$

where e is the electronic charge, M is the mass of the ion, and v is its velocity after acceleration. The motion of the ion is perpendicular to the uniform magnetic field (2) as shown in Fig. 1.1. It is deflected into a circular orbit by the field. The radius R_m of the orbit is derived from the basic formula for centripetal motion

$$Mv^2/R_m = evB \qquad (1\text{-}2)$$

where B is the magnetic induction.

Eliminating v from equations (1-1) and (1-2) yields

$$R_m = (2MU/e)^{1/2}/B \qquad (1\text{-}3)$$

If B is expressed in tesla, M in atomic mass units (a.m.u.), U in volts, and R_m in metres, then

$$R_m = 1.44 \times 10^{-4} (MU)^{1/2}/B \qquad (1\text{-}4)$$

Thus for a given $U^{1/2}/B$, a light ion travels in an orbit with a small radius,whilst a heavy ion travels in a larger orbit.

Ions of one particular mass are not only deflected but also focussed by the magnetic field. The image of the source is formed after ion deflection through 180° as illustrated in Fig.1.1. Hence a collector (3) should be located at this point to obtain maximum resolution.

2/ 60° sector field instrument

Besides the above 180° deflection other configurations of magnetic deflection are also practical. The 60° magnetic sector mass spectrometer was first introduced by Nier (1/2) in 1940. The operating principles were described by Herzog (1/3). This is : Ions entering a magnetic sector orthogonally will leave the sector also orthogonally. A magnetic sector field has a focussing function with respect to ions similar to that which a combination of an optical prism and a cylindrical lens has with respect to light beams.

A symmetric type 60° sector spectrometer is illustrated schematically in fig. 1.2. This has equal object-image distances from the magnetic boundary. For

the same curvature of ion deflection it requires much less material than the 180° deflection instrument.

3/ Practical operation as a spectrometer

For all types of magnetic spectrometer, successive ion separation can be achieved by sweeping either U or B. Operation by sweeping U (usually employed in small magnetic spectrometers) has the disadvantage that the accuracy of the analysis is poor. This is because sweeping U also varies the source parameters. Commonly, high resolution instruments are operated by sweeping B. This is because the source operation is completely independent of the magnetic field intensity. A magnetic spectrometer with a radius R_m up to 1,000 mm can give a resolution up to the order of 100,000 by employing special designs of source to ensure monoenergetic ion beams.

1.4. The Quadrupole Mass Filter

The quadrupole mass filter was first introduced by Paul (1/4) in 1953. His instrument is illustrated schematically in Fig.1.3. It has three sections. Ions are produced and focussed into a beam in the ion source (1). Then they are ejected towards the collector (5) which can be either a simple plate or an electron multiplier. There are four circular rods (3) between the source and the collector. They are supplied with d.c. plus a.c. (radio frequency or r.f.) voltages to form an effective mass filter.

In the xy plane the d.c. voltage sets up a "saddle"

d.c. field between the rods. The potentials at the z axis and mid-way between the adjacent rods are zero relative to ground. The potentials close to the rods are positive in the x direction and negative in the y direction. Thus the d.c. field has a focussing effect in the x direction for positive ions. The natural oscillations of the ions are harmonic and stable in this direction. The superposition of the r.f. field set up by the r.f. voltage adds a defocussing effect on the ions forcing them to vibrate synchronously with the field. The light ions are easily synchronized and therefore resonate with the r.f. field. This means that they are easily lost in the x direction. The heavy ions are more stable and hence can pass down the length of the rod assembly to reach the collector.From the point of view of filtering, the pair of rods in the x direction constitute a high mass pass filter. In contrast, the d.c. field has a defocussing effect in the y direction. Ions tend to escape outwards in this direction. The heavy ions have a greater tendency to be lost than the light ions because of their greater inertia. The superposition of the r.f. field forces all the ions to vibrate synchronously with the field, and therefore adds a focussing effect. This focussing has more influence on the light than on the heavy ions. The light ions are not so easily lost in the y direction. They are stable and thus can reach the collector. From the point of view of filtering, the pair of rods in the y direction constitute a low mass pass filter.

Whilst both high and low mass ions are ejected radially (light in x, heavy in y directions) there is the possibility that ions with some intermediate mass may just be stable in both directions. These ions, and these only, can reach the collector. When this occurs the "critical" mass for transmission is given by

$$M = 1.38 \times 10^{7} V / f^{2} r^{2} \qquad (1\text{-}5)$$

where M is the mass of the ions in a.m.u.; V is the amplitude of the r.f. voltage, in volts; f is the radio frequency, in Hz; r_o is the radius of the quadrupole field, in metres. From equation (1-5) it can be seen that any particular ion mass can be selected by controlling the frequency or amplitude of the applied voltage.

1.5. The Monopole Mass Spectrometer

The monopole mass spectrometer was first introduced by Von Zahn (1/6) in 1963. It is illustrated schematically in Fig.1.4. A circular rod and a right angle V electrode form a quarter of the quadrupole filter. Indeed it is a development of the quadrupole filter. Its properties are, however, considerably different.

The figure shows a method of ion injection in which the ions enter at an angle to the main axis. The rod is supplied with a d.c. plus an r.f. voltage. The electric fields and the ion motion for the monopole are the same as for a corresponding quarter of the quadrupole. For ion

separation the y direction is of interest. The d.c. field has a defocussing, and the r.f. field a focussing, effect. The heavy ions tend to be defocussed by the resultant field, vibrate towards the rod, and eventually are lost. The light tend to be focussed by the fields and therefore vibrate towards the corner of the V electrode. Eventually they strike this electrode. There is a probability that a portion of species of light ion will pass through the small "collector defining" hole in the V electrode. The mass M of the species of ion is given by

$$M = KV/f^2$$

where K is a function of the distance from the corner of the V electrode to the rod. V and f are the amplitude and frequency of the r.f. voltage. These ions of mass M are stable and do not strike the V electrode. To focus on the hole the flight time in the monopole field should be exactly

$$T = 2\pi/\beta\omega \qquad (1\text{-}6)$$

where $\omega = 2\pi f$; β is determined by the d.c. and r.f. voltages and will be defined in section 2.3. As with the quadrupole the deflection of ions can be controlled by variation of the frequency or amplitude of the r.f. voltage.

1.6. The Time of Flight Mass Spectrometer

The time of flight (TOF) mass spectrometer was introduced by Stephens (1/7) in 1946. Following his ideas a number of TOF mass spectrometers have been developed utilizing slightly different approaches to ion separation. Here the simple linear direct type is discussed as an example of the general principle. Fig. 1.5 is a schematic diagram of this instrument. Ions generated in the source (1) are drawn out by a pulsed electric voltage applied to grid (2). They are accelerated by a high negative voltage U on the drift tube (3). Hence they all have the same energy when they enter this drift tube. Inside the tube the ions travel with different speeds depending upon their mass. Therefore they arrive at the collector (4) at different times.

If the mass-charge ratio of a singly charged ion is M/e, and the length of the ion path L, then the flight time of the ion through the drift tube is given by

$$T = L(M/2eU)^{1/2} \qquad (1\text{-}7)$$

The time difference (ΔT) for ions of masses M_1 and M_2 is

$$\Delta T = L(M_1^{1/2}-M_2^{1/2})/(2eU)^{1/2} \qquad (1\text{-}8)$$

Thus a mass spectrum is obtained by timing the arrival of the "bunches" of ions as they reach the collector.

1.7. The Omegatron

The omegatron was first introduced by Hipple (1/8) in 1949. His instrument is illustrated schematically in Fig. 1.6. The top and the bottom plates (1) and (2) shown in this diagram are connected to a radio frequency voltage generator (5). The guard rings (3) between the plates are supplied with r.f. potentials from a potential divider (6). This configuration ensures a homogeneous r.f. field inside the chamber. By applying a homogeneous magnetic field orthogonally a circular multiple accelerator is formed. The magnetic induction is usually about 5 tesla.

Ions, generated by the impact of an electron beam, describe circular orbits in the magnetic field. For singly charged ions of mass M the angular frequency ω_m is given by

$$\omega_m = eB/M \qquad (1\text{-}9)$$

This frequency is independent of the orbit radius. If the angular frequency of the r.f. field is equal to ω_m, the ions gain energy from the r.f. field and describe a spiral path of the form illustrated in Fig. 1.6. In this resonant case the radius of the curvature R_m of the ion path increases linearly with time T as given by

$$R_m = E_o T/2B \qquad (1\text{-}10)$$

where E_o is the amplitude of the r.f. field. Eventually the ions must strike the collector (4). All the other ions (i.e. not in resonance) remain near the central axis of the system. Eventually they "drift" to the guard rings, where a trapping voltage (7) is applied as shown in the diagram.

If the collector is placed at a distance R_o from the central axis and the resolution is defined by

$$M/\Delta M = \omega_m / | \omega_m - \omega |$$

then the resolving power of the omegatron is

$$M/\Delta M = eR_o B^2 / 2E_o M \qquad (1\text{-}11)$$

Obviously the heavier the ions, the lower the resolution of the instrument.

1.8. Selection of the Mass Spectrometer for This Application

The omegatron is a compact device for measurement of partial pressures in a vacuum system. The magnet can be removed for degassing. It has a very high resolving power at low mass. (A resolution of 45,000 adequate for the separation of hydrogen and doubly charged deuteron has been reported). This instrument needs both magnetic and r.f. fields. To achieve high resolving power at high mass, a strong magnetic field of the order of 5 tesla and a small

r.f. voltage of the order of 0.1 to 1 volt (resolving power is proportional to B^2/E_oM) are required. There are practical limits to magnetic field strength, and the r.f. voltage must be very small for operation at high mass. Hence the instrument suffers great problems with contamination. This is why it has not found any significant applications in the last decade. Thus the omegatron is discounted.

The TOF mass spectrometer has the fastest response time of all the mass spectrometers. In one second, up to 100,000 spectra can be scanned. Therefore the instrument is uniquely useful for studying the growth and decay of fast gas phase chemical reactions.

However, the ion source of the instrument has to be made with great precision. Also to reproduce ion pulse signals faithfully a complex difficult design of wide band amplifier is needed. These involve complicated operation and reduce the reliability of the instrument. Up to the present time it has therefore had only specialized applications. Moreover its resolving power is proportional to the length of the drift tube (see equation (1-8)); to cover the required mass range would need a long drift tube. (A drift tube of over one metre is common). This would be incompatible with high pressure measurement. Thus the TOF mass spectrometer is also discounted.

The quadrupole and the magnetic deflection mass spectrometer are extremely useful for many applications. Either instrument can meet the requirements defined for

this project. In general terms the advantages of the quadrupole are as follows :

(a) The focussing effect is proportional to the mass of the selected ion (the heavier the ions, the higher the r.f. voltage required).

(b) The behaviour is resistant to contamination.

(c) It is small.

(d) It is convenient to install.

From the point of view of small size and convenient installation the magnetic mass spectrometer with permanent magnet must be considered. However it requires low accelerating voltage to focus the heavy ions ($U \alpha 1/M$, see equation (1-4)). This leads to problems with high mass ions when the spectrometer is contaminated. From the point of view of long term stability and resistance to contamination the magnetic mass spectrometer with an electro-magnet is a serious contender. Its sensitivity is similar to that of the quadrupole. Nevertheless its disadvantage is that it requires a heavy electro-magnet and the associated complicated electronic circuits. Thus because of the advantage of weight, size, and convenience of operation the quadrupole is chosen rather than the magnetic spectrometer (with variable magnetic field) for this application.

The monopole mass spectrometer has a similar performance to that of the quadrupole mass filter in clean high vacuum environments. It has the following main advantages over the quadrupole :

(a) Its construction is simpler.

(b) The resolving power is independent of the ratio U/V. No accurate U/V circuit is required.

However, unlike the quadrupole the monopole requires a constant ion injection energy. It is expected to have serious problems with contamination because ion focussing is affected by small changes in surface potentials. This vital disadvantage eliminates any possibility of the instrument being used in the current project.Therefore the quadrupole mass filter is left as the best choice for the present work.

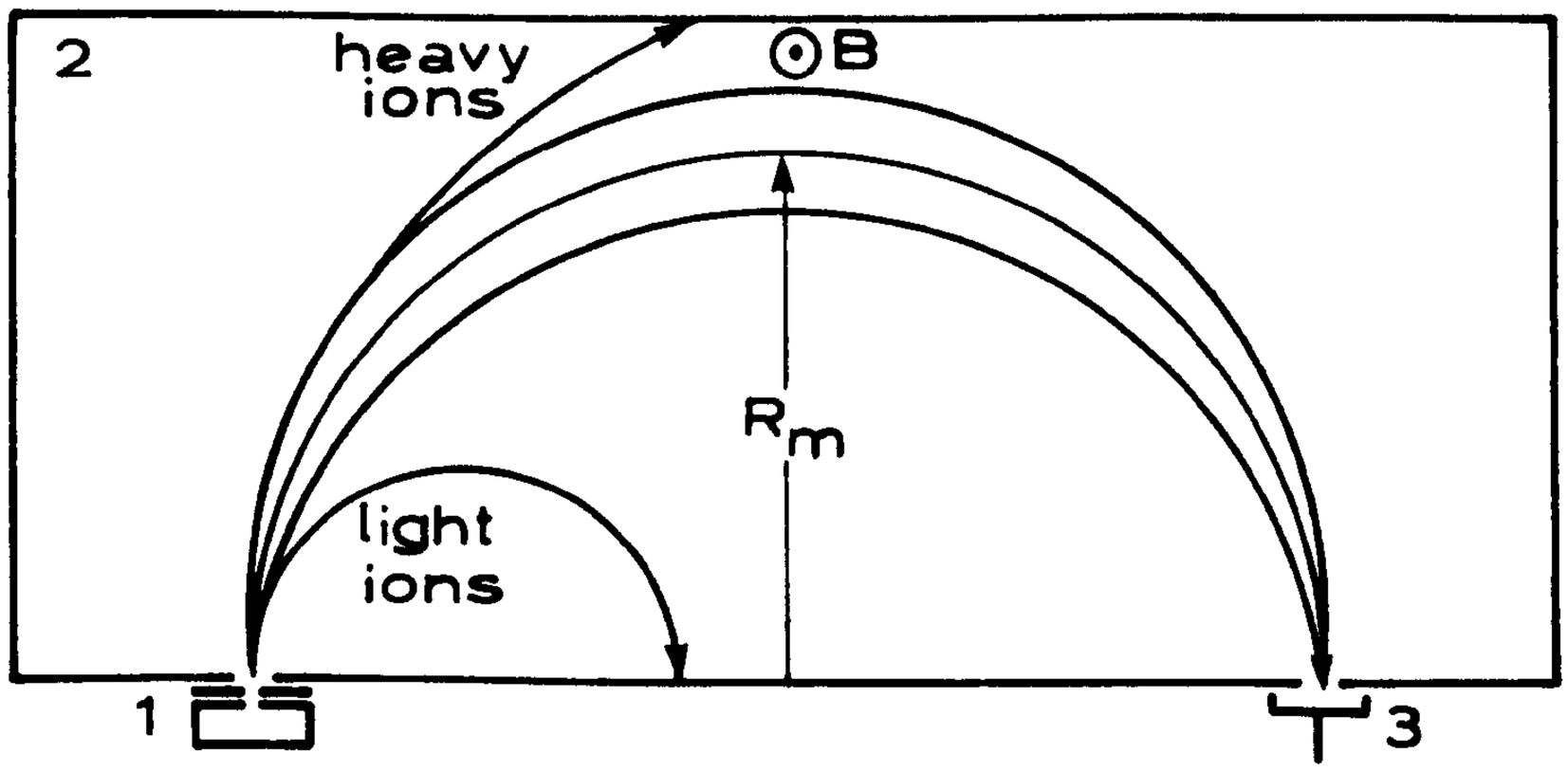

FIG. 1.1. 180° MAGNETIC DEFLECTION MASS SPECTROMETER.

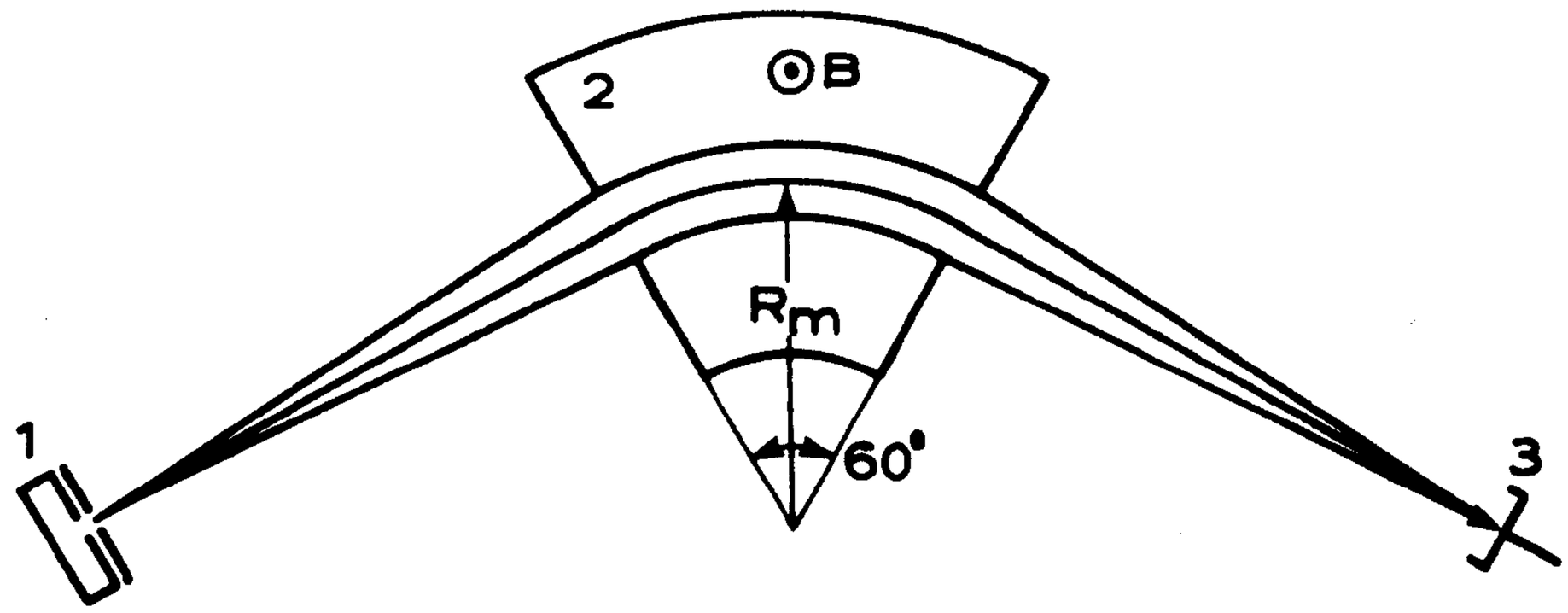

FIG. 1.2. 60° MAGNETIC DEFLECTION MASS SPECTROMETER.

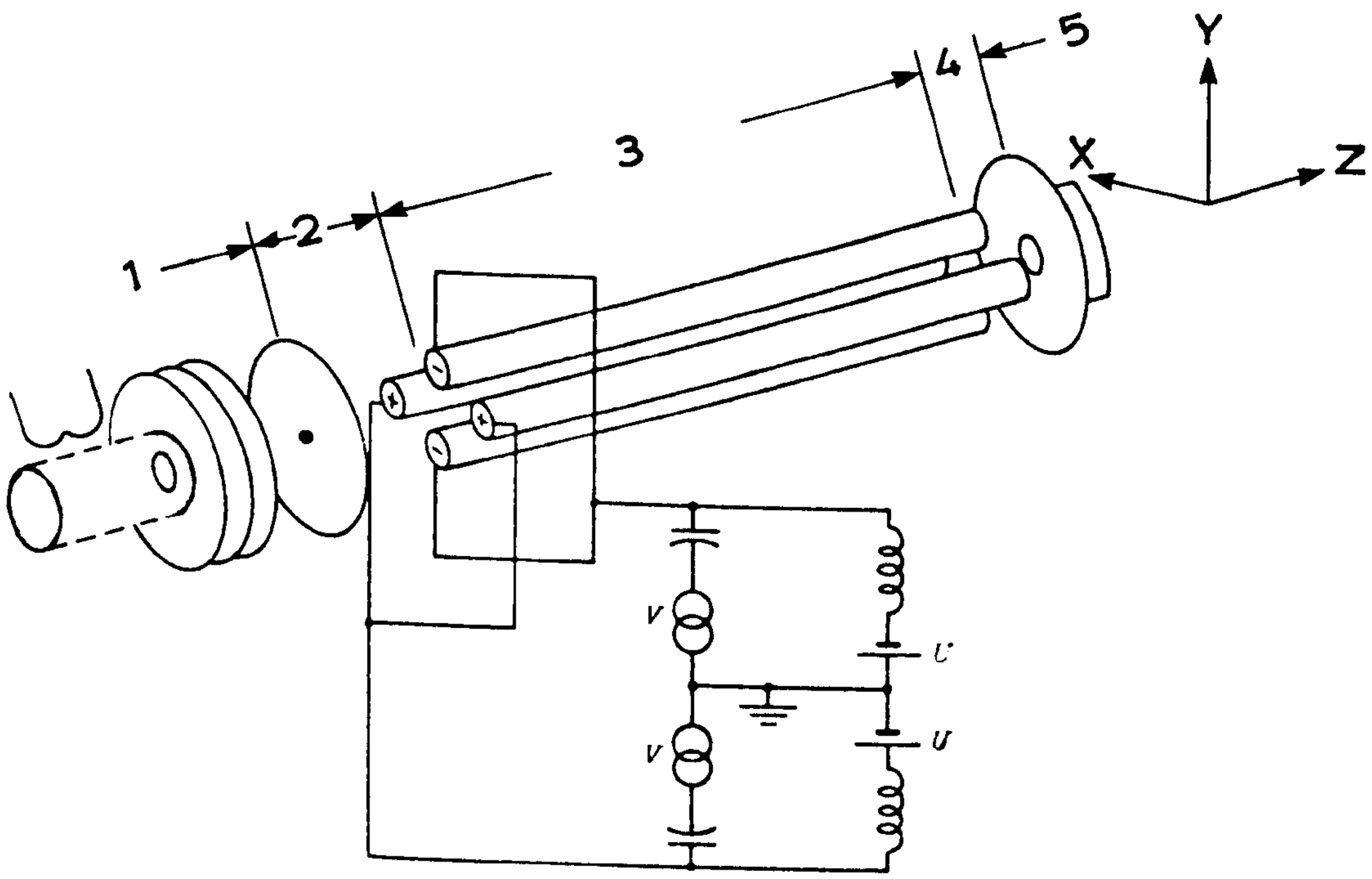

FIG. 1.3. QUADRUPOLE MASS SPECTROMETER. (1/5)

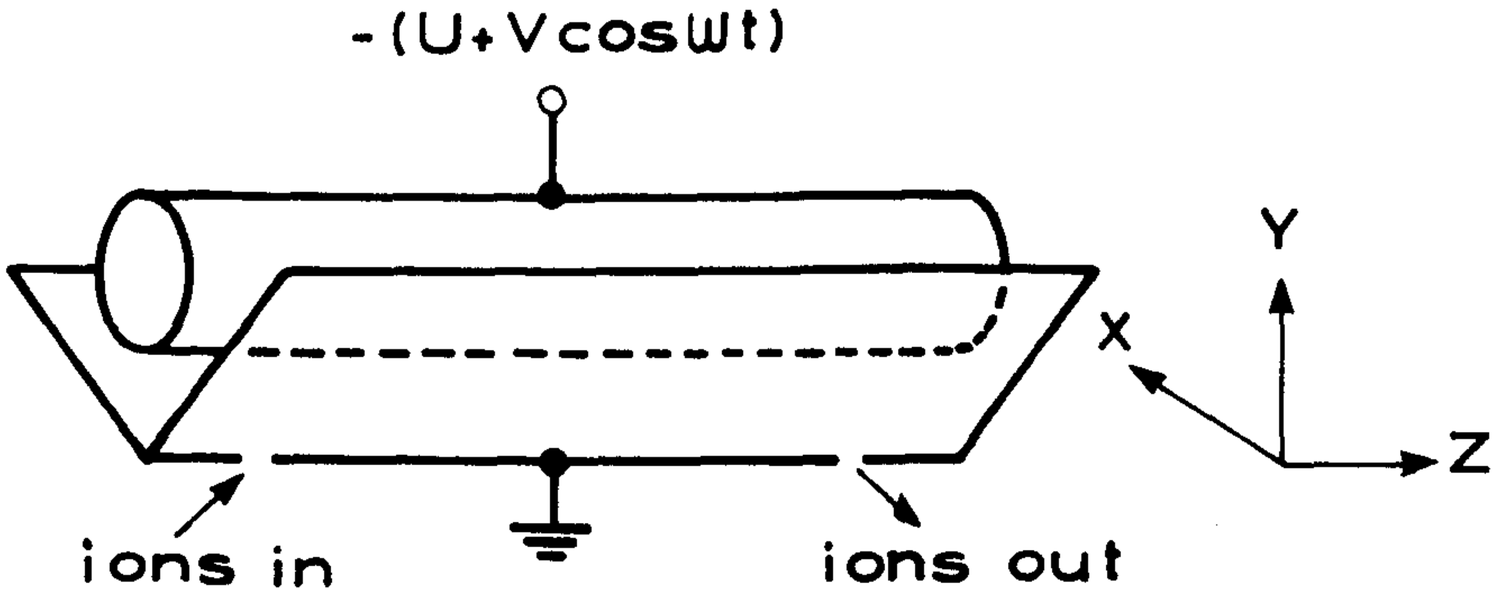

FIG. 1.4. MONOPOLE MASS SPECTROMETER.

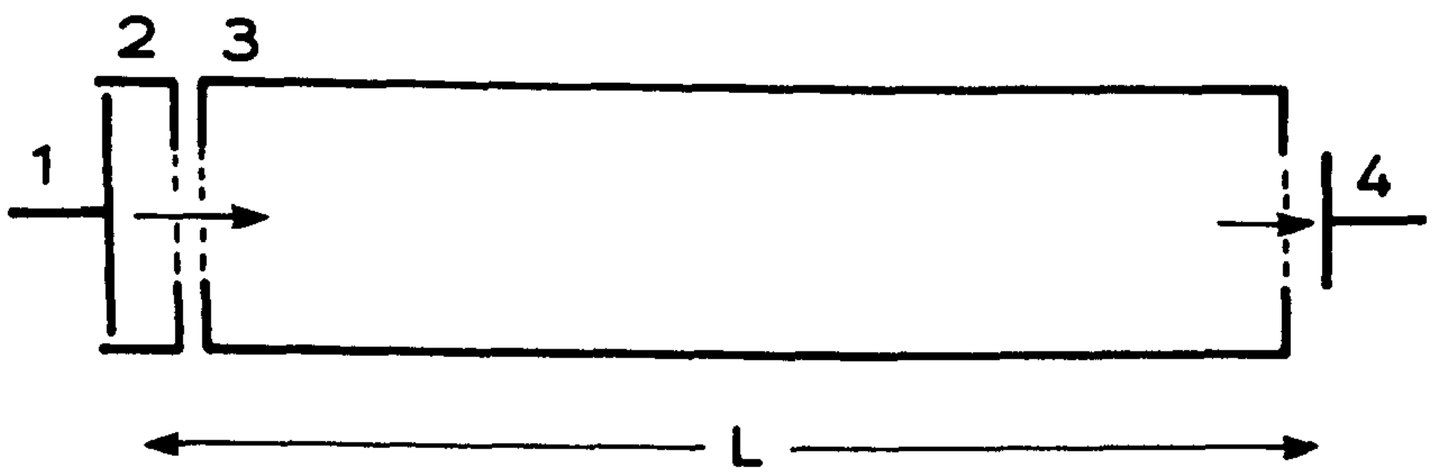

FIG. 1.5. TIME OF FLIGHT MASS SPECTROMETER.

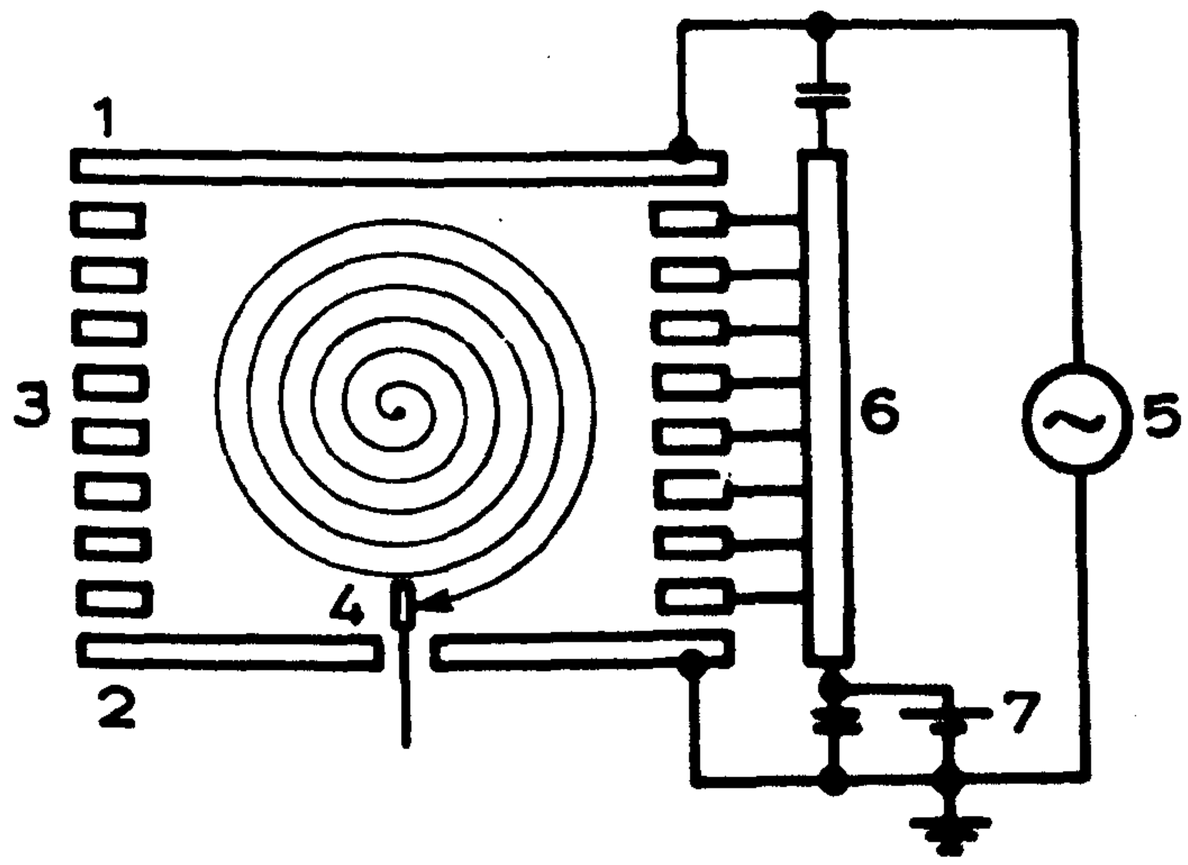

FIG. 1.6. OMEGATRON.

CHAPTER 2. Principle of Operation of the Quadrupole Mass Filter

2.1. History

In 1953 Paul (2/1) and Steinwedel, at the University of Bonn, and Post (2/2), at the University of California, recognized the possibility of employing a strong focussing effect electrodynamic quadrupole field as a mass filter. Paul and Steinwedel were the first to publish in this field. The pioneering group, Paul (2/3, 2/4) and his colleagues, developed quadrupole mass filters (QMFs) during the 1950s and obtained basic patents on their devices in 1956 (2/5).

In the early 1960s, there were greatly growing demands in high and ultra high vacuum technology application and upper atmosphere and space research for residual gas analysis. Because of their simplicity, compactness, economy, absence of magnetic field, ability to control the ion transmission and resolution electrically, QMFs were rapidly developed to meet these needs.

Since the late 1960s, in spite of a slowdown in its evolution, the combinations of QMF with other mass spectrometers, for instance, gas-liquid chromatograph, high pressure liquid chromatograph, magnetic mass spectrometer, etc., have been developed and widely applied.

In 1972 an alternative operation of QMF, called r.f. mode or a.c. mode was reported by Brinkmann (2/6). This new principle was taken up and developed at

Liverpool. The work in this novel mode has continued for over a decade. The review of evolution on the a.c. mode will be presented in detail in a later section.

A comprehensive review of the QMF's theory, design and application entitled "Quadrupole Mass Spectrometry" was published by Dawson (Ed.)(2/7) in 1976. Since 1975 the development of the quadrupole mass spectrometer and its applications has been surveyed closely by Todd ((2/8) to (2/11)) at approximately three-yearly intervals.

2.2. Profile

With reference to Fig. 1.3, sample ions are produced and focussed in the ion source (1) and are injected along the central axis of the rod system. They obtain extra kinetic energy in the entrance fringing field (2). During their travel between the rods (3), which are subject to r.f. and d.c. voltages, ions of one specific value of M/e are focussed near to the central axis of the rods by the quadrupole field, whereas the other ions are "defocussed" and travel outwards to the rods. Passing through the exit fringing field (4), the selected ions are collected by the collector (5).Their intensity is measured by conventional electronic circuits.

2.3. Electric Field of QMF

The basic theory of QMF operation has been well established (2/1). In this chapter it is reproduced with only small changes.

To simplify the explanation of QMF operation, the following assumptions are made :

(a) The quadrupole rods have hyperbolic cross sections as shown in Fig 2.1, where the co-ordinate system is also defined. r_o is half of the distance between opposite electrodes, and called the field radius; φ_o is the potential applied to the electrodes.

(b) The rods are infinitely long, so that fringing fields can be neglected.

(c) The three dimensional fields in the three orthogonal co-ordinates are uncoupled.

(d) The space charge field generated by the ions is small enough to be neglected.

The potential at a point, P(x,y,z), in an ideal quadrupole field can be expressed as

$$\varphi(x,y,z,) = \varphi_1(x) + \varphi_2(y) + \varphi_3(z) \qquad (2\text{-}1)$$

Since there is no z-direction potential applied, that is

$$\varphi_3(z) = 0$$

then

$$\varphi(x,y,z) = \varphi(x,y)$$

$$= \varphi_1(x) + \varphi_2(y) \qquad (2\text{-}2)$$

Considering only the x direction, the focussing force F_x acting upon an ion increases according to its displacement from zero. That is

$$F_x = eE_x = -e\,\partial\varphi_1(x)/\partial x\ \alpha\ x \qquad (2\text{-}3)$$

where E_x is the x direction electric field.

Integrating (2-3), $\varphi_1(x)$ can be defined by

$$\varphi_1(0) = 0, \qquad \varphi_1(r_o) = \varphi_o$$

as

$$\varphi_1(x) = \varphi_o x^2/r_o^2 \qquad (2\text{-}4)$$

In the field, Laplaces' equation must be satisfied, yielding

$$\nabla^2\varphi = \nabla^2\varphi_1 + \nabla^2\varphi_2 = 0$$

so that

$$\nabla^2\varphi_2 = -\nabla^2\varphi_1 = -2\,\varphi_o/r_o^2$$

i.e.

$$\partial^2\varphi_2/\partial y^2 = -2\,\varphi_o/r_o^2 \qquad (2\text{-}5)$$

Integrating (2-5), substituting $\varphi_2(0)=0$ and examining with $\varphi_2(r_o)=-\varphi_o$, then $\varphi_2(y)$ is given by

$$\varphi_2(y) = -\varphi_o y^2/r_o^2 \qquad (2\text{-}6)$$

Normally φ_o is chosen as

$$\varphi_o = U + V\cos\omega t \qquad (2\text{-}7)$$

where U is the d.c. voltage, V is the peak amplitude of the radio frequency voltage, ω is the angular frequency ($\omega = 2\pi f$, f is the radio frequency), t is time.

Thus the potential at the point is

$$\varphi(x,y) = (U + V\cos\omega t)(x^2-y^2)/r_o^2 \qquad (2\text{-}8)$$

The result here indicates that the assumption (a) is valid.

Therefore the electric fields are written as

$$E_x = -\partial\varphi(x,y)/\partial x = -2(U + V\cos\omega t)x/r_o^2 \qquad (2\text{-}9)$$

$$E_y = -\partial\varphi(x,y)/\partial y = 2(U + V\cos\omega t)y/r_o^2 \qquad (2\text{-}10)$$

$$E_z = -\partial\varphi(x,y)/\partial z = 0 \qquad (2\text{-}11)$$

2.4. The Stability Regions of Ion Motion

In the field, an ion motion can be described as

$$d^2x/dt^2 + 2e(U + V\cos\omega t)x/Mr_0^2 = 0 \qquad (2\text{-}12)$$

$$d^2y/dt^2 - 2e(U + V\cos\omega t)y/Mr_0^2 = 0 \qquad (2\text{-}13)$$

$$d^2z/dt^2 = 0 \qquad (2\text{-}14)$$

where M is the mass of the ion. Equation (2-14) indicates that the ion moves along the z directon with constant velocity, i.e. the axial velocity with which it entered the quadrupole field. In an ideal field, as put forward in assumption (c), (2-12) and (2-13) describe two independent components of the ion motion.

Let u represent x or y, and

$$\xi = \omega t/2 \qquad (2\text{-}15)$$

$$a = 8eU/Mr_0^2\omega^2 \qquad (2\text{-}16)$$

$$q = 4eV/Mr_0^2\omega^2 \qquad (2\text{-}17)$$

then equations (2-12) and (2-13) can be simplified to

$$d^2u/d^2\xi + (a + 2q\cos 2\xi)u = 0 \qquad (2\text{-}18)$$

This is the well-known Mathieu equation (2/12). Its stable solutions are

$$u(\xi) = A_0 \sum_{n=-\infty}^{\infty} C_{2n} \cos(2n+\beta)\xi + B_0 \sum_{n=-\infty}^{\infty} C_{2n} \sin(2n+\beta)\xi \qquad (2\text{-}19)$$

where A_0 and B_0 are defined by the initial conditions of u, $du/d\xi$, and the r.f. phase angle ωt_o. C_{2n} and β are functions of "a" and "q".

The stable solutions in x and y directions can be superimposed in (a.q) space and illustrated by a stability diagram as shown in Fig 2.2. In the diagram, the x stable regions are formed by the points whose "a" and "q" make the solutions of equation (2-12) stable; the y stable regions correspond to the stable solutions of (2-13); the different signs between the equations (2-12) and (2-13) are expressed by the opposite directions of the coordinates.

There are some regions, for instance regions (1), (2), etc., where x stable and y stable overlap. These are called stability regions. If the values of (a,q) are of such magnitude as to lie in a stability region, the ion will have a stable trajectory in the quadrupole field. If they do not lie in this region the ion's trajectory will be unstable.These are attractive properties for the design of a mass filter. Theoretically all the stability regions can be used. However region (1) is of the most interest owing to its simplest realization in practical design. Up to the present time all instrument manufacturers have

concentrated upon region (1). Therefore usually region (1) is called the "stability region" for the convenience of narration. Its details are depicted in Fig. 2.3. The stable trajectories of an ion with respect to the apex of the stability region are shown in Fig. 2.4.

2.5. The Operation of QMF

The stability diagram in Fig.2.5 has been developed from Fig. 2.3, the co-ordinates being U and V (U and V are d.c. and a.c. voltages as defined in Fig. 2.1.). Three different masses are chosen such that $M_1 > M_2 > M_3$.

If the mass analyser is operated by varying the voltages U and V. maintaining the ratio U/V constant, all the operating points lie on a straight line. It passes through the origin, and is illustrated by the line OP in Fig. 2.5. The slope of this line is given by $\tan\theta = U/V$. Usually OP is called the "operating line". This operating line, as drawn in Fig. 2.5, intersects each of the triangles. Each segment inside a triangle represents a stable operation for the particular ions. Scanning down from high voltage to zero as shown in Fig.2.5 from P to O means that the ions of M_1, M_2, and M_3 are selected in turn. During a selection, if the ions of M_2 are stable, the heavier ions, M_1, will be unstable in the y direction, whilst the lighter ions, M_3, will be unstable in the x direction.

The resolving power of the analyser depends upon the length of the intersection of the operating line. The

shorter this length, the higher the resolving power. To obtain a higher resolving power the most convenient method is to increase the ratio U/V, i.e. tan θ.

2.6. The Effects of Practical Factors

In practice the assumptions in section 2.3 are never satisfied. The length of the rods is limited. The construction of the rod system is not perfect. These limitations influence the performance of a quadrupole mass filter as follows.

1) The effects of limited length of the rod system

The limited length of the rod system has the following results:

(a) Fringing fields at the entrance and the exit of the quadrupole structure become significant.

(b) The number of cycles an ion experiences in an r.f. quadrupole field is not infinite.

A) The fringing fields

Dawson (2/13) has calculated the ion transmission of a mass filter for many conditions and described the effects of the fringing fields.

The fringing field at the entrance is formed between the emittance plane of the ion source and the entrance of the rod system. It strengthens gradually from zero to a full quadrupole field. In a simplified situation, a linear entrance field is assumed. If V_o is the r.f. voltage used, the increment of the potential along the axis from zero to full corresponds to the movement of an ope-

rating point along the operating line from the origin to the apex (arrow 1 shown in Fig. 2.6). Thus the ions desired to be selected will be unstable in the y direction. If they spend a large number of r.f. cycles passing through the entrance fringing field, their y displacements become very great. Many of them will be lost, and therefore the transmission of these ions will be very low.

In addition, there are some other more complex effects of the entrance fringing field. They can benefit the transmission of the ions. It follows that there is an optimum length for the entrance fringing field. According to Dawson's calculation, the length of one to two r.f. cycles gives an optimum match between the ion source emittance and the quadrupole acceptance.

The fringing field at the exit of the quadrupole is formed between the exit of the rod system and the collector plane. It has a diverging rather than converging effect on the ion beam. Dawson's calculation shows that the selected ions tend to be accelerated through the exit fringing field, particularly in the x quadrant when the displacements are large. However, the change of the field from full at the quadrupole exit to zero at the collector corresponds to the movement of the operating point from the apex to the origin (arrow 2 shown in Fig. 2.6.). Therefore in the exit fringing field the ions again follow unstable paths in the y direction. Some slow-moving ions may be trapped in the fringing field for many r.f. cycles or even reflected back into the quadrupole.

B) The effects of the number of cycles

As explained earlier the stability diagram was derived mathematically from an infinitely long rod system. This raises problems for a finite rod system. If the length of an analyser is too short to enable a distinction to be made between the trajectories of ions of adjacent mass number, the analyser will fail to distinguish them. That is, the resolving power of the analyser will be restricted.

Paul(2/4) has suggested that the limiting resolving power of an analyser is proportional to the square of the number "N" of the cycles a specific ion experienced in the r.f. field, i.e.

$$M/\Delta M = N^2/K \qquad (2\text{-}20)$$

where ΔM is measured at 10% of the peak height, and K is a constant. In a number of experimental studies (2/14) the power of "N" was found to be either exactly or very close to 2, and that the value of K about 20.

For a given instrument (2/15) with K assumed to be 20, then

$$M/\Delta M = 8.35\times10^{-29} f^2 L^2 M/2eU_z$$

or

$$\Delta M = 4\times10^9 U_z/f^2 L^2 \qquad (2\text{-}21)$$

where U_z is the voltage determining the ion injection energy (eUz), in volts; f, in Hz; L, in metres; M, in a.m.u.; e, in coulomb.

Equations (2-20) and (2-21) apply only when: (a) the imperfection in the electric field is neglected; (b) the resolving power examined is in the range below 1,000.

With attempts to increase the resolving power by increasing the number of r.f. cycles, the effect of the field imperfection becomes evident. Experiments have shown that the graph of the maximum resolution versus number of r.f. cycles saturates below or just about 1,000 at 10% peak height for a commonly used device.

2) The effects of imperfect construction

The imperfections of a quadrupole construction arise because: (a) The cross section of the rods is circular instead of hyperbolic; (b) There must inevitably be some errors of construction. Both result in field imperfections. An imperfect quadrupole field can be regarded as a combination of a principal perfect round quadrupole field and other weak round multipole fields (2/16, 2/17, and 2/18). The field inside a quadrupole structure can be expressed by

$$\varphi = \sum_n A_n (r_c/r_o)^n \cos n(\psi-\psi_o)[U-V\cos\omega(t-t_n)] \qquad (2\text{-}22)$$

Where r_c and ψ are polar co-ordinates; A_n is weighting

factor; ωt_n is a phase factor. For a perfect quadrupole field n=2, $A_n=1$.

Because of the existence of the multipole fields, ion trajectories are perturbed. From those calculations quoted above some ions resonating in the multipole fields now take unstable trajectories in the quadrupole structure and are lost radially. This is often the cause of the so-called "split peaks" in a practical instrument. In the stable region, this is represented by the "unstable" resonance lines shown in Fig. 2.7.

The calculation by Dawson (2/17, 2/18) shows that the most significant perturbances result mainly from the third, fourth, and sixth order terms of equation (2-22). The experiments by Holme (2/19) have strongly confirmed Dawson's calculation.

A) The effects of round rods

Substituting round for hyperbolic rods introduces the sixth order field distortion. Denison (2/20) showed that the effect of round rods could be minimised by making the housing radius $R_h=3.54r_o$, and $r=1.1468r_o$, where r is the radius of the individual rods.

B) The effects of positional errors

The positional errors cause mainly third and fourth order field distortions (2/20). Dawson has stated that as well as peak splitting, they reduce the maximum resolving power by a factor of $\epsilon^{1.3}$, where ϵ is the error (2/7).

2.7. The A.C. Mode

In 1972 Brinkmann (2/6) published the results obtained with a quadrupole mass filter in an a.c. mode. This was so named because it relied upon a form of an "energy" in addition to the conventional path filtering technique.

The apparatus he used to illustrate the principle is shown schematically in Fig. 2.8.A. The rods were supplied with only an a.c. voltage. The collector was biassed positively so that it operated as a crude form of energy filter.

The operation of the spectrometer in the a.c. mode can be described as follows. When it is functioning, its operating point is P as shown in Fig. 2.9. The amplitudes of oscillations of the selected ions grow rapidly so that they pass very close to the rods. These ions when they pass through the exit of the quadrupole structure gain maximum energy from the r.f. field. Therefore they are able to overcome the retarding field in the collector region and reach the collector. However, in the case of all the undesired ions, the operating point of the quadrupole is not P. They are ejected either by the r.f. field, because they are unstable, or by the retarding field, because their energy is not great enough. Therefore they cannot reach the collector.

Using the apparatus shown in Fig. 2.8.A, Brinkmann recorded a spectrum resolving the ions of masses 414 and 415. His results showed that a resolution greater than

1,000 at M=500 could be obtained. The transmission of ions (and hence sensitivity) was about ten times greater than that obtained by the same instrument operating in the normal mode at the same resolution. Brinkmann concluded that his modified quadrupole mass filter in the a.c. mode could be best for high masses.

In a similar series of experiments Holme (2/22) reported results with a simplified arrangement of collector assembly. His apparatus is shown in Fig. 2.8.B. With this arrangement the resolution in the a.c. mode was considerably greater than in the normal mode for the same instrument at the same sensitivity.

Holme's initial work was followed by a more comprehensive study (2/19) at Liverpool. The collector assembly for this later study is shown in Fig. 2.8.C. The results confirmed the initial conclusions, giving better performance in the a.c. mode for both well and poorly constructed analysers. To obtain these results, several analysers in lengths of 50mm and 150mm were used. Some were constructed with one pair of rods made 0.1 mm oversize in diameter to simulate effects of a poor constructional technique.

The results also showed that even with the poorly constructed systems, very good "peak shapes" were always obtained. There was no evidence of peak splitting which was certainly the case when operating in the normal mode. Instead of "peak splitting", however, satellite peaks were observed. The results obtained in one particular series of experiments are indicated by the peaks in

Fig. 2.7. When the positions of the satellite peaks on the the "mass" scale are compared with the locations of resonance lines in the stability region calculated by Dawson, they are found to be well correlated. This can be understood in qualitative terms by the explanation of Holme (2/19) and Brinkmann (2/6) for the a.c. mode and the analysis of Busch (2/16) and Dawson (2/17 and 2/18) for the effect of imperfection of the quadrupole field. With reference to Fig. 2.7, when the mass filter is scanning from high mass to low mass, its operating point moves from "A" to "B", to "C", to "D". At "A" the desired ions are resonant with the quadrupole field. At "B", "C", or "D", where the resonance lines intersect the q-axis, the ions in resonance with the quadrupole field are resonant again at a high order multipole field (first the third order resonance point). Their trajectories expand outwards from the central axis. They gain maximum energy from the corresponding multipole field. Hence they can reach the collector by the effect of energy filtering and form satellite peaks. Furthermore the results also show the particular inhibition of satellite peaks at the higher retarding potential, suggesting a retarding potential determines the "cut off" energy of the ions.

Following this work, Leck (2/23) proposed an alternative collector assembly which combines "spatial" and "energy" filtering. This is shown in Fig. 2.10.A. The collector assembly consists of two coaxial collectors: an

inner disc biassed at a negative potential to attract "low energy" unwanted ions,and an outer annular ring to collect the selected ions.

The operation can be described as follows by referring to Fig. 2.10.B. The triangle here is the stability region for the ions of mass M. The operating line of the analyser is OP. An r.f. voltage V_{ac} is applied to the rods.

For $V_{ac} > V_o$. The ions are light with respect to V_{ac}. Their vibrations are easily synchronized to the r.f. field. They are unstable and therefore quickly ejected radially from the filter before reaching the collector region.

For $V_{ac} << V_o$. The ions are heavy with respect to V_{ac}. Their inertia resists the influence of the r.f. field. Their rotational rate is asynchronous to the r.f. field. They gain very little energy from it. They rotate at low speed and travel close to the central axis.

For $V_{ac} = V_o$. The ions are resonant to the r.f. field. The rate of rotation of the ions as they follow helical paths along the length of the analyser coincides precisely with that of the a.c. field. They leave the analyser at some considerable distance from the central axis, and have maximum chance of gaining energy from the r.f. field. With this energy they overcome the attraction of the "trapping field", which is set up by the negative potential on the inner collector, and "spray out" to the outer collector. The geometric and electric arrangements

of the collector assembly make the "spatial" and "energy" filtering effective.

Some initial experiments at Liverpool indicated that a mass filter with the new collector assembly produced an equally good or rather better performance than the previously used instrument. The investigation on the performance of the a.c. mode with this new collector assembly was continued by Ross (2/24 and 2/25).

Ross's basic experiment confirmed that the effect of "spatial" and "energy" filtering was realized by the outer collector at virtual zero potential and the inner collector at -15V. Increasing the potential of the inner collector to -210V, however, did not change significantly the instrument's performance, with regard to either the sensitivity or the resolution.

Ross's results strongly comfirmed that the resolution with the new collector assembly was always better than the normal mode for the same sensitivity. Ross pointed out that up to 300 a.m.u. the mass discrimination of the new instrument would not change even with a significant change in operating parameters and instrument contamination.

Further experiments by Ross indicated that the resolution of the instrument depended upon the number of cycles experienced by the focussed ions in the r.f. field. A better resolution could be obtained if the ions spent a larger number of cycles in a unit longitudinal length of the rod system.

With a rather different collector assembly (shown in Fig.2.11.A) Dawson (2/26) investigated the performance of a 150 mm filter for the a.c. mode. Dawson found that at high ion energy

$$R_{lim} \alpha M^2 \alpha (\text{ion energy})^2 \alpha N^4$$

where R_{lim} is the limiting resolution.

In the a.c. mode an indication light of peak splitting shown in Fig. 2.12 can be observed when the ion injection energy is taken to an excessively high level. This is in fact an entirely different fundamental property of the filter. To distinguish them from "split peaks" the peaks in Fig. 2.12 are called multi-peaks.

Using the phase space dynamic method Dawson (2/26) calculated the acceptance area for the new mode. He also transformed the stop at the exit of the rod system back to a shadow at the entrance of the r.f. field. Comparing the acceptance area with the shadow area, in the light of source radius limit, Dawson illustrated the formation of a peak when the acceptance area was free from the shadow. Also he pointed out the possible appearance of the multi-peaks when the acceptance area was partially covered by the shadow. For instance, Fig. 2.11.B shows that a single peak will appear when the source radius is $0.35r_o$, whilst double peaks will appear when the radius is $0.50r_o$.

Alternatively, multi-peaks can be explained in

qualitative terms by looking at the details of the ion trajectories. The calculations by Leck (2/27) show that the ion trajectories are in the forms of beats.Two typical paths, obtained from computer analysis for q=0.9054 and 0.9078 are shown in Fig. 2.13.

As the a.c. voltage amplitude sweeps down through and just below V_o (see Fig.2.10.B), the contour of the ion trajectories in the r.f. field changes from a half of the fundamental beat to a full beat, to two beats, three beats and so on. Meanwhile the amplitude becomes smaller and smaller. If L is the length of the analyser, n is an integer, $2D_n$ is the distance between the adjacent two nodes of a beat, then when

$$L = 2nD_n$$

a dip in the ion current on the outer collector will occur. But when

$$L = (2n + 1)D_n$$

a spike will occur. Therefore multi-peaks are formed. Fig. 2.13 shows that the first spike of an ion current occurs at q = 0.9078 and the second at q = 0.9054. At this point double peaks may have already appeared.

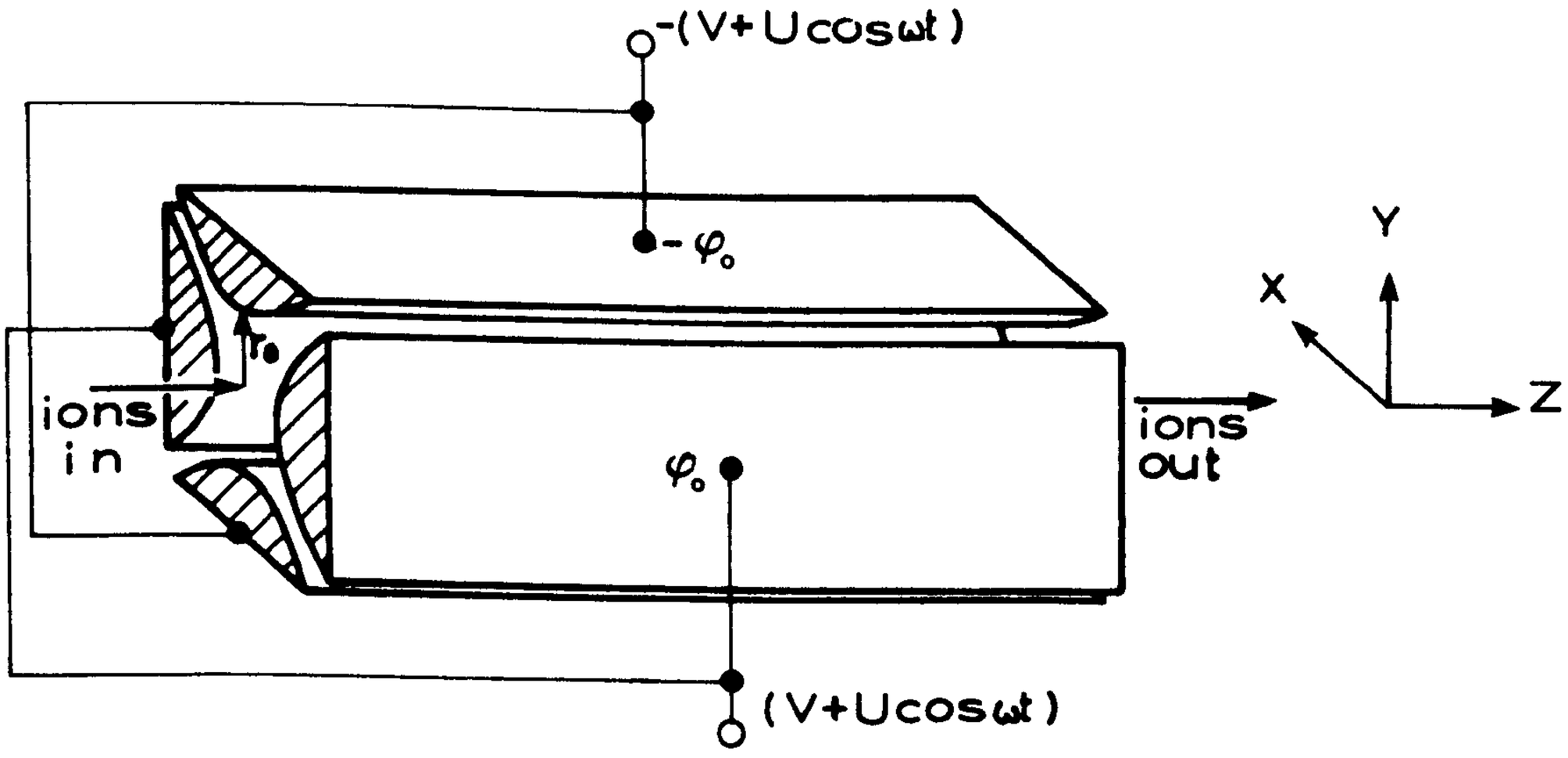

FIG. 2.1. CONFIGURATION OF QUADRUPOLE.

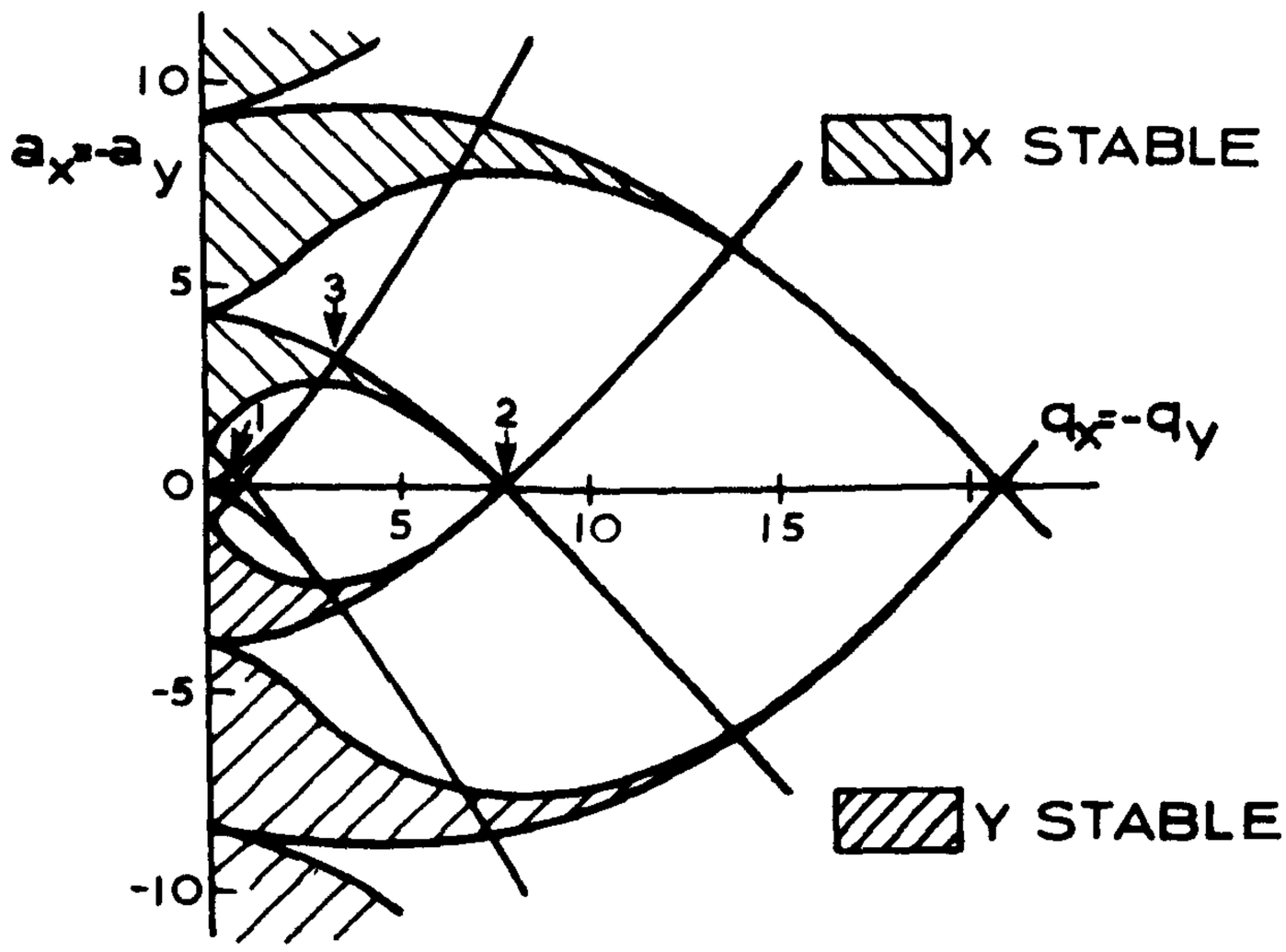

FIG. 2.2. MATHIEU STABILITY DIAGRAM SHOWING THE STABLE REGIONS IN BOTH X AND Y DIRECTIONS.

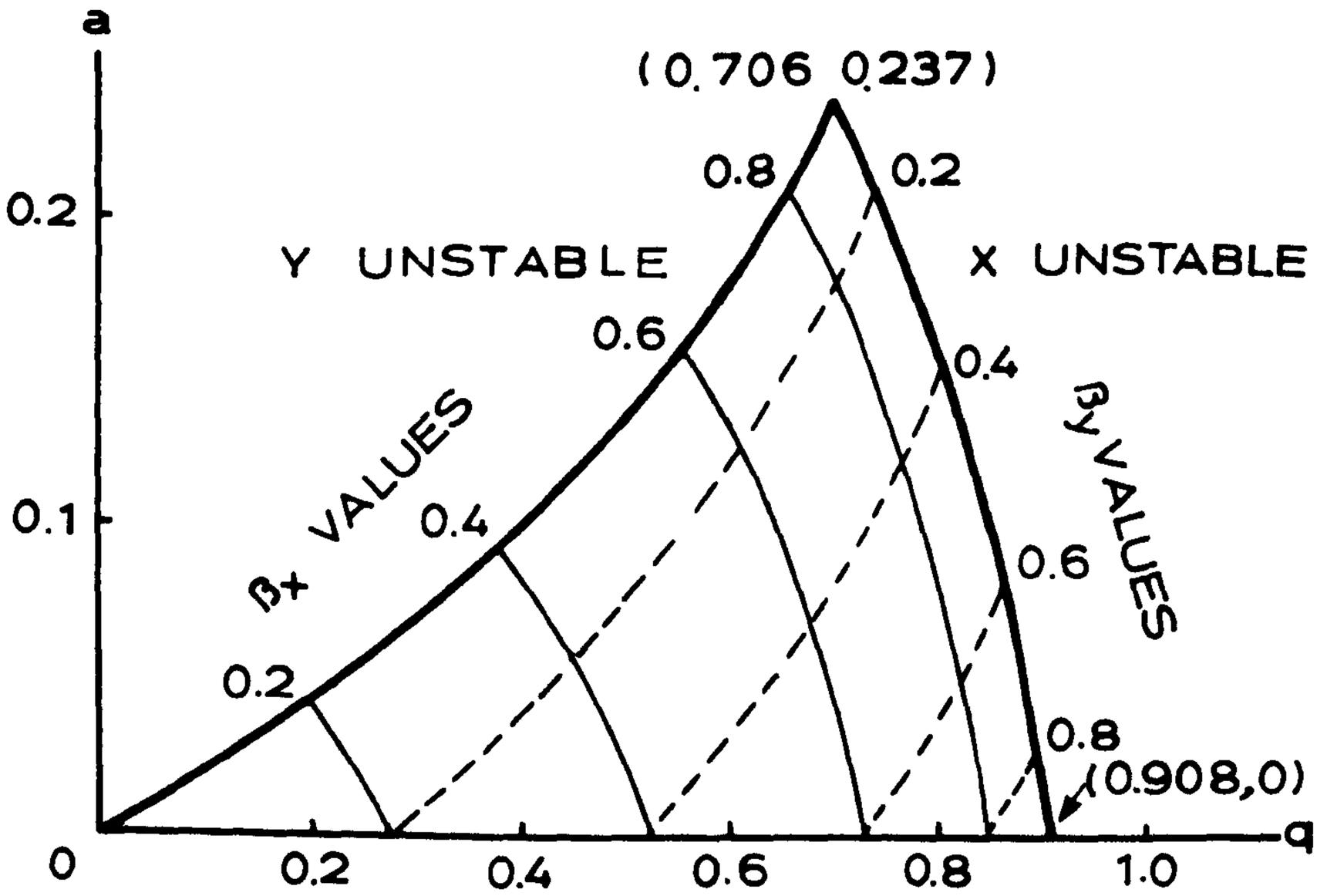

FIG. 2.3. STABILITY REGION.

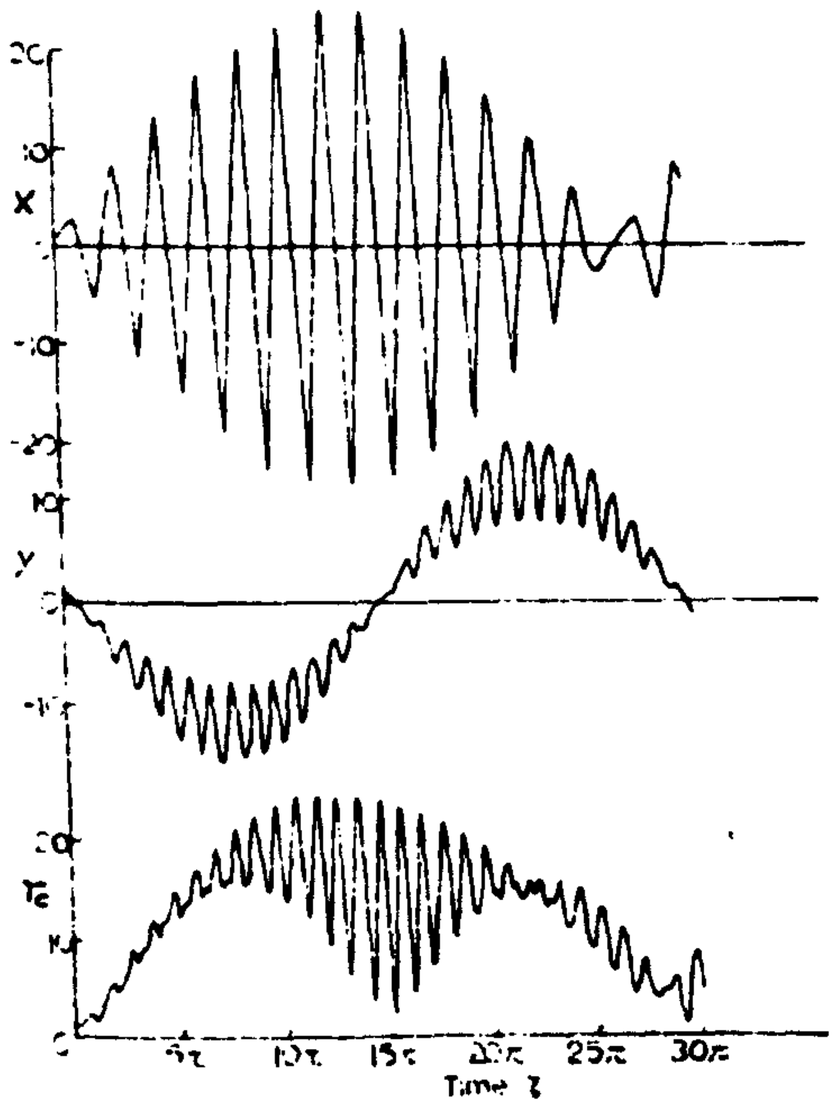

FIG. 2.4. TYPICAL ION TRAJECTORIES TAKEN BY AN ION NEAR THE APEX OF THE STABILITY REGION.(2/7)

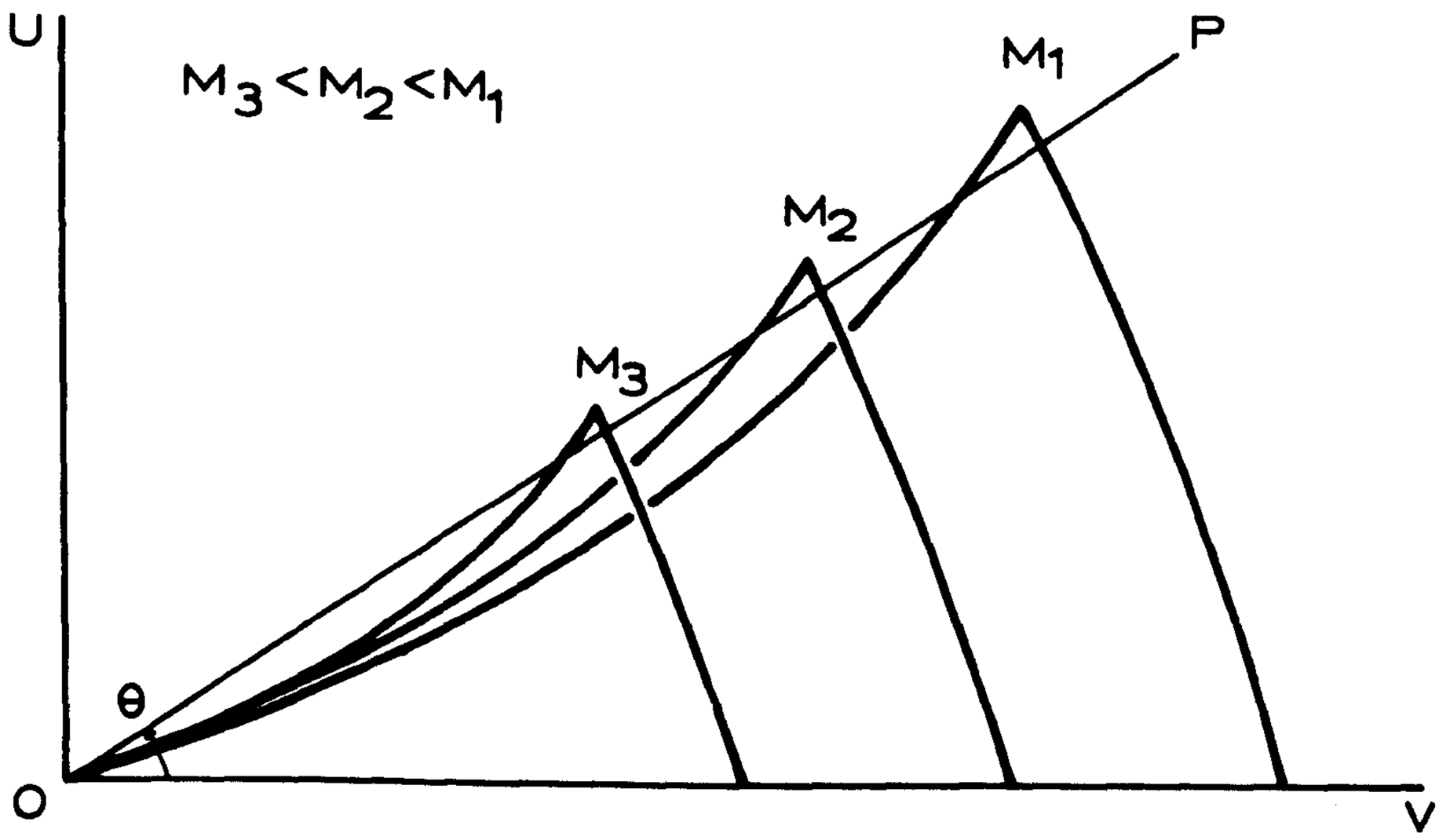

FIG. 2.5. OPERATION OF QUADRUPOLE MASS FILTER BY VARYING V AND U WITH CONSTANT RATIO U/V.

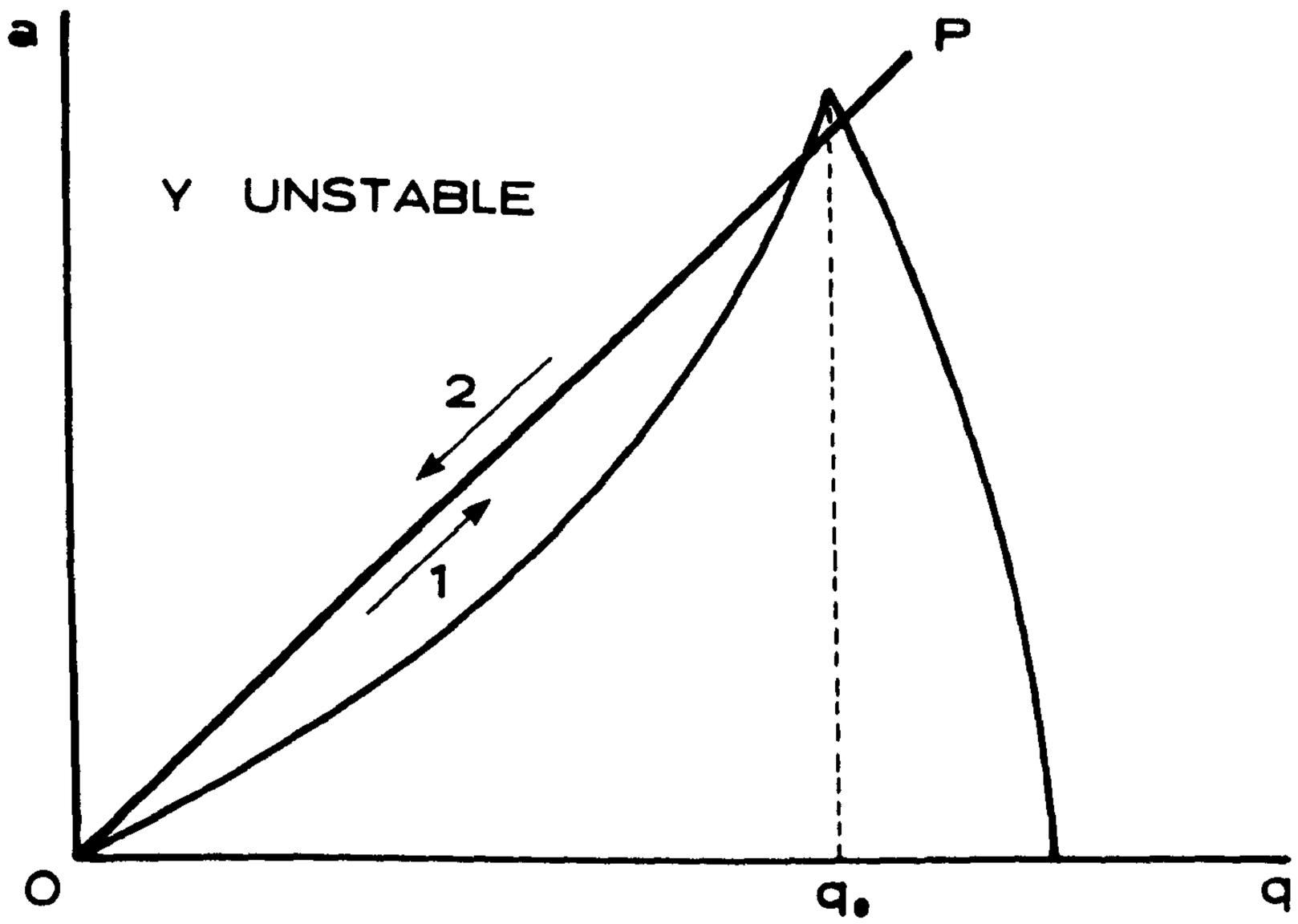

FIG. 2.6. TRANSITIONS IN THE FRINGING FIELDS.

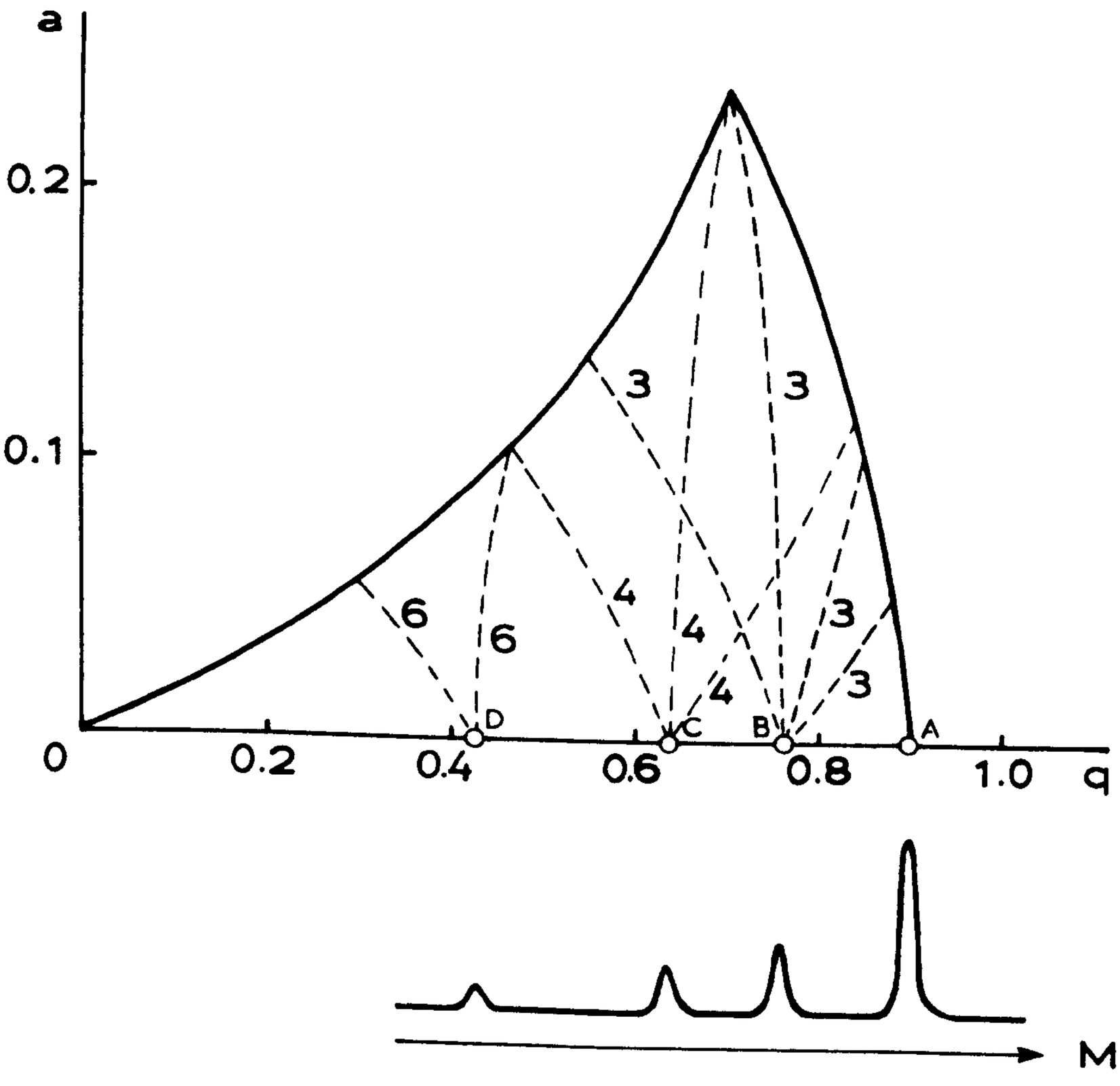

FIG. 2.7. HIGH ORDER RESONANT LINES AND SATELLITE PEAKS.

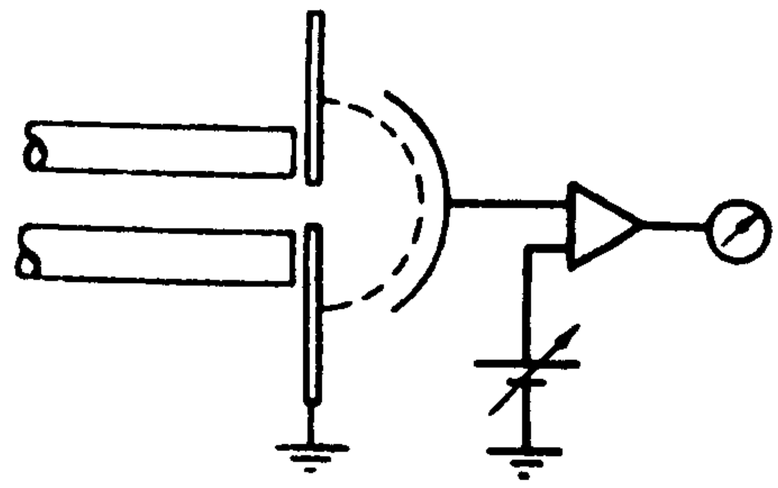

(A)

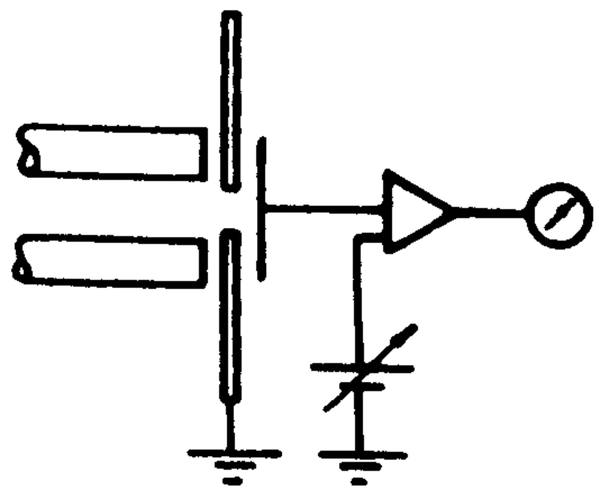

(B)

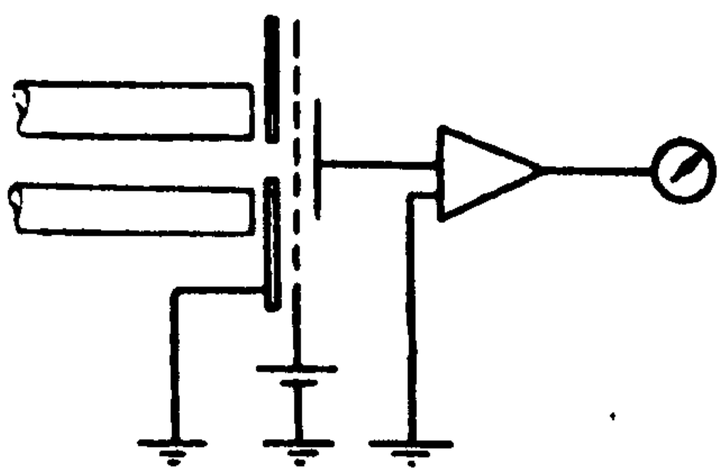

(C)

FIG. 2.8. SOME EARLY CONFIGURATIONS OF COLLECTION SYSTEM IN THE A.C. MODE.(2/22)

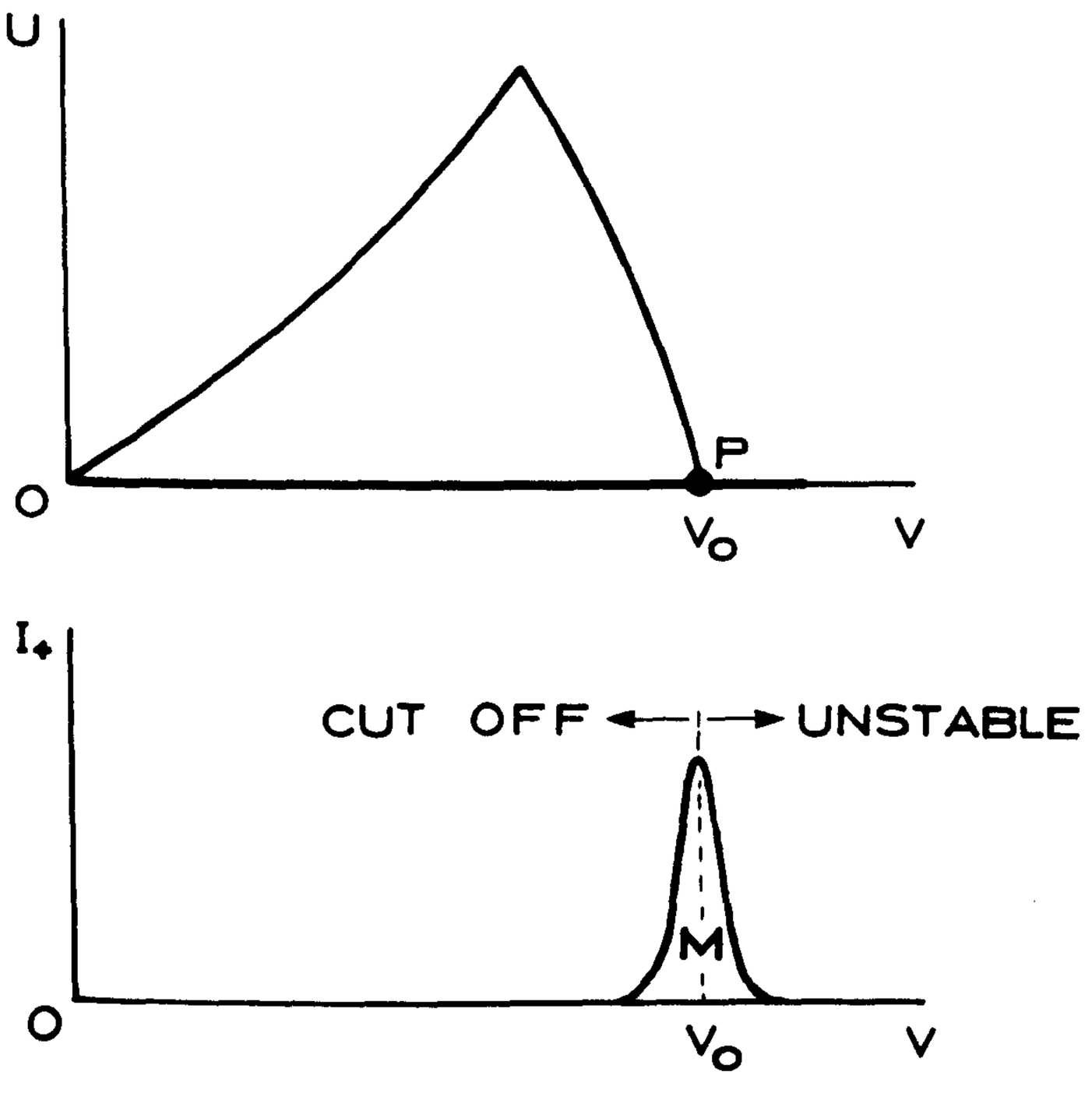

FIG. 2.9. OPERATION WITH BRINKMANN'S CONFIGURATION OF COLLECTION SYSTEM IN THE A.C. MODE.

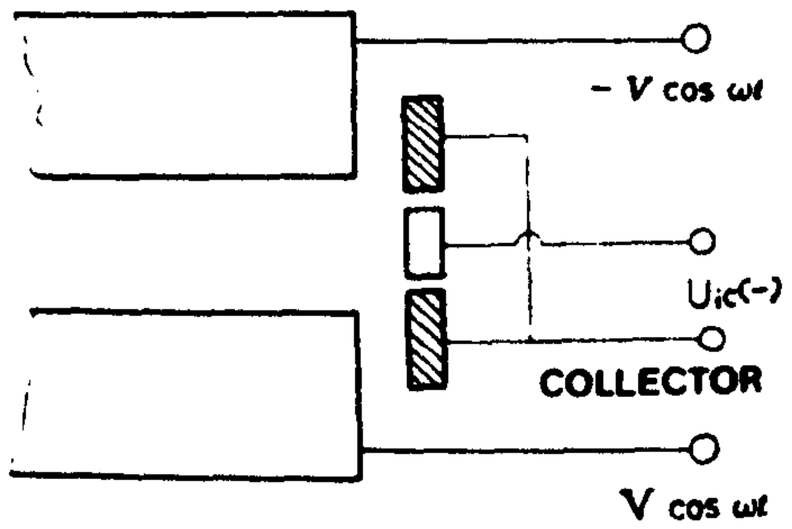

(A)

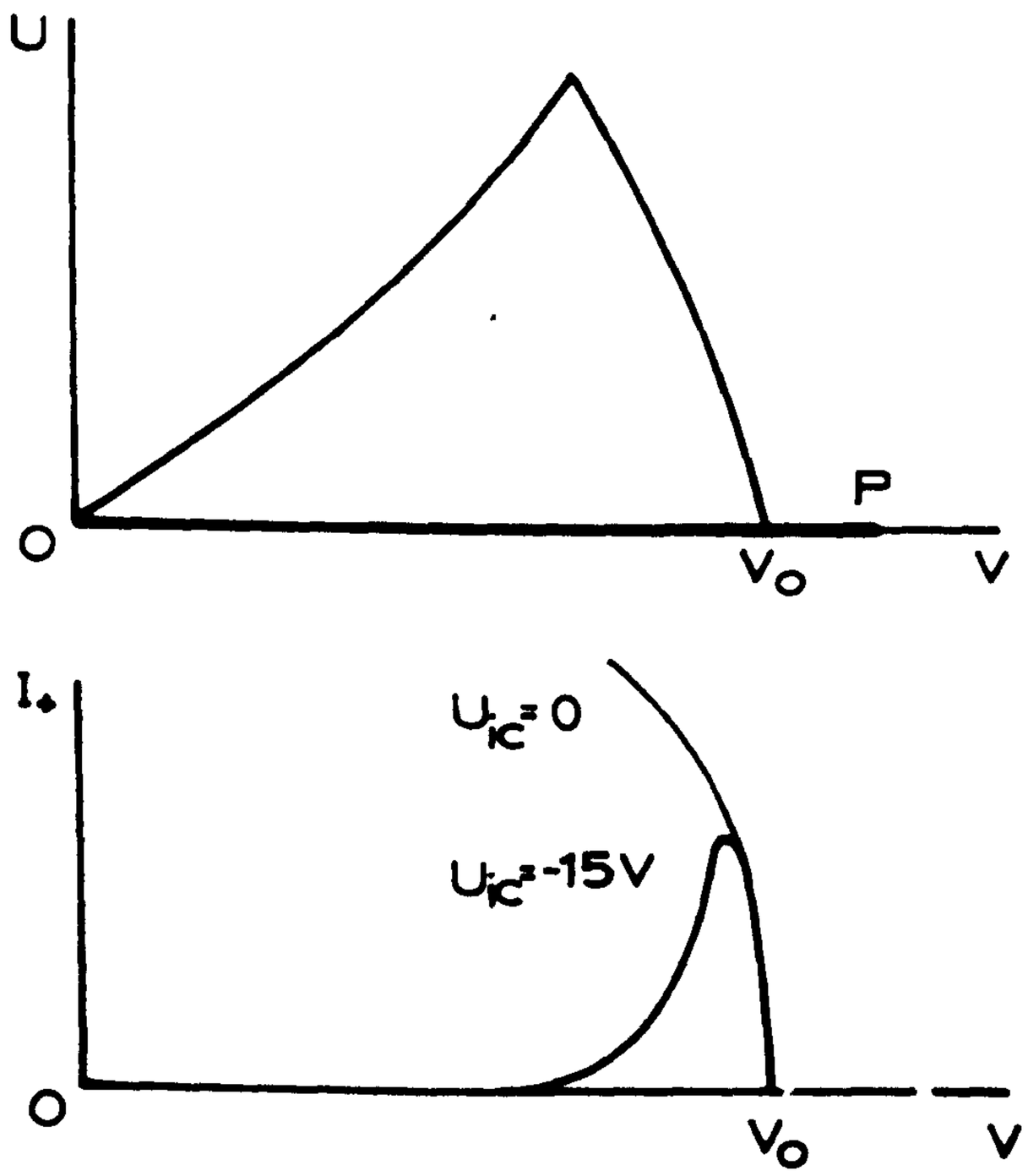

(B)

FIG. 2.10. THE PRESENT CONFIGURATION OF COLLECTION SYSTEM AND THE OPERATION USING THIS SYSTEM IN THE A.C. MODE.

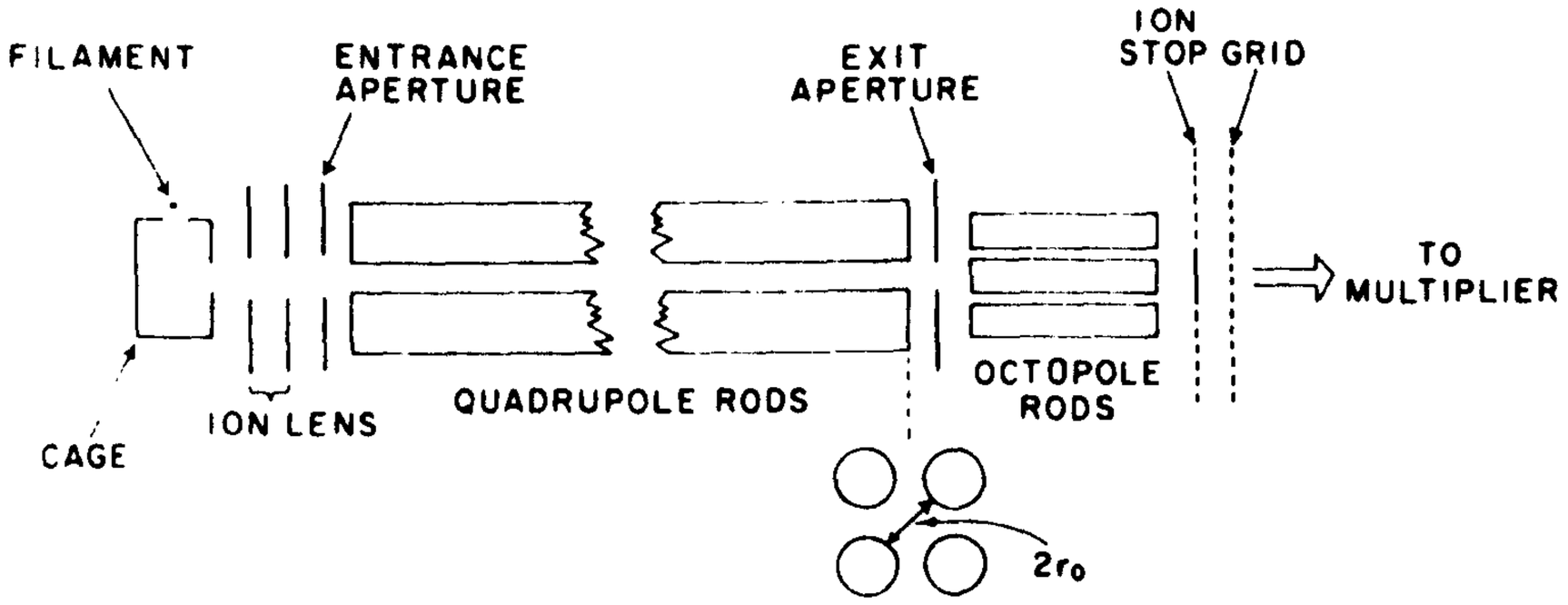

(A)

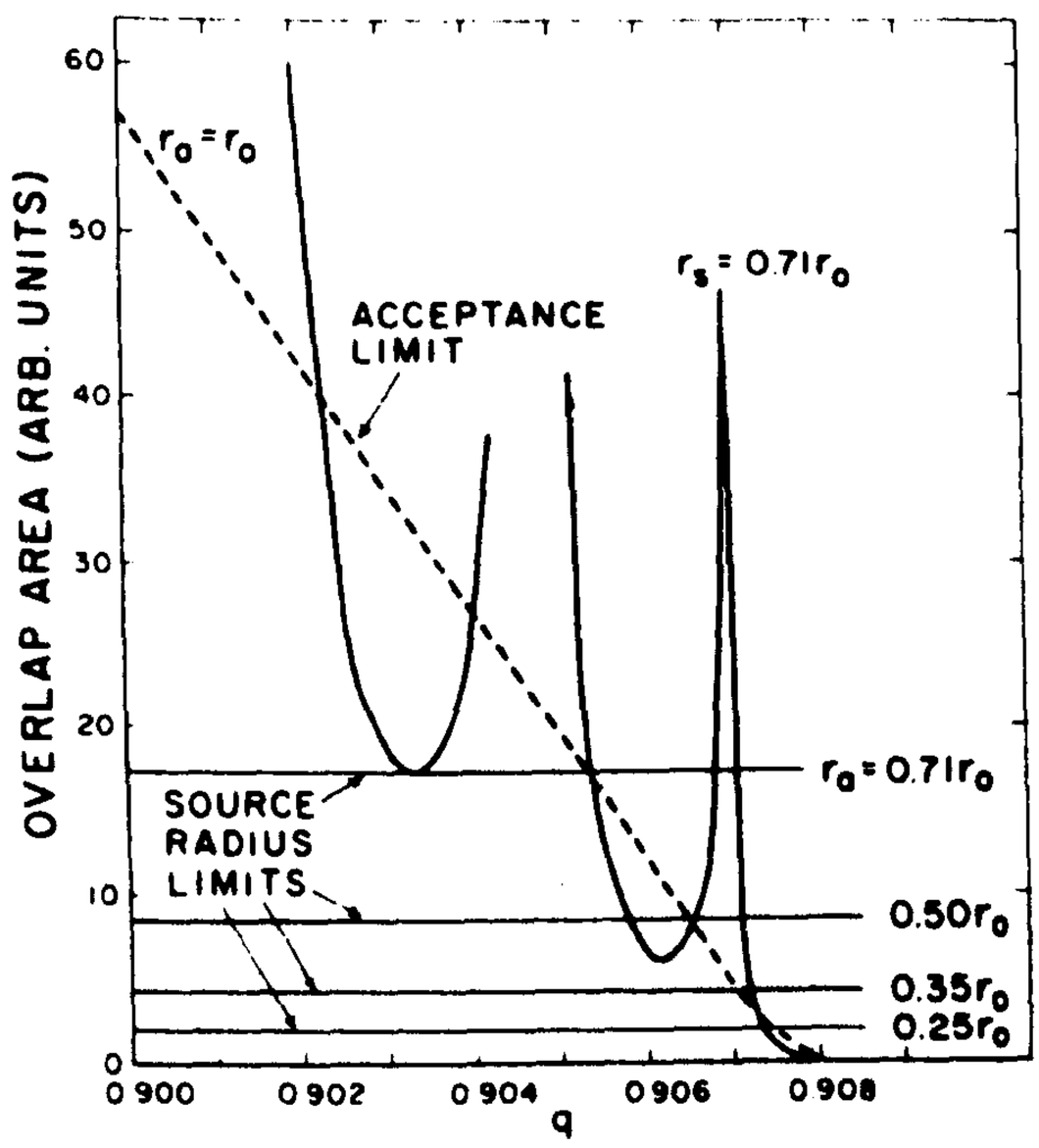

(B)

FIG. 2.11. CONFIGURATION OF A COLLECTION SYSTEM AND COMPARISON OF ACCEPTANCE WITH SHADOW AREA BY DAWSON. (2/26)

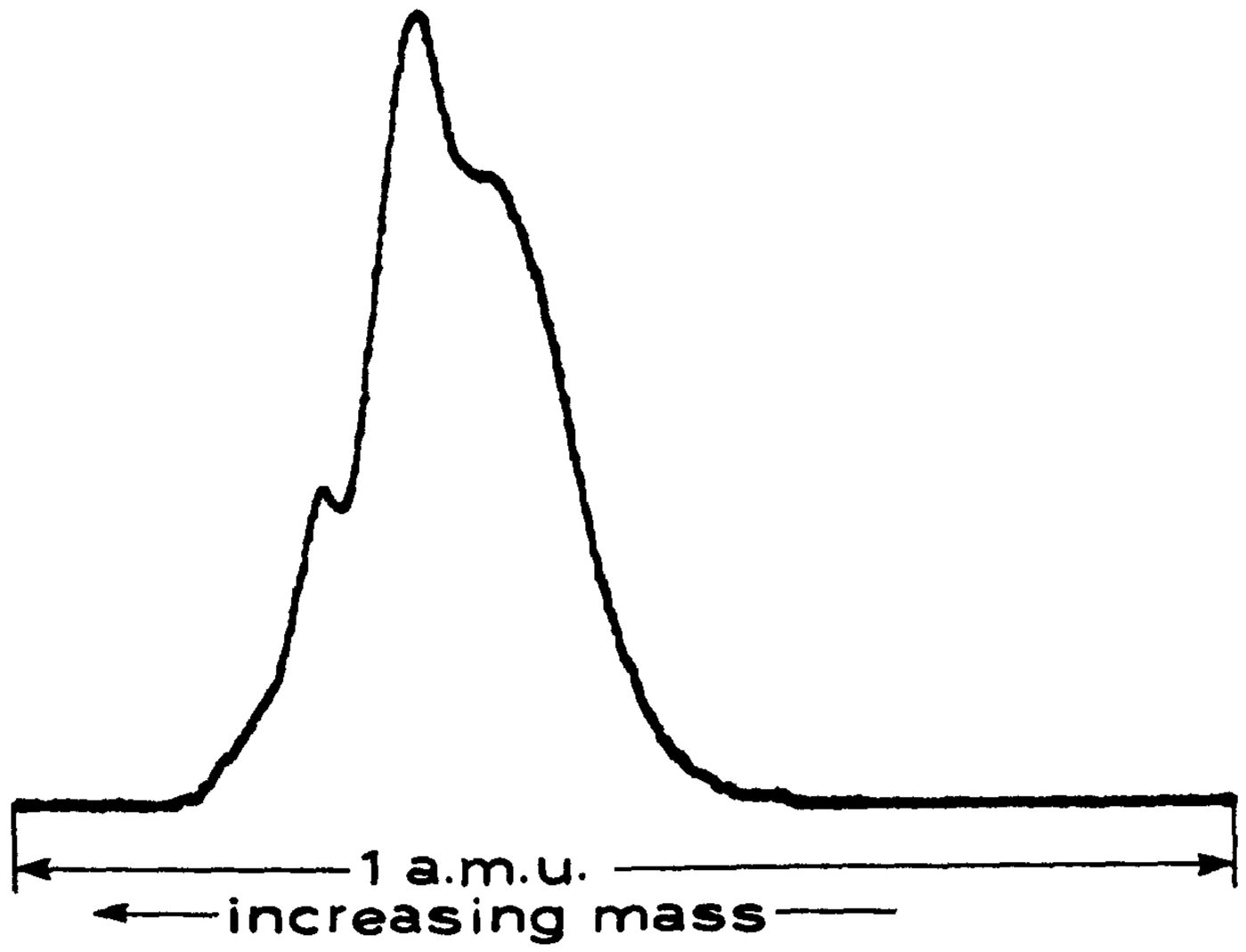

FIG. 2.12. THE MULTI-PEAKS.

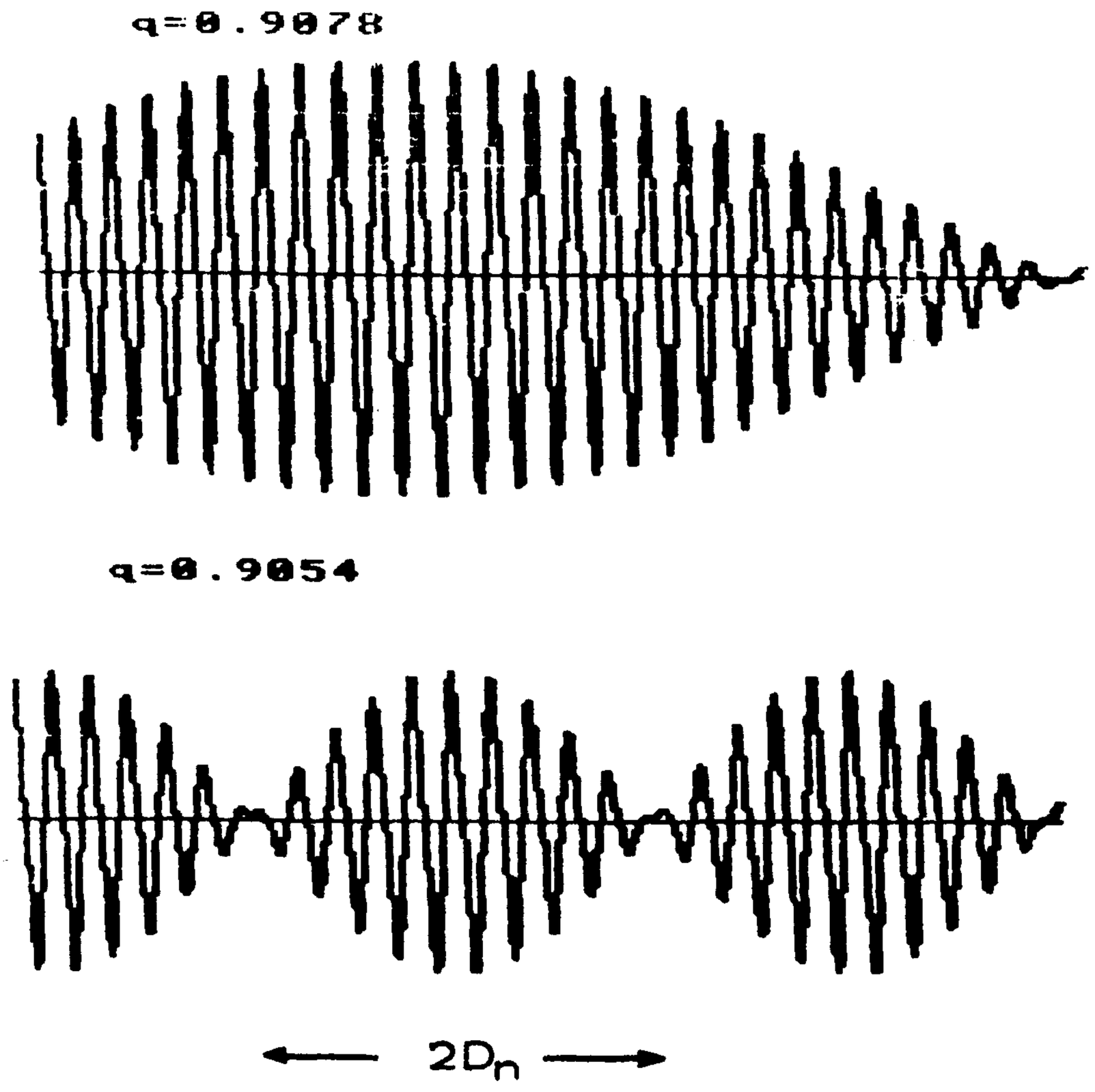

FIG. 2.13. BEAT FORM OF ION TRAJECTORIES IN THE A.C. MODE.(2/27)

CHAPTER 3. Experimental Equipment

Fig. 3.1. shows an outline of the experimental equipment. Throughout the investigation the experiments were carried out using several versions of the basic quadrupole head, and the corresponding electronics. Two vacuum systems, plant No.1 and plant No.2, were used.

3.1. The Quadrupole Head

The quadrupole heads which were used during the investigation consisted of different combinations of two types of ion source, five different lengths of rod assembly, and a collector assembly.

1) The ion source

(A) Conventional ion source

Fig. 3.2.A is a schematic diagram of an ion source purchased from Edwards High Vacuum Co. The lens system has circular symmetry about the central axis.All its component plates are manufactured from stainless steel discs. The filament assembly has two tungsten helical filaments. They are insulated from the filament plate by ceramic supporters. Lens 3 has a cylindrical stainless steel mesh surrounding the filaments to increase ionization efficiency and to shield the electron emission region from the other parts. The cage is also cylindrical made from molybdenum mesh. The cage encompasses the main part of the ionization region.

The component lens plates are separated from one

another by ceramic washers. The lens assembly is built up from the base. A jig made in the department, shown in Fig. 3.2.B, was used to align the source. With careful use of this jig the whole lens assembly could be aligned with errors of less than 0.1 mm in eccentricity.

With reference to Fig.3.2.A, the filament assembly, lens 3 and cage form the ionization section; lens 1, lens 2 and the base constitute an ion focusing system. By applying potentials on the source, electrons are emitted from one of the filaments and oscillate through the cage. Hence ions are produced in the ionization region. Then they are focussed by the lens system into a parallel beam and ejected into the rod system.

(B) Nier source

Fig. 3.3.A is a schematic diagram of the Nier source. A Nier source used in a leak detector of Edwards High Vacuum Co., as an ionization section, is mounted on the ion focussing system of the conventional ion source. There is an isolation region located between the two. All the parts of the source are made of non-magnetic material.

The whole source is assembled with the jig shown in Fig. 3.3.B. The assembly is built up from the base. An overall eccentricity of less than 0.1 mm in the lens assembly can be obtained.

A small magnetic field axial to the electron path is essential to focus the electrons through the ionization region. This field is obtained from a small permanent magnet placed outside the vacuum system. The ion focussing

system draws ions from the isolation region,focusses them, and then ejects them to the rod system.

2) Rod assembly

The five rod assemblies are the same except for their lengths. For convenience they are numbered 1 to 5. They are listed below.

Table 3.1 Rod assemblies.

No.	Rod Assembly Length (mm)	Thesis Chapter Reference
1	50	4.1 - 4.3, 4.6
2	50	4.4, 4.5, 4.7, 4.8
3	25	4.2
4	85	4.5 - 4.7
5	100	4.2 - 4.3

All the rod assemblies have the same construction. The rods are circular, 6.35 mm in diameter (2r), with the distance ($2r_o$) between the opposite rods 5.47 mm. A sectional view of an assembly is given in Fig. 3.4. The rods are fixed at each end by a screw and two ruby balls. The ruby balls and the ceramic washer serve to insulate the rods from the housing. The alignment of the assembly is determined by the accuracy of these components. The rods, the housing, and the body are all made of stainless steel.

3) Collector assembly

Fig. 3.5. illustrates schematically a collector assembly. It was designed to fit a commercial flange, which has only one lead-through connector in the centre. Component (1) is the outer collector, an annular ring with internal diameter 7 mm and external diameter 17 mm. (2) is the inner collector 4 mm diameter. (3) is a shield earthed to screen the outer collector from the inner. It is equidistant, 0.5 mm, from each collector. These three components are aligned perpendicular to the four rods. (4) are ruby washers to insulate the electrodes. (5) is the body on which the components are assembled. (6) is a length of wire to connect the inner collector to a peripheral lead-through connector. (7) is the connector from the outer collector to the central lead-through on the flange. Except for the ruby washers and the wire, all the components are made of stainless steel.

4) Assembly of a mass filter

The ion source, rod assembly,and collector assembly are aligned by a spigot with a slide fit. The distance between the base of the ion source and the rods is 0.5 mm. The distance between the rods and the collectors is 2.0 mm. Neither distance is critical.

3.2. Electronic Equipment

Except for EQ10 and EQ50 which are made by Edwards High Vacuum Co., all the electronic equipment, i.e. the "High Voltage Quadrupole Mass Spectrometer (HVQMS)" analy-

ser supply, ion source control unit, and picoameter were made in the department.

The block diagram of the analyser supply is given in Fig. 3.6. The frequency is determined by a crystal and a corresponding coil. The r.f. voltage is stabilized by the feedback circuit. The analyser supply can provide a maximum of 2.5 KV peak to ground r.f. voltage. For the purpose of experiment, a switch has been arranged to select an operation mode of either normal or a.c.

For convenience the ion source control unit provides four ranges of stabilized electron emission current: 10uA, 0.1mA, 1mA, and 10mA. With reference to Fig. 3.2.(A) the unit provides all the potentials for the ion source. The potential of the central disc in the collector assembly (see Fig.2.10.A) is normally held at lens 1 potential, i.e. -145 volts.

The picoameter is a standard negative voltage feedback amplifier. Its minimum measurable current under ideal operating conditions is 10^{-15} A.

3.3. The Vacuum Systems

Two vacuum plants were used for the experimental work.

1) Plant No.1

Plant No.1, as shown in Fig. 3.7, is a stainless steel high vacuum system. The quadrupole mass filter is pumped by the rotary pump and the diffusion pump. The ultimate pressure of the system is of the order of 10^{-7}

mbar. The sublimation pump was not required and was in fact very rarely used.

There are two ionization gauges, type IOG 12, on the system. One, No.1, was chosen as a standard gauge used for calibration of the other gauges. It was well maintained throughout the whole of the work. Another, No.2, was used as an operating gauge. It was calibrated before use.

There are two gas introduction systems on the plant. The system via valve 10 has the finer control for gas introduction. This was used when only a single gas component was required.

2) Plant No.2

Plant No.2, shown in Fig. 3.8, is a miniature model of a vacuum furnace. The purpose was to simulate the conditions in which a quadrupole mass filter was working inside a practical vacuum furnace. The mass filter, the glass bell jar and the high pressure ionization gauge IR10 are mounted on the vacuum chamber. The mass filter is pumped by the rotary pump and the diffusion pump via a baffle of 3.3 l/s. The baffle was used to maintain a high pressure (10^{-3} mbar) during a processing experiment. The ultimate pressure of the system was in the order of 10^{-6} mbar. The ionization gauge IR10 was calibrated before being installed on the plant. The simple auxiliary gas introduction system was used for a quick test of quadrupole performance. Usually argon was the test gas.

In association with the plant, a 1 kW radio frequency heater was used to bake the samples inside the

glass bell jar. The temperature of the sample was monitored by a thermocouple. The gases evaporated from the sample simulate the hostile atmosphere of a vacuum furnace.

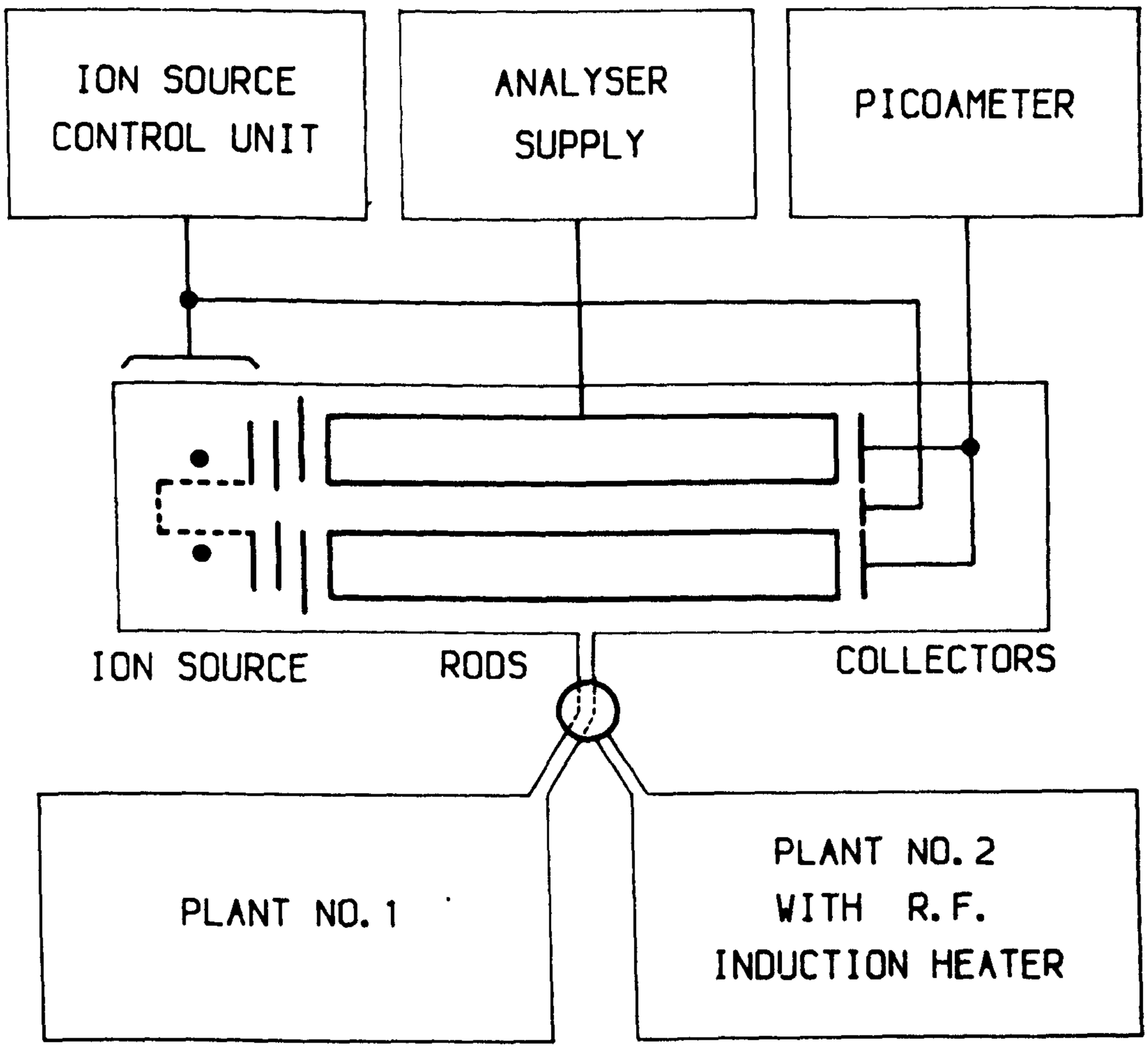

FIG. 3.1. OUTLINE OF EXPERIMENTAL APPARATUS.

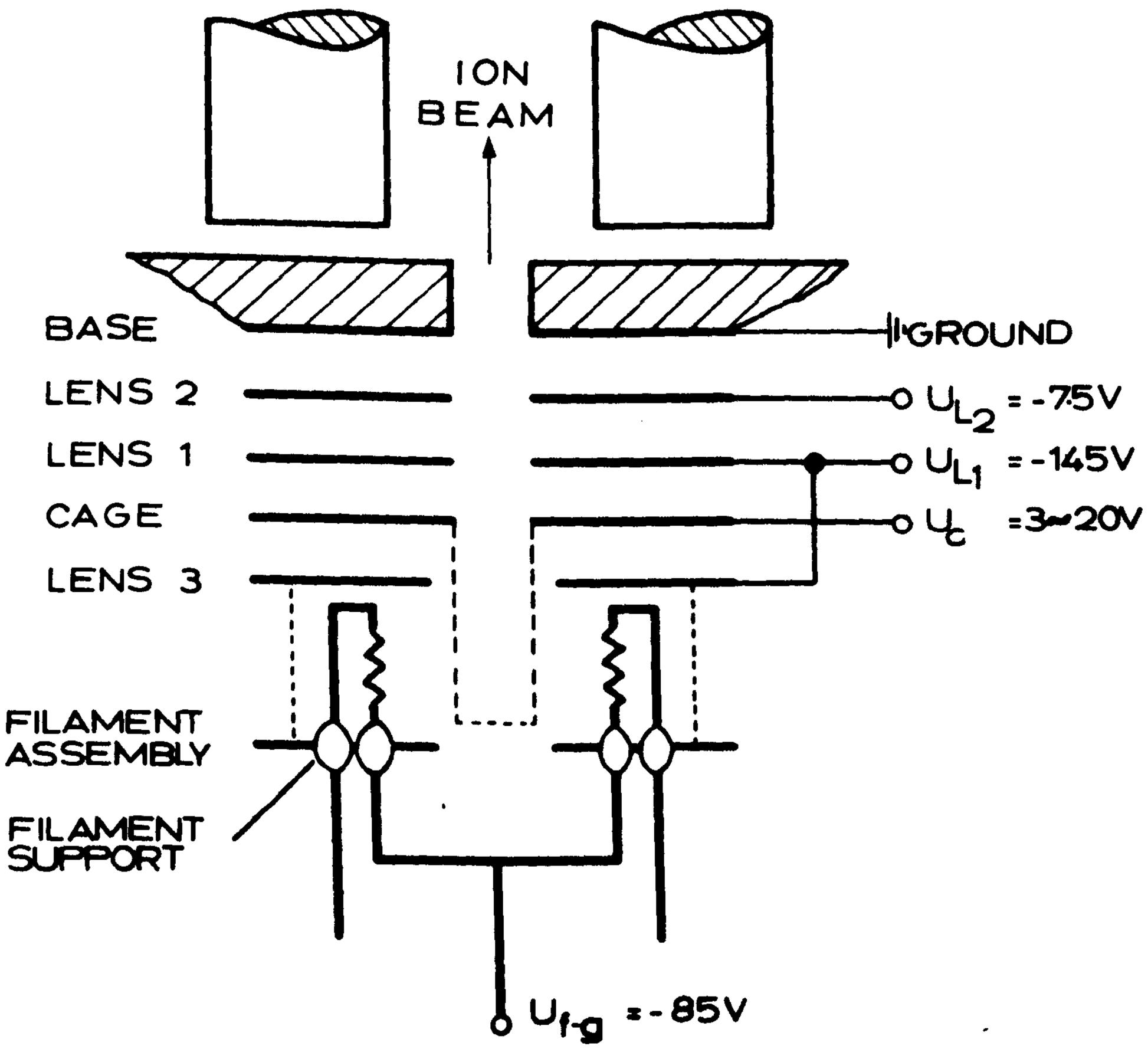

FIG. 3.2.A. CONFIGURATION OF A CONVENTIONAL ION SOURCE.

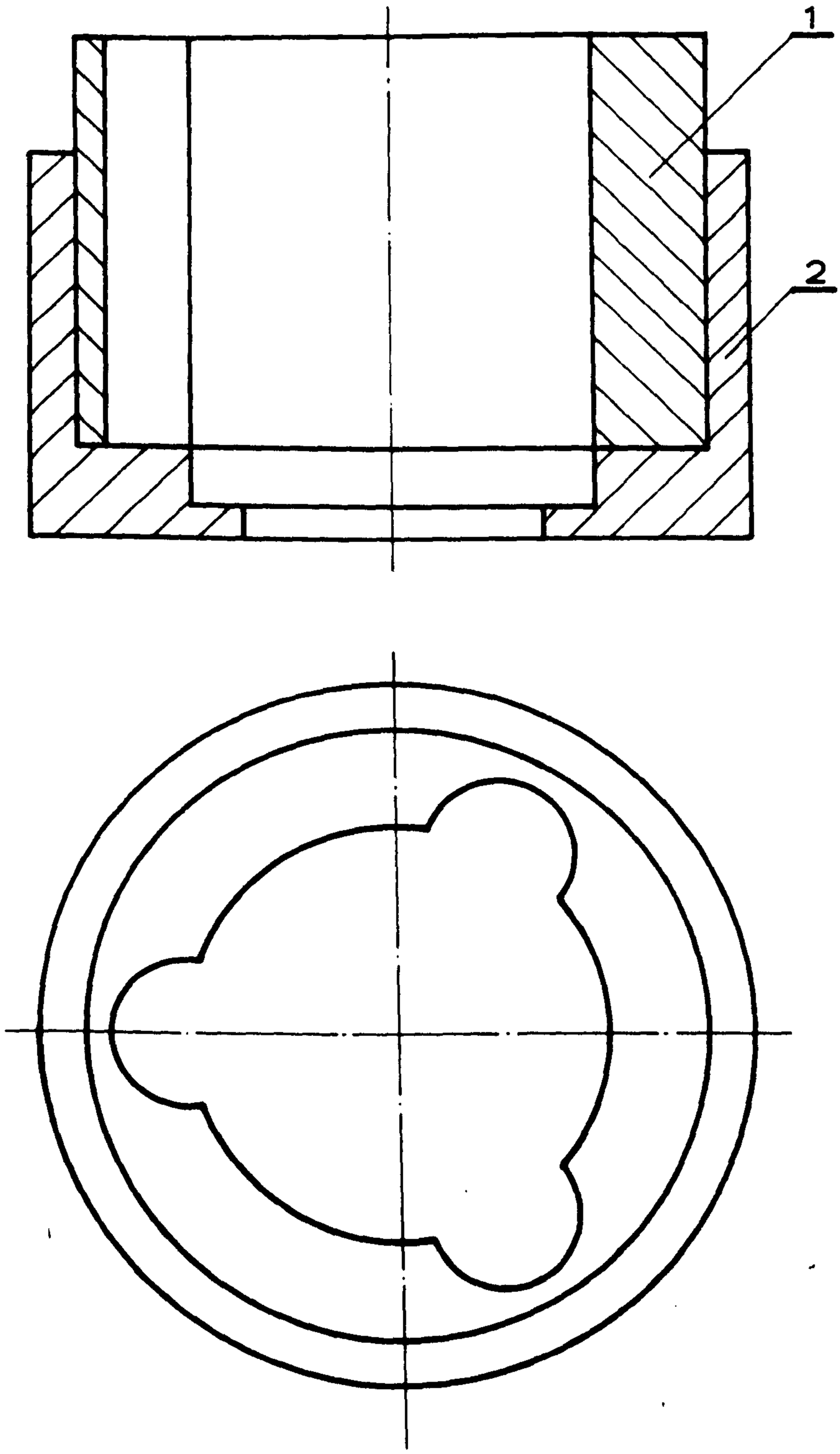

FIG. 3.2.B. A JIG FOR ASSEMBLY OF THE CONVENTIONAL ION SOURCE.

1-UPPER JIG 2-LOWER JIG

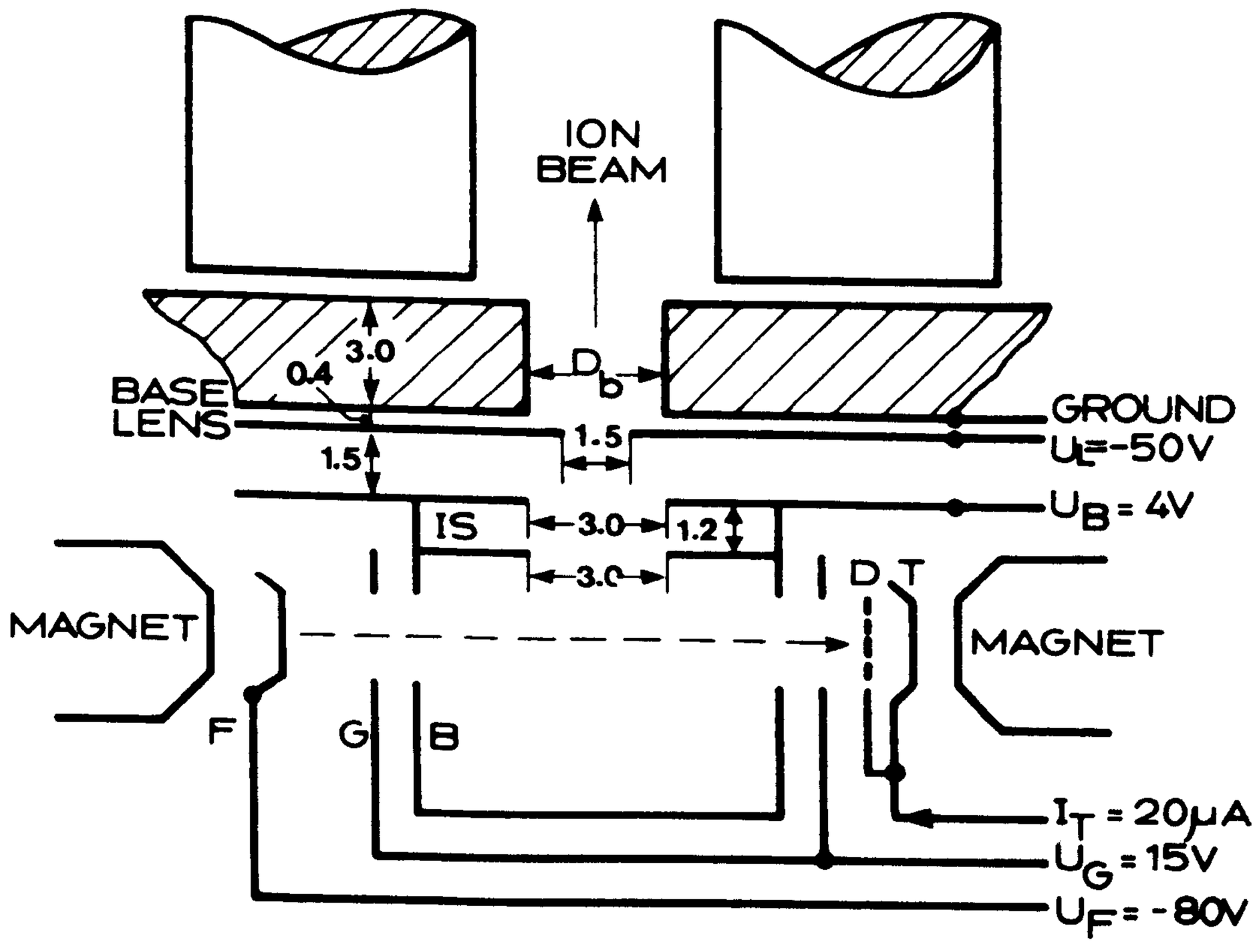

FIG. 3.3.A. CONFIGURATION OF A NIER SOURCE.

B- IONIZATION CHAMBER (BOX)

D- SECONDARY ELECTRON DEPRESSOR

F- FILAMENT

G- GATE

IS-ISOLATION CHAMBER

T- ELECTRON TRAP

ALL DIMENSIONS ARE IN MM

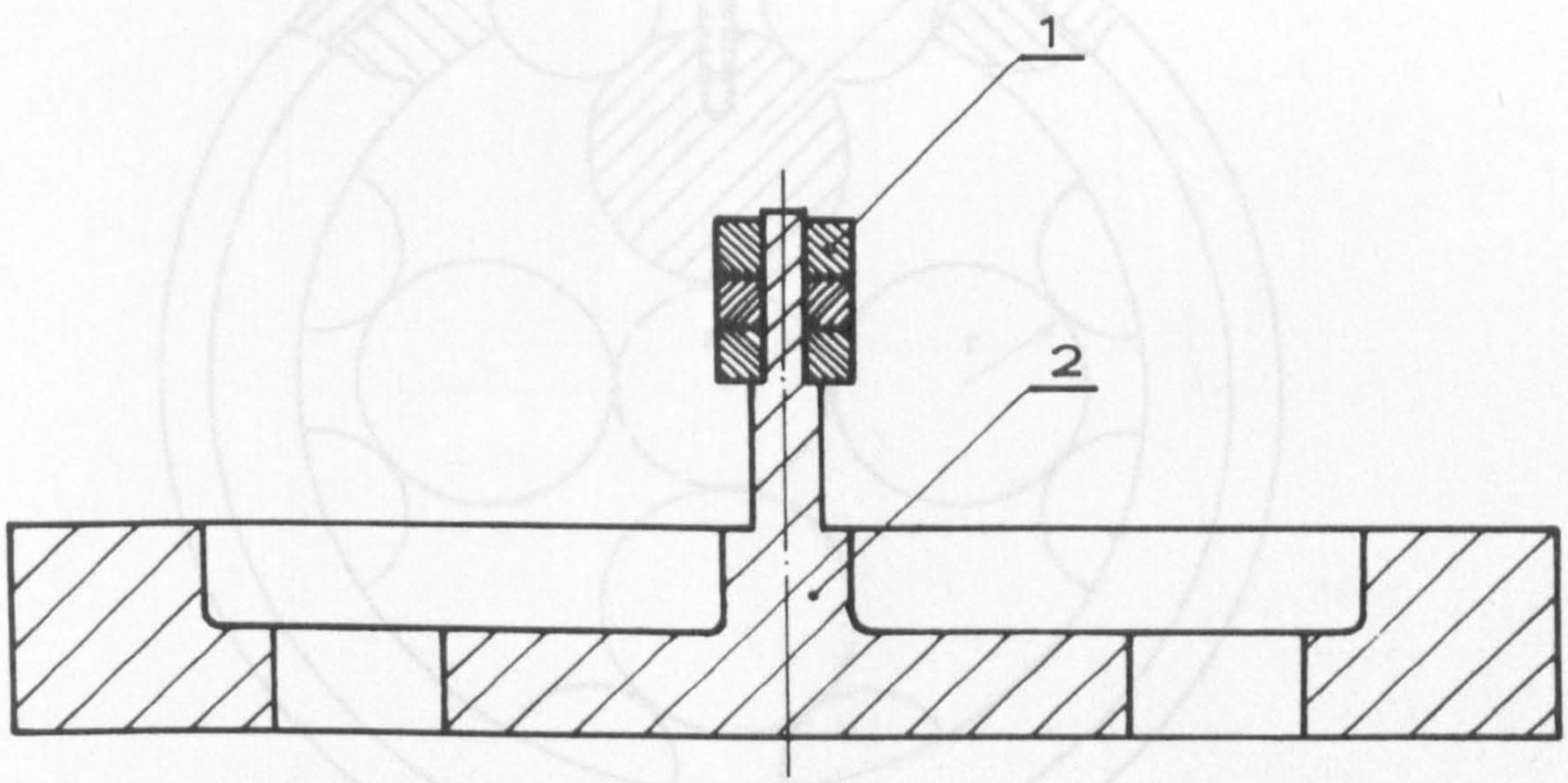

FIG. 3.3.B. A JIG FOR ASSEMBLY OF THE NIER SOURCE.
1-SLIDE RING 2-JIG BASE

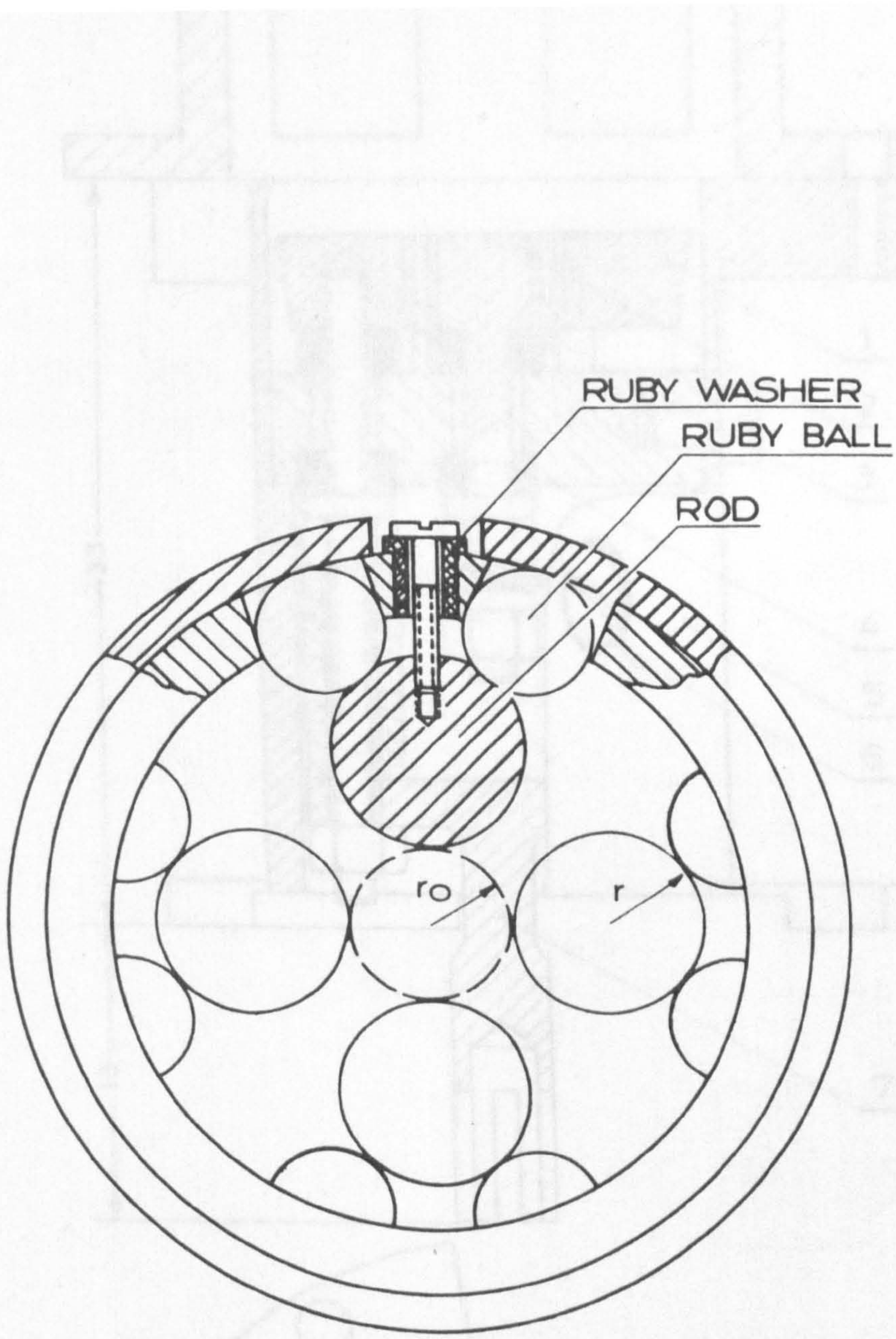

FIG. 3.4. A SECTIONAL VIEW OF ROD ASSEMBLY AND MOUNTING WITHIN ITS HOUSING.

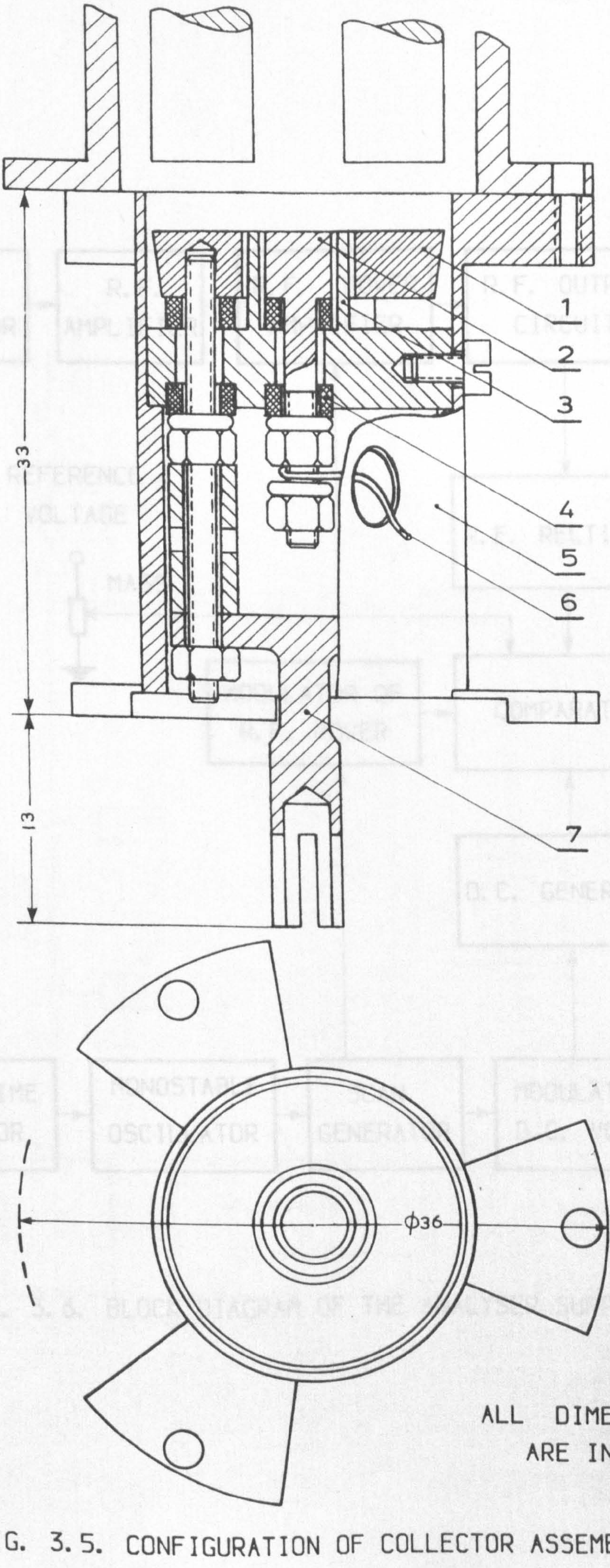

FIG. 3.5. CONFIGURATION OF COLLECTOR ASSEMBLY.

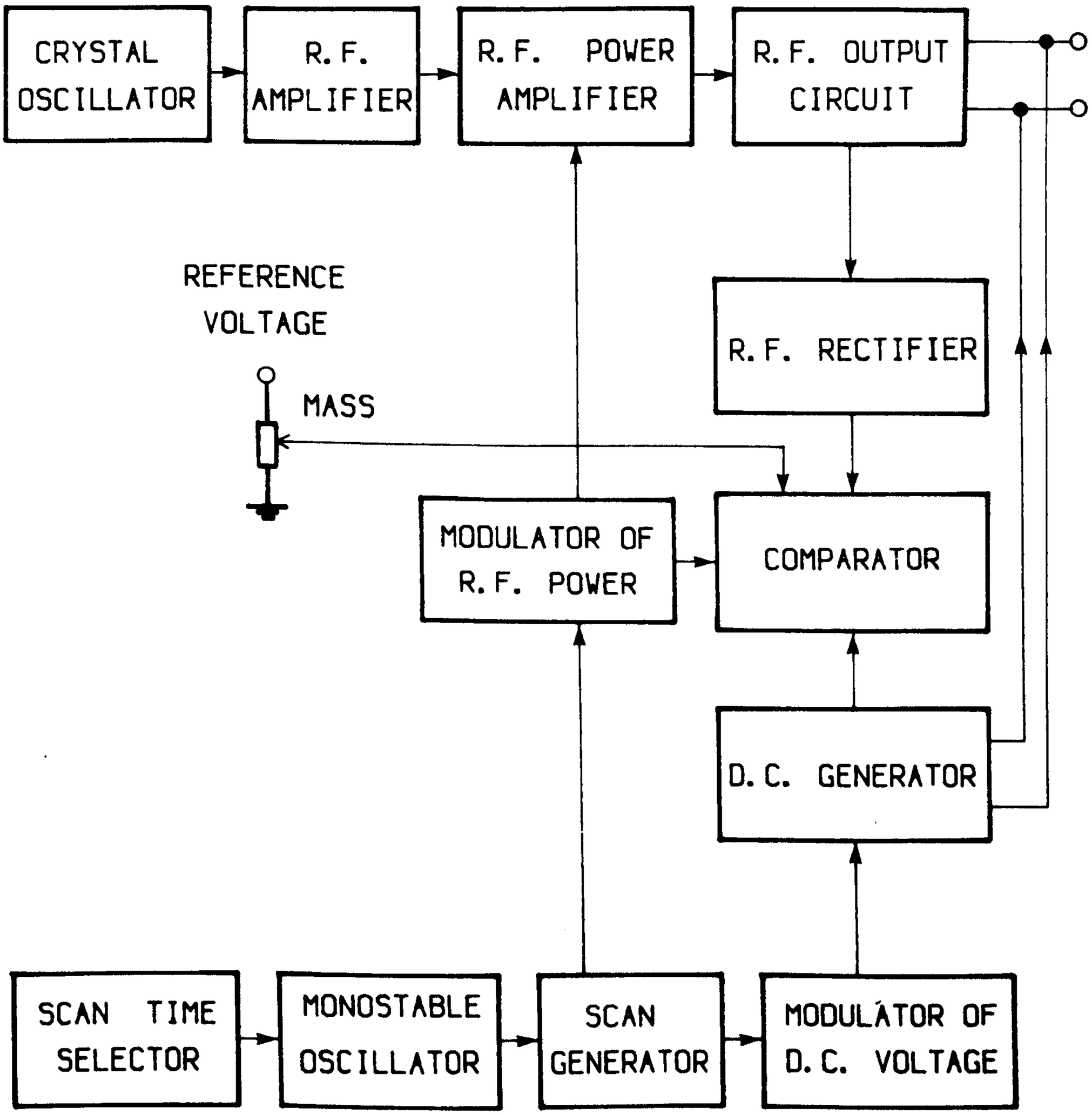

FIG. 3.6. BLOCK DIAGRAM OF THE ANALYSER SUPPLY.

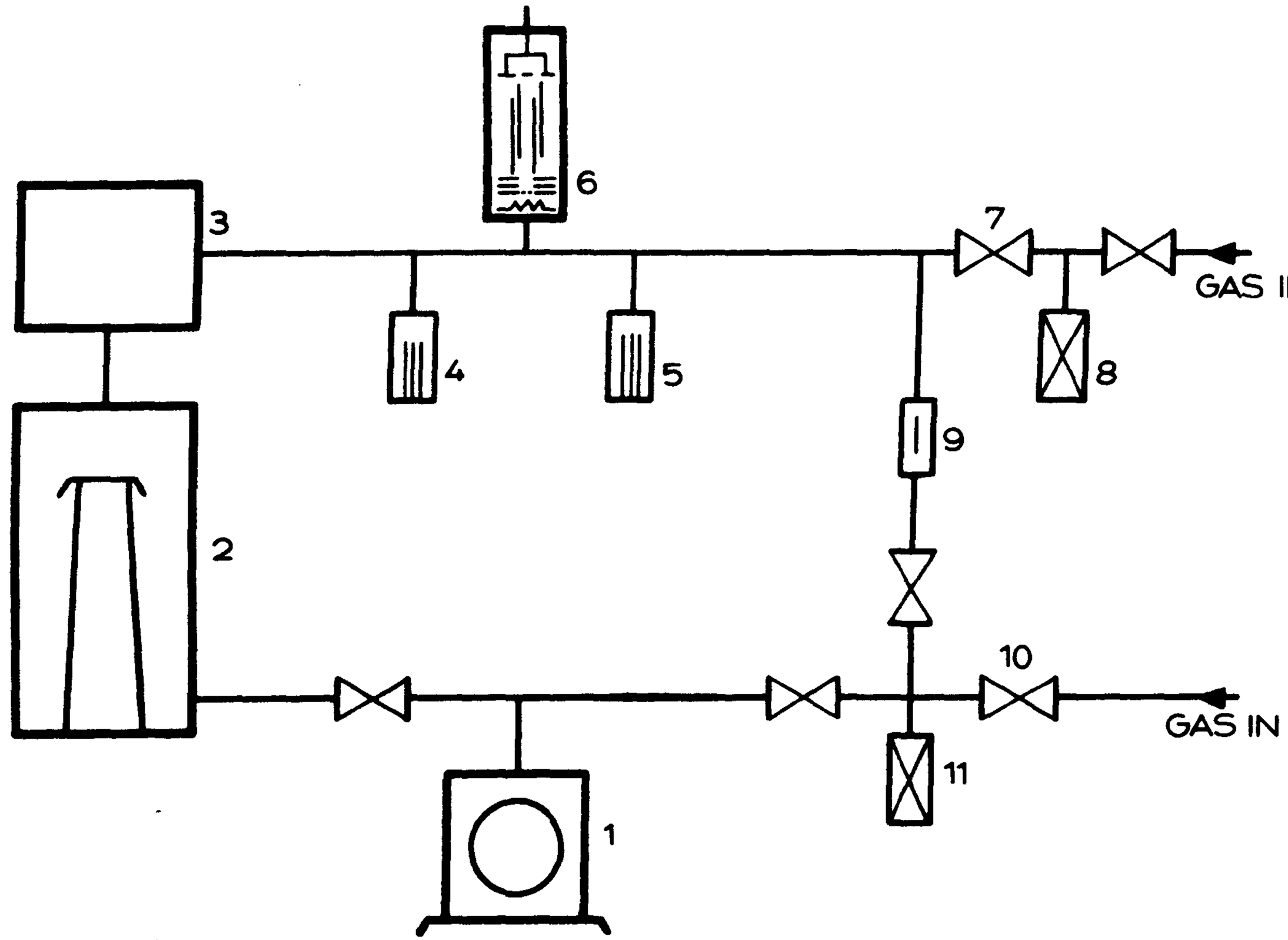

FIG. 3.7. SCHEMATIC DIAGRAM OF PLANT NO. 1.

1-ROTARY PUMP	2-DIFFUSION PUMP
3-SUBLIMATION PUMP	4,5-IONIZATION GAUGES
6-QUADRUPOLE MASS FILTER	7,10-NEEDLE VALVES
8,11-PIRANI GAUGES	9-POROUS PLUG

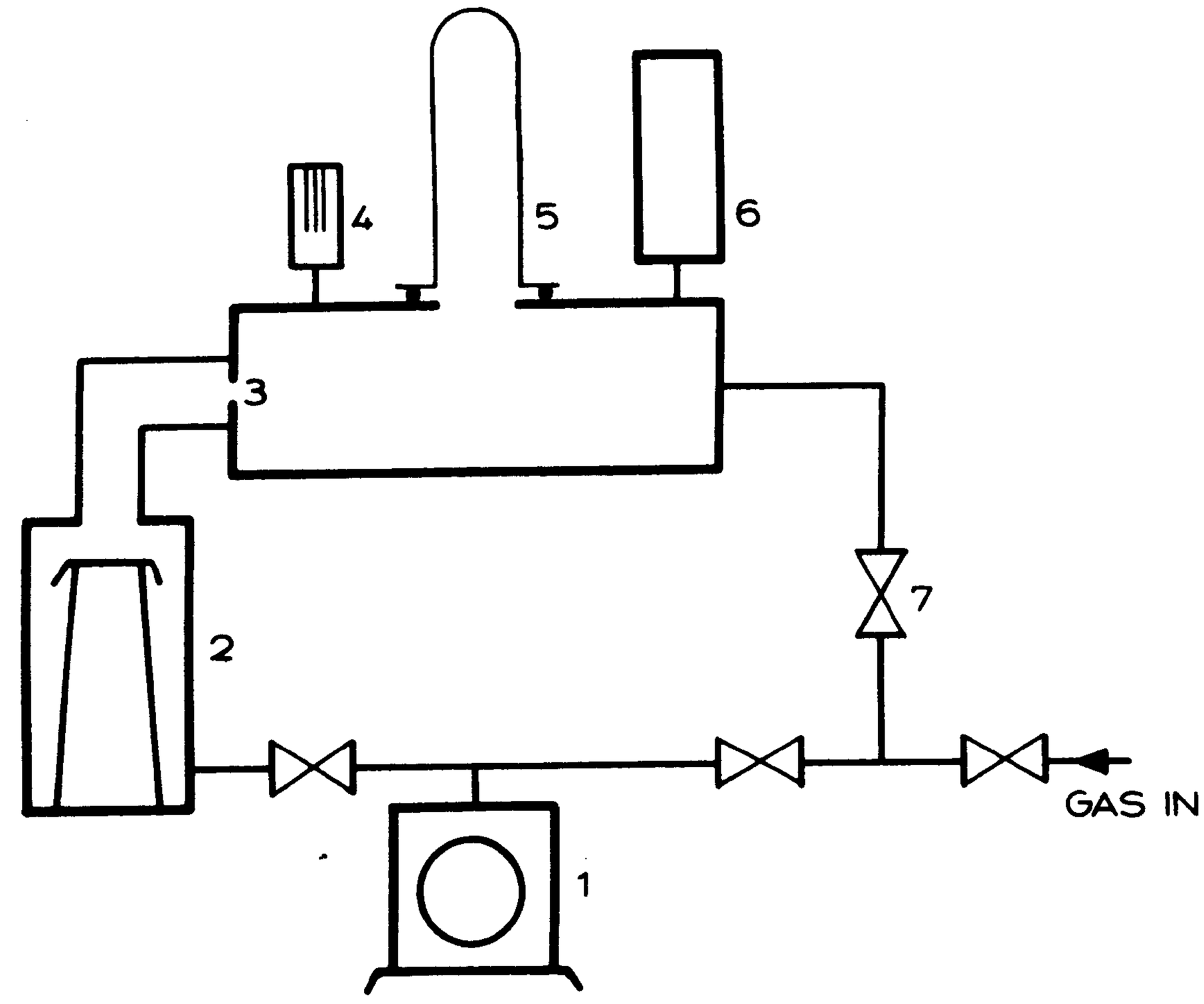

FIG. 3.8. SCHEMATIC DIAGRAM OF PLANT NO. 2.

1-ROTARY PUMP 2-DIFFUSION PUMP 3-BAFFLE

4-IONIZATION GAUGE IR10 5-GLASS BELL JAR

6-QUADRUPOLE MASS FILTER 7-NEEDLE VALVE

CHAPTER 4. Experimental Procedure and Results

4.1. General Performance

To investigate the general performance of a quadrupole mass filter the 50 mm quadrupole(No.1) was employed. The experiments were carried out on plant No.1. The background pressure of the system was always of the order of $5x10^{-7}$ mbar before any test gas was introduced. The pressure of the test gas was usually $5x10^{-6}$ mbar. Most of the experimental work was carried out with ions entering the quadrupole filter with relatively high energy. This energy was controlled by varying the potential of the cage in the ion source. Although, as will be pointed out later, the potential of the cage (with respect to ground) was not always identical to ion energy, the terms "cage voltage" and "ion energy" will be, for convenience, considered synonymous in this and the following sections up to section 4.5.

To compare the two modes of operation (the normal and the new, or a.c.), the mass filter was operated at an emission current of 0.1 mA and a frequency of 4 MHz. The resolution setting in the normal mode was set to give the same sensitivity* as that of the a.c. mode at an ion energy of 10 eV. The test gas was argon. The relationship

---

Note: The sensitivity is defined by $S = I^+/I_eP$. Here I^+ is the ion current, in ampere; I_e the emission current in mA; P the pressure in mbar.

between sensitivity and ion energy over the range 6 eV to 18 eV is shown in Fig. 4.1.1.

The performance of the mass filter in the a.c. mode for different values of emission current was examined at 2.5 MHz. Only the sensitivities obtained at emission currents of 0.1 mA and 1 mA are shown in Fig. 4.1.2. The test gas was argon. Identical results, not shown, have been obtained for krypton.

Since the emission current affected experimental resu-lts, it was fixed at 0.1 mA for all the following experiments unless otherwise stated.

4.2. High Pressure Limitation

As mentioned in Chapter 1 the "high pressure limit" of the spectrometer is of considerable practical importance. The pressure giving maximum output and the upper limit for the linear relation between pressure and output are particularly significant. The experiments to measure these limitations were carried out on plant No.1 with argon as the test gas. The 25 mm (No.3), the 50 mm (No.1), and the 100 mm (No.5) quadrupole heads were examined. All three were operated in both the a.c. and normal modes. However because the resolution of the 25 mm filter (No.3) was very poor, no systematic experiments were carried out with this filter. The experimental results with the 50 mm (No.1) and the 100 mm (No.5) filters are as follows.

1/ Importance of the operating mode

The relationship between the ion current and the

pressure for the two modes is shown in Fig. 4.2.1. These results are for the 50mm mass filter (No.1) at 4 MHz. They show little difference between the two modes. Other experiments showed that changing either the potential on the inner collector for the a.c. mode or the resolution setting for the normal mode had no effect on the "shapes" of the curves shown in Fig. 4.2.1.

2/ Importance of the operating frequency

The effects of the operating frequency are shown in Fig.4.2.2. The results were obtained with the 50 mm filter (No.1) at cage voltage U_c=5.3 V in the normal mode. It can be seen that using 2 MHz instead of 4 MHz extends the high pressure limitation from $2x10^{-4}$ mbar to $4x10^{-4}$ mbar.

3/ Importance of the length of the filter

The high pressure limitations of the filters of different lengths are shown in Fig. 4.2.3. Decreasing from 100 mm to 50 mm increases the useful pressure range by a factor of two. The results were obtained for the a.c. mode at 4 MHz and U_c=6.8 V.

4/ Importance of other electric parameters

It has been found that except for the ion energy, the other electric parameters, such as the emission current, the potentials of lens 1, lens 2 and the inner collector, do not affect the pressure limit. The influence of the ion energy on the pressure limit is shown in Fig. 4.2.4. The points are derived from the graphs of ion current versus pressure for different values of ion energy. These results were obtained for argon with the 50 mm

filter (No.1) in the a.c. mode operating at 4 MHz.

4.3. Mass Discrimination and Wide Mass Range

Ideally a mass spectrometer is required to have constant sensitivity and resolution over its operating mass range. Unfortunately, this is not always the case, the transmission efficiency varying as a function of ion mass. This "mass discrimination" is an important factor for mass spectrometer operation.

To investigate this discrimination, the 100 mm quadrupole mass filter (No.5) was operated on plant No.1. A high voltage r.f. power supply delivering 2.5 kV was used in order to extend the mass range to 600 a.m.u. at 2 MHz. Heptacosafluorotributytamine $C_{12}F_{24}N$ (Heptacosa) was selected as the main test gas. This gas is used extensively as a cracking pattern standard. It has been analysed precisely in many magnetic and electric sector mass spectrometers. Its cracking pattern is stable and covers a wide range from M=31 to M=600 a.m.u.

The sensitivity of the quadrupole was measured for a number of ion fragments over a wide range of ion energies. Fig.4.3.1 shows the relationship between sensitivity and ion energy for these different ions. Clearly the sensitivity depends on ion energy over the mass range of 69-576 a.m.u..

The graph plotted in Fig. 4.3.2 is derived from Fig. 4.3.1. In Fig. 4.3.2 the black bars represent the ranges of ion energy where the mass analyser has a

sensitivity greater than 90% of the maximum. The graph shows that the heavier the ion, the higher the ion energy needed for maximum sensitivity. For example, at M=69 a.m.u. the energy required is about 6.5 eV; at M=576 a.m.u., it is about 15 eV. It can be noted that varying the cage voltage linearly from 6 V at M=0 to 16 V at M=600 (as the dashed line shows in Fig. 4.3.2), gives a near maximum sensitivity over this mass range.

To turn this to practical advantage the ion source control unit was modified so that the ion energy varied linearly (6-16 eV) as the spectrometer swept through the mass range (0-600 a.m.u.). The value of this technique is illustrated in Table 4.3.1. The table shows the cracking pattern obtained for the 100 mm quadrupole (No.5) (variable ion energy) compared with the standard analysis obtained on a large double focussing sector field spectrometer. The two instruments are in good agreement. The peak widths (Δ)* over the mass range are shown in Fig. 4.3.3. Also plotted in this graph are the data obtained in an identical series of experiments for the 50 mm filter (No.1). To illustrate the type of spectra obtained, Fig. 4.3.4 represents a portion of a spectrum spectrum of Heptacosa recorded with the 100 mm filter (No.5) at 2 MHz. Heavy hydrocarbons differing from each other by 7 a.m.u. are clearly separated.

Note: Peak width and resolution are defined with reference to 50% peak height level in this work.

The sensitivities of the 50 mm (No.1) and the 100 mm (No.5) quadrupole mass spectrometers for different gases are listed in Table 4.3.2.

4.4. A.C. Voltage on Lens 2 of the Ion Source

Whilst examining the influence of the construction of the conventional ion source, an interesting phenomenon was observed. The performance of the 50 mm quadrupole mass filter (No. 2) was seriously affected by moving the r.f. cable when by error the d.c. power supply was not connected to lens 2 leaving it "floating". This suggested that the performance was influenced by the stray capacitance between lens 2 and the rods. Even when the cage voltage was zero (i.e. apparently zero ion energy), a finite sensitivity was observed. Simple experiments showed that there was an effective capacitance from lens 2 to ground. This capacitance and the stray capacitance to the rods constituted an a.c. voltage divider. It was the a.c. voltage from this divider which affected the performance of the mass filter. To investigate further, a series of systematic experiments was planned. For the sake of convenient narration, this operation where an a.c. potential is applied to lens 2 is called "unusual" to be distinguished from the "usual" operation of the a.c. mode.

In order to set up the unusual operation, an a.c. voltage divider was built as shown in Fig. 4.4.1. The effects of amplitude and phase angle were examined separately. The amplitude was measured with respect to

ground, and the phase angle with respect to that on one of the rods. During the experiments the phase angle was found scarcely to affect the performance of the filter except when it was near 90^{o}. Therefore while examining the effect of the varying voltage amplitude the phase angle was always set far from 90^{o}. The experimental results are as follows.

1/ The dependence on ion mass and the frequency of the a.c. voltage

The performance of the mass filter versus mass in the unusual operation was examined for argon and krypton. The frequency was fixed at 4 MHz. The a.c. potentials on lens 2 were 65 V and 31 V peak to ground for Kr^{+} and Ar^{+} respectively. The phase angles were far from 90^{o}. The results are shown in Figs. 4.4.2.A and B. The performance versus frequency was examined for argon with an a.c. voltage of 31 V on lens 2. Fig. 4.4.3 shows the results for f=2.5 MHz and f=4 MHz.

2/ The dependence on the a.c. voltage

The experiments were carried out for argon at 4MHz and U_{c}=0 V.

(A) The dependence on the amplitude

To alter the amplitude, the circuit in Fig. 4.4.4 was used. By carefully varying the resistance of the potentiometer the amplitude of the a.c. voltage was adjusted (with the phase angles well removed from 90^{o}). The measured values of sensitivity and resolution as a function of the a.c. amplitude are shown in Fig. 4.4.4.

(B) The dependence on the phase angle

To vary the phase angle, the R-L-C circuit shown in Fig. 4.4.5 was used. The values of the inductor and resistor were adjusted to change the phase angle with the voltage amplitude fixed at 25 V peak to ground. The observed values of sensitivity and resolution plotted as a function of phase angle are shown in fig. 4.4.5.

3/ The dependence on d.c. bias

To investigate the effect of a d.c. bias on lens 2, the circuit in Fig. 4.4.6 was used. An adjustable d.c. voltage and a fixed a.c. voltage (31V amplitude, less than 60^{o} in phase angle, and 4 MHz frequency) were applied to lens 2. The test gas was argon. The cage voltage was zero. The plots of sensitivity and resolution as a function of d.c. bias are shown in Fig. 4.4.6.

4/ Overall comparison of the "usual" with the "unusual" operation

To compare the two methods of operation of the a.c. mode, results for the "usual" and "unusual" operation are presented together in Fig. 4.4.7. There the ratio

$$|dS/S| \; / \; dU_c$$

is chosen as an ordinate. This ratio is a measure of the stability of the filter with respect to the changes in cage voltage. Clearly a small value of this ratio indicates a stable performance.

4.5. The Multi-Peaks

Although, with the a.c. mode, good peak shapes are always observed when the ion energy is low, there is a form of peak splitting at high ion energies. The behaviour is regular and reproducible. This is quite different from that of the normal mode, where the phenomenon depends upon the contamination and the imperfections of the rod system. The term "multi-peaks" has been introduced (see section 2.7) to distinguish this phenomenon from the peak splitting of the normal mode. The effect is illustrated by the set of characteristics plotted in Fig. 4.5.1. These are standard plots of the argon ion peak obtained at various ion energies. (These peaks were recorded on a "memory" oscilloscope using an amplifier with a short time constant in order to capture all the fine details.)

For comparison and analysis the multi - peak structure can be portrayed quantitatively by defining the distance between the "sister peaks" on an a.m.u. scale as Δ_1, Δ_2, Δ_3, etc. (as shown in figure 4.5.1).

For a detailed investigation the experiments were carried out first to determine the effects of the potentials of the inner collector and the ion focussing system, and second to determine the effects of the ion energy. Two rod assemblies, 50 mm (No.1) and 85 mm (No.4) were used.

First, by varying the potential of the inner collector, or lens 1, or lens 2, the relation of the width between sister peaks and these potentials was obtained.

The results are shown in Figs. 4.5.2.A, B, and C. These results were obtained with a "dirty" ion source, i.e. one which had been used for many hours on the 50 mm quadrupole (No.1).

Second, the separation of sister peaks was measured as a function of ion energy for three different operating frequencies. The relationship of the distance (width Δ) between sister peaks and the ion energy is shown in Figs. 4.5.3 and 4.5.4. In this experiment a "clean" ion source was used. Similar results were also obtained for the "dirty" source. However the values of (Δ) increased by about 35% at 2 MHz. The increase was rather less at 4 MHz. The results in Figs.4.5.3 and 4.5.4 are replotted in Fig. 4.5.5 with the number of cycles ions spend in the r.f. field as the abscissa.

4.6. Effect of Contamination

The investigation of the effect of contamination comprised a study of the short term effect produced by specific gases and the long term effect produced by typical hostile vapours found in vacuum furnaces.

1/ Short term effect produced by specific gases

In this investigation the 50 mm quadrupole mass filter (No. 1) was operated in the a.c. mode at 4 MHz on plant No.1.

At the start of the experiment, the residual pressure of the vacuum system was reduced to less than 5×10^{-7} mbar. The reference gas, argon, was introduced and main-

tained at a pressure of $5x10^{-6}$ mbar. The experiment then proceeded as shown in Fig. 4.6.1:

(a) The height of the argon peak was recorded.

(b) A contaminant gas was introduced also to a pressure of $5x10^{-6}$ mbar.

(c) As soon as stability had been reached, the sensitivity for argon was measured.

(d) The contaminant gas was pumped from the system.

(e) When the system had stabilised once more the sensitivity for argon was recorded again.

The experiments were carried out with different values of cage voltage in the range of 3 - 8 volts for various contaminant gases. The results obtained for air are shown in Table 4.6.1. The results obtained for a number of other contaminant gases are shown in Table 4.6.2 for the cage voltage of 7 volts.

2/ Long term effect produced by hostile vapours

(A) Apparatus and samples

To investigate the ability of a mass filter in the a.c. mode to withstand contamination in a vacuum furnace, the long term effect of hostile vapours on the filter was examined. The 50 mm quadrupole used was the same as that used for the "short term effect" experiments. To cover a wide mass range it was essential to use the high voltage r.f. generator with an output up to 2.5 KV. For simulating a miniature vacuum furnace, plant No.2 (see Fig. 3.8) was used. The ionization gauge IR10 was used as a pressure monitor for plant No.2. As a calibration system plant No.1

(see Fig. 3.7) was employed. Argon was the reference gas.

To stimulate hostile environments in plant No. 2, a sample in the glass dome was baked by the radio frequency induction heater. A number of samples, such as copper shim, copper mesh, steel wool, workshop swarf, etc., were used. These samples were assumed to be typical of the type of load for an industrial vacuum furnace. In addition viton samples were baked to give extremely hostile environments.

(B) Experimental procedure

Before this series of experiments started, the sensitivity of the mass filter was carefully measured on plant No. 1. To simulate the worst possible pressure in processing as well as to reduce the time of the experiment, a hostile vapour pressure was maintained at 10^{-3} mbar on plant No.2. This was realized by reducing the pumping speed with the baffle and by baking the samples. The mass filter was operated with the usual electrical parameters. To simulate the situations of full use of the quadrupole, it was swept continuously through the whole mass range, i.e. 0-125 a.m.u. at 4 MHz or 0-500 a.m.u. at 2 MHz, over the whole of the outgassing period.

From time to time, the quadrupole was recalibrated on plant No. 1. The ion source was cleaned by electron bombardment (this was 10 mA at 500 V, i.e. 5 watts, for 60 minutes). Calibration was carried out immediately before and after this cleaning.

(C) Results

The experiments were carried out over a period of nine months. Over this time the mass filter operated in the extremely hostile atmosphere for a total of one hundred hours. The ion source had to be replaced once and a total of four filament assemblies used. Also a ruby washer between a rod and its housing had to be replaced. The collector assembly was cleaned twice. The rods, however, were never touched. The performance (with the a.c. mode at 4 MHz and U_c=8 V) when operating at 10^{-3} mbar during baking of the viton is shown in Fig.4.6.2. The residual gas spectrum of plant No.2 is shown in Fig.4.6.3.

Due to contamination the performance of the filter gradually changed. The initial performance compared with that after the 45th hour of contamination is shown in Figs. 4.6.4.A and 4.6.4.B. The calibration was made at 4 MHz for argon. After 45 hours contamination the maximum sensitivity fell by 20%. (To restore the original sensitivity at 6 V the cage potential had to be increased by approximately 2 volts. To give the same peak width the cage voltage had to be increased by only 0.5 volts). The values of the maximum sensitivity, which is less sensitive to the ion energy, throughout the whole series of experiments are shown in Table 4.6.3.

In addition to the experiments on the 50 mm quadrupole (No. 1) at 4 MHz, the 85 mm quadrupole (No. 4) was also examined at 3 MHz for one month. Table 4.6.4 shows the results in relative sensitivity for both argon and krypton after 50 hours contamination (40 hours in

hydrocarbons and 10 hours in fluorides evaporated from a viton sample).

During the experiments on the 50 mm quadrupole, attention was always paid to a comparison of the two modes. Even after 45 hours contamination, the performance in the a.c. mode was always repeatable. However,the normal mode was not stable. Fig. 4.6.5 shows the decay of the sensitivity in the normal mode over a period of 20 minutes. The measurements were made at a relatively high cage voltage of 12 volts in order to reduce change to minimum.

A comparison of the two modes was made after 78 hours contamination. The spectra for argon (Ar^+ and Ar^{++}) were recorded under different resolution settings for the normal mode, and also for the a.c. mode. The results are shown in Figs. 4.6.6.A, B, C, D, and E. The ratio of the Ar^+ to the Ar^{++} peak height is indicated on each graph. (The difference of the d.c. voltage on the rods between the successive spectra for the normal mode was 0.87 volts at M=40).

Two further experiments were carried out. The purpose was to observe the different behaviour in the two modes due to changes of d.c. potential on the rods. In the first experiment the d.c. potential on the rods was changed by adjusting the slope of the operating line. Thus, balanced d.c. voltages were always applied to the rods. The changes in sensitivity relative to singly and doubly charged argon ions are shown in Fig. 4.6.7. In the

second experiment, a battery of variable voltage was inserted between one of the rods and its r.f. supply cable. Thus an unbalanced offset d.c. voltage was introduced. The changes in sensitivity due to this unbalanced voltage are shown in Fig. 4.6.8. Again the effects are greater for the normal than for the a.c. mode. (Note: in each experiment the instruments were preset to have the same initial sensitivity for both modes before the disturbing voltages were applied).

4.7. Distribution of Ions Over the Collector System

The "ion burn" of the collector system suggested a complex pattern to the ion beam. This pattern was observed after operation in hydrocarbon vapours at high pressure. A typical pattern is indicated in the photograph Fig.4.7.1. This picture was obtained after 20 hours contamination described in section 4.6. The deposit on the inner collector has a square brown area. The border of the square is very sharp. From the border inwards to the centre, the deposit film becomes thicker. The geometric relation of the square film to the rod assembly is shown in Fig. 4.7.2. The corners of the square face the rods.

These observations of non-uniformity led to an investigation of the importance of the shape and position of the inner collector. Three special inner collector assemblies (two were square and one was circular) were used. An example of a square inner collector is shown schematically in Fig.4.7.3.A. In Fig.4.7.3.B the symbols

show the positions of the square inner collector related to the four rods. The square represents the collector, the circles represent the rods. Two sets of experiments were carried out. The first set was to compare the performance of the three inner collectors A, B, and C. A is the original circular collector, 12.5 mm^2 area. B is also a circular collector 25 mm^2, and C is a square collector 25 mm^2 area. For each assembly sensitivity and resolution were measured as a function of the potential on lens 1. Results for N_2^{++} are shown in Figs. 4.7.4.A and B. The reason for using N_2^{++} was to observe the possible deterioration in resolution. The second set of experiments was to observe the effects of rotating a square collector with respect to the rods. Measurements were made with the square collector 49 mm^2 area, (A), with the sides of the square facing the rods, and (B), with the corners facing the rods. The results for argon and krypton at different ion energies are shown in Figs. 4.7.5.A and B and Figs.4.7.6.A and B respectively. It was found that the potential of the inner collector was not critical.

4.8. Nier Source

The Nier source shown in Fig. 3.3.A of section 3.1 was tested with the 50 mm rod assembly (No. 2) in the a.c. mode. Measurements were all made on plant No.1. Refering to Fig. 3.3.A, the electrical parameters applied to the source were as follows: The potentials on the box and the gate were the same: $U_b = U_g = 4$ V. The potentials on the trap,

lens, and inner collector were U_t=6.7 V, U_l=-80 V, and U_{ic} =-145 V respectively. The trap electron current I_t= 20 μA. The magnetic induction was 0.2 tesla.

1/ The general performance of the Nier source

(A) The effect of the ionization section

The sensitivity* of the mass filter was found to depend upon the position of the magnet. With a bad alignment the performance was extremely poor. The magnet position was therefore always adjusted to make the ratio of trap to emission current a maximum which gave the best performance. (At optimum the ratio of trap to emission current was approximately 0.1) The distribution of the electron current to the various source plates was measured at this optimum. The measured values are shown in Fig. 4.8.1. This was the normal operating condition for all the experiments described here.

The sensitivity and resolution as a function of the trap current at 4 MHz for krypton M/e=84 were examined.The results are shown in Figs. 4.8.2.A and B. Other measurements have showed the performance to be almost independent of the potentials of the trap and the gate electrodes. For example, typical results relating to the gate are shown in Figs. 4.8.3.A and B.

(B) The influence of the ion isolation region

Note: The sensitivity in this section is defined as

$$S = I^+/pI_t$$

where I^+ is in amperes, I_t in mA, and P in mbar.

In the basic design of the source, steps were taken to prevent electrons entering the filter. The extra small chamber (isolation region in Fig.3.3.A),introduced to stop this flow of the electrons, also minimized the penetration of the focussing fields into the ionization region. (Before the isolation region was introduced there was a long "tail" on the low mass sides of all the peaks, presumably caused by field penetration.) The size of the entrance and exit orifice of this chamber was chosen to optimize the performance.

(C) The influence of the alignment

Without special assembly techniques the tolerance in the Nier source was probably no better than 0.5 mm. Non-reproducible results were obtained in the preliminary experiments. This led to a special jig (described in section 3.1) being made for assembly. Also a travelling microscope was employed to check the eccentricity of the source. Using the jig for assembly the eccentricity had been less than 0.1 mm. Consistent results and improved performance were now obtained. In Fig. 4.8.4.A curve B shows the sensitivity obtained with an aligned source. For comparison, curve A in Fig.4.8.4.A shows the best result obtained with an non-aligned source for the same source structure.

(D) The influence of the ion focussing system

Curves B and C in Fig. 4.8.4.A show that a much higher sensitivity was obtained for an ion focussing system with a narrower exit (i.e. a smaller diameter D_b in

Fig. 3.3.A). The results in Fig.4.8.4.B indicate that the resolution is also better with the narrower channel. The potential of the lens plate is not critical. This can be seen from the results in Figs. 4.8.5.A and B.

(E) The overall performance

The performance of the mass filter with the Nier source was examined up to mass 100 a.m.u. The performance was found to depend critically upon the potential of the ionization chamber. The sensitivity of the instrument for krypton, argon and methane at 3 MHz is shown in Fig.4.8.6. The spectra of the filter for krypton, argon, methane, and hydrogen under different operating conditions are shown in figures 4.8.7. to 4.8.10. The corresponding sensitivities and peak widths are listed in Table 4.8.1.

2/ A detailed investigation of the resolving power

(A) Technique

The foregoing results indicate that the resolving power of the mass filter when using the Nier source is much better than when using the conventional source. This very good resolving power falls into the range usually associated with magnetic sector mass spectrometers. Therefore a special technique, i.e. measuring the interference at adjacent peaks, was used for examining resolving power. Argon was chosen as the test gas. By measuring the interference at M=39 and M=41 of the argon mass 40 peak, the resolving power could be estimated. Extracting the signal from the noise was a major problem. Three methods of measurement were used.

The first method was conventional. Signal averaging was used and amplifier time constants were made as long as possible. For the second method, the ion beam was switched on and off. For the third method, the test gas was introduced and then removed rapidly from the system.

(B) Results

(1) At the high mass side of a peak

The interference at the high mass side of an argon peak was examined with methods 1 and 2. The experimental procedure and the results are shown in Fig. 4.8.11. First, the argon peak was recorded (lower curve of Fig. 4.8.11). Then the sensitivity of the output amplifier was increased by a factor of 100, and the signal at M=41 was recorded (the upper curve of Fig. 4.8.11). It can be seen that the interference at M=41 from mass 40 is less than 0.2%.

For more precise measurement, method 2 was employed. The experimental procedure and the results can be seen in Fig. 4.8.12. For curve A, the procedure was as follows. The filter was tuned to the top of an argon peak. Then the ion beam was switched on and off (i.e. the ion energy was switched between 2 and 4 eV) as indicated on the time scale in Fig. 4.8.12. The experiment was repeated with the filter tuned to mass 42 and then 41 with an increased amplifier sensitivity. The interference of argon 40 at M=41 can be seen to be less than 0.05%. At M=42 it is effectively zero; the small peak at this mass is almost certainly residual Kr^{++}.

(2) At the low mass side of the peak

The interference at the low mass side of the argon peak was examined with method 1. Fig. 4.8.13 shows the spectrum at 3 MHz. The mass 40 peak has a long tail. The same spectrum for 4 MHz is shown in fig. 4.8.14. Clearly the interference has been suppressed. The interferences up to M=36 at different frequencies are listed in Table 4.8.2. Also it was found that the interference at the low mass side of the peak changed at different operating pressures. Fig.4.8.15 shows the results for the effect of pressure variation with the quadrupole operating at 4 MHz.

(3) The interference at M=4 from a mass 2 hydrogen peak

With the Nier source, recognisable peaks were observed at M=2 and 4. Interference at M=4 due to the hydrogen peak at "2" was investigated with method 3. The procedure for the first set of experiments can be seen in Fig. 4.8.16.A. First the background was recorded. Then helium was introduced to 10^{-6} mbar to provide a reference signal. The background was again recorded (curve 1 in Fig. 4.8.16.B). Finally two spectra extending from M=2 to 6 a.m.u. were recorded at the hydrogen pressures of $1x10^{-5}$ mbar and $2x10^{-5}$ mbar (curves 2 and 3). During the experiments the zero on the amplifier was not adjusted. Fig. 4.8.16.B shows clearly that the interference at M=4 was less than 2%.

The second set of experiments is illustrated in Fig. 4.8.17. This figure is in three sections: A, B, and

C. Each section corresponds to scanning through the mass range 4.5 to 3.0 a.m.u. Section A shows a scan obtained with the helium pressure $1x10^{-6}$ mbar and the hydrogen presure zero. Section B shows a scan obtained with the helium pressure zero and the hydrogen pressure $2x10^{-5}$ mbar. Section C shows a scan obtained with the helium pressure zero and the hydrogen pressure falling from 10^{-5} mbar at the start to zero at the finish.

The experiments were carried out with a slow scan and a long amplifier time constant to reduce the output signal interference. The zero drift in the amplifier and also gas scattering effects due to the relatively high hydrogen pressure tend to obscure the true interference at mass 4 from the mass 2 peak. However the interference, including gas scattering effects, can be seen to be less than 2%.

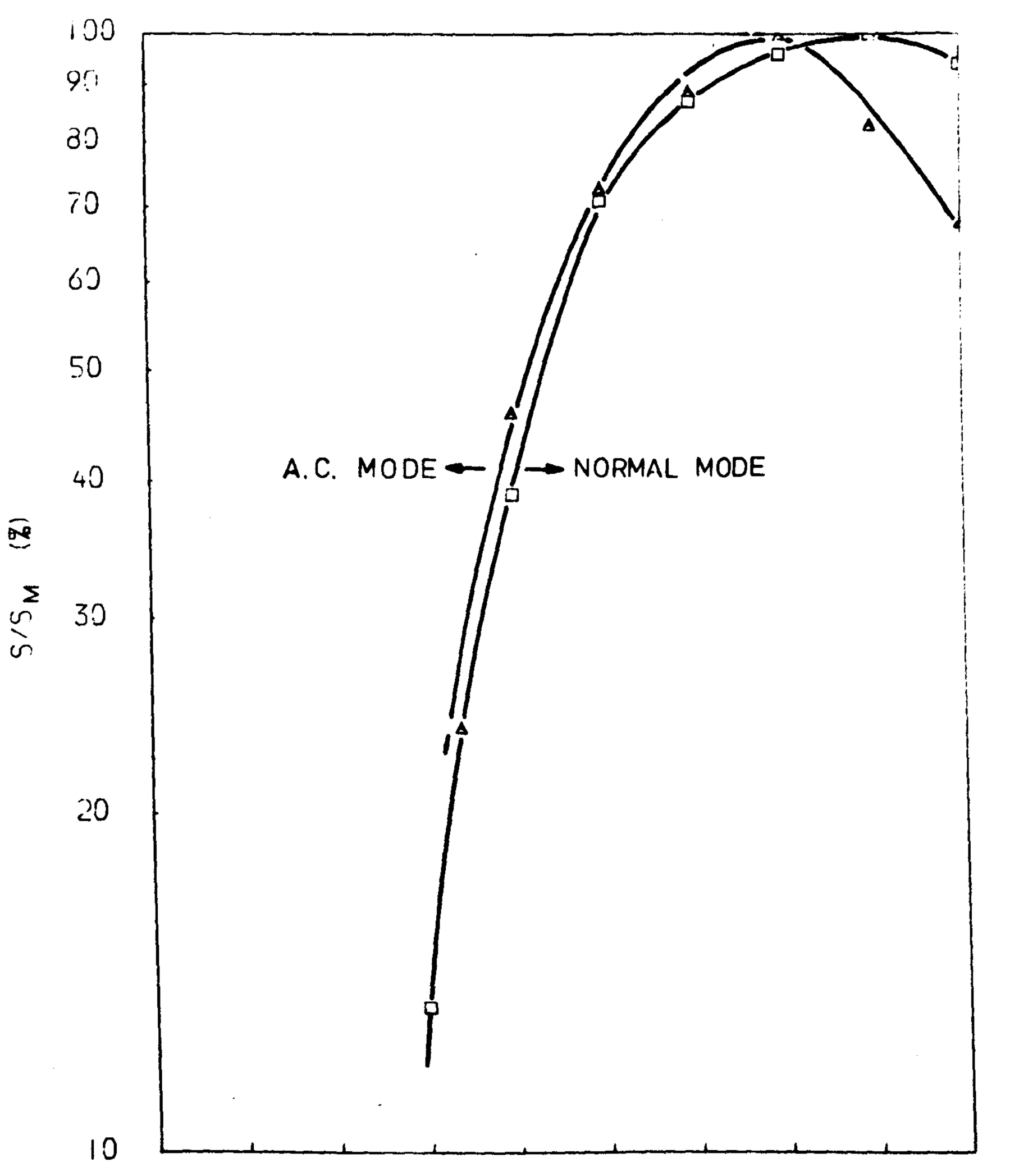

FIG. 4.1.1. SENSITIVITY AS A FUNCTION OF ION ENERGY IN THE NORMAL MODE AND A.C. MODE.

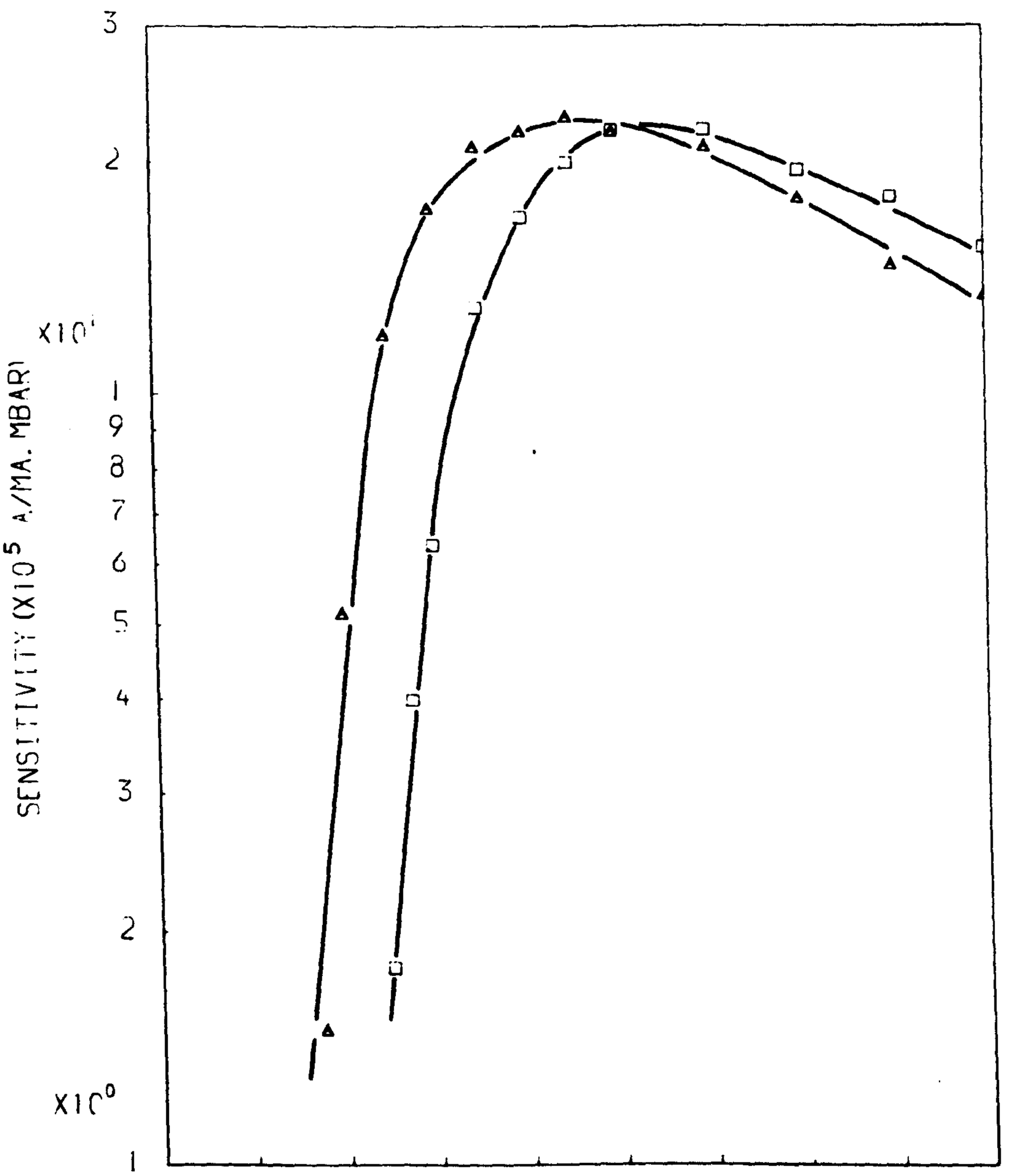

FIG. 4.1.2. SENSITIVITY AS A FUNCTION OF ION ENERGY FOR DIFFERENT VALUES OF EMISSION CURRENT.

△ 0.1MA □ 1.0MA

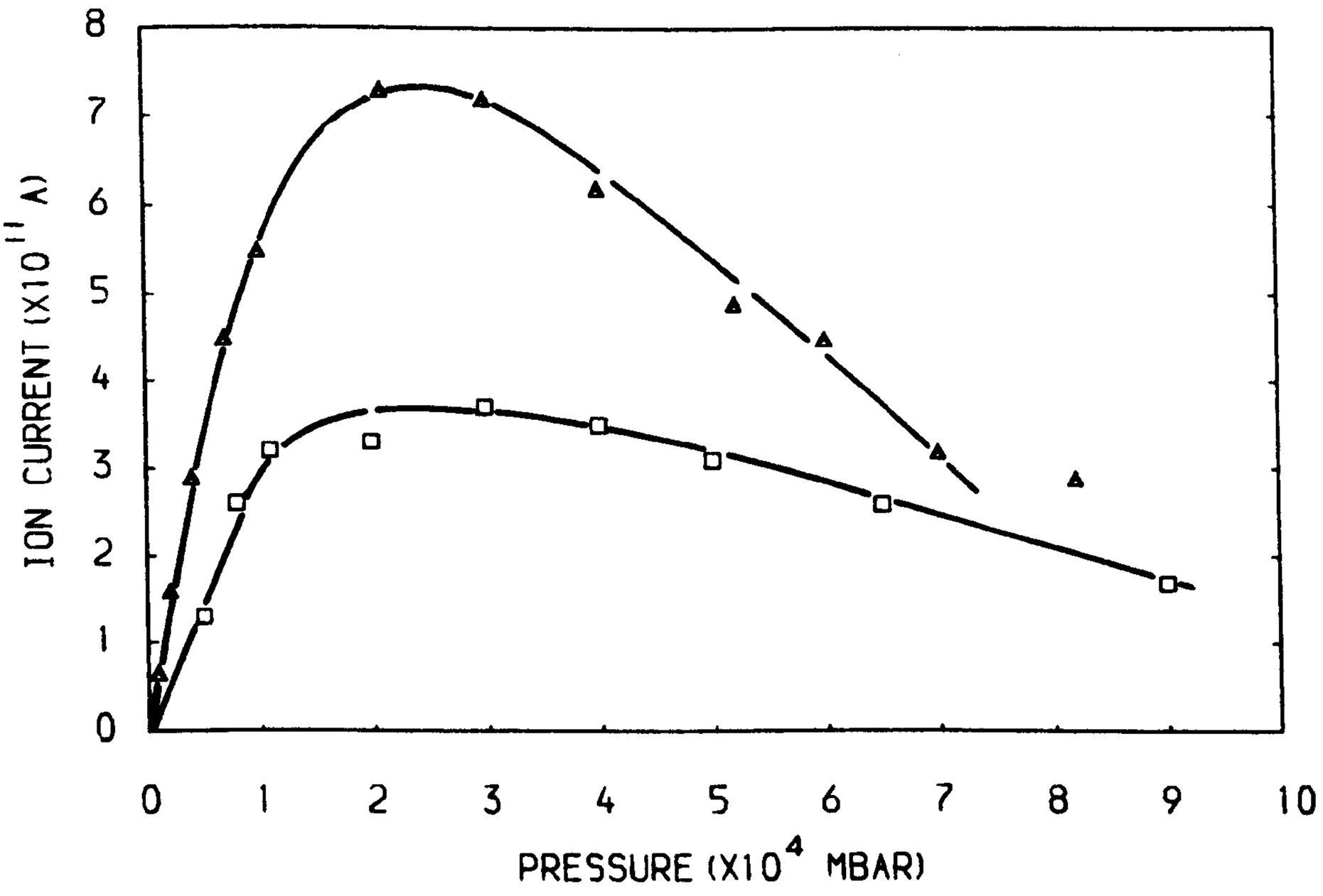

FIG. 4. 2. 1. ION CURRENT AS A FUNCTION OF PRESSURE FOR THE NORMAL MODE AND A. C. MODE AT HIGH PRESSURES.

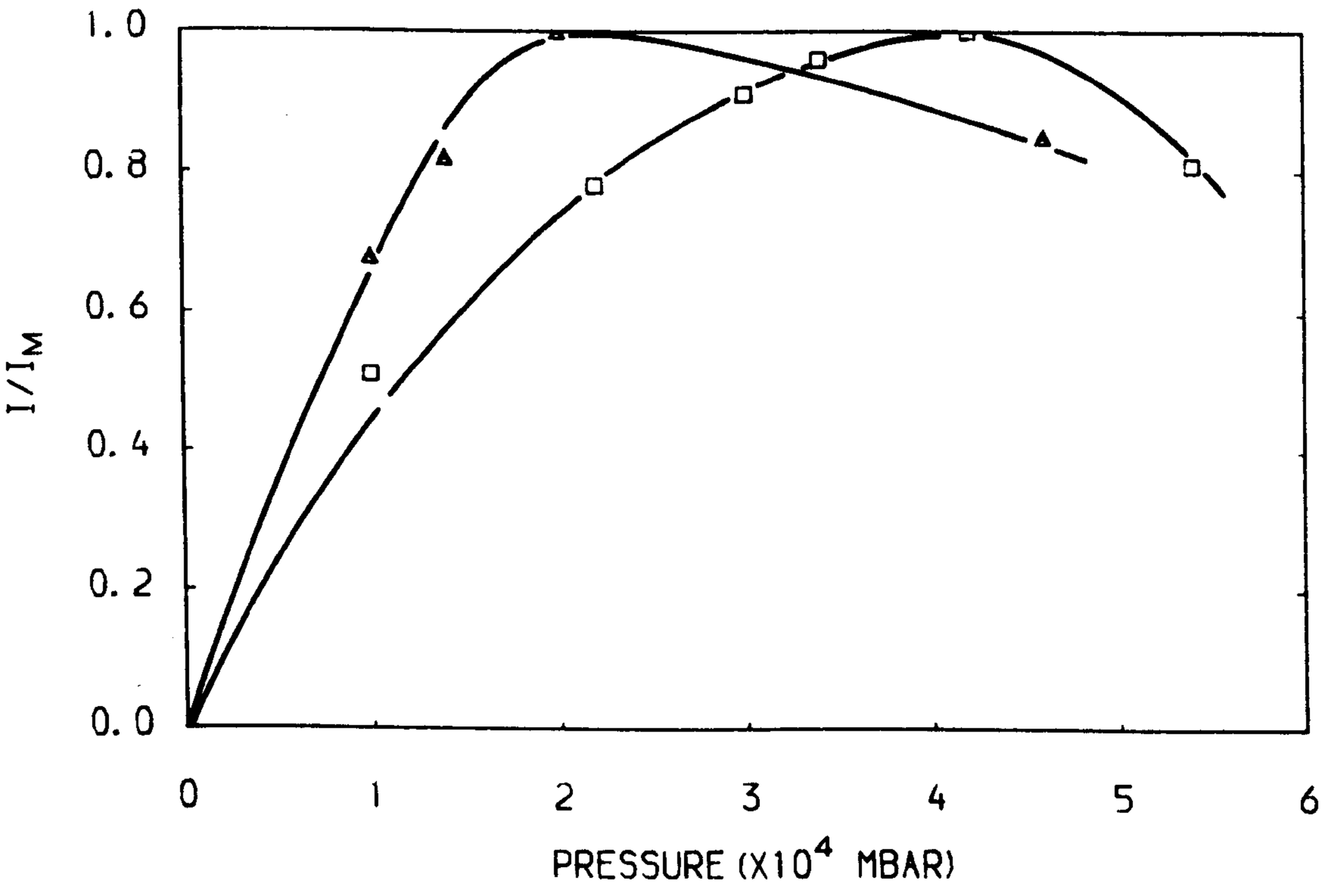

FIG. 4. 2. 2. ION CURRENT AS A FUNCTION OF PRESSURE FOR DIFFERENT VALUES OF FREQUENCY AT HIGH PRESSURES.

□ F=2MHZ △ F=4MHZ

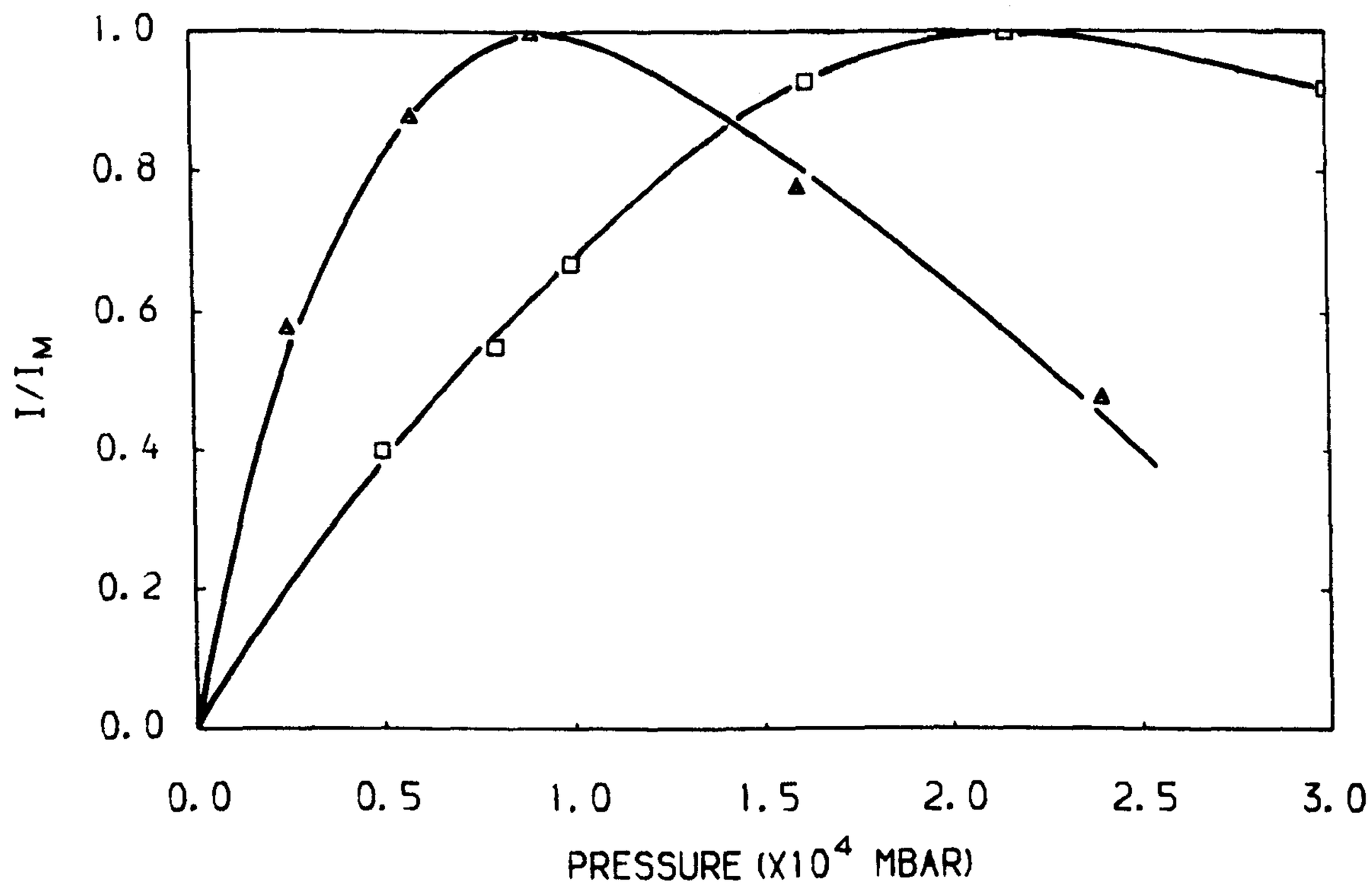

FIG. 4.2.3. ION CURRENT AS A FUNCTION OF PRESSURE FOR DIFFERENT VALUES OF ROD LENGTH AT HIGH PRESSURES.

□ L=50MM

△ L=100MM

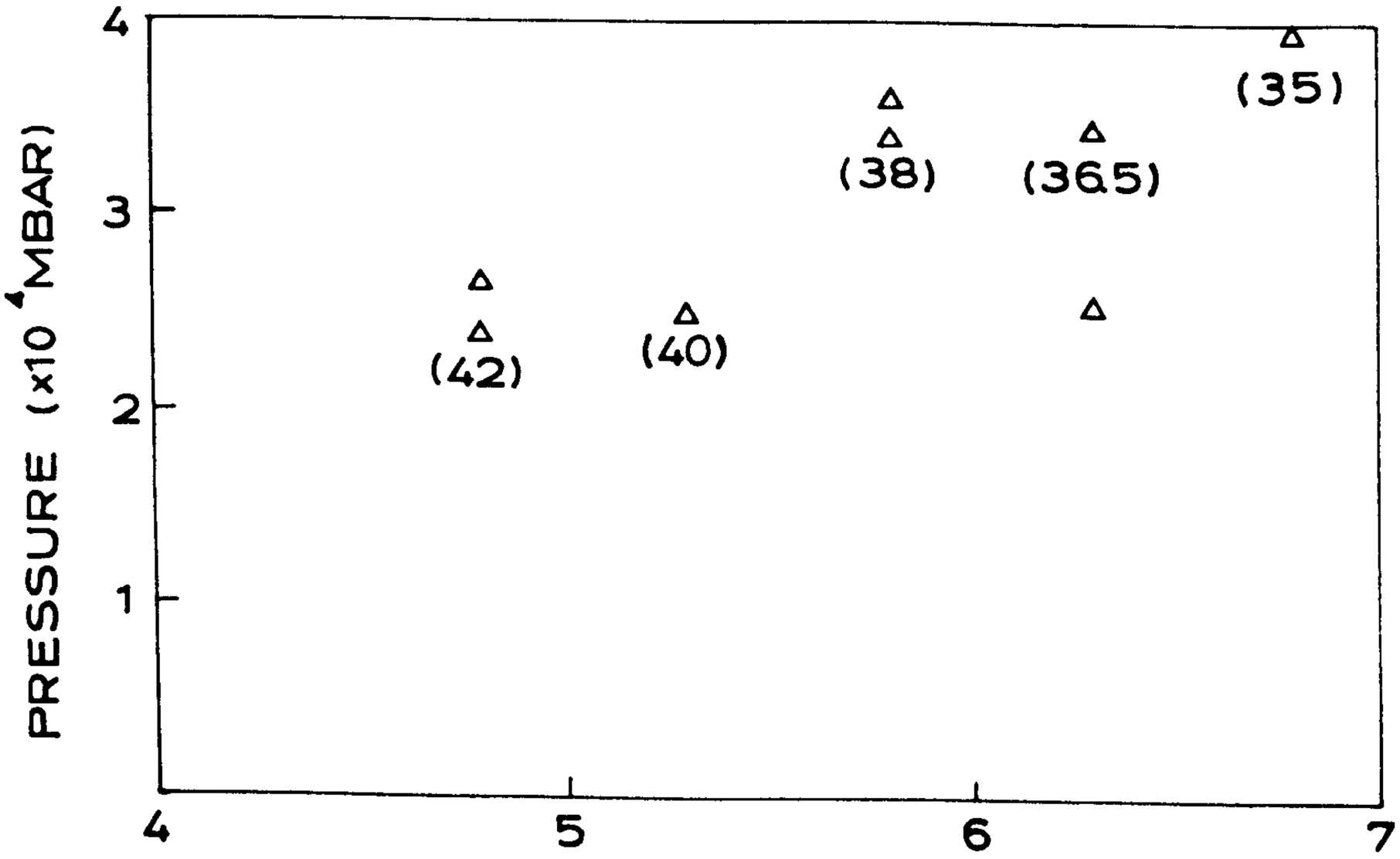

FIG. 4.2.4. THE POINTS IN THE DIAGRAM SHOWING THAT THE HIGH PRESSURE LIMIT IS RELATED TO THE ION ENERGY. THE NUMBERS IN BRACKETS INDICATE THE NUMBER OF CYCLES IONS SPENT IN THE R.F. FIELD.

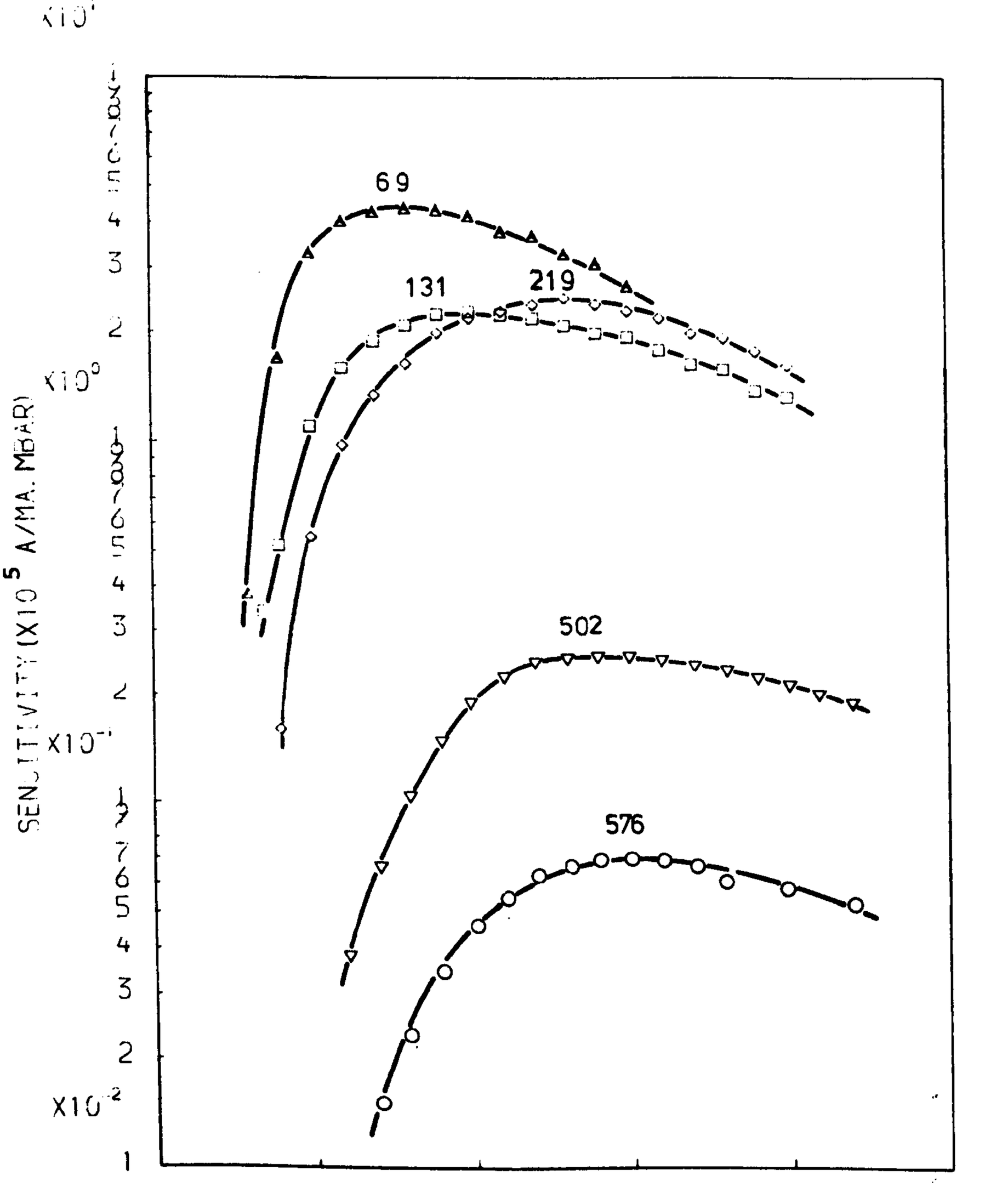

FIG. 4.3.1. SENSITIVITY AS A FUNCTION OF ION ENERGY FOR THE MAJOR PEAKS IN HEPTACOSA.

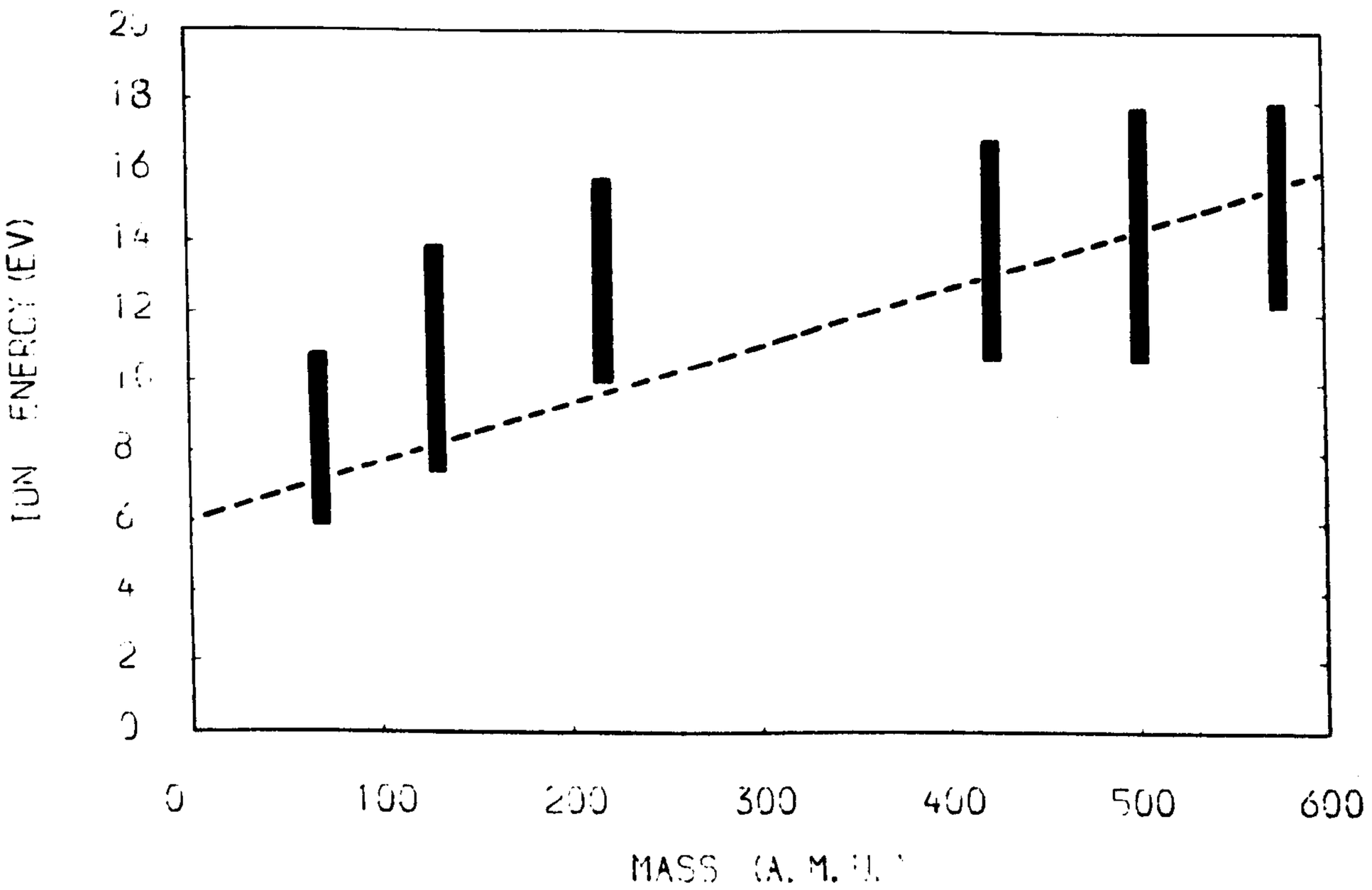

FIG. 4.3.2. THE RANGES OF ION ENERGY FOR THE MAJOR PEAKS WHICH COVER 90-100% OF THE MAXIMUM SENSITIVITY. THE STRAIGHT DASHED LINE SHOWS THAT THE ION ENERGY INCREASES LINEARLY FROM 6 EV TO 16 EV FOR A CONSTANT SENSITIVITY OVER THE MASS RANGE 0-600 A. M. U.

TABLE 4.3.1. A comparison of the "cracking pattern" obtained with a 100 mm quadrupole mass filter with that obtained with an analytical magnetic sector mass spectrometer (MS9). The filter was shifting an ion energy from 6 eV for M=0 to 16 eV for M=600 a.m.u.. The peak intensity of mass 69 is regarded as 100.

Nominal mass	Quadrupole	MS9	Ion fragment
31	3.2	2.3	CF
50	3.5	1.0	CF_2
69	100	100	CF_3
100	16.2	12	C_2F_4
114	11.0	3.7	C_2F_4N
119	11.9	8.3	C_2F_5
131	49	31	C_3F_5
150	2.5	2.1	C_3F_6
164	2.4	0.66	C_3F_6N
169	5.6	3.6	C_3F_7
176	2.8	0.99	C_4F_6N
181	2.8	1.9	C_4F_7
214	2.1	0.64	C_4F_8N
219	51.9	62	C_4F_9
226	1.2	0.69	C_5F_8N
231	1.0	0.93	C_5F_9
264	15	10	$C_5F_{10}N$
276	0.56	0.21	$C_6F_{10}N$
314	0.88	0.44	$C_6F_{12}N$
326	0.96	0.40	$C_7F_{12}N$

(Table 4.3.1. cont'd)

Nominal mass	Quadrupole	MS9	Ion fragment
364	0.56	0.16	$C_7F_{14}N$
376	1.5	0.93	$C_8F_{14}N$
395	0.39	0.21	$C_8F_{15}N$
414	5.8	5.1	$C_8F_{16}N$
426	2.8	2.5	$C_9F_{16}N$
464	4.0	3.8	$C_9F_{18}N$
476	0.21	0.12	$C_{10}F_{18}N$
488	0.16	0.09	$C_{11}F_{18}N$
502	6.5	8.6	$C_9F_{20}N$
514	0.24		
526	0.42		
538	0.42	0.40	$C_{12}F_{20}N$
557	0.10		
564	0.35	0.18	$C_{11}F_{22}N$
576	1.7	1.7	$C_{12}F_{22}N$

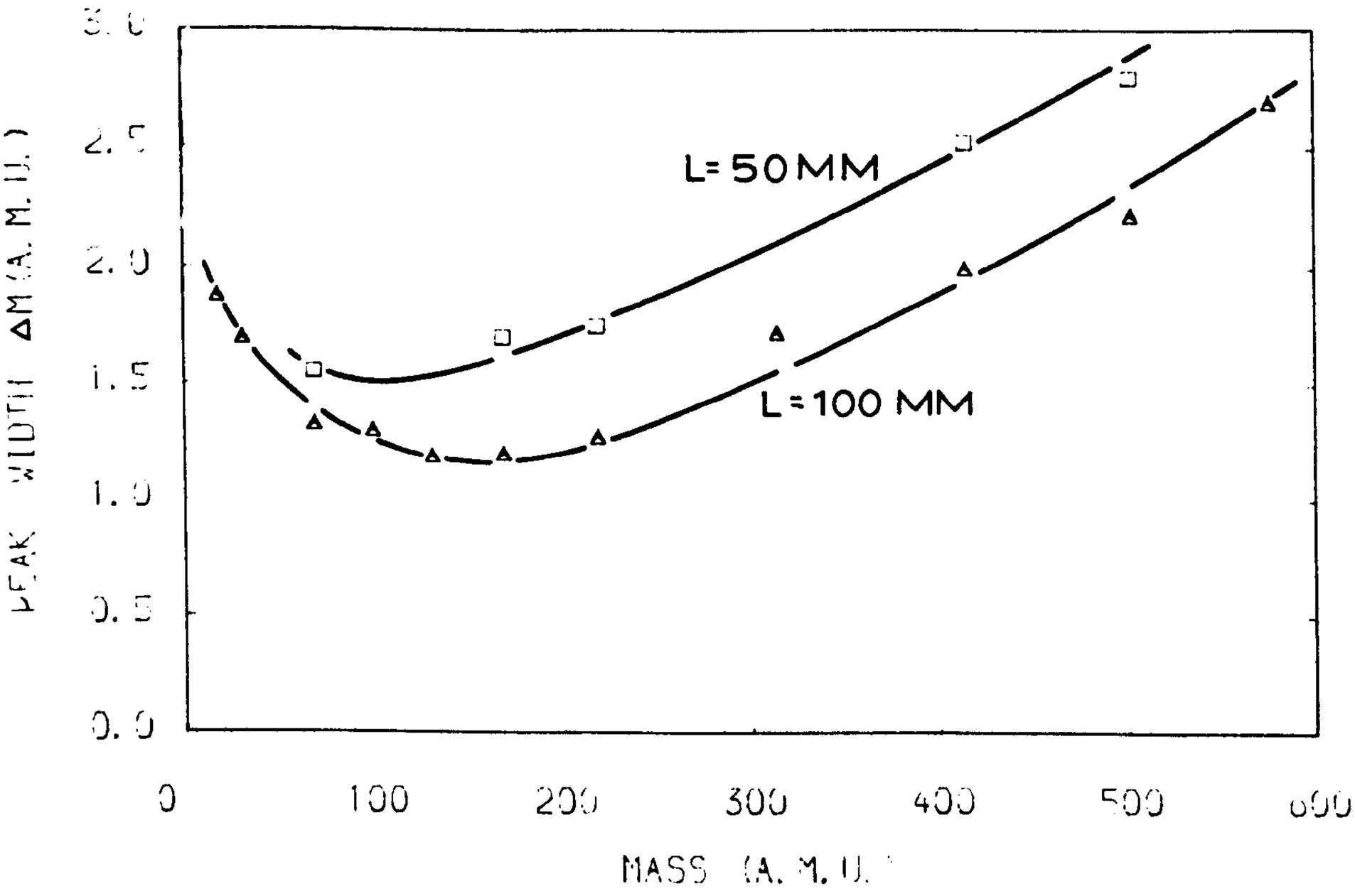

FIG. 4.3.3. PEAK WIDTH AS A FUNCTION OF ION MASS FOR THE QUADRUPOLES WITH A VARIABLE ION ENERGY.

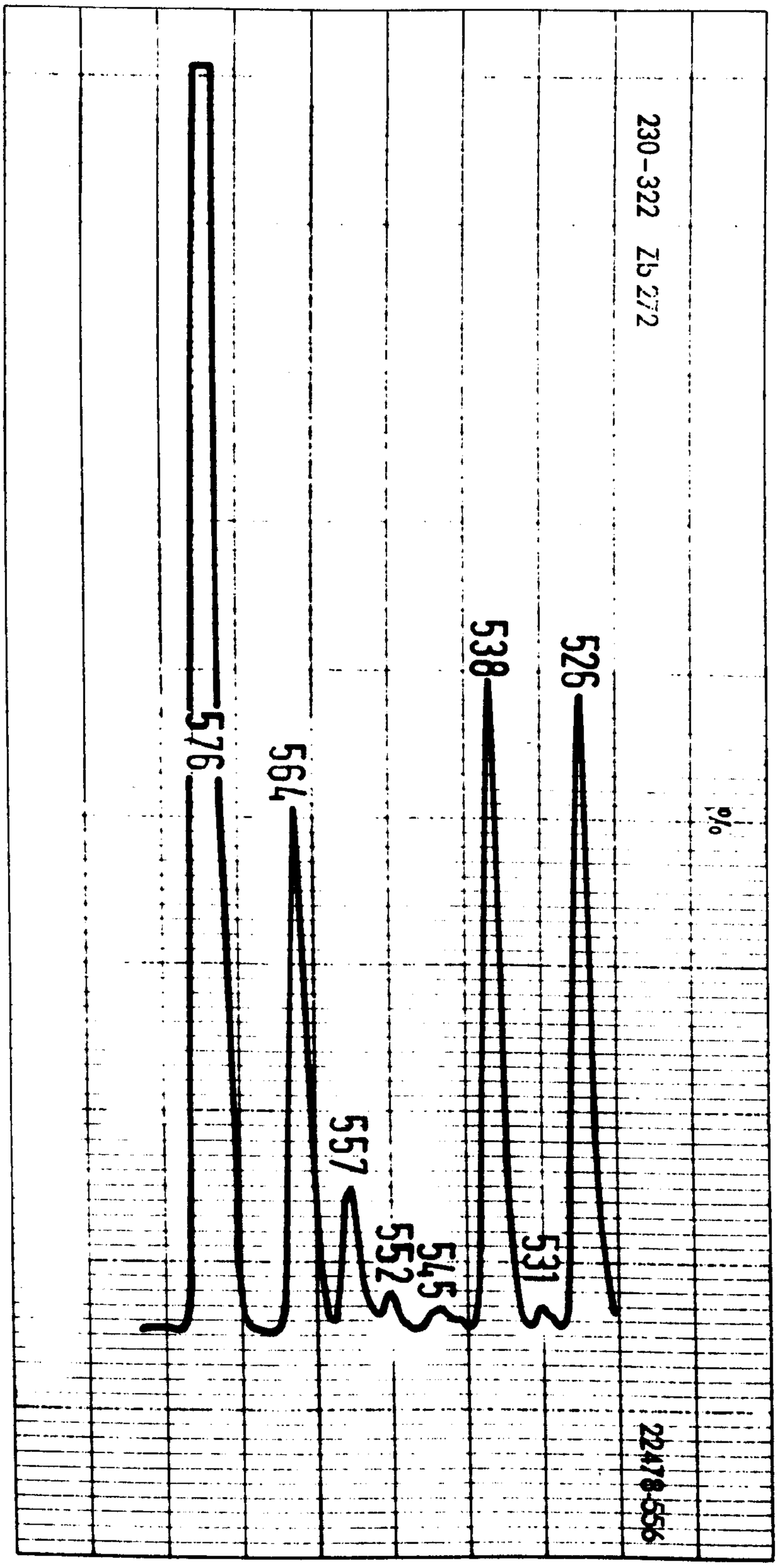

FIG. 4.3.4. A PORTION OF TYPICAL SPECTRUM OBTAINED WITH THE 100 MM FILTER BY SHIFTING THE ION ENERGY FROM 6 EV TO 16 EV OVER THE MASS RANGE 0-600 A.M.U.

TABLE 4.3.2. Sensitivity of the quadrupole (a.c. mode) operating as a total pressure gauge.

Gas	Sensitivity ($torr^{-1}$) (nitrogen equivalent)	
	50 mm lens	100 mm lens
Argon	0.19	-
Xenon	0.15-0.20	0.15-0.20
Heptacosa	0.14	0.19

Note: Values obtained by summing all the individual peaks in the mass spectrum. The calibration was made by comparison with the IOG 12 ionization gauge. Thus "nitrogen equivalent" referes to this gauge. The relatively small spread in the above values indicates: (a) the characteristics of the ion source are similar to that of the IOG 12 ; (b) the ion transmission efficiency of the lenses is approximately constant throughout the operating mass range.

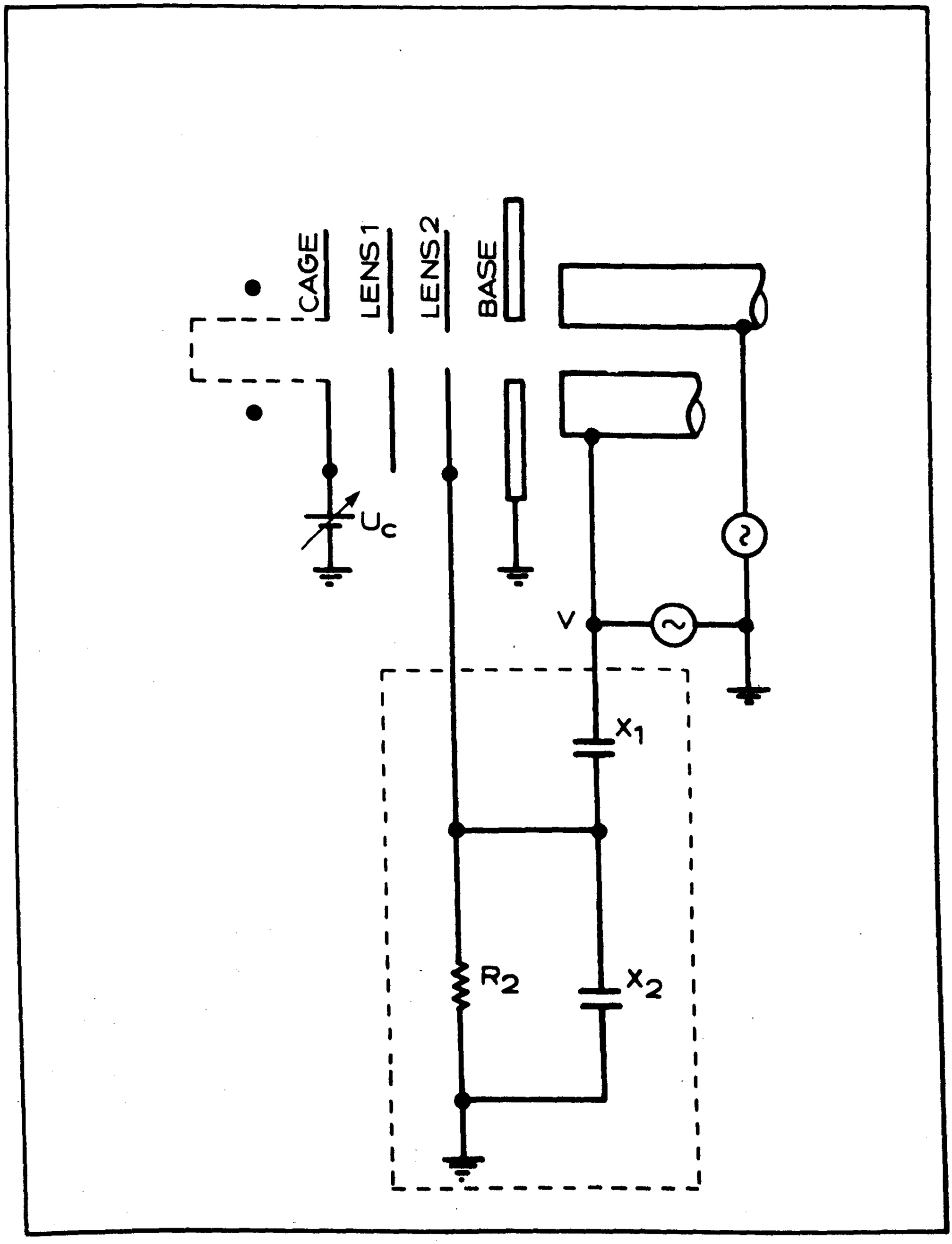

FIG. 4.4.1. CONFIGURATION FOR AN A.C. POTENTIAL ON LENS 2.

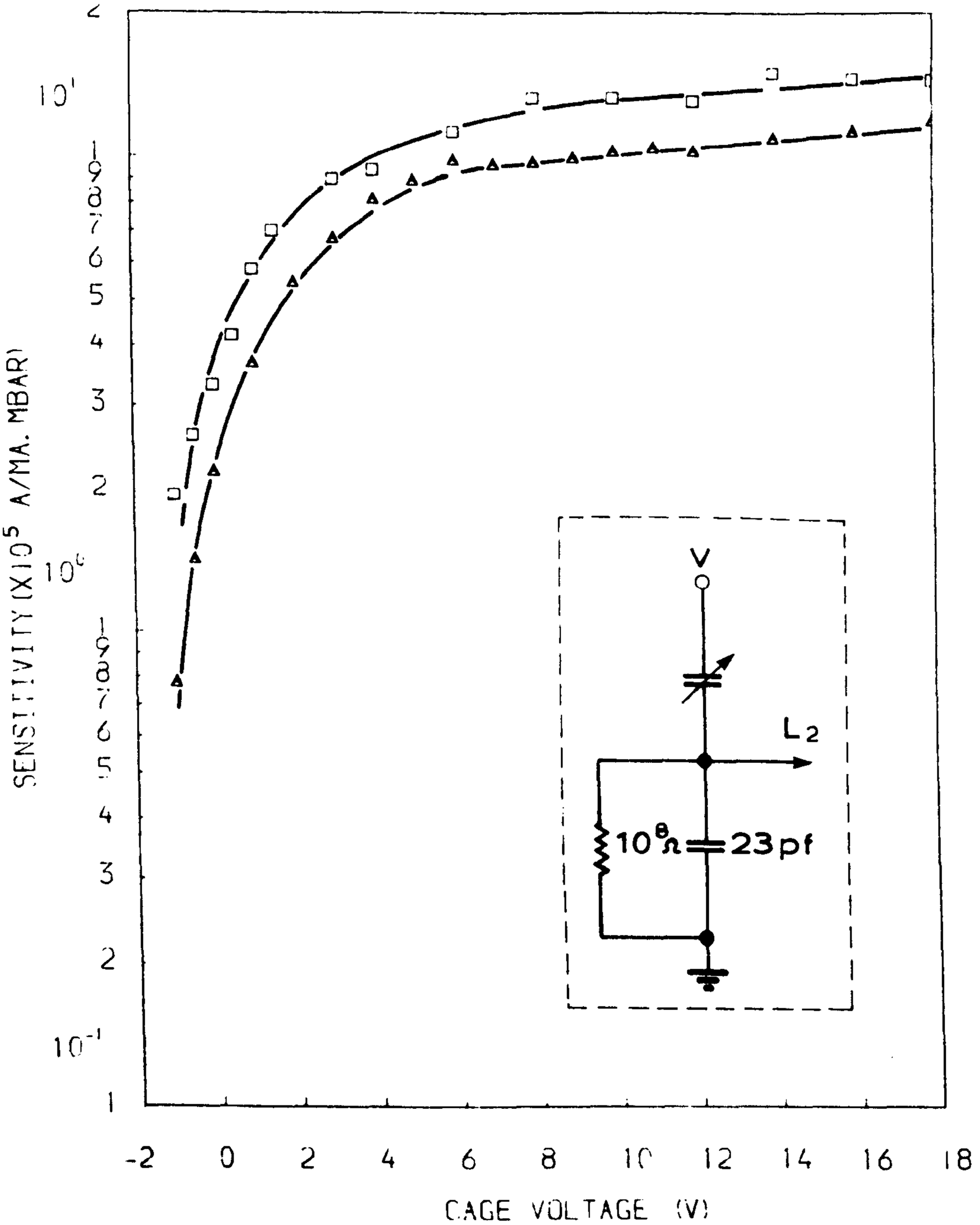

FIG. 4.4.2.A. SENSITIVITY AS A FUNCTION OF CAGE VOLTAGE IN THE PRESENCE OF AN A.C. POTENTIAL ON LENS 2 FOR DIFFERENT MASSES.

□ M/E=84 △ M/E=40

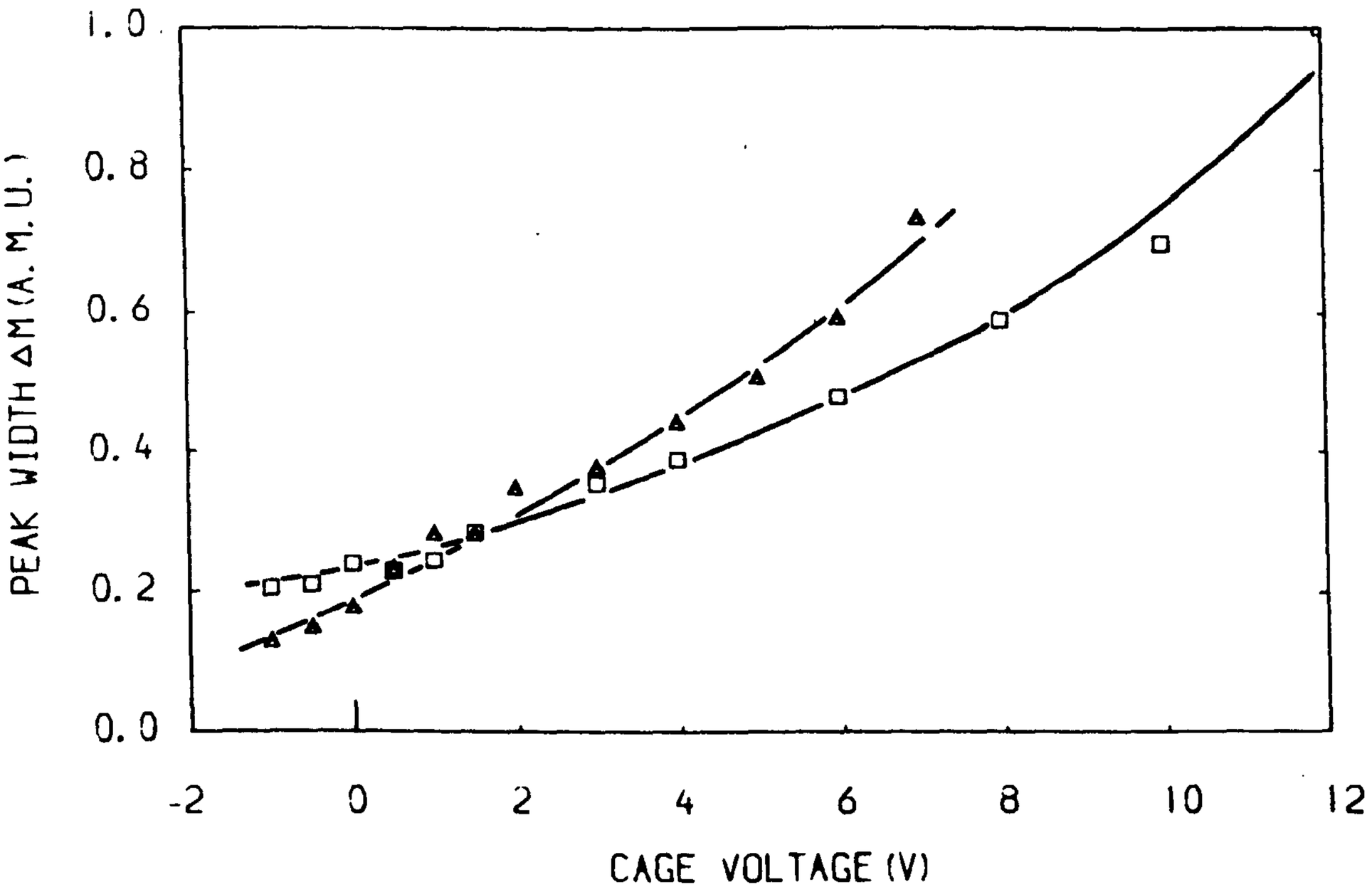

FIG. 4.4.2.B. PEAK WIDTH AS A FUNCTION OF CAGE VOLTAGE IN THE PRESENCE OF AN A.C. POTENTIAL ON LENS 2 FOR DIFFERENT MASSES.

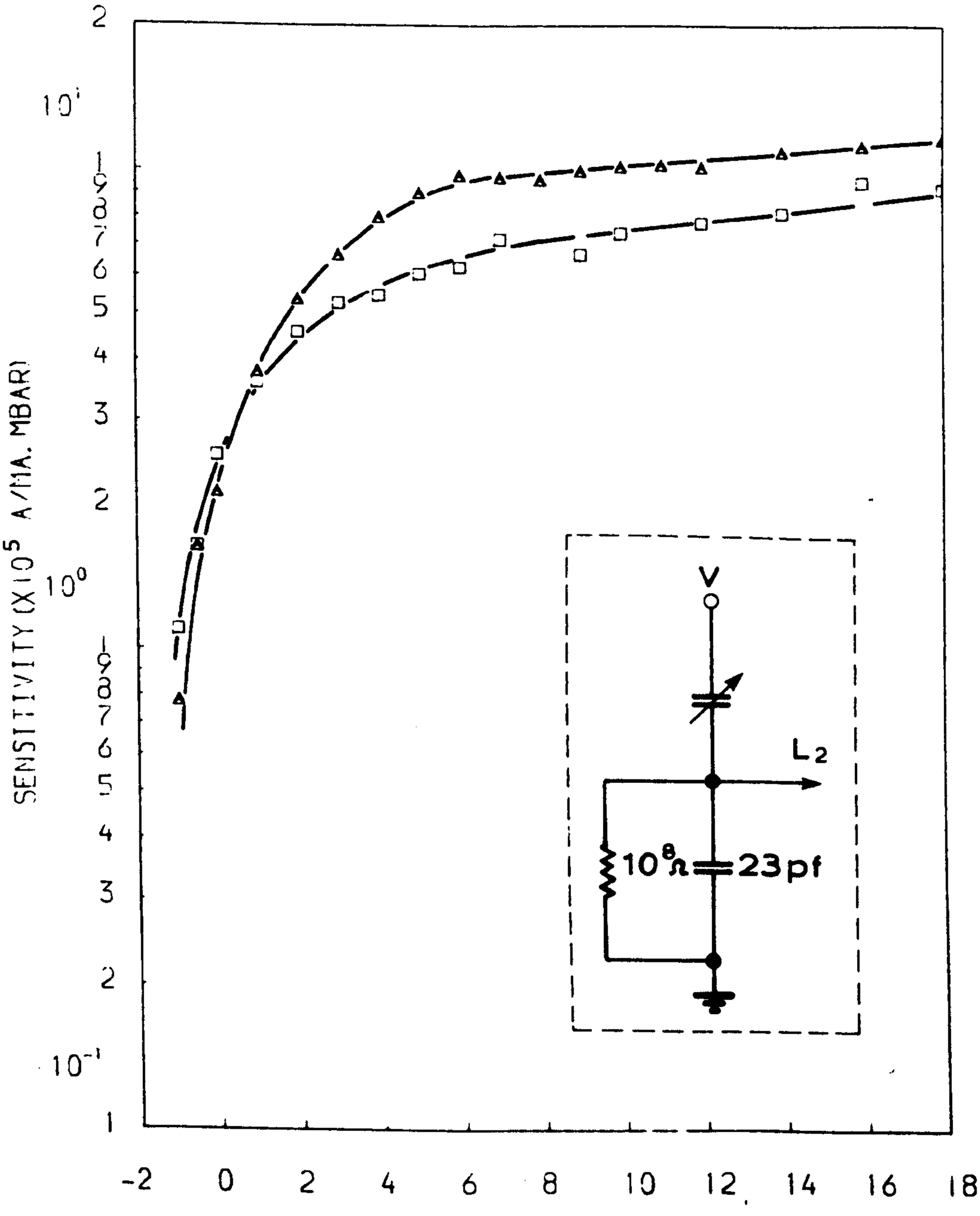

FIG. 4.4.3. SENSITIVITY AS A FUNCTION OF CAGE VOLTAGE IN THE PRESENCE OF AN A.C. POTENTIAL ON LENS 2 FOR DIFFERENT VALUES OF FREQUENCY.

□ F=2.5 MHZ △ F=4MHZ

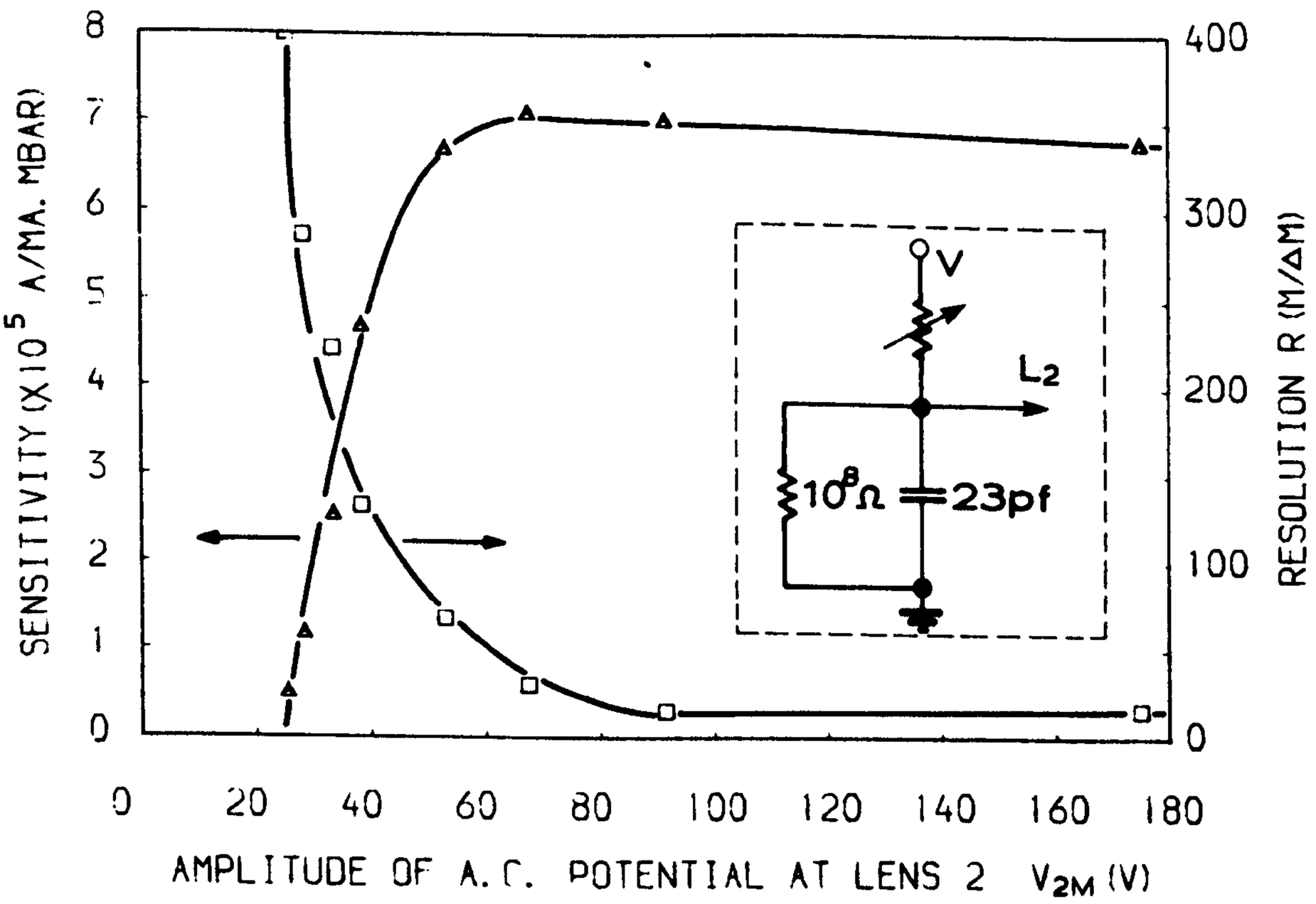

FIG. 4. 4. 4. EFFECT OF THE AMPLITUDE OF AN A. C. POTENTIAL AT LENS 2 ON THE PERFORMANCE OF THE QUADRUPOLE MASS ANALYSER.

△ SENSITIVITY

□ RESOLUTION

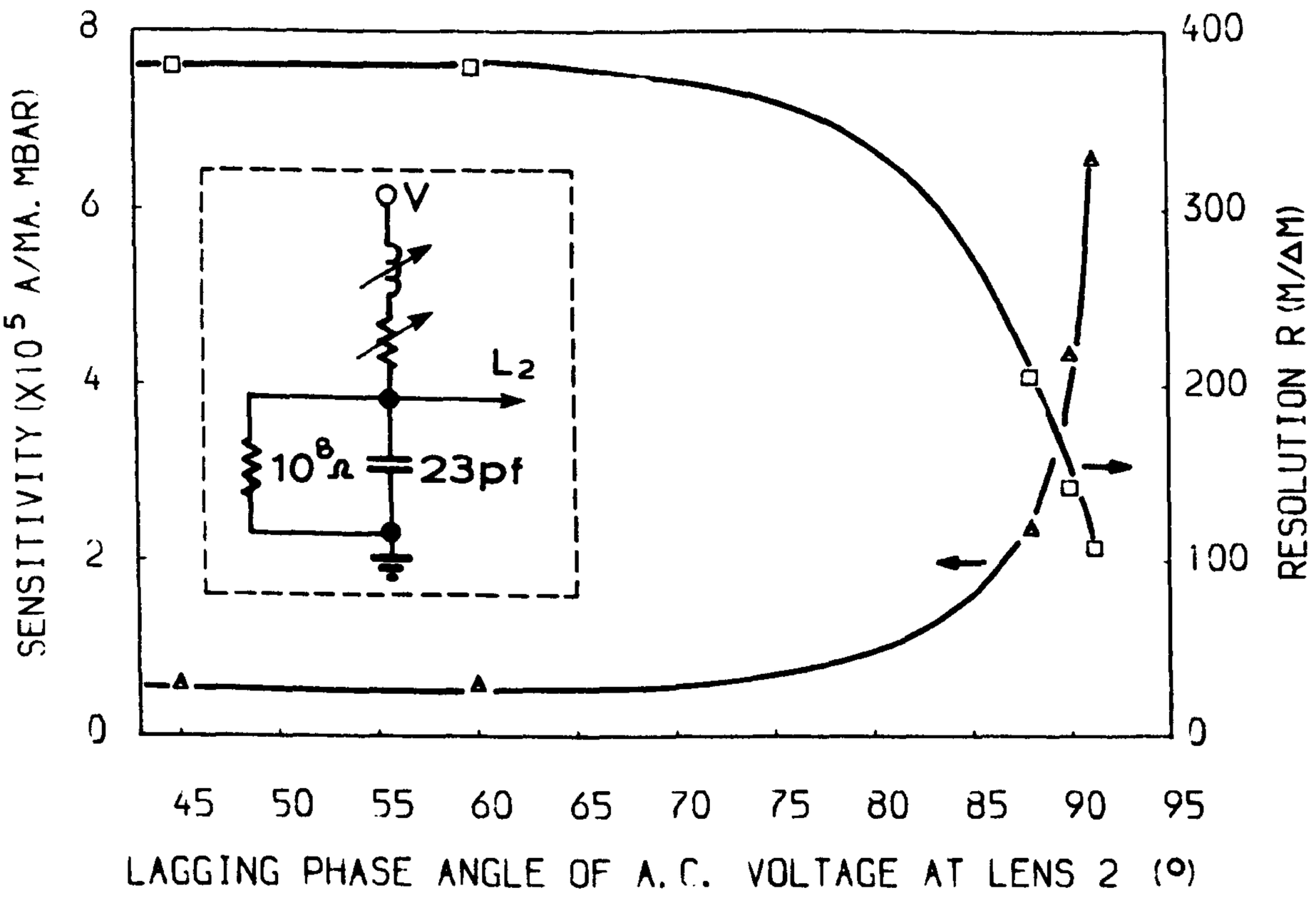

FIG. 4.4.5. EFFECT OF THE PHASE ANGLE OF AN A.C. POTENTIAL AT LENS 2 ON THE PERFORMANCE OF THE QUADRUPOLE MASS ANALYSER.

△ SENSITIVITY ▫ RESOLUTION

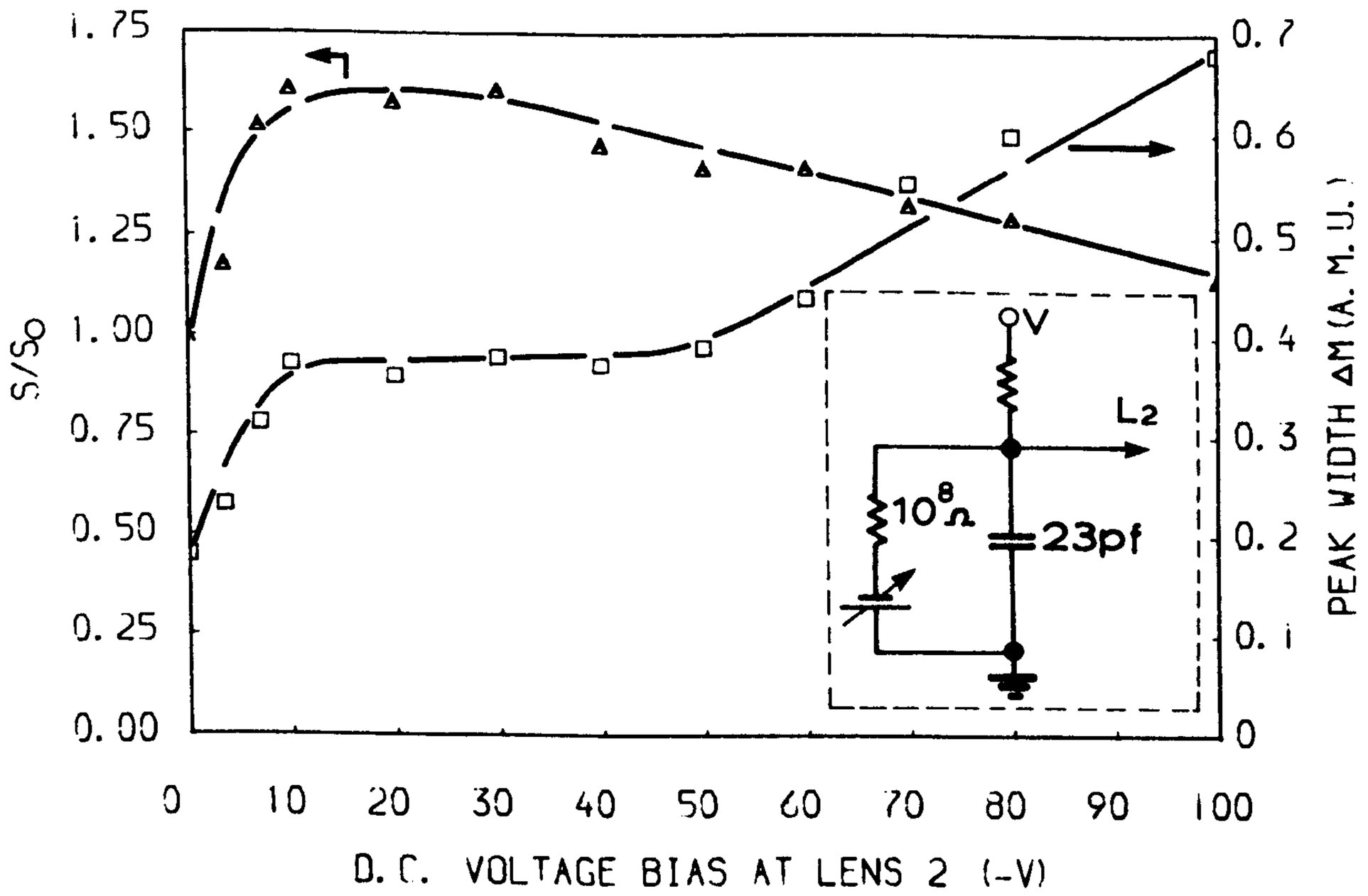

FIG. 4.4.6. EFFECT OF A D.C. BIAS AT LENS 2 ON THE PERFORMANCE OF THE QUADRUPOLE MASS ANALYSER.

△ S/S0 □ ΔM

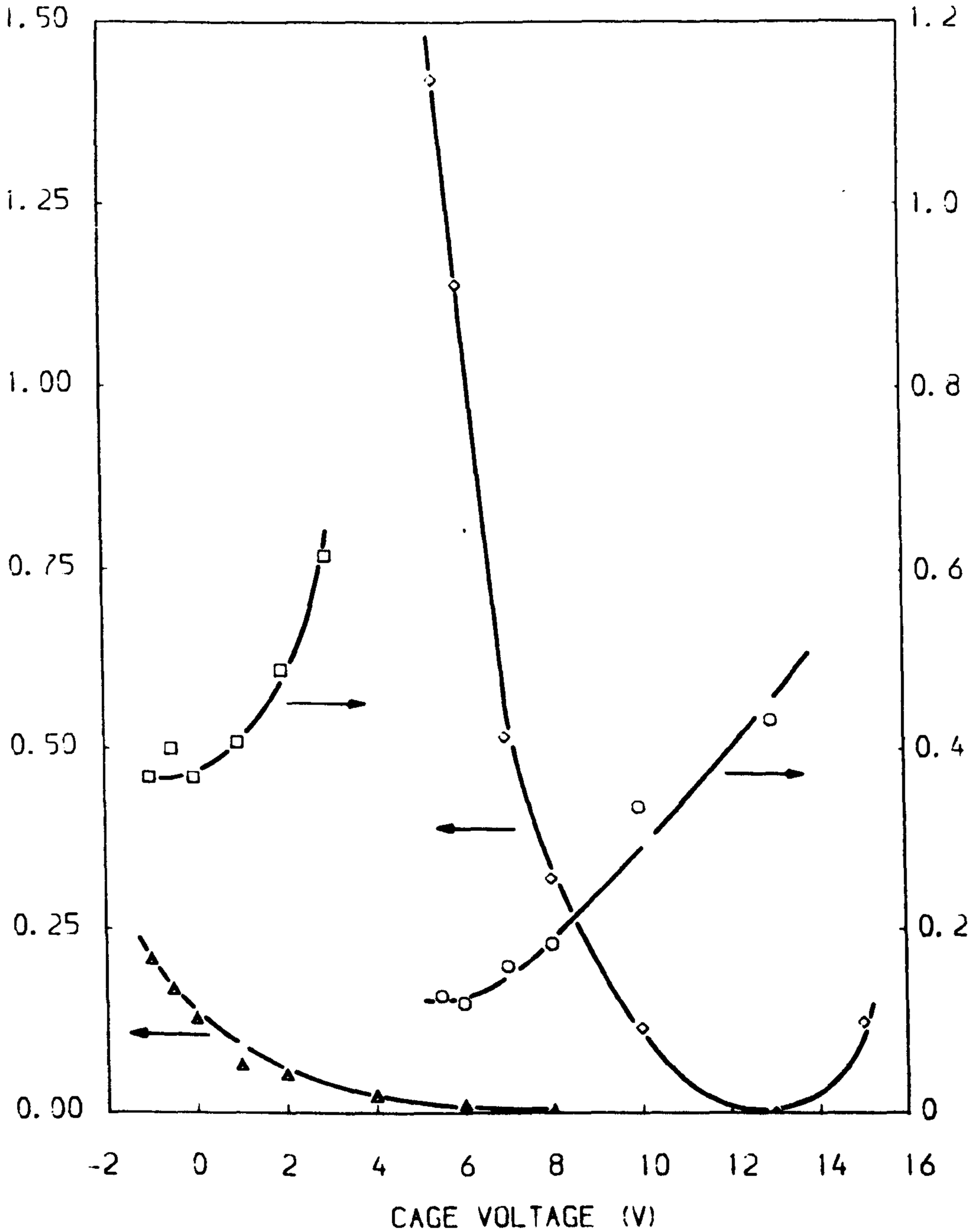

FIG. 4.4.7. COMPARISON OF THE PERFORMANCE BETWEEN THE USUAL OPERATION AND THE UNUSUAL OPERATION.

◇ $|\Delta S/S|/U_C$, ○ ΔM, FOR THE USUAL OPERATION

△ $|\Delta S/S|/U_C$, □ ΔM, FOR THE UNUSUAL OPERATION

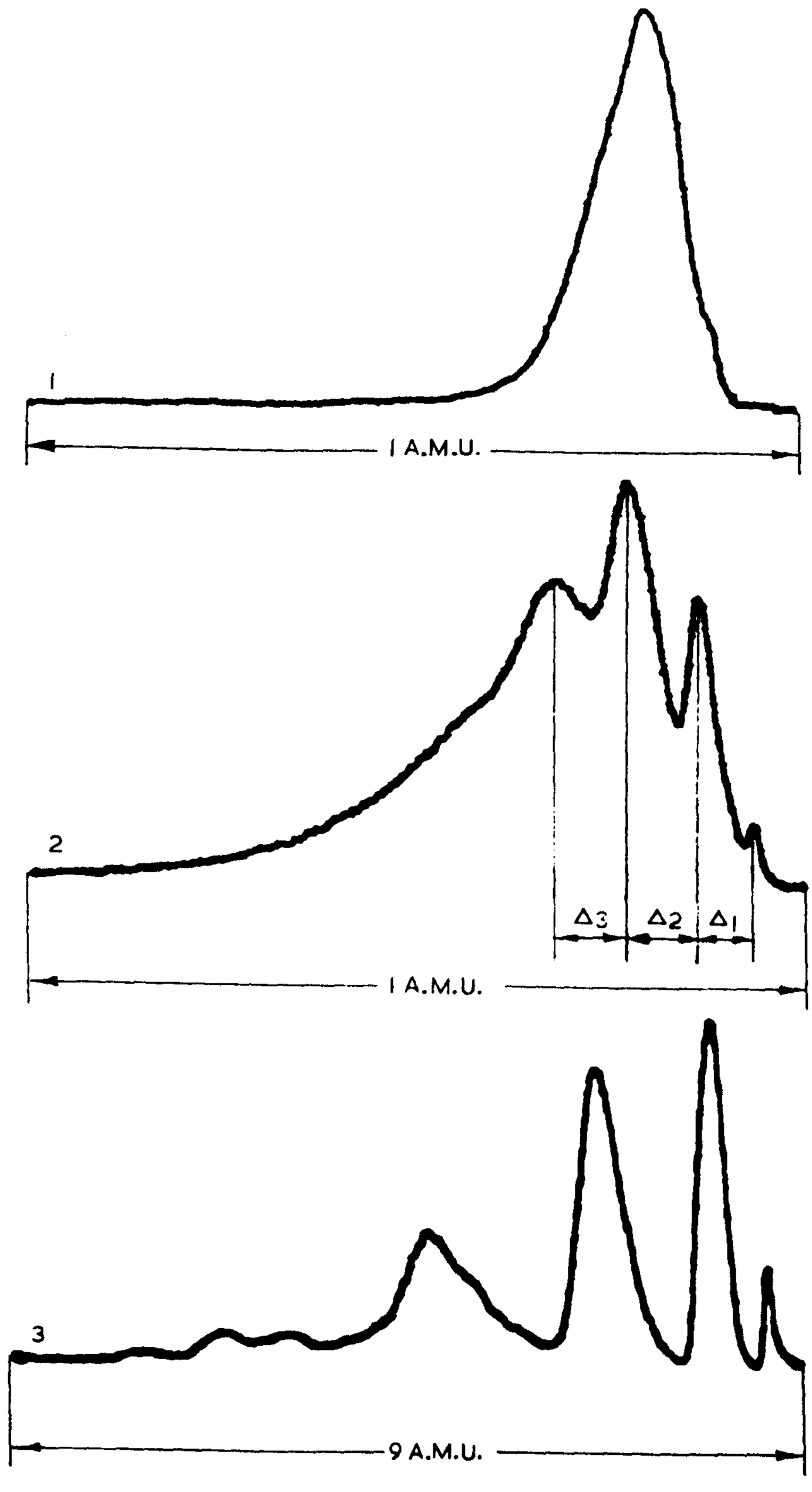

FIG. 4.5.1. MULTI-PEAKS OF ARGON. L=50MM.

1- F=4MHZ, ION ENERGY=7EV.

2- 4MHZ, 12EV.

3- 2MHZ, 16EV.

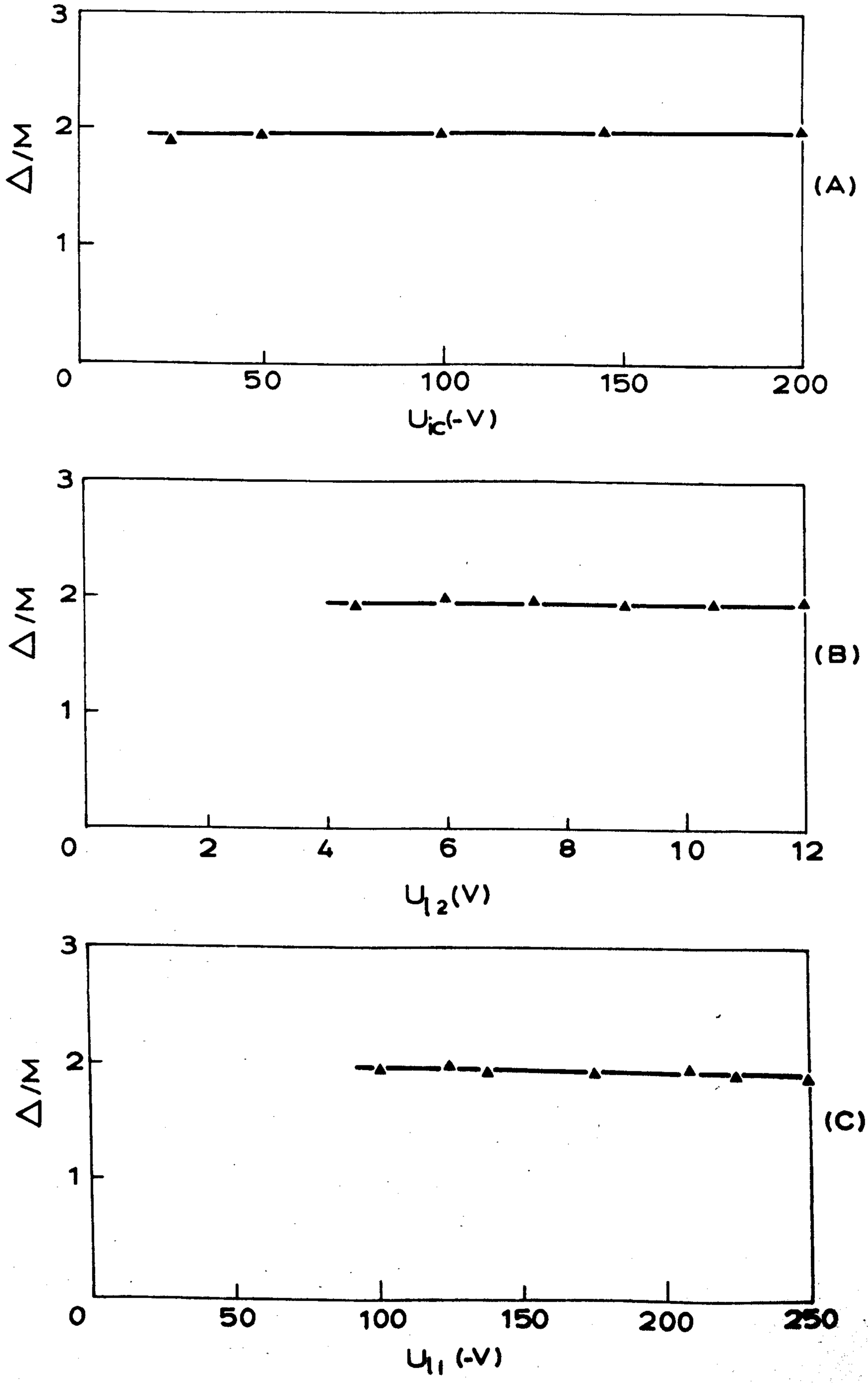

FIG. 4.5.2. WIDTH BETWEEN SISTER PEAKS AS A FUNCTION OF U_{ic}, U_{12}, AND U_{11}. (L=50 MM, ION ENERGY=16 EV, F= 2MHZ, $\Delta = \Delta_1 + \Delta_2$)

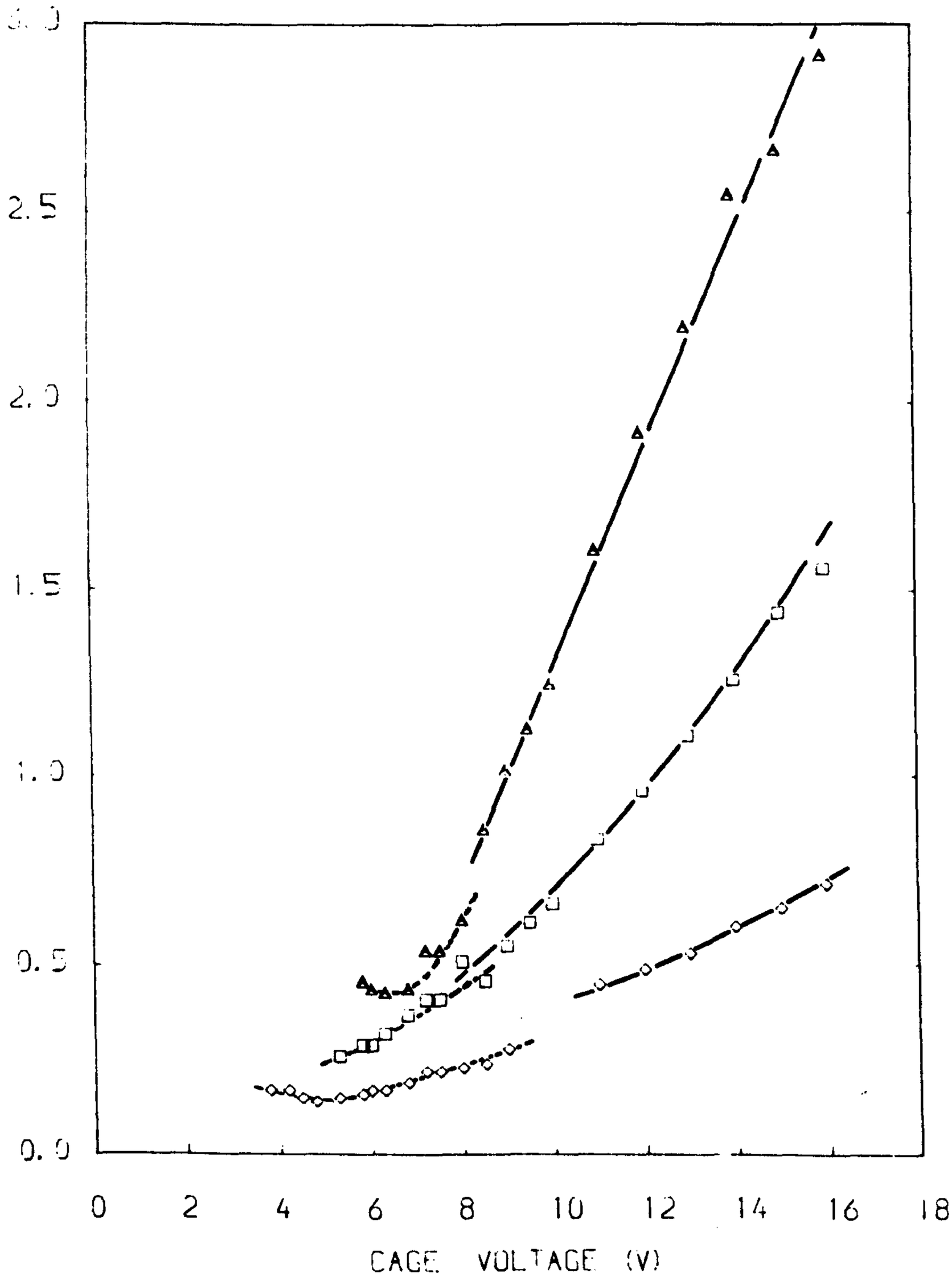

FIG. 4.5.3. Δ IS SHOWN AS A FUNCTION OF CAGE VOLTAGE FOR DIFFERENT VALUES OF FREQUENCY. M/E=40, L=50MM. THE DOTTED CURVES SHOW THE WIDTH OF CORRESPONDING SINGLE PEAKS. $\Delta = \Delta_1 + \Delta_2 + \Delta_3$.

△ F=2MHZ □ F=2.5MHZ ◇ F=4MHZ

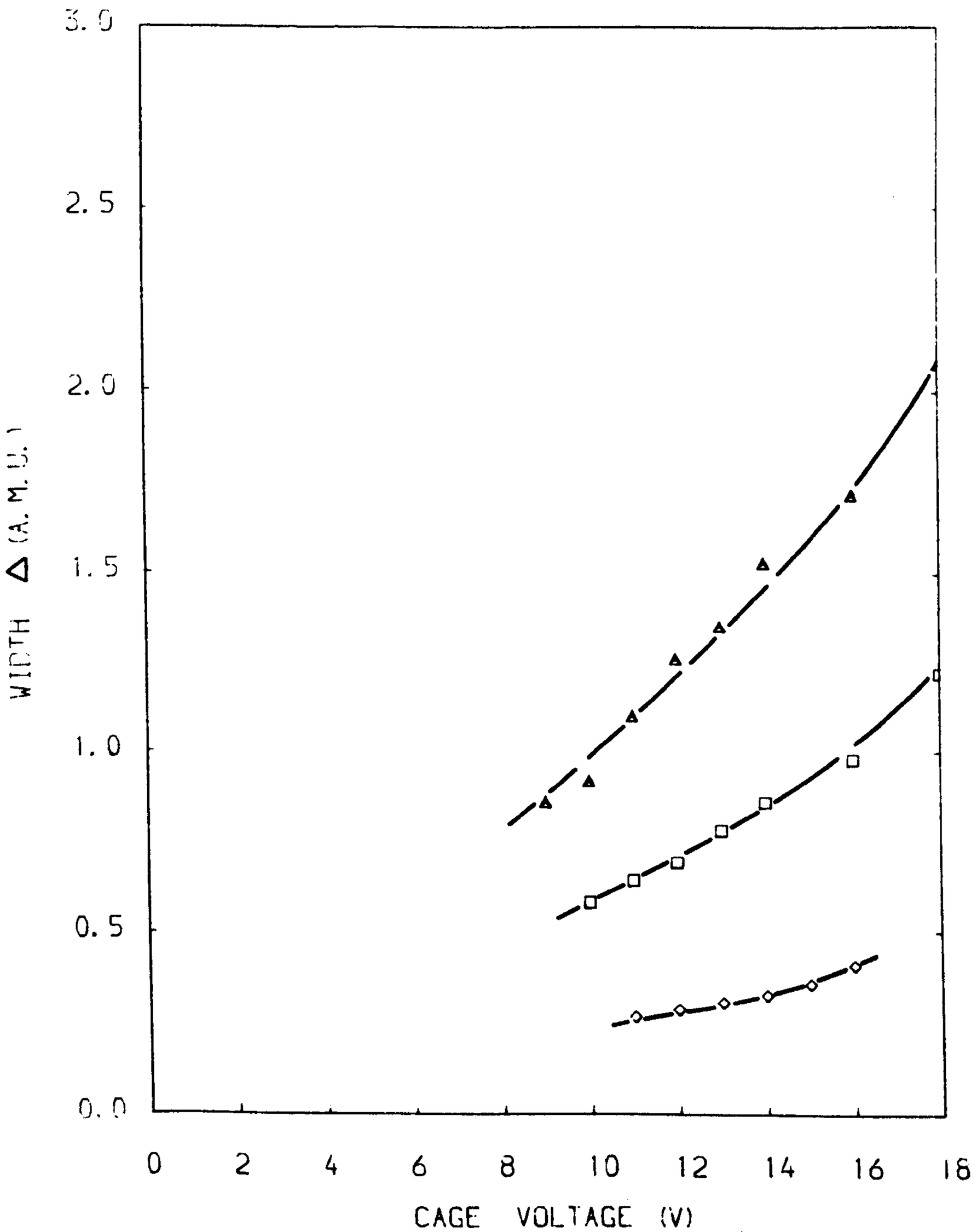

FIG. 4.5.4. Δ IS SHOWN AS A FUNCTION OF CAGE VOLTAGE FOR DIFFERENT VALUES OF FREQUENCY. M/E=40, L=85MM. $\Delta = \Delta_1 + \Delta_2 + \Delta_3$.

△ F=2MHZ □ F=2.5MHZ ◇ F=4MHZ

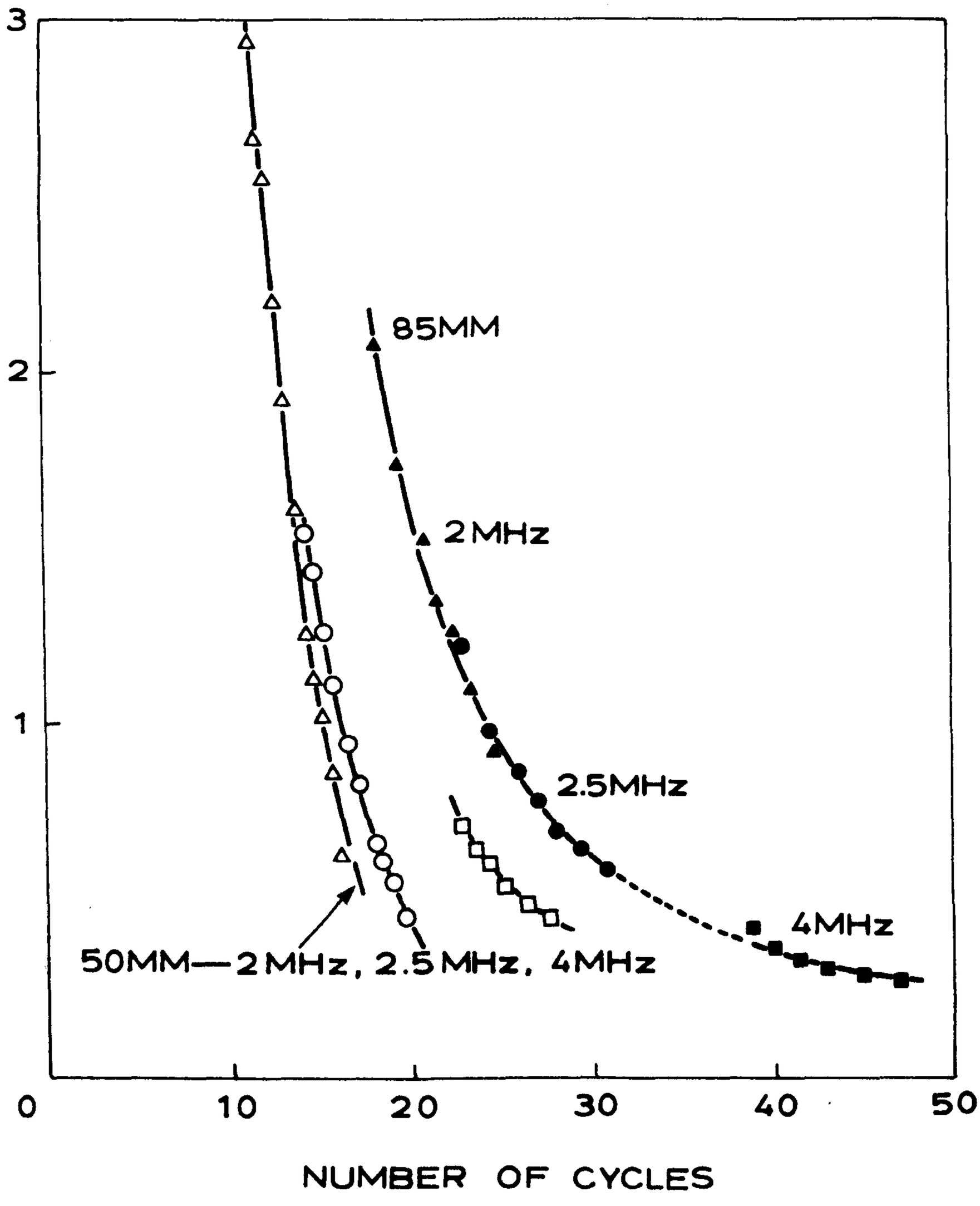

FIG. 4.5.5. WIDTH BETWEEN SISTER PEAKS AS A FUNCTION OF NUMBER OF CYCLES. $\Delta = \Delta_1 + \Delta_2 + \Delta_3$.

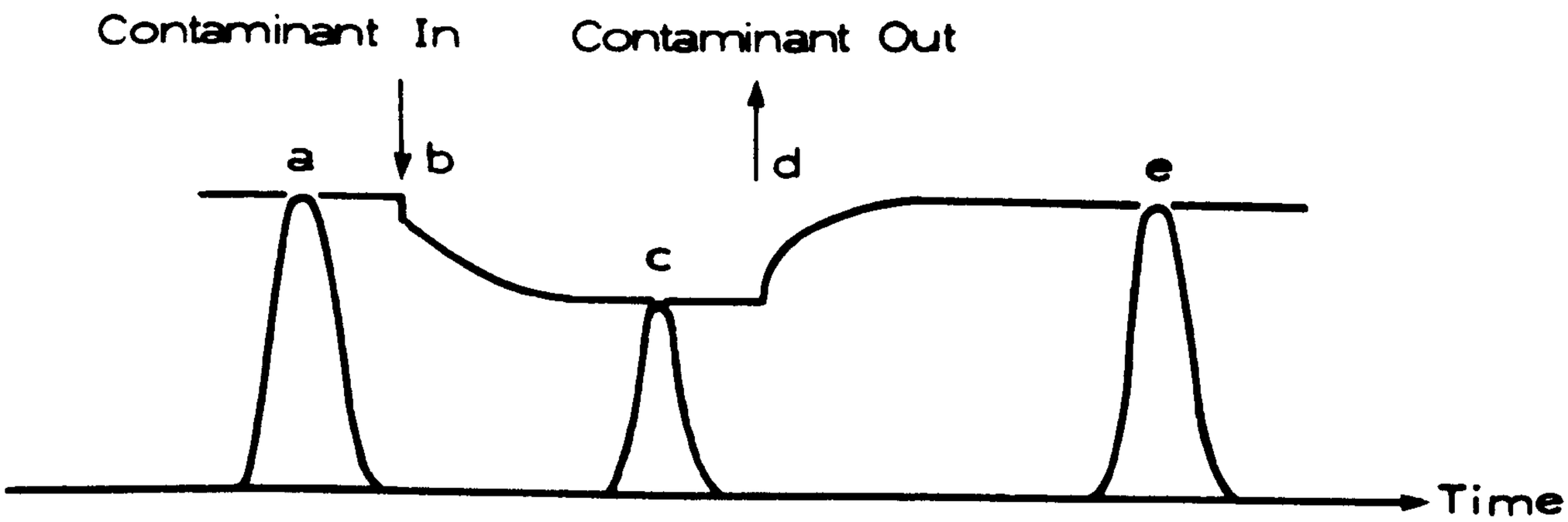

FIG. 4.6.1. THE PROCEDURE OF THE EXPERIMENT FOR SHORT TERM CONTAMINATION.

A) LET THE MASS ANALYSER BECOME STABLE AND RECORD THE ARGON PEAK

B) INTRODUCE 'CONTAMINATIVE' GAS

C) LET THE MASS ANALYSER BECOME STABLE AND RECORD THE ARGON PEAK

D) PUMP OUT THE 'CONTAMINANT'

E) RECORD THE ARGON PEAK

TABLE 4.6.1.* Change of the performance of the 50 mm QMF after introduction of air. The data were obtained at the air pressure of $5x10^{-6}$ mbar for diferent values of ion energy.

U (V)	3.9	4.6	5.6	6.3	7.3
ΔS (%)	-45	-28	-8	-2	-1
ΔM (%)		-18	-15	-7	0

TABLE 4.6.2.* Change of the sensitivity of the 50 mm QMF for different gases of pressure $5x10^{-6}$mar at ion energy 7 eV.

Gas	H_2	H_2O	N_2	Air	O_2	Methane	Aceton
S(%)	100	-20	0	0	-30	4(6.3eV)	15(7.7eV)

Note: A) $\Delta S(\%)=(S-S_o)/S_o$, S_o is the original value.

B) $\Delta M(\%)=(\Delta M-\Delta M_o)/\Delta M_o$, ΔM_o is the original value.

C) "-" means decreasing.

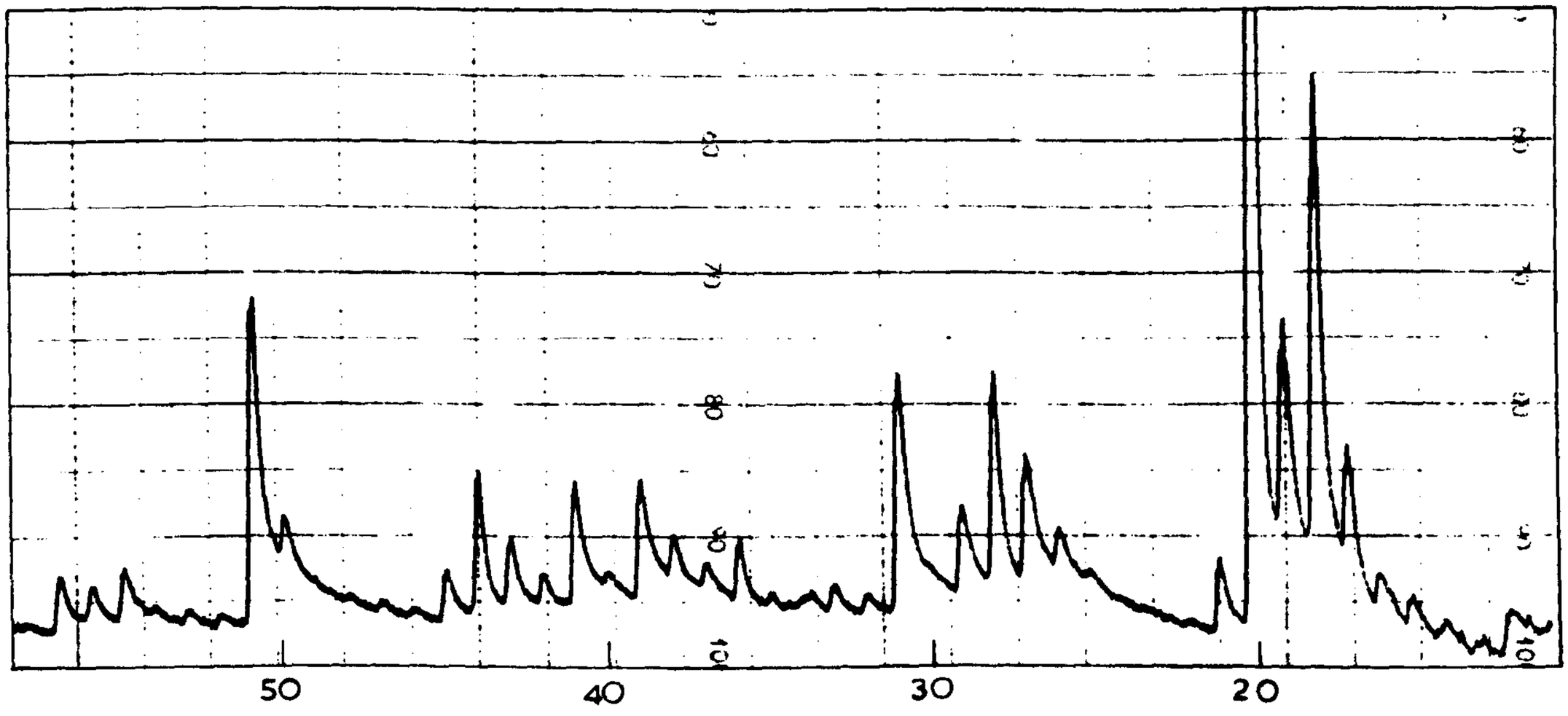

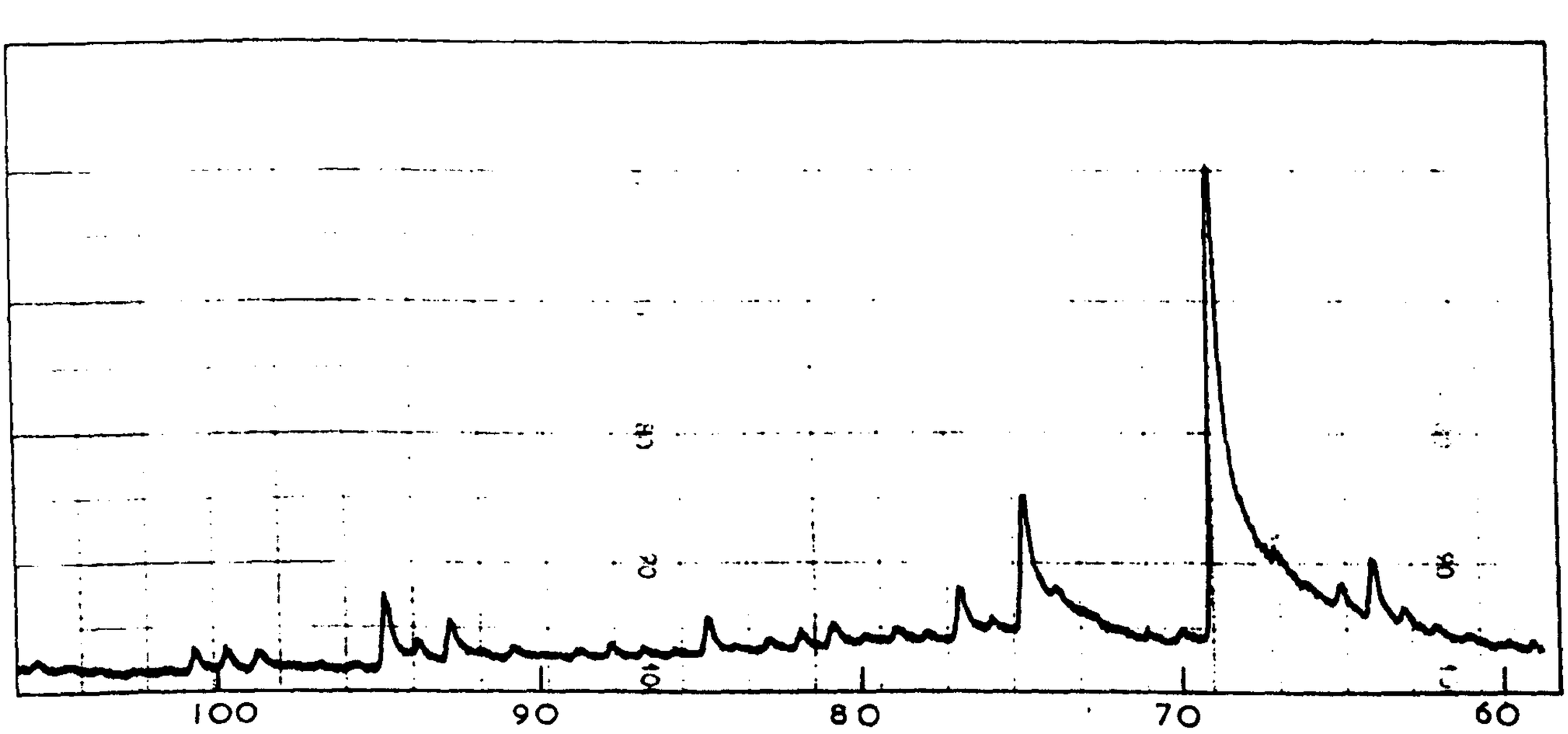

FIG. 4.6.2. A TYPICAL MASS SPECTRUM OF DECOMPOSITES EVAPORATED FROM A VITON "O" RING AT 10^{-3} MBAR.

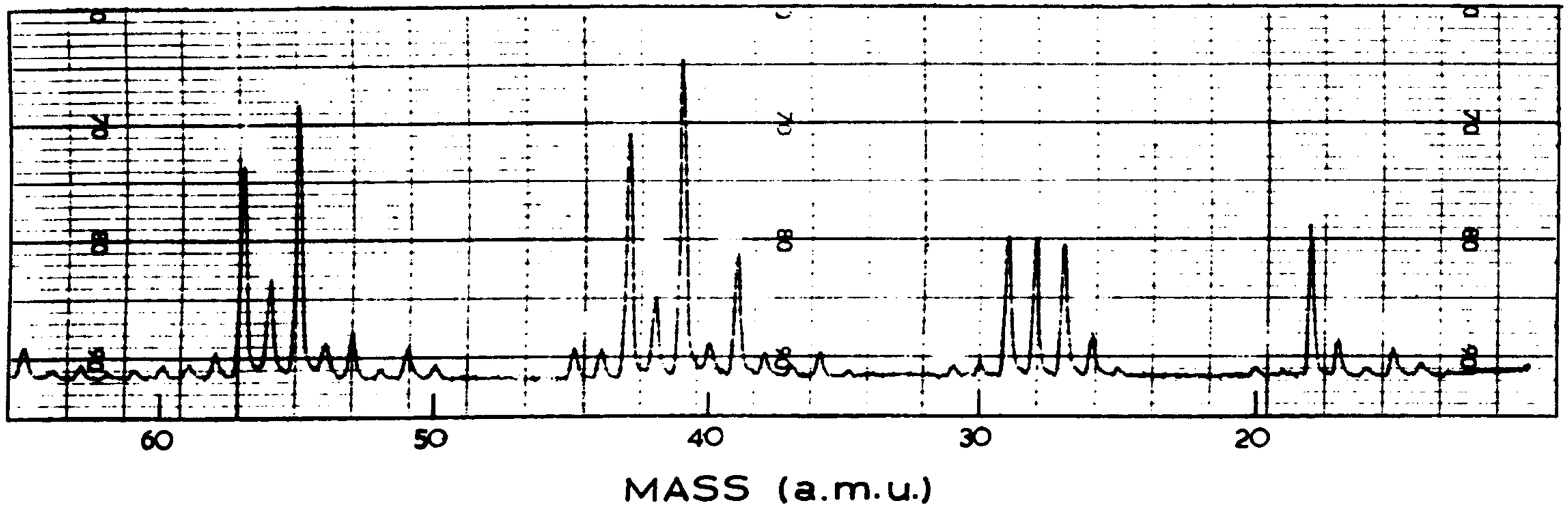

FIG. 4.6.3. A TYPICAL MASS SPECTRUM AT 10^{-5} MBAR ON PLANT NO. 2.

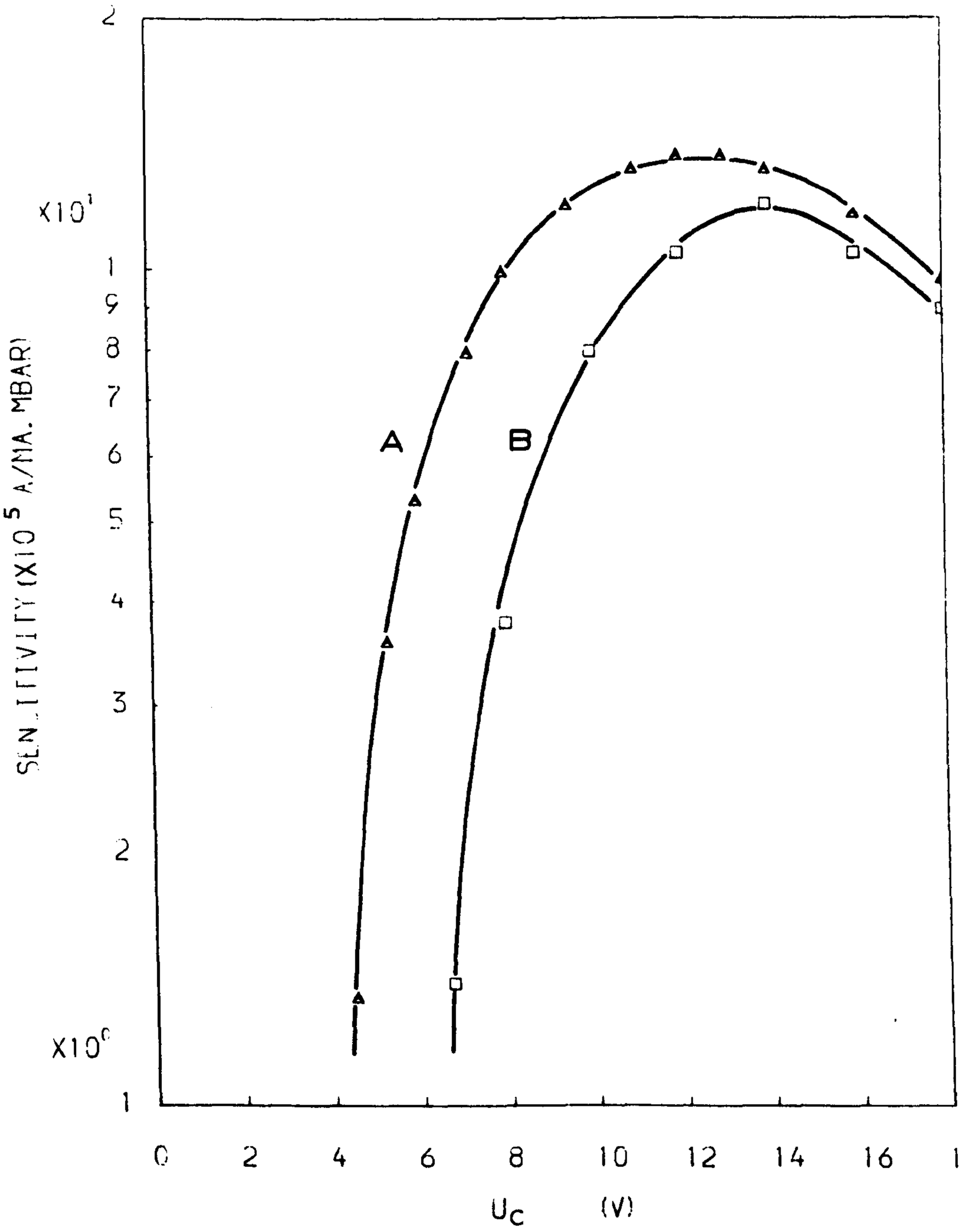

FIG. 4.6.4.A COMPARISON OF SENSITIVITIES OBTAINED BEFORE CONTAMINATION AND AFTER 45 HOURS CONTAMINATION IN THE A.C. MODE.

A △ BEFORE CONTAMINATION

B □ AFTER 45 HOURS CONTAMINATION

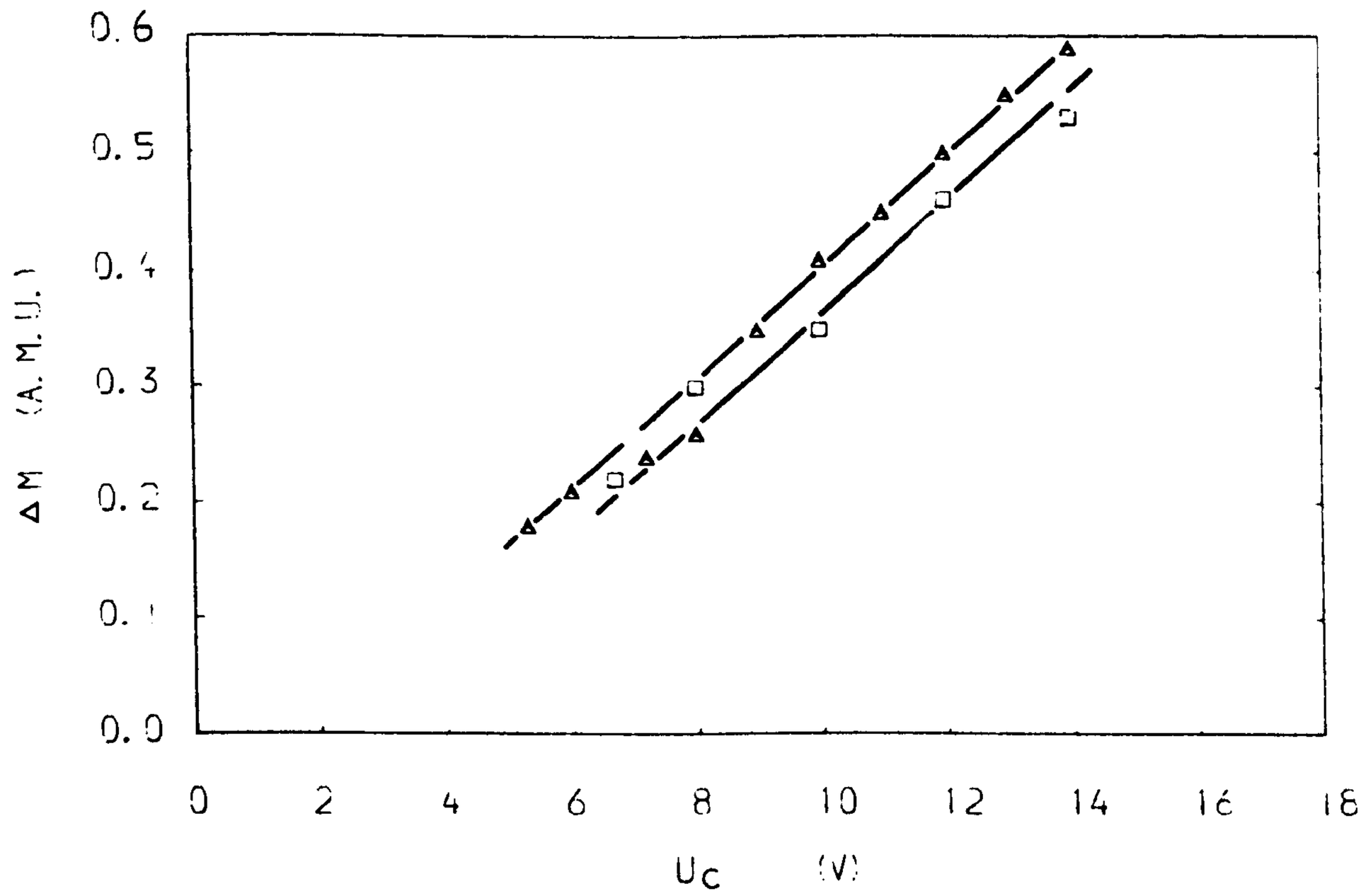

FIG. 4.6.4.B COMPARISON OF PEAK WIDTHS OBTAINED BEFORE CONTAMINATION AND AFTER 45 HOURS CONTAMINATION IN THE A.C. MODE.

△ BEFORE CONTAMINATION

□ AFTER 45 HOURS CONTAMINATION

TABLE 4.6.3. The variation of the maximum sensitivity of a 50 mm quadrupole mass filter during 100 hours contamination. The hydrocarbons were evaporated from copper mesh, workshop swarf, etc. The fluorocarbons were decomposited from viton "o" rings. The rods were never cleaned during the experiments. The data were obtained at 4 MHz. The sensitivity is defined as a collected ion current for an emission current of 1 mA at a pressure of 1 mbar.

Date	Time	S(10^5A/mA.mbar)	Contaminants
9. 9.82	0	1.4	Hydrocarbons
28. 9.82	18	1.0	
11.10.82	18	1.4	
12.11.82	32	1.6	
26. 1.83	51	1.2	Fluorocarbons
17. 2.83	78	0.9	
10. 5.83	98	0.9	

TABLE 4.6.4. The changes in the relative sensitivity* of an 85 mm quadropole filter after 50 hours contamination for various cage voltages. In the first 40 hours the filter was operating in a hydrocarbon atmosphere of 10^{-3} mbar, in the final 10 hours in a fluorocarbon pressure of 10^{-3} mbar. The data were obtained at 3 MHz. The maximum sensitivity changed from 5×10^{-5} A/mA.mbar at the start to 3.5×10^{-5} A/mA.mbar at the end.

U_c (V)	6	7	8	9	10
(S_{40}/S_{20}) (%)	-5	-7	-15	-5	-12
(S_{84}/S_{42}) (%)	0	-1	- 6	2	- 7

Note: The variation in relative sensitivity, i.e. the ratio S_{40}/S_{20} and the ratio S_{84}/S_{42}, is defined as:

(a new ratio - the original ratio)/the original ratio, in percentage.

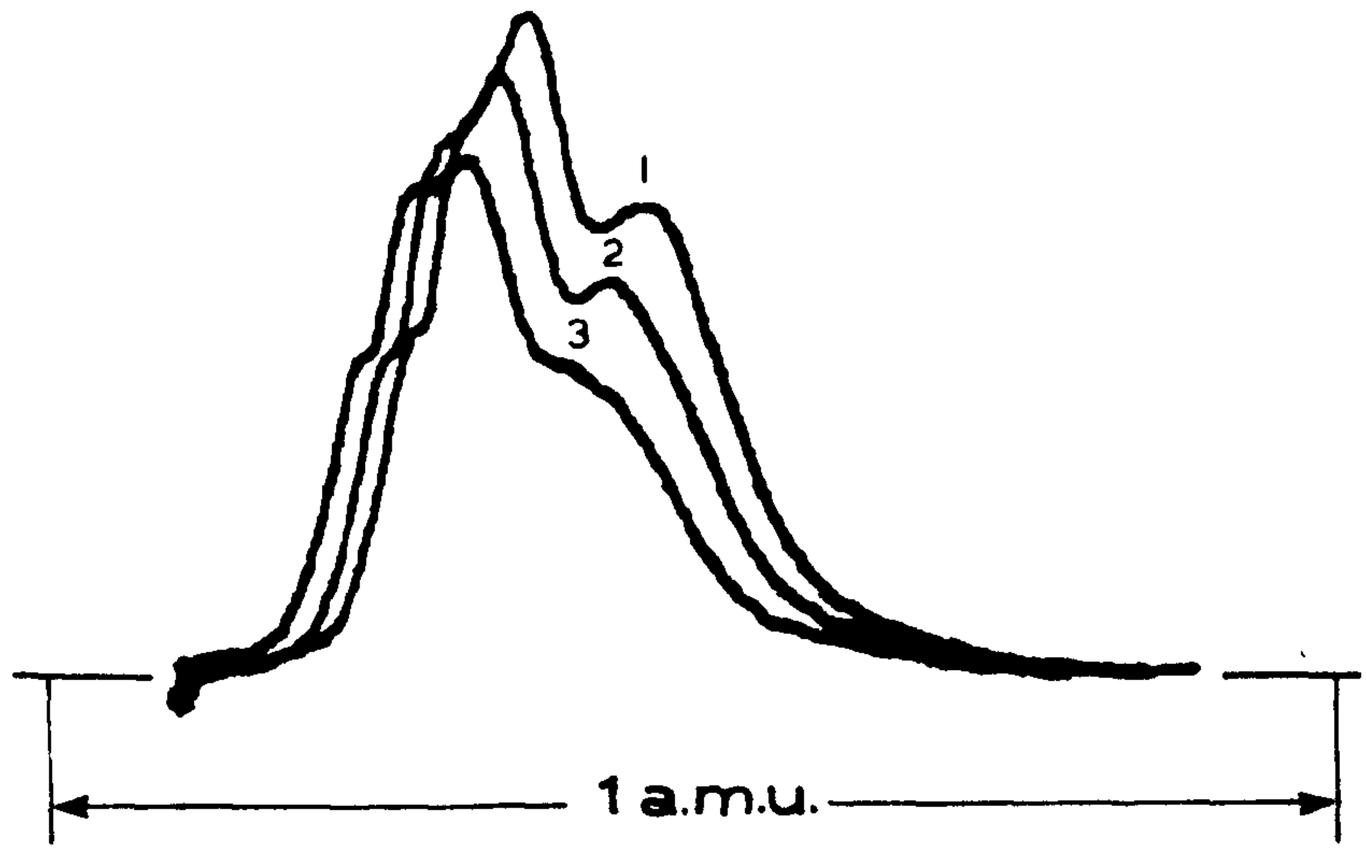

FIG. 4.6.5. AN UNSTABLE ARGON PEAK OBTAINED IN THE NORMAL MODE AFTER 45 HOURS CONTAMINATION.

1- AT THE BEGINNING

2- 10 MINUTES LATER AFTER 1

3- 20 MINUTES LATER AFTER 1

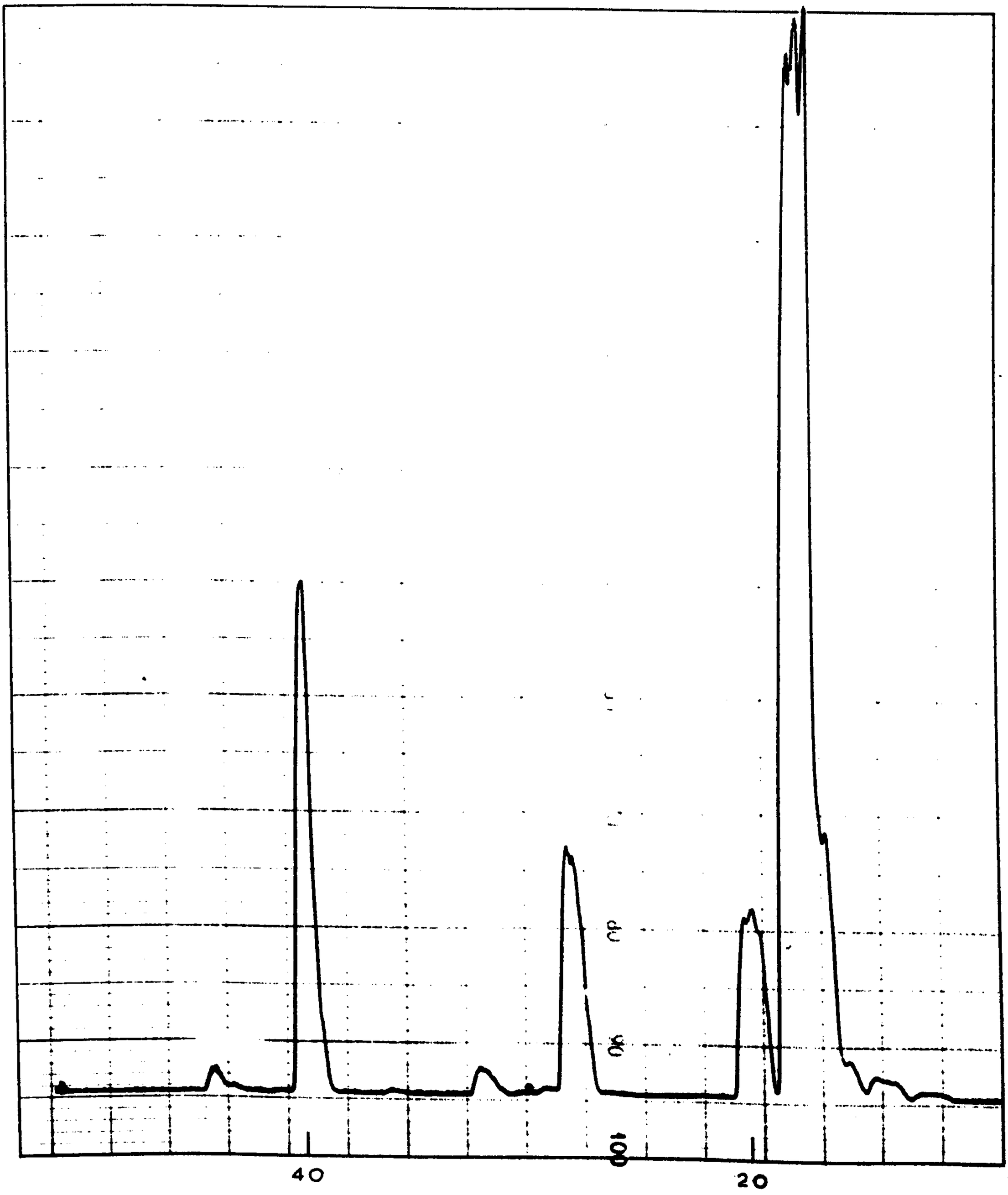

FIG. 4.6.6.A. A SPECTRUM SHOWING THE ABUNDANCE OF ARGON IN THE NORMAL MODE. U=77.73V, I_{40}/I_{20} =2.7.

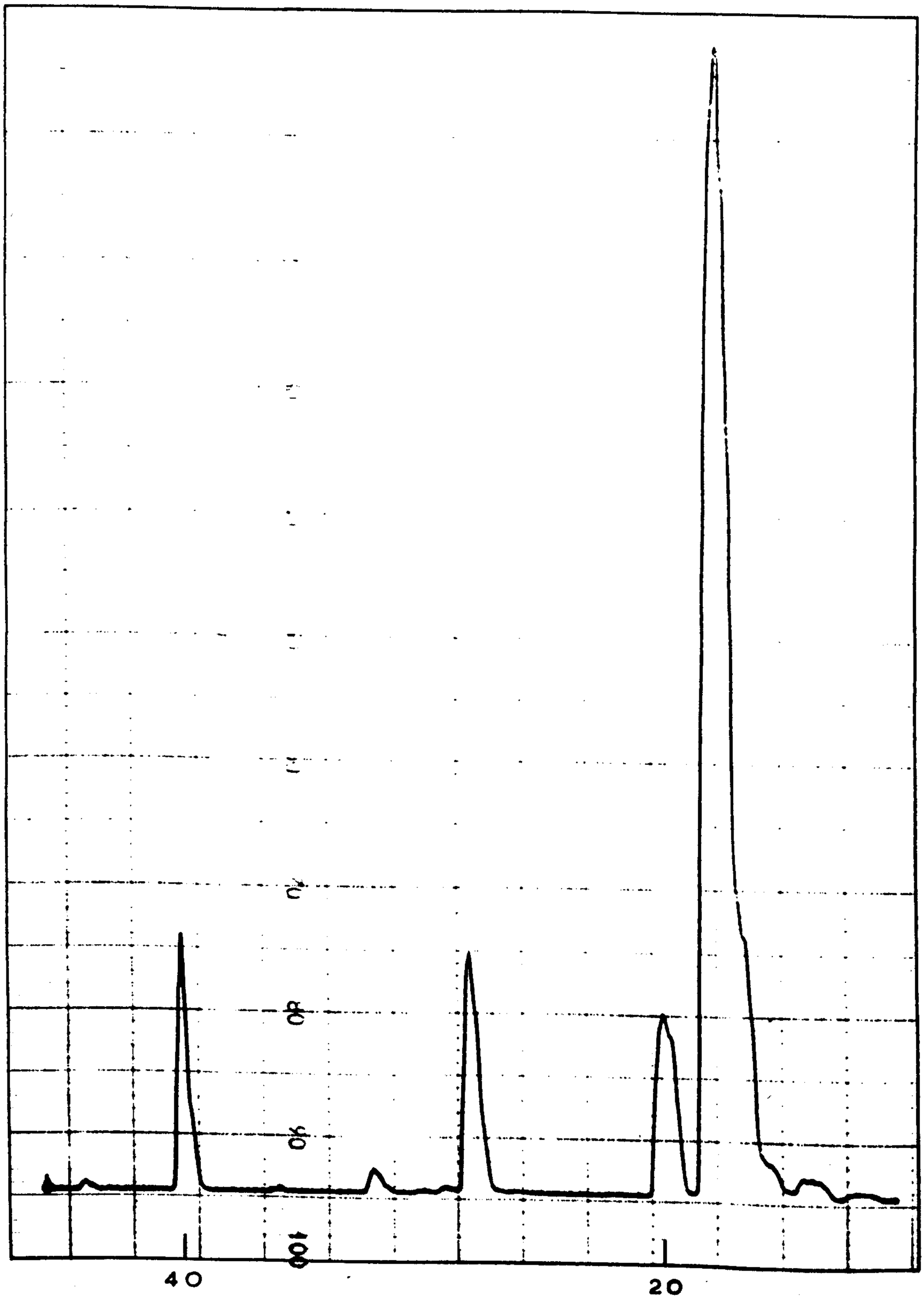

FIG. 4.6.6.B. A SPECTRUM SHOWING THE ABUNDANCE OF ARGON IN THE NORMAL MODE. U=78.60V, $I_{40}/I_{20}=1.4$.

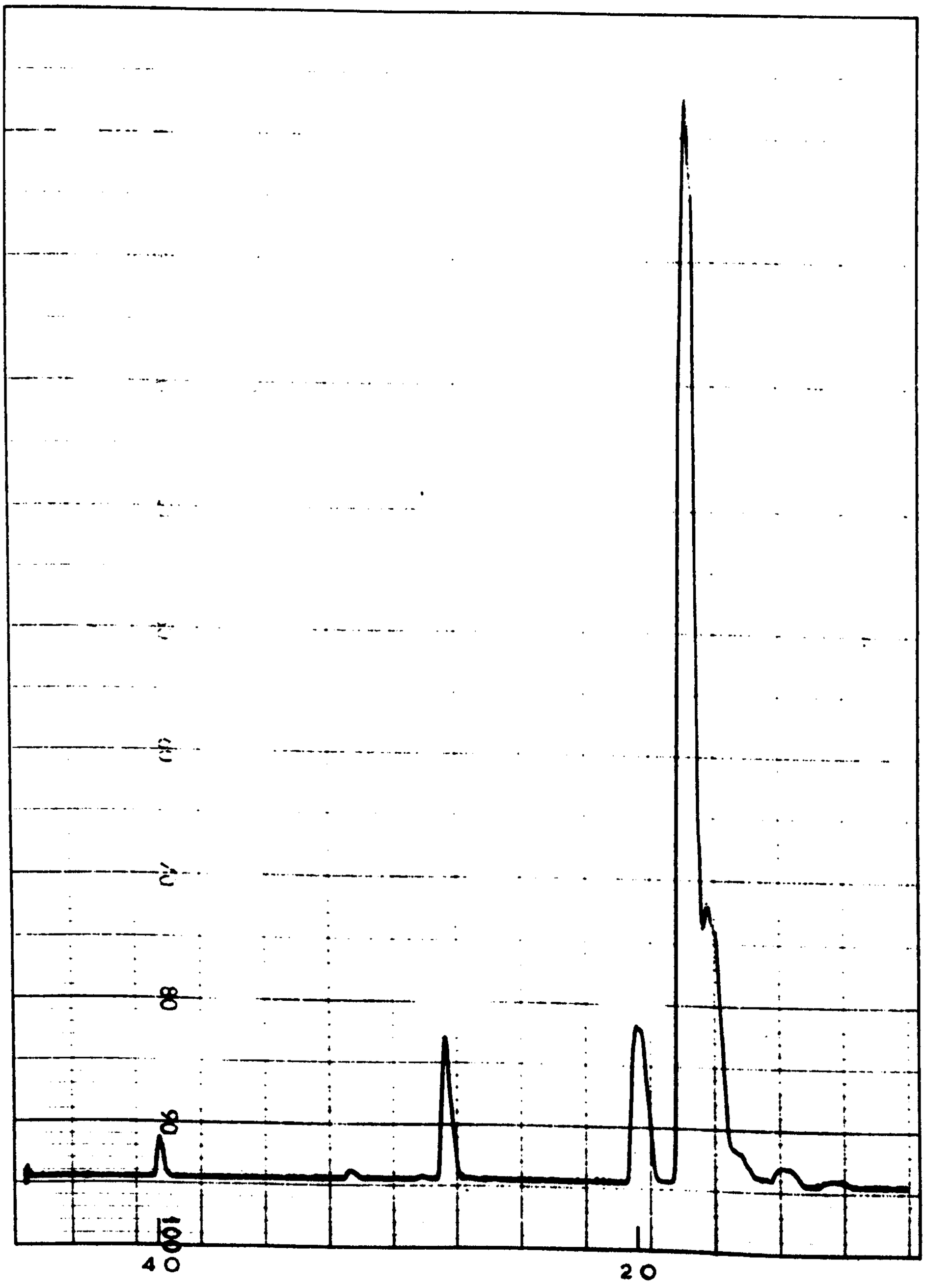

FIG. 4.6.6.C. A SPECTRUM SHOWING THE ABUNDANCE OF ARGON IN THE NORMAL MODE. U=79.47V, I_{40}/I_{20}=0.2.

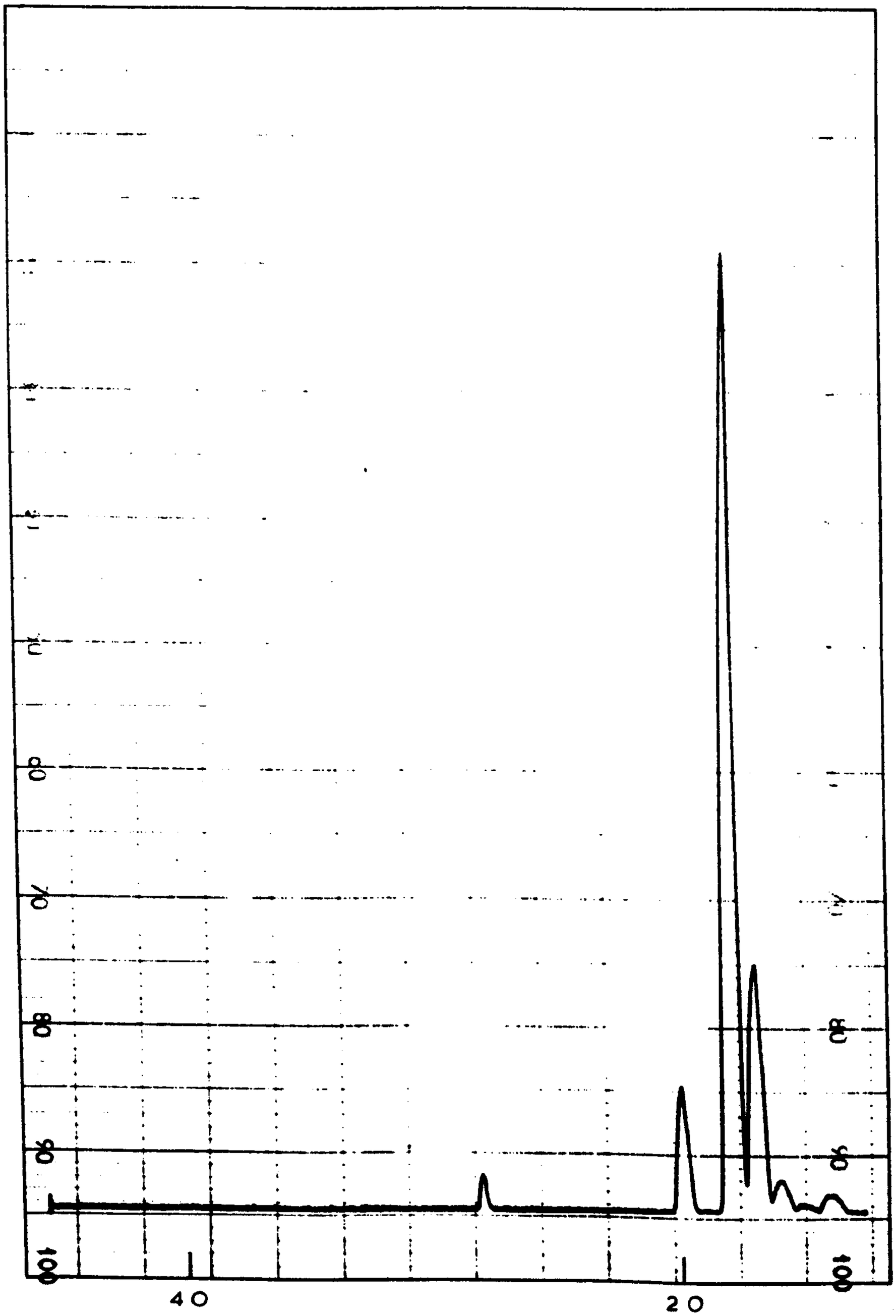

FIG. 4.6.6.D. A SPECTRUM SHOWING THE ABUNDANCE OF ARGON IN THE NORMAL MODE. U=80.35V, I_{40}/I_{20}=0.0.

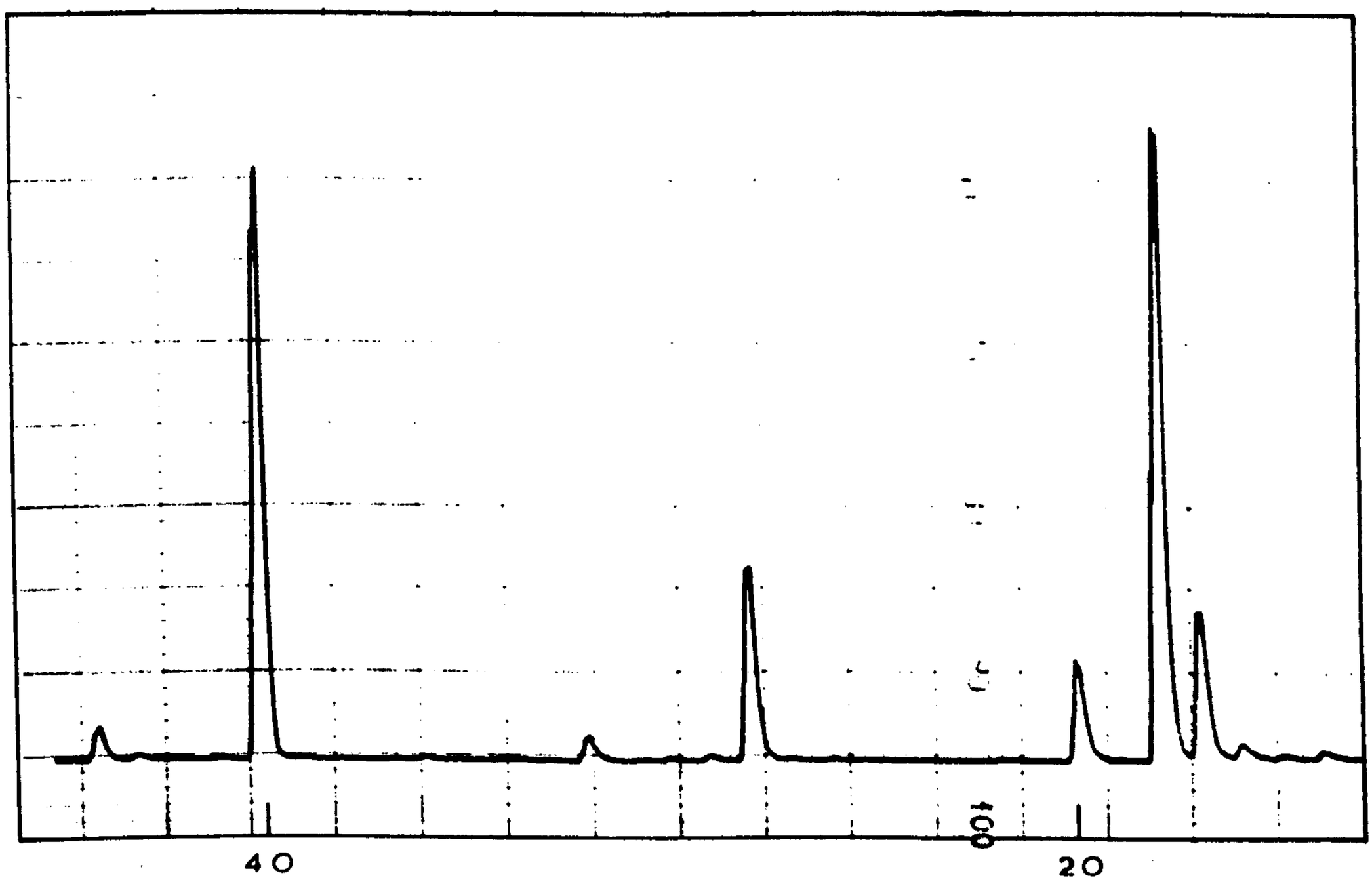

FIG. 4.6.6.E. A SPECTRUM SHOWING THE ABUNDANCE OF ARGON IN THE A.C. MODE. $I_{40}/I_{20}=6.0$.

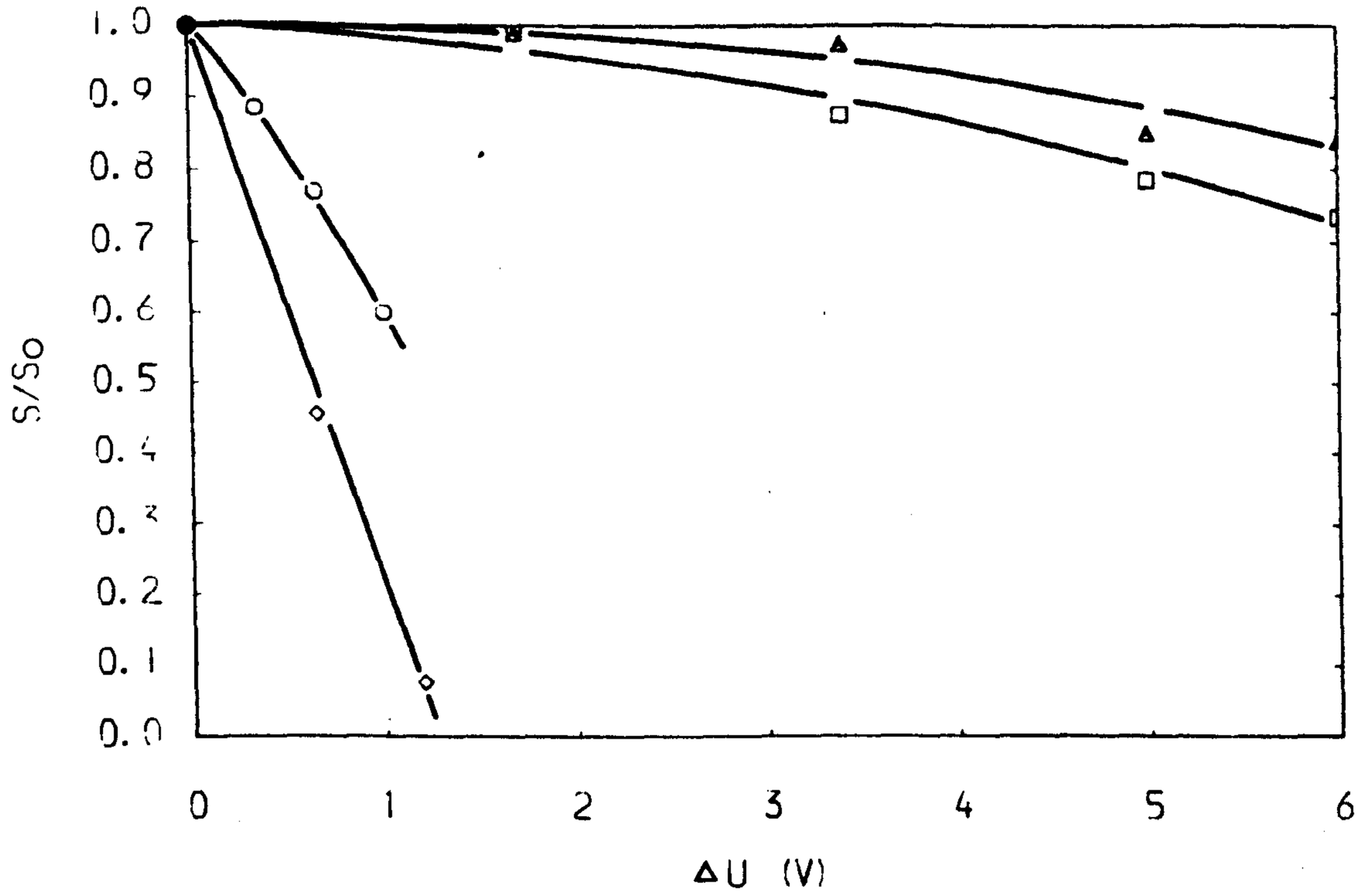

FIG. 4.6.7. CURVES SHOWING THE FRACTIONAL CHANGES IN SENSITIVITY (S/S_o) RESULTING FROM CHANGES IN THE D.C. POTENTIALS APPLIED TO THE RODS. THE SMALL INCREMENTS IN D.C. VOLTAGE WERE EFFECTED BY ALTERING THE SLOPES OF THE SCAN LINES.

◇ M/E=40, NORMAL MODE ○ M/E=20, NORMAL MODE

△ M/E=40, A.C. MODE □ M/E=20, A.C. MODE

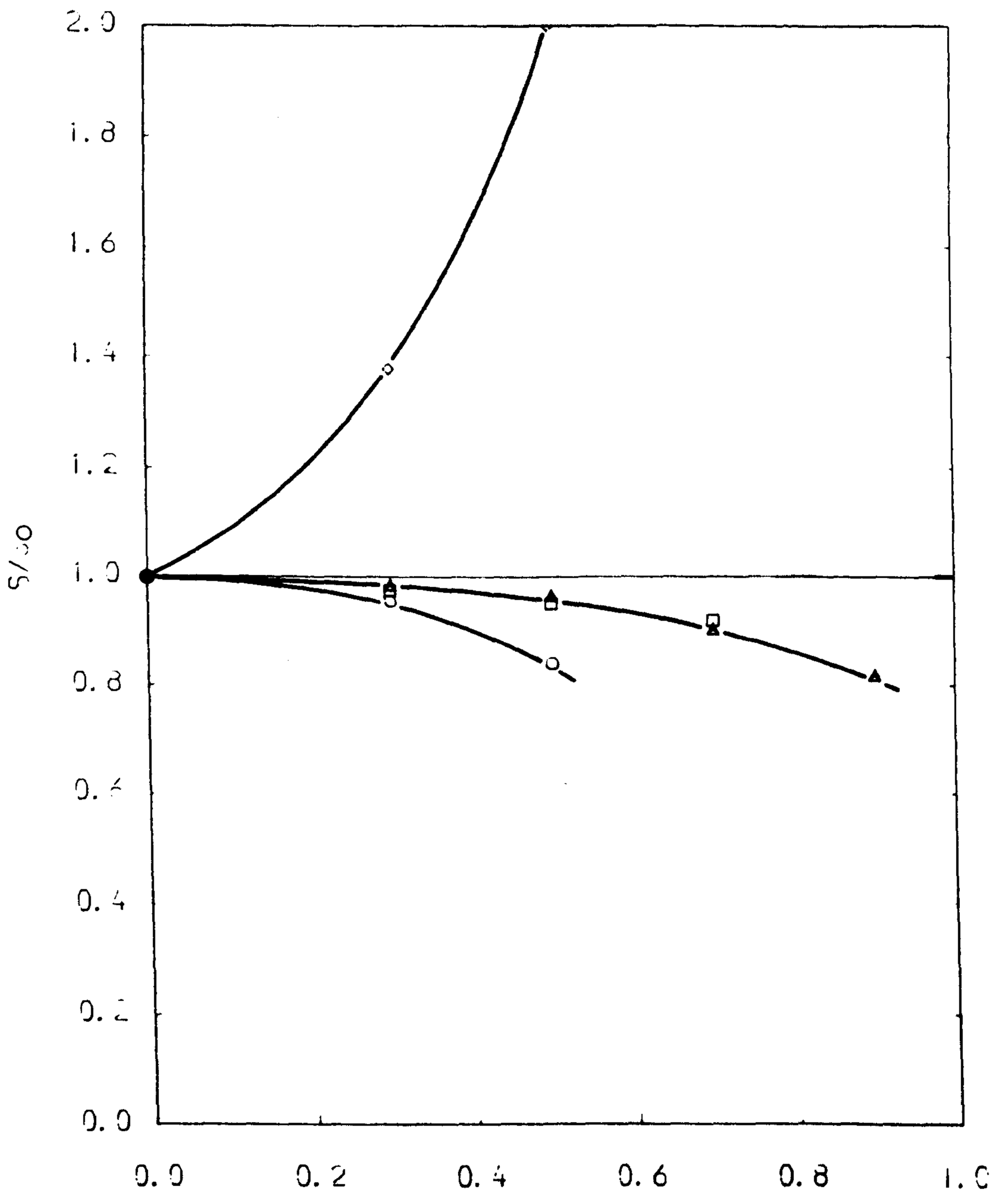

FIG. 4. 6. 8. FRACTIONAL CHANGES IN SENSITIVITY (S/S_o) CAUSED BY A SMALL IMBALANCE IN THE D. C. POTENTIAL APPLIED TO THE RODS.

◇ M/E=40, NORMAL MODE
○ M/E=20, NORMAL MODE
△ M/E=40, A. C. MODE
□ M/E=20, A. C. MODE

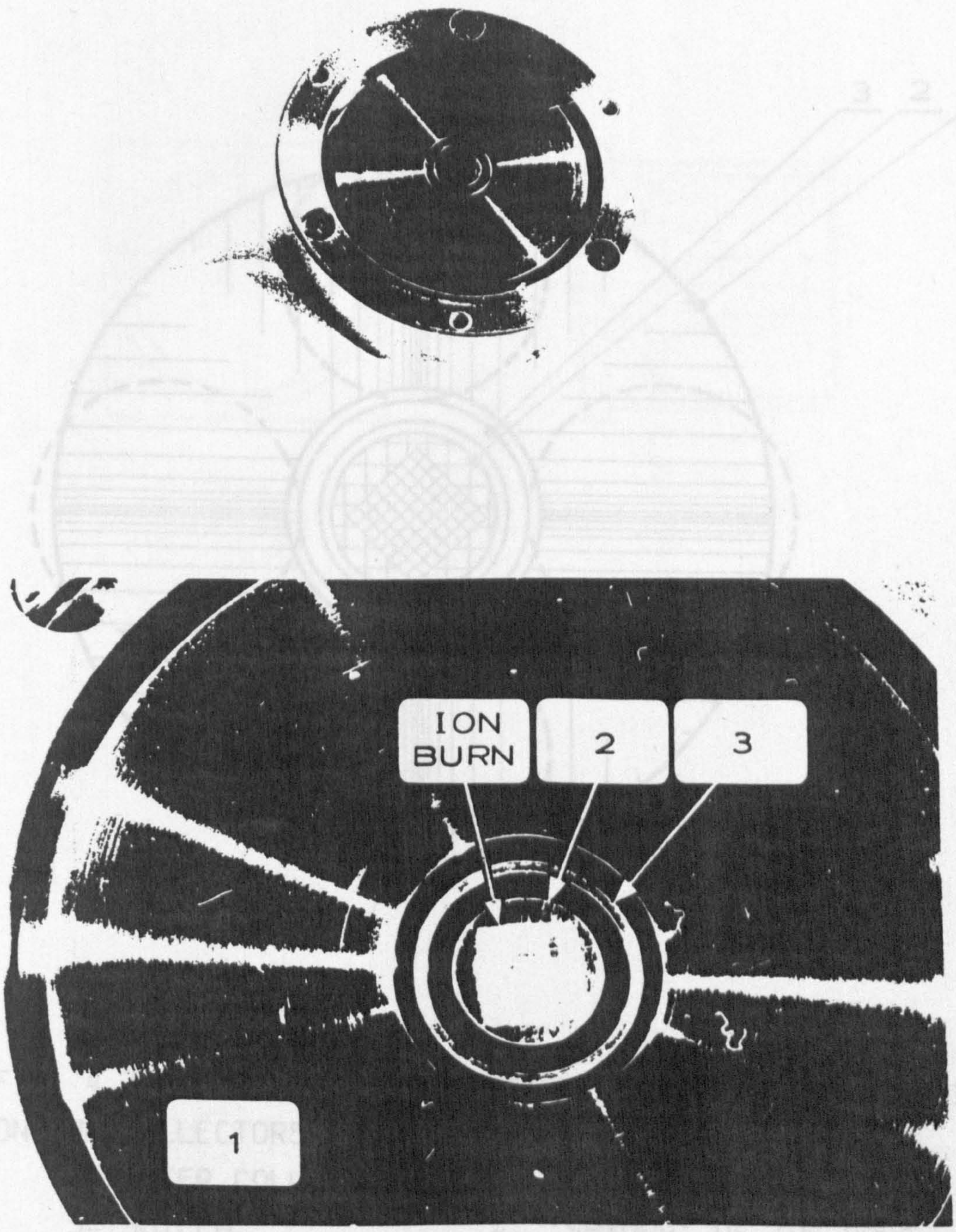

FIG. 4.7.1. A CONTAMINATED COLLECTOR ASSEMBLY.
1-OUTER COLLECTOR 2-INNER COLLECTOR 3-SHIELD

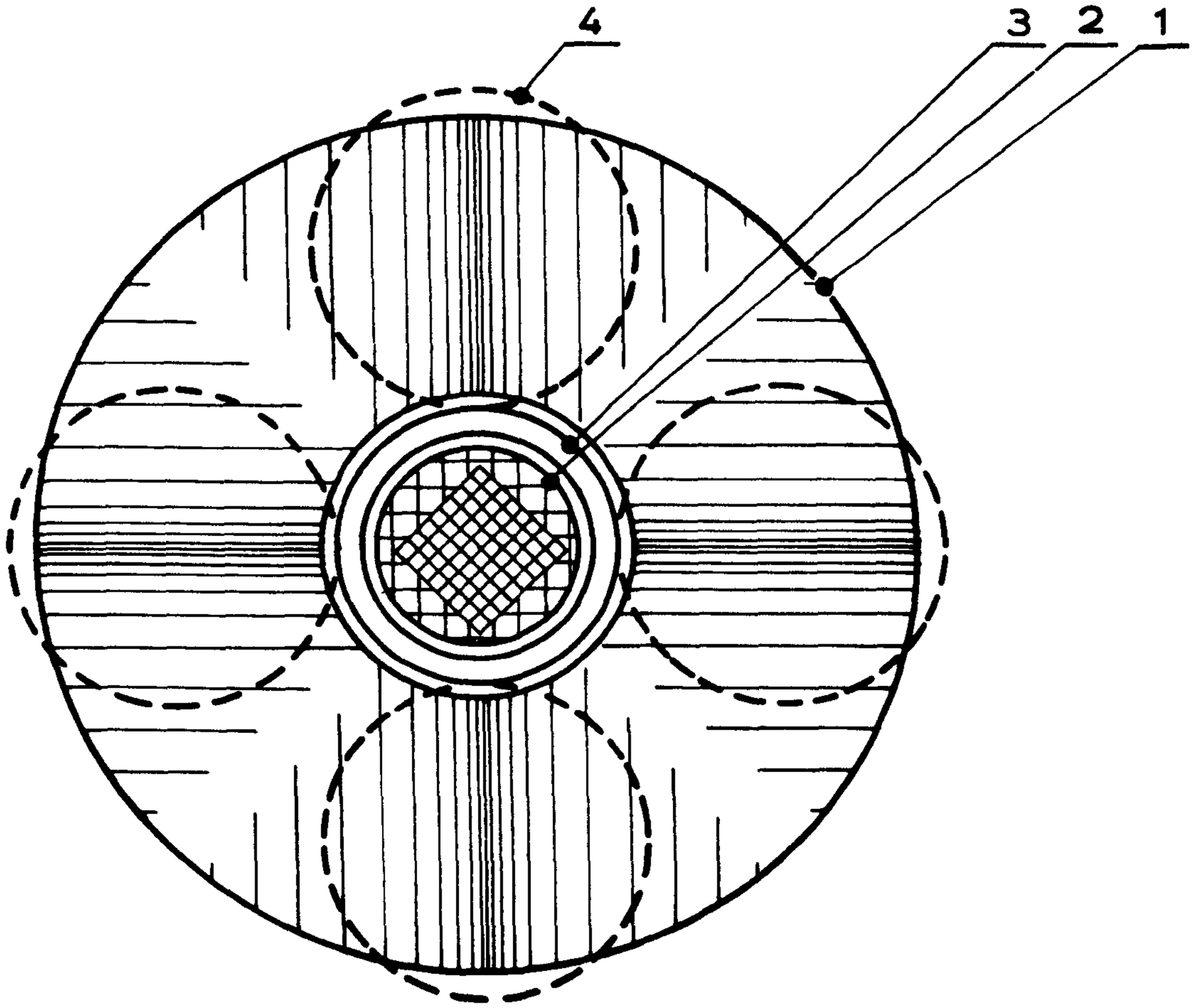

FIG. 4.7.2. DETAILS OF THE CONTAMINATED AREA (SHADED) ON THE COLLECTORS.

1- OUTER COLLECTOR.
2- INNER COLLECTOR.
3- SHIELD.
4- 'SHADOW' OF THE RODS.

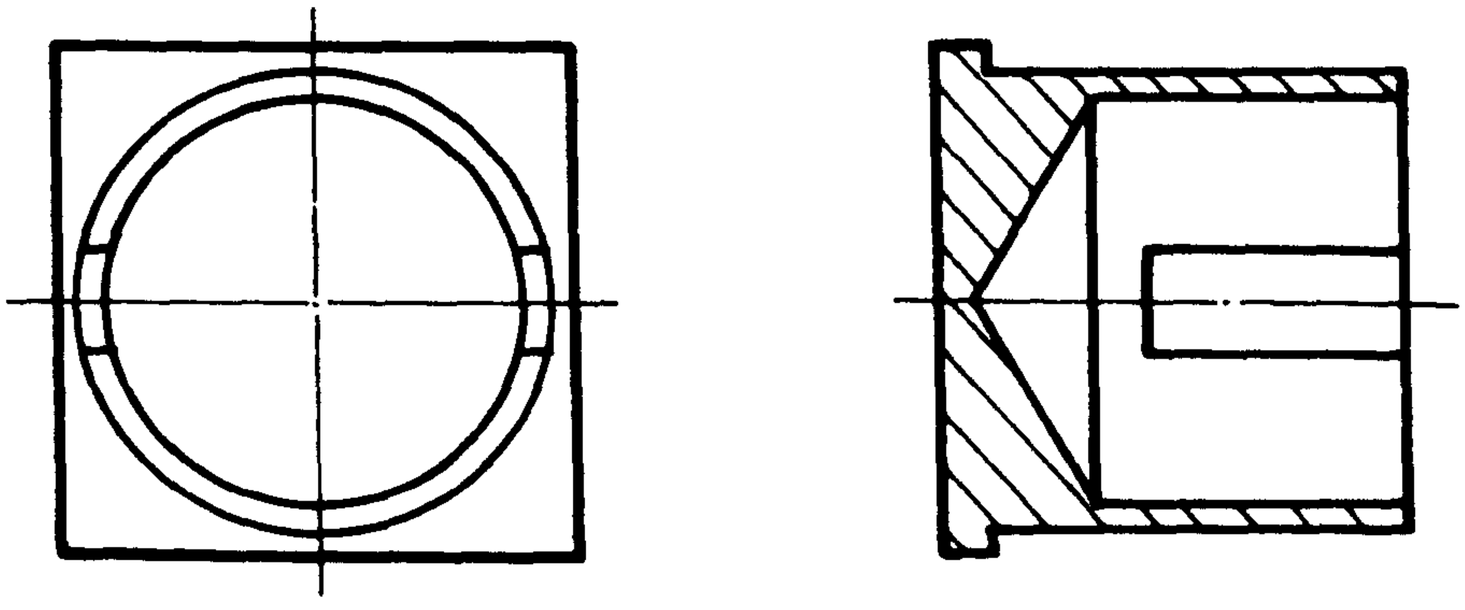

(A)

(B)

FIG. 4.7.3. SQUARE INNER COLLECTOR AND ITS POSITION RELATIVE TO THE RODS.

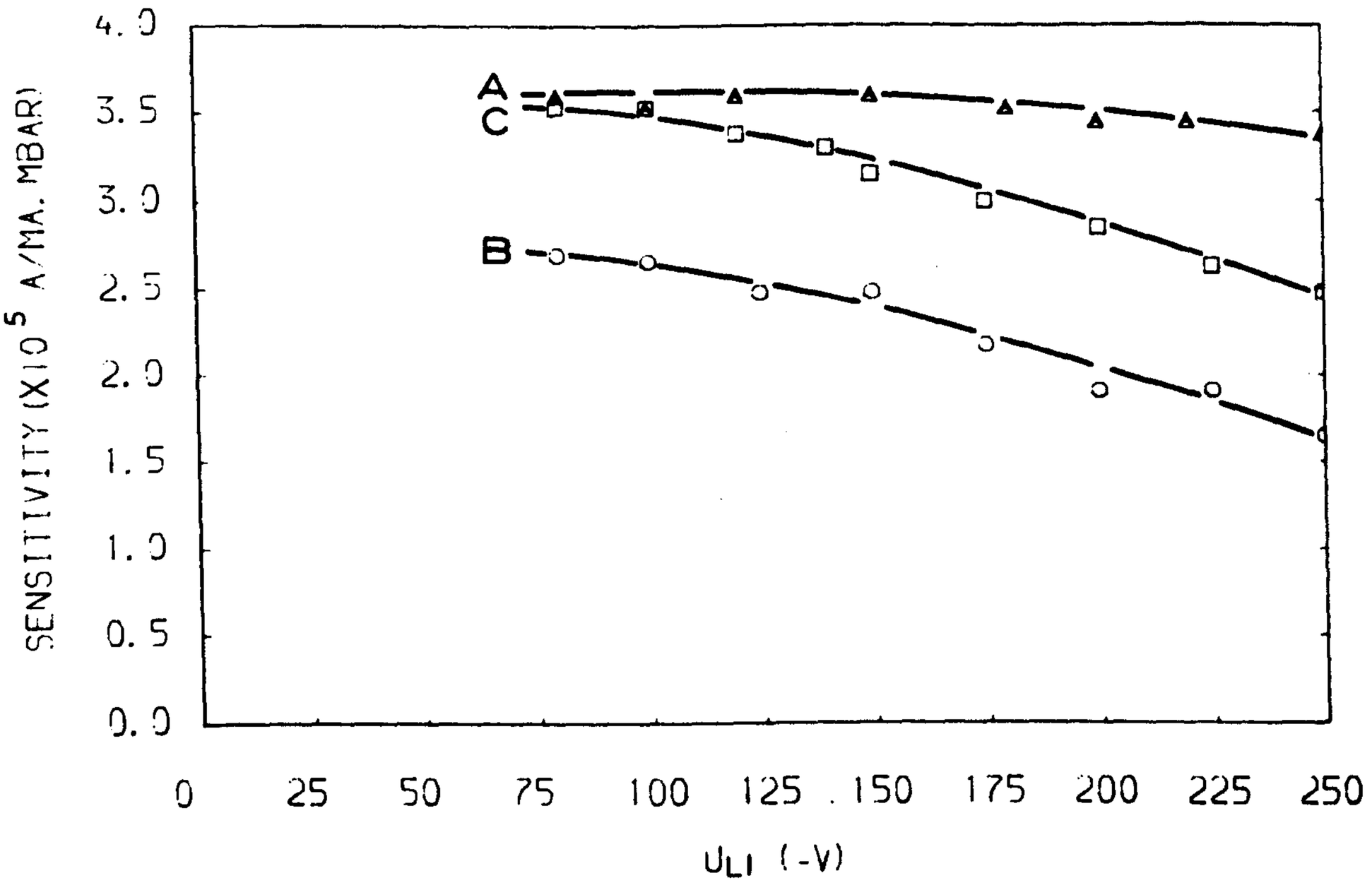

FIG. 4.7.4.A. SENSITIVITY AS A FUNCTION OF THE POTENTIAL ON LENS 1 FOR DIFFERENT SHAPES OF INNER COLLECTOR. M/E=14.

(A) ○ (B) ○ (C) ○□○

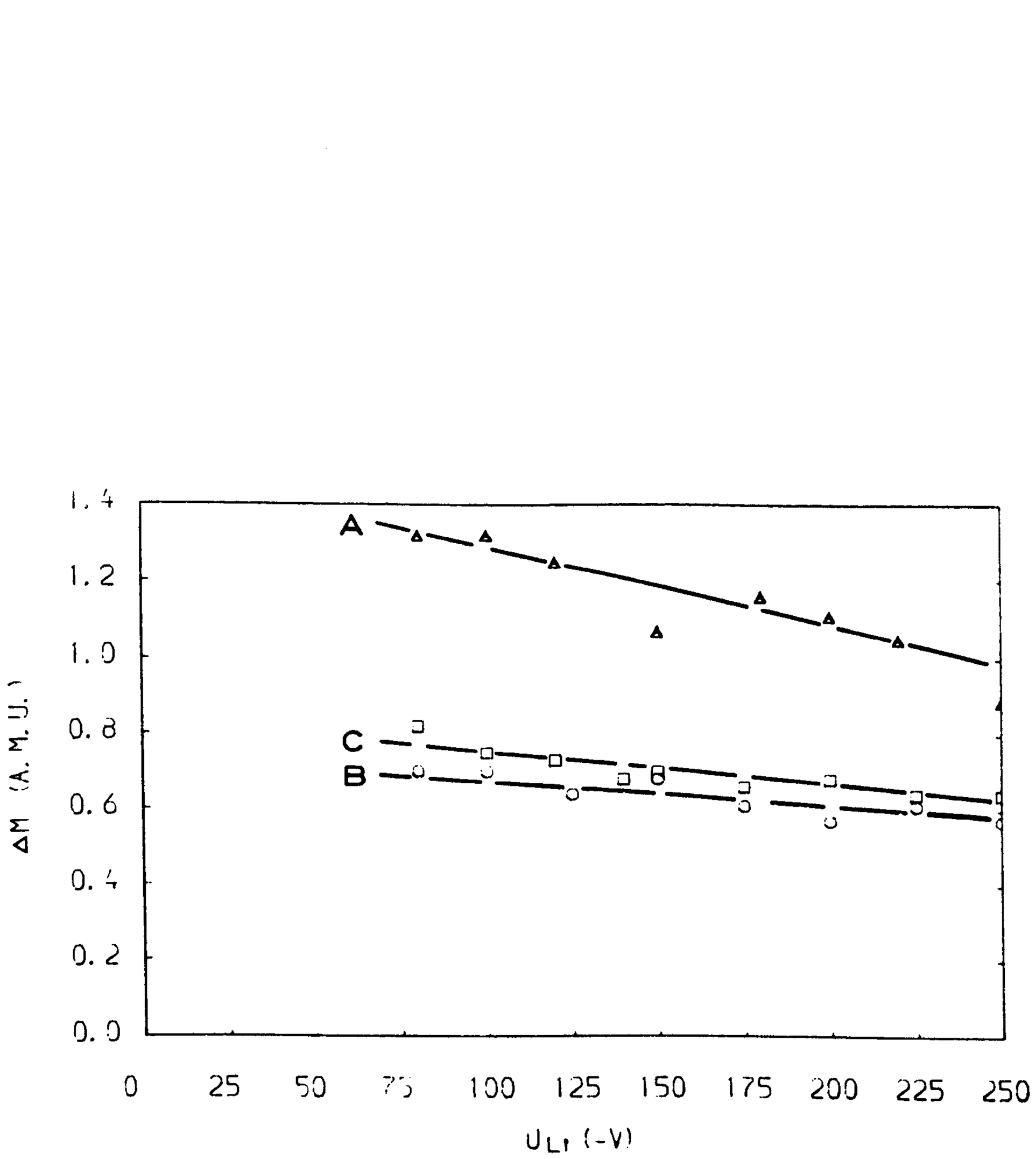

FIG. 4.7.4.B. PEAK WIDTH AS A FUNCTION OF THE POTENTIAL ON LENS 1 FOR DIFFERENT SHAPES OF INNER COLLECTOR. M/E=14.

(A) ○ (B) ○ (C) ○□○

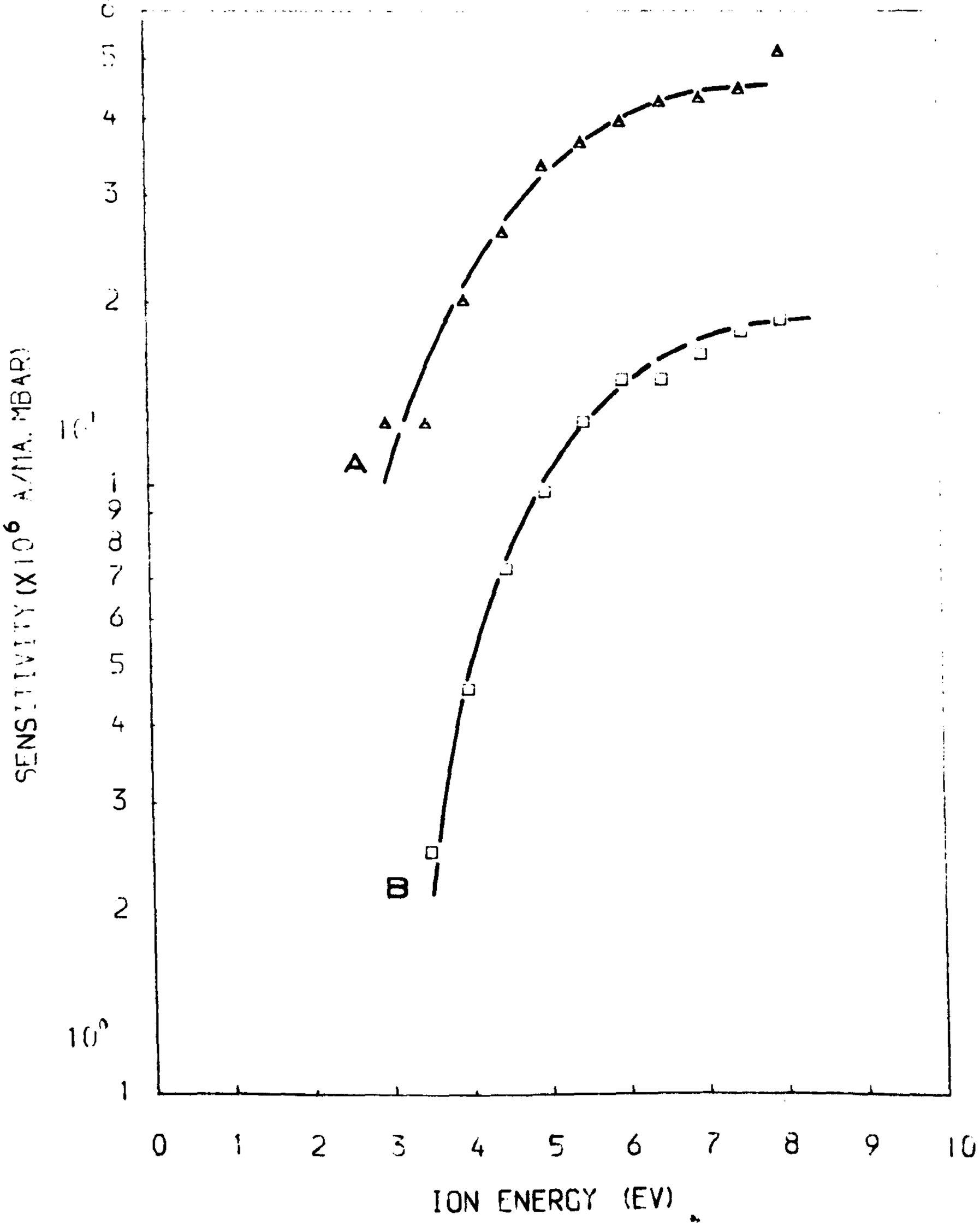

FIG. 4.7.5.A. SENSITIVITY AS A FUNCTION OF ION ENERGY FOR DIFFERENT POSITIONS OF A SQUARE INNER COLLECTOR. M/E=40. (A) ○□○, (B) ○◇○.

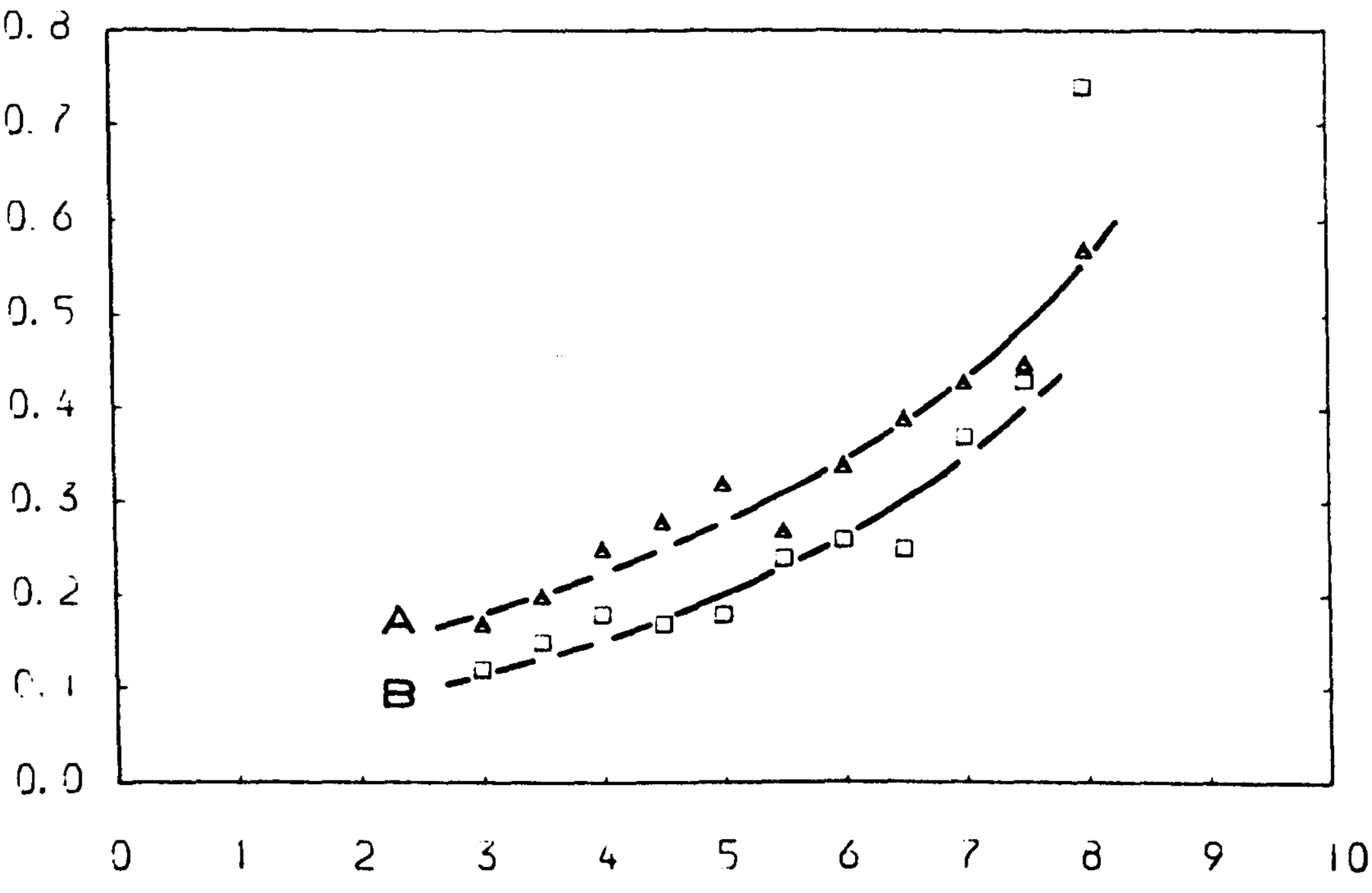

FIG. 4.7.5.B. PEAK WIDTH AS A FUNCTION OF ION ENERGY FOR DIFFERENT POSITIONS OF A SQUARE INNER COLLECTOR.
M/E=40. (A) ○□○ ○ (B) ○◇○ ○.

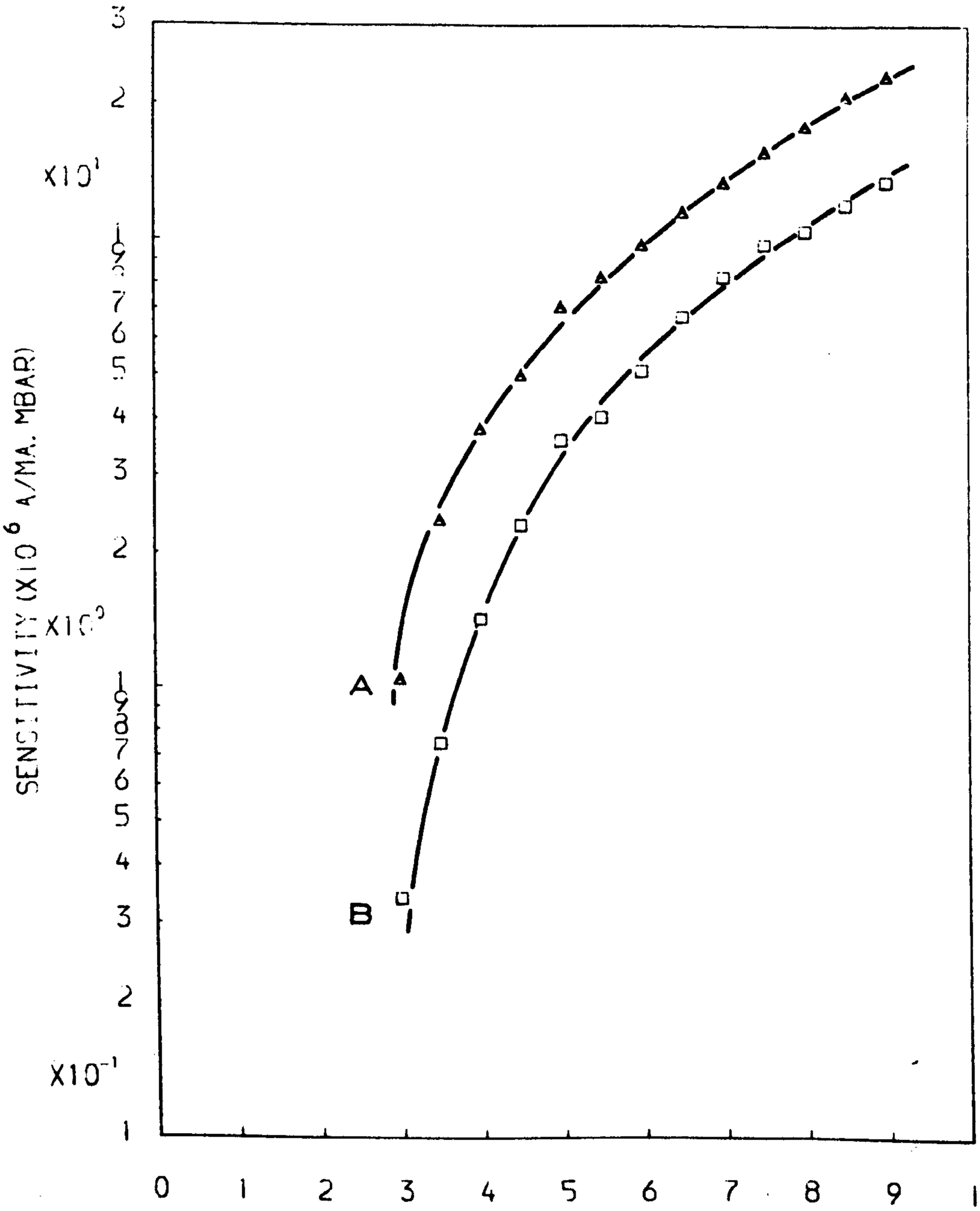

FIG. 4.7.6.A. SENSITIVITY AS A FUNCTION OF ION ENERGY FOR DIFFERENT POSITIONS OF A SQUARE INNER COLLECTOR.

M/E=84 (A) (B)

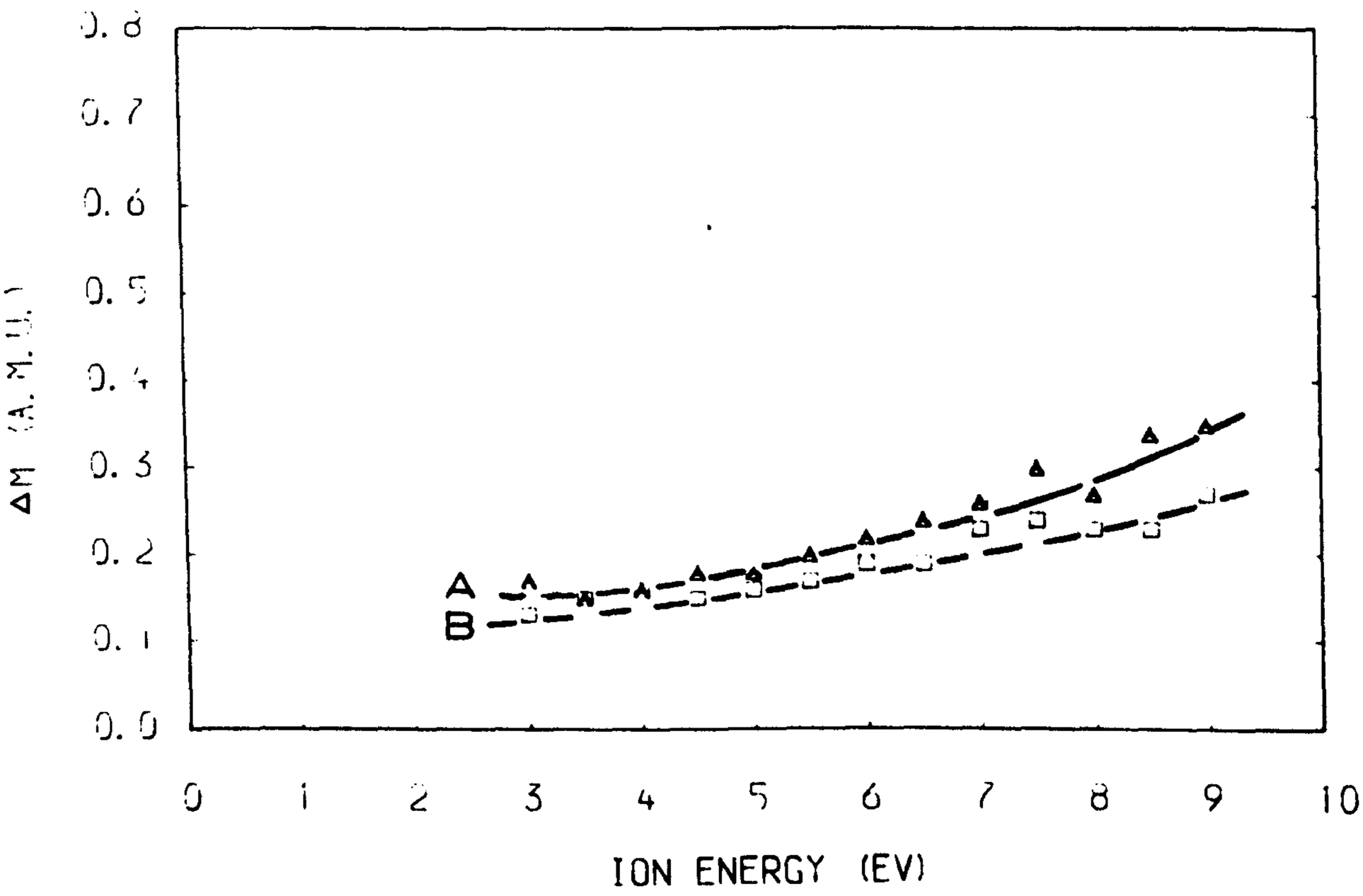

FIG. 4.7.6.B. PEAK WIDTH AS A FUNCTION OF ION ENERGY FOR DIFFERENT POSITIONS OF A SQUARE INNER COLLECTOR.

M/E=84 (A)  (B) 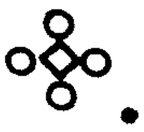

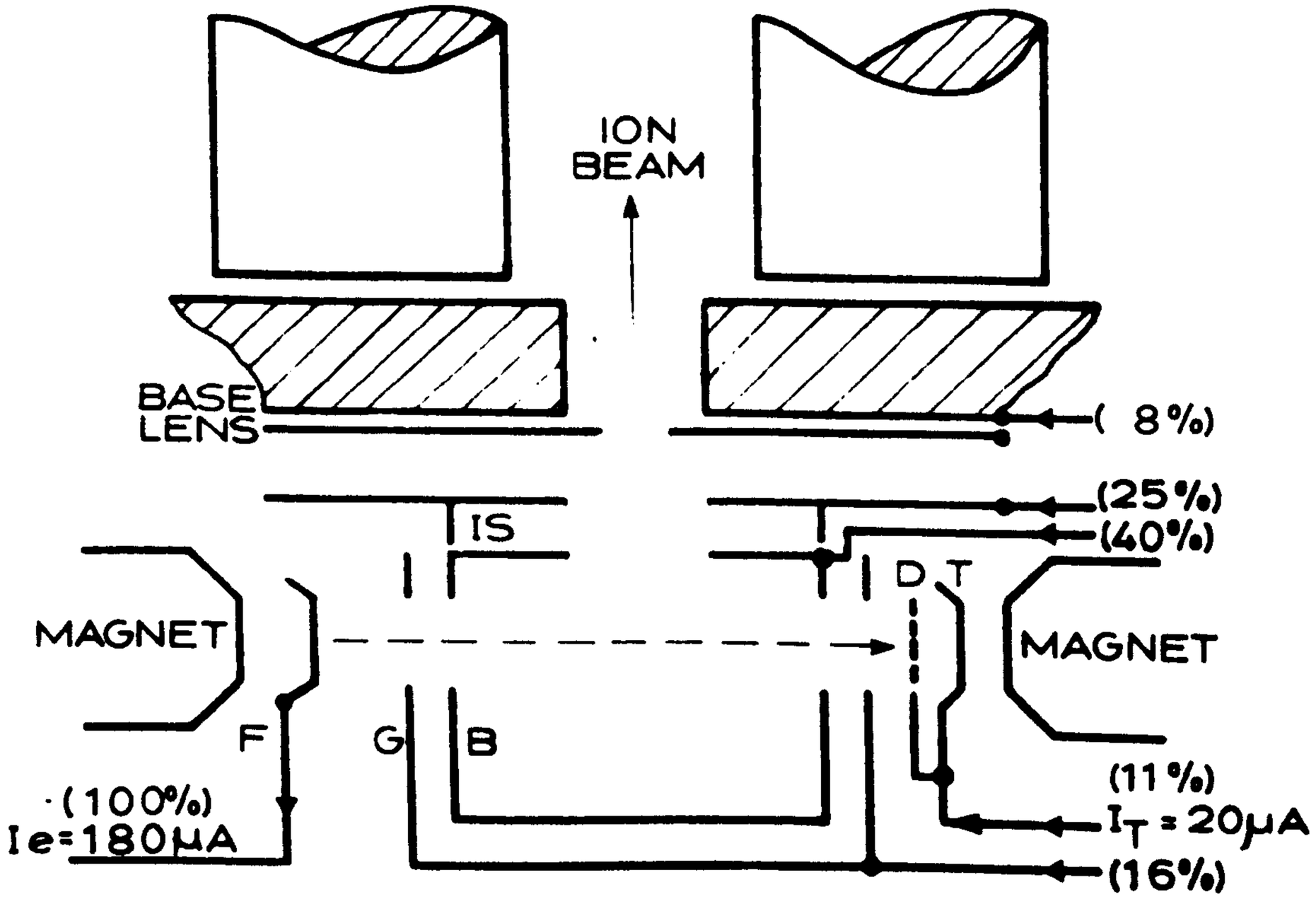

FIG. 4.8.1. DISTRIBUTION OF EMISSION CURRENT IN THE NIER SOURCE.

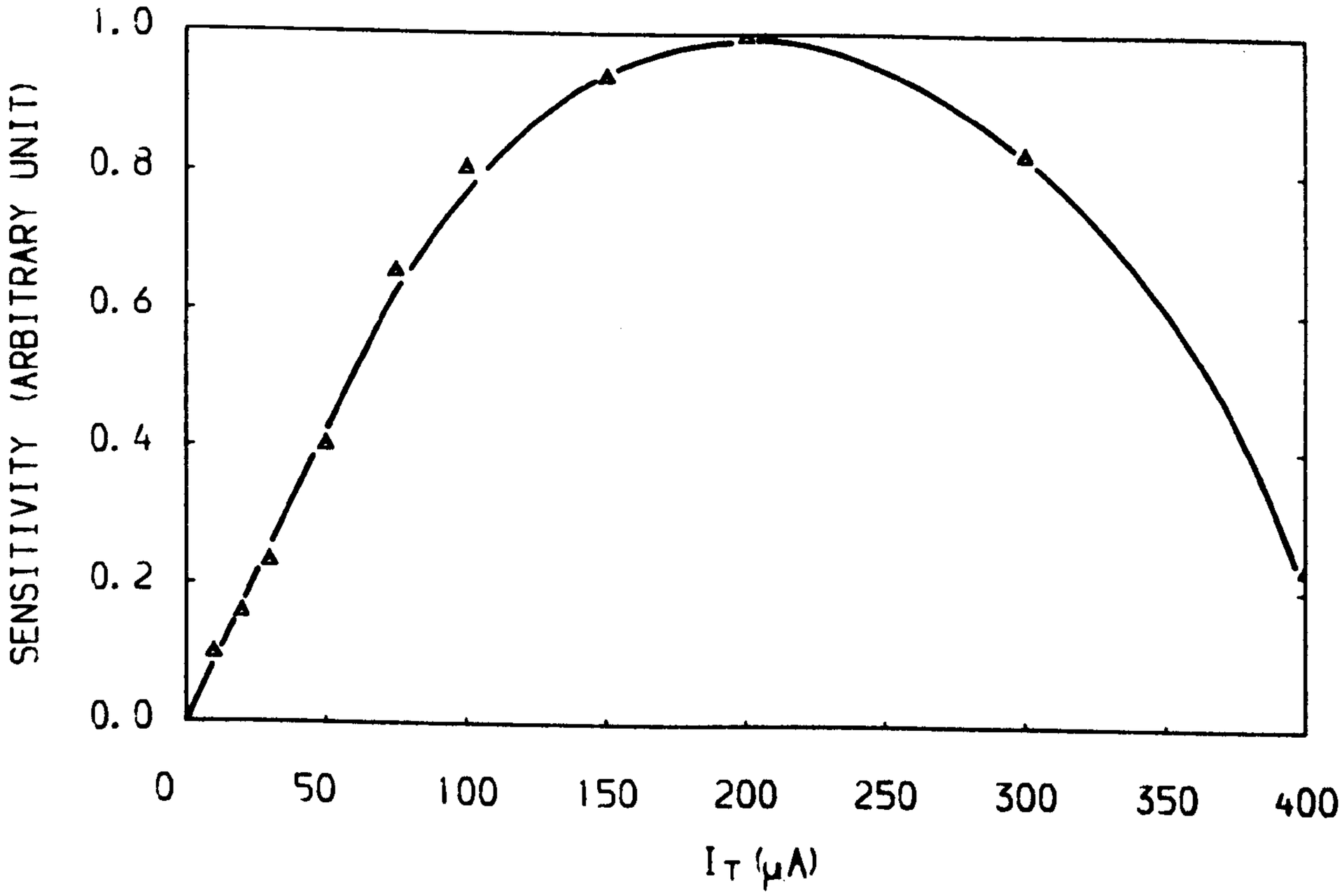

FIG. 4.8.2.A. SENSITIVITY AS A FUNCTION OF THE TRAP CURRENT.

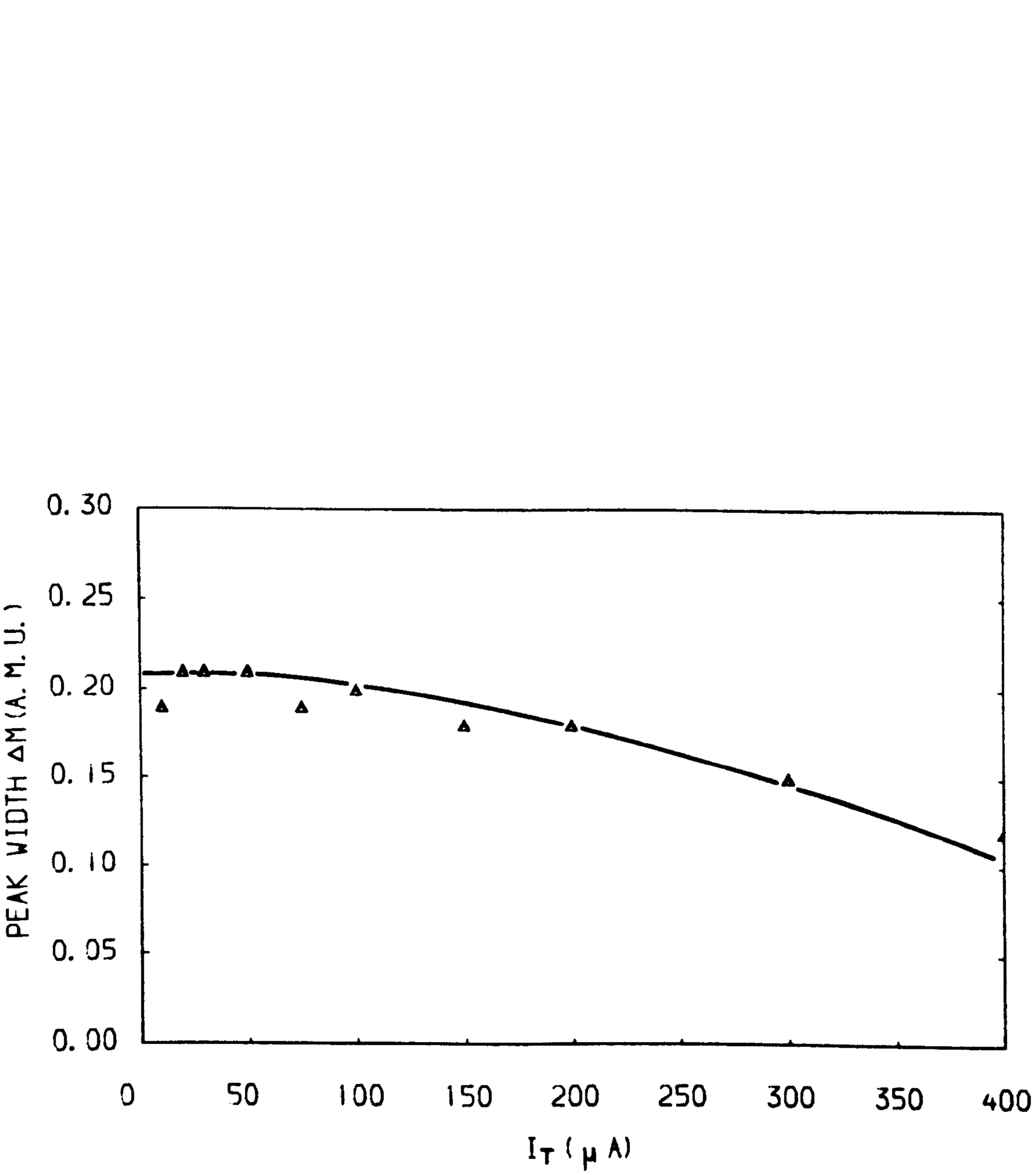

FIG. 4. 8. 2. B. PEAK WIDTH AS A FUNCTION OF THE TRAP CURRENT.

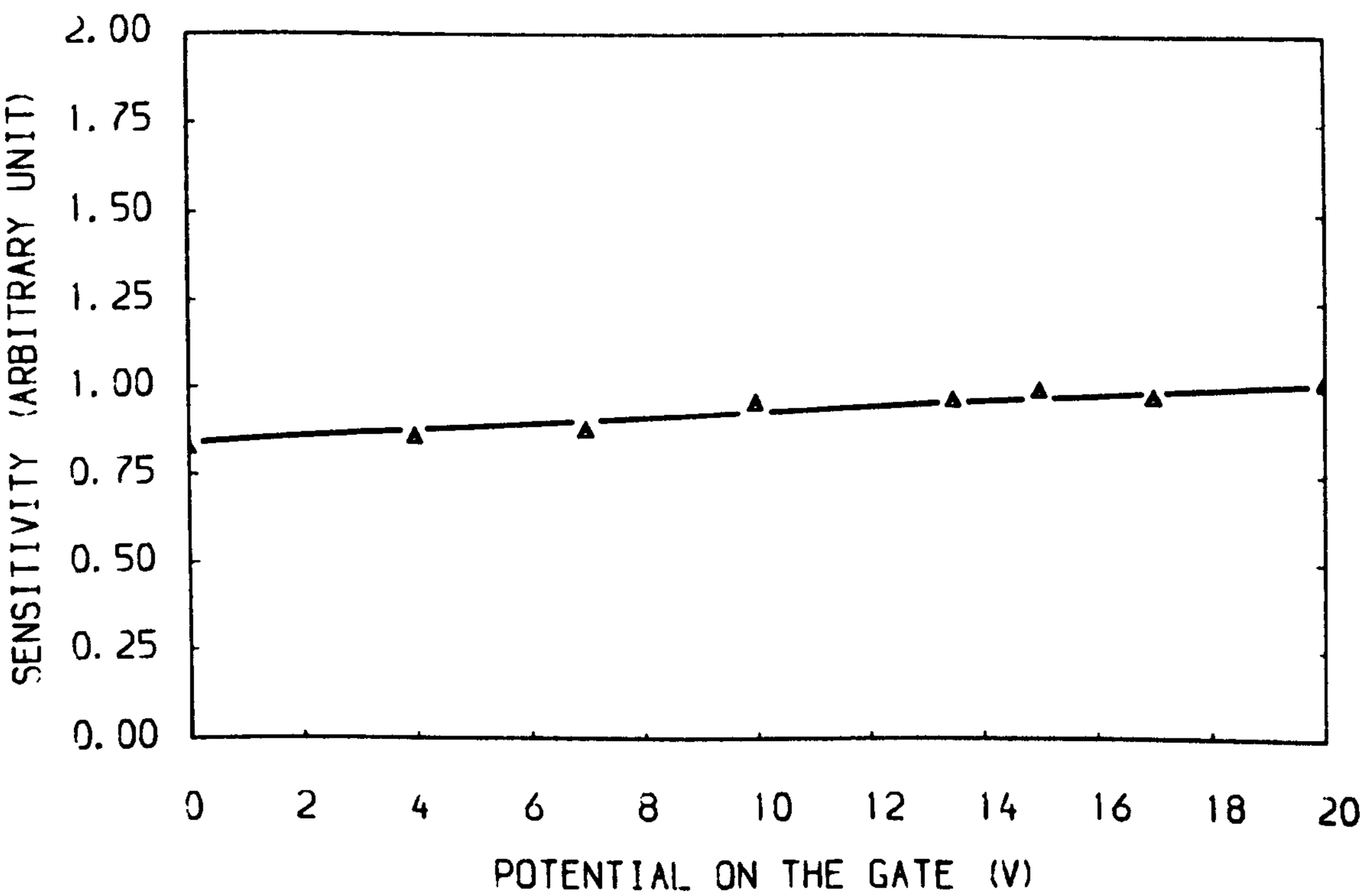

FIG. 4. 8. 3. A. SENSITIVITY AS A FUNCTION OF THE GATE POTENTIAL. THE SENSITIVITY AT U_G=15V WITH U_B=4V, U_L=-50V, U_T=6V, I_T=20μA IS REGARDED AS 1. M/E=14, F=4MHZ.

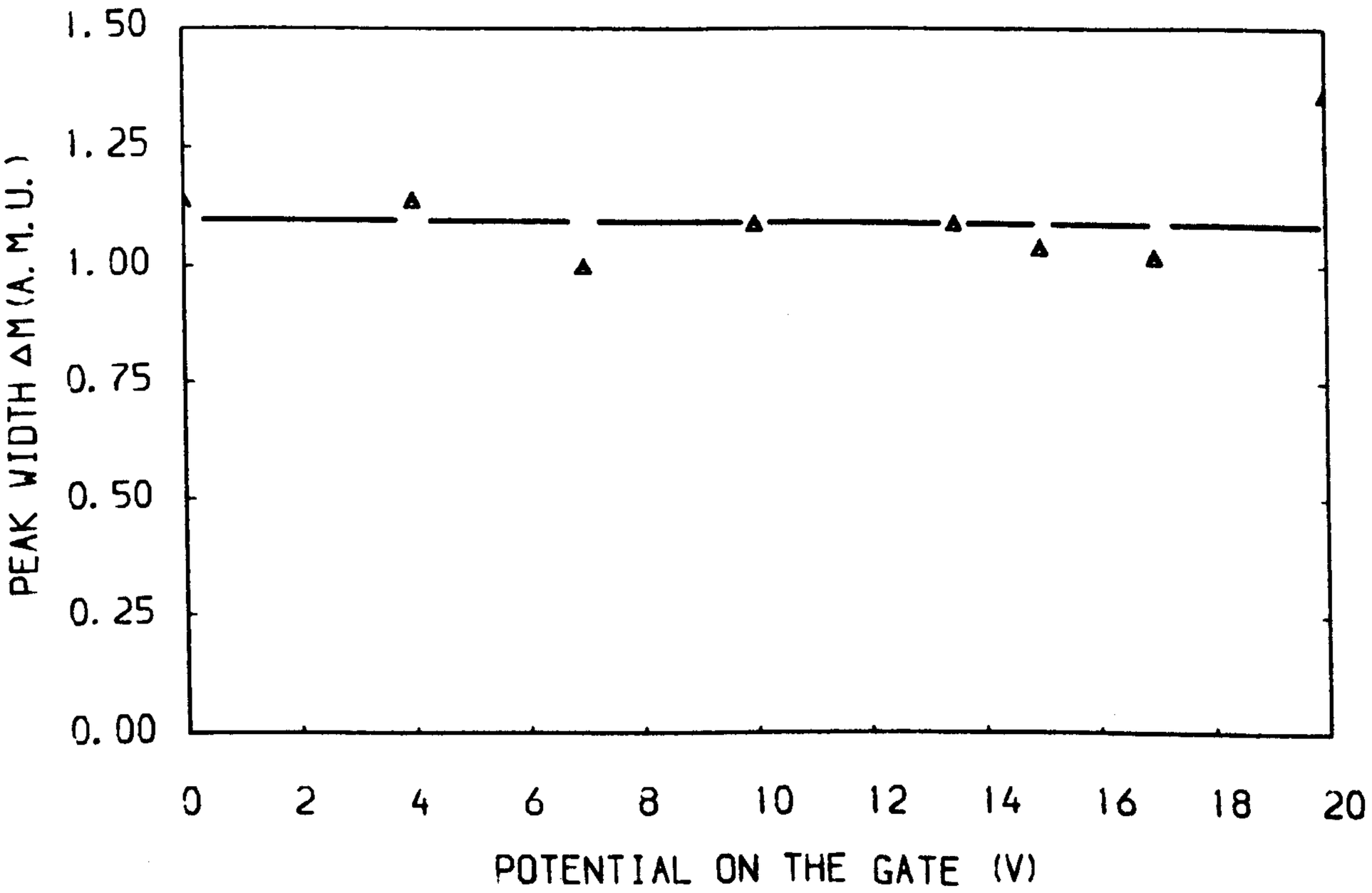

FIG. 4.8.3.B. PEAK WIDTH AS A FUNCTION OF THE GATE POTENTIAL.

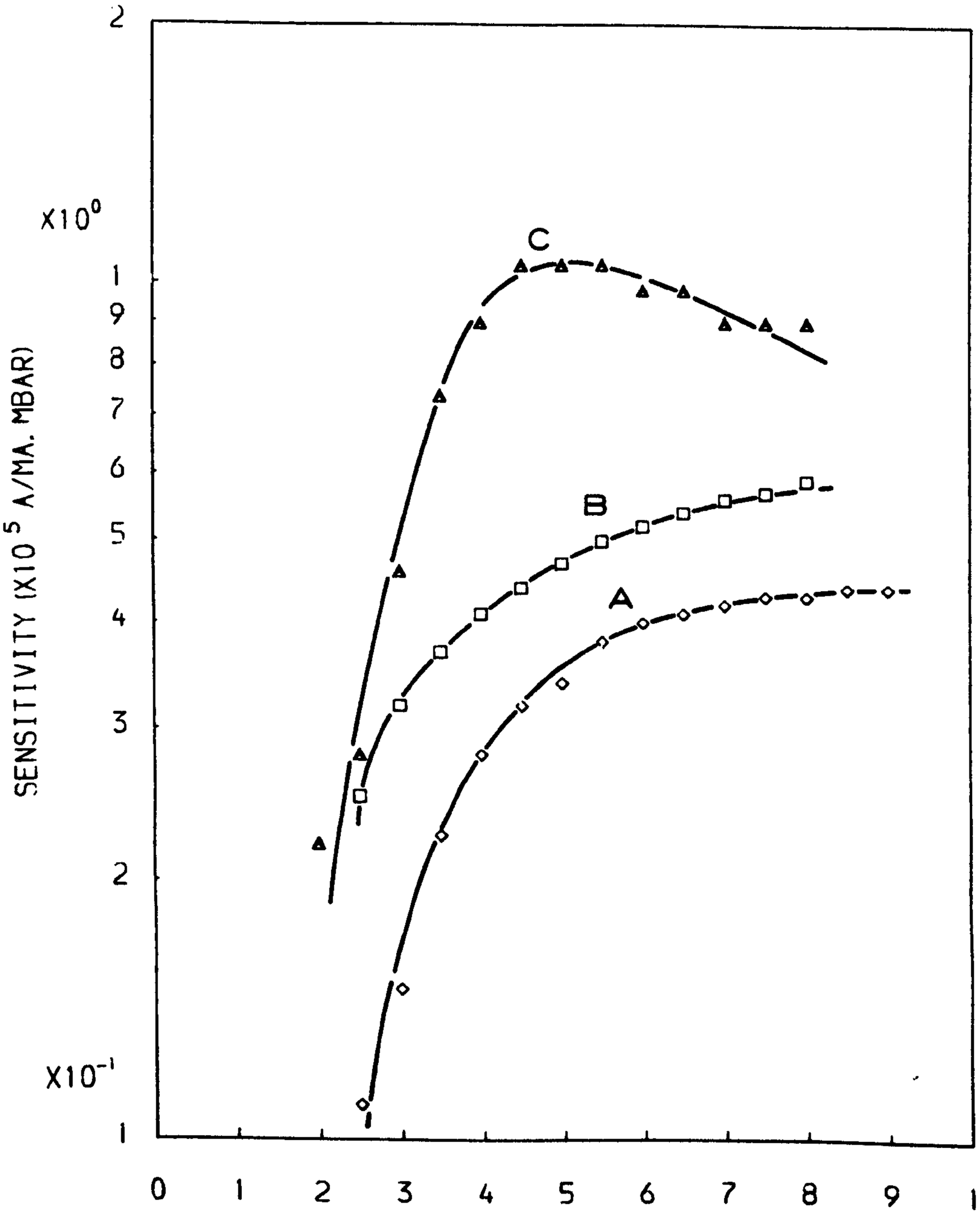

FIG. 4.8.4.A. EFFECT OF ALIGNMENT AND CONSTRUCTION OF ION OPTIC SYSTEM ON THE SENSITIVITY OF THE ANALYSER.

A ◇ NON-ALIGNED WITH 5.2MM OUTLET

B □ ALIGNED WITH 5.2MM OUTLET

C △ ALIGNED WITH 3.0MM OUTLET

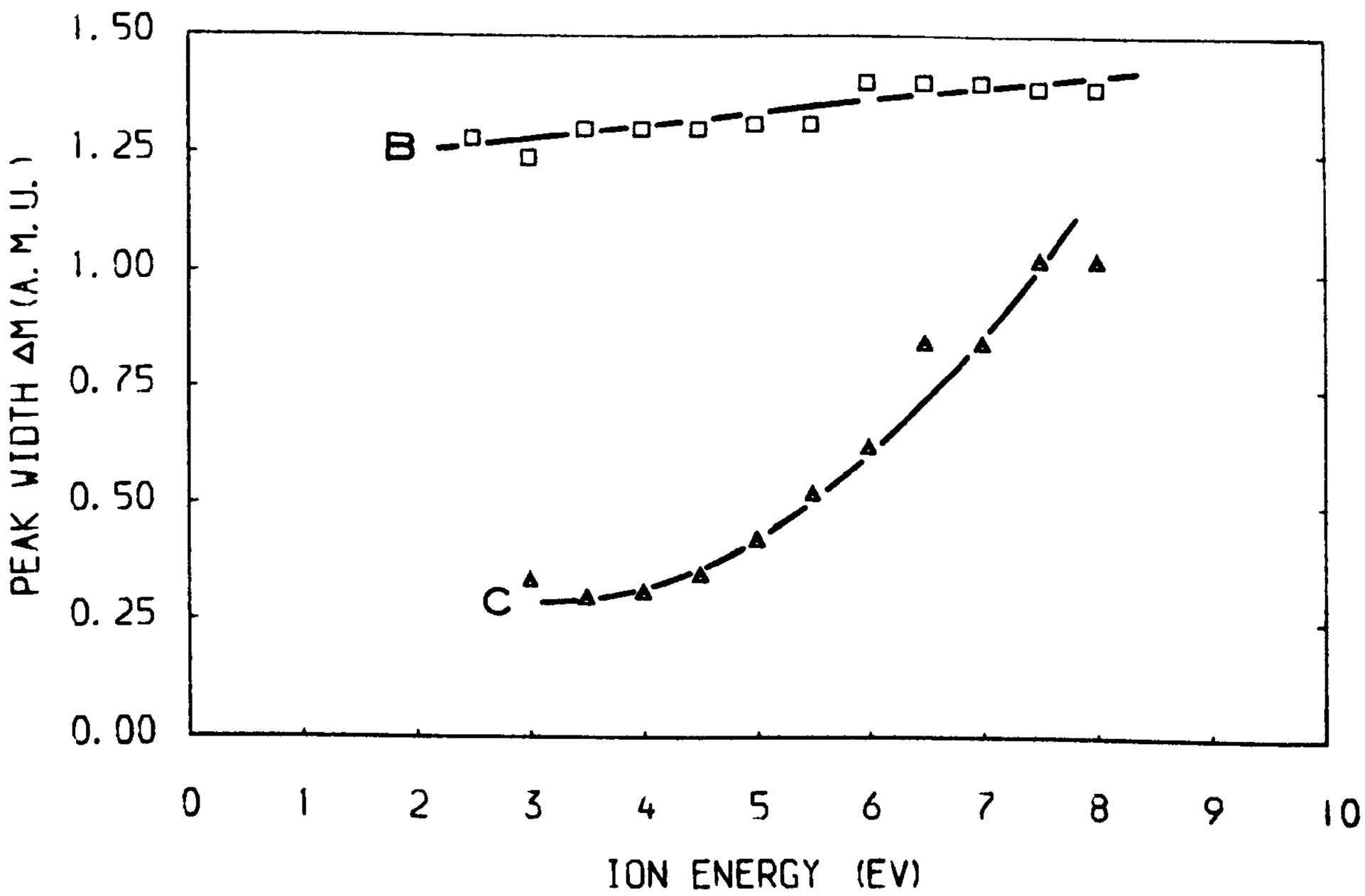

FIG. 4.8.4.8. EFFECT OF THE CONSTRUCTION OF ION OPTIC SYSTEM ON THE PEAK WIDTH.

B □ ALIGNED WITH 5.2MM OUTLET

C △ ALIGNED WITH 3.0MM OUTLET

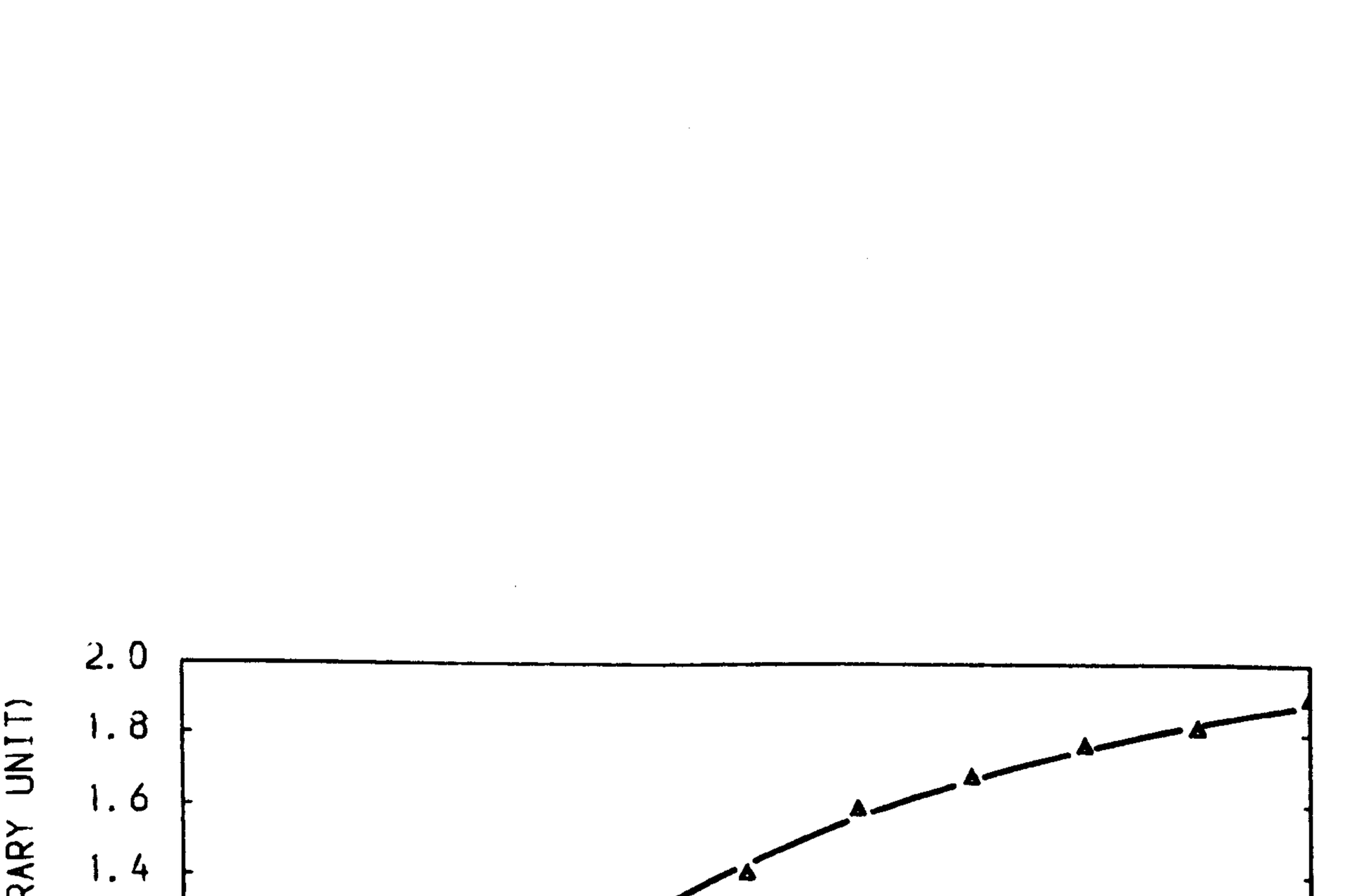

FIG. 4.8.5.A. SENSITIVITY AS A FUNCTION OF POTENTIAL ON THE LENS. THE SENSITIVITY AT U_L=-50V WITH U_B=4V, U_G=15V, U_T=6V, I_T=20μA IS REGARDED AS 1. M/E=14, F=4MHZ.

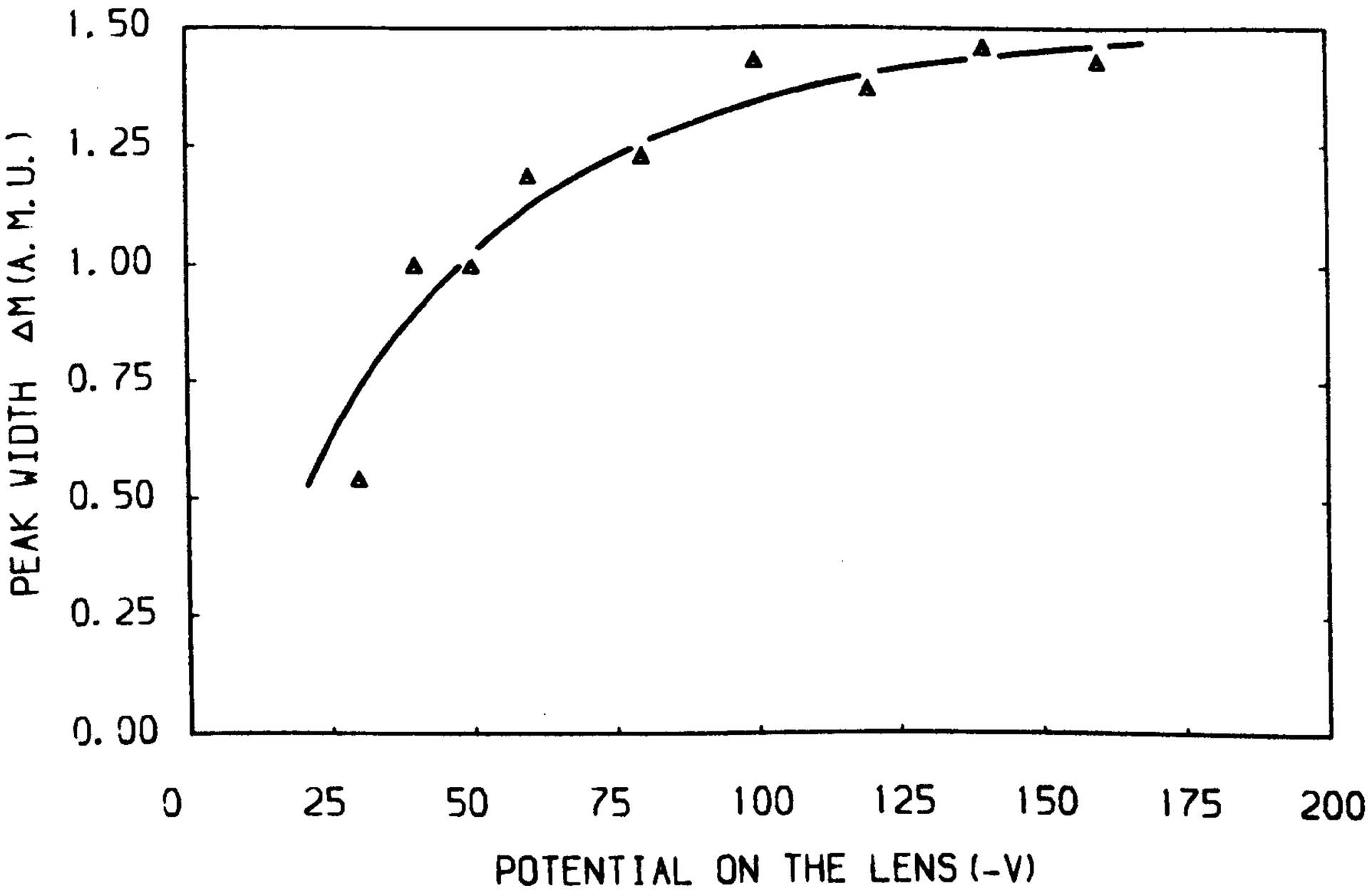

FIG. 4.8.5.B. PEAK WIDTH AS A FUNCTION OF POTENTIAL ON THE LENS OF THE NIER SOURCE. M/E=14, F=4MHZ.

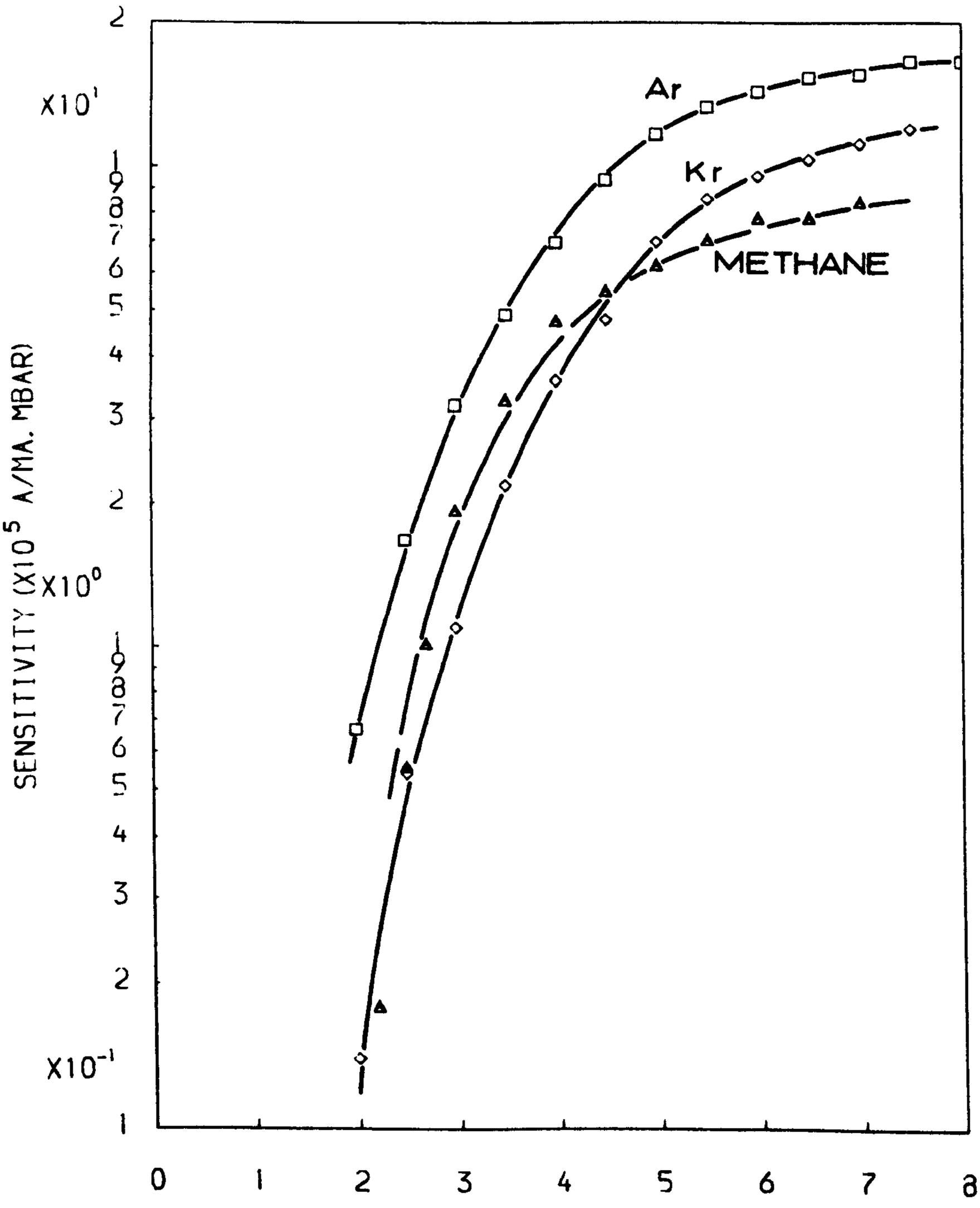

FIG. 4.8.6. SENSITIVITY AS A FUNCTION OF ION ENERGY.
METHANE (△), ARGON (□) AND KRYPTON (◇). F=3MHZ.

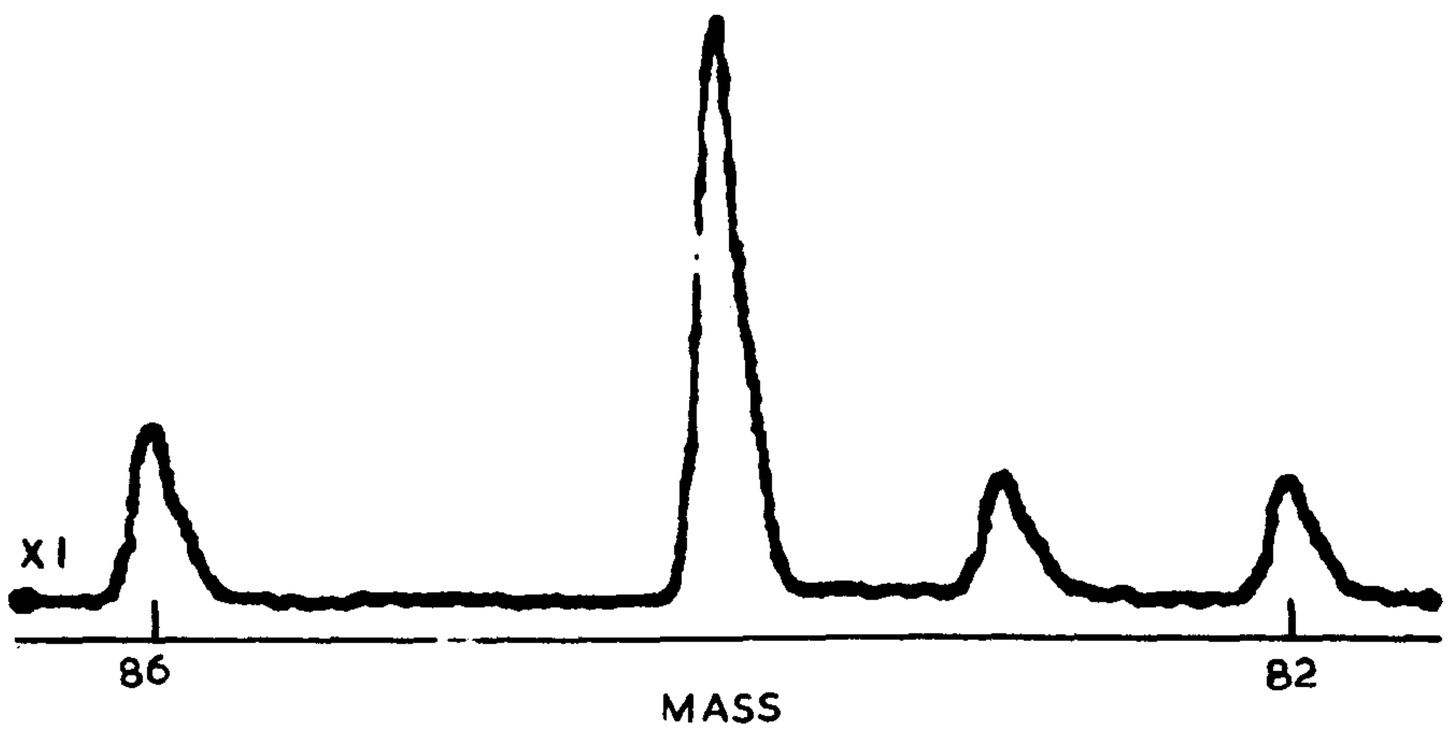

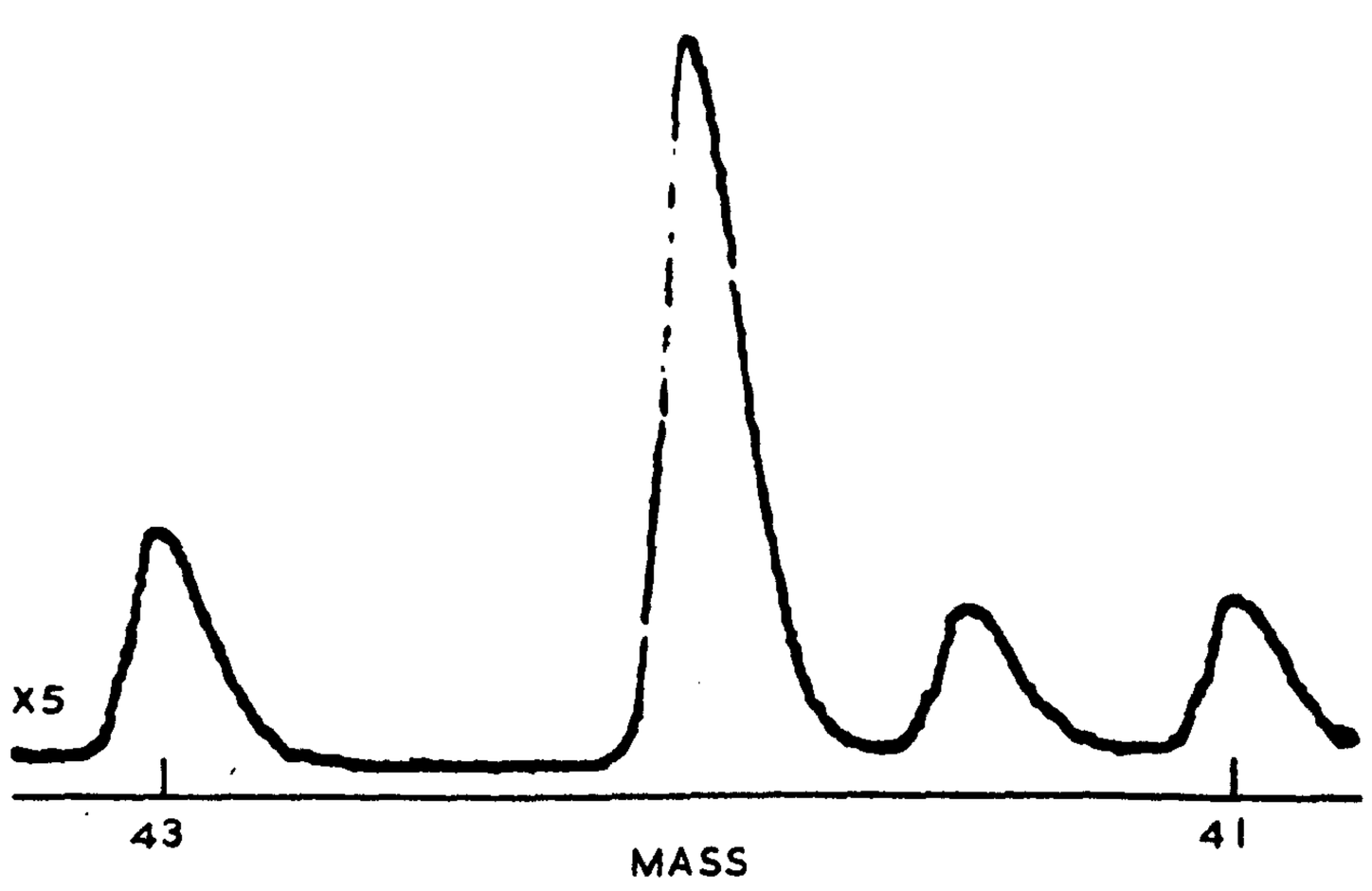

FIG. 4.8.7. RELEVANT PORTIONS OF KRYPTON SPECTRUM.
F=4MHZ, U_B=4V.

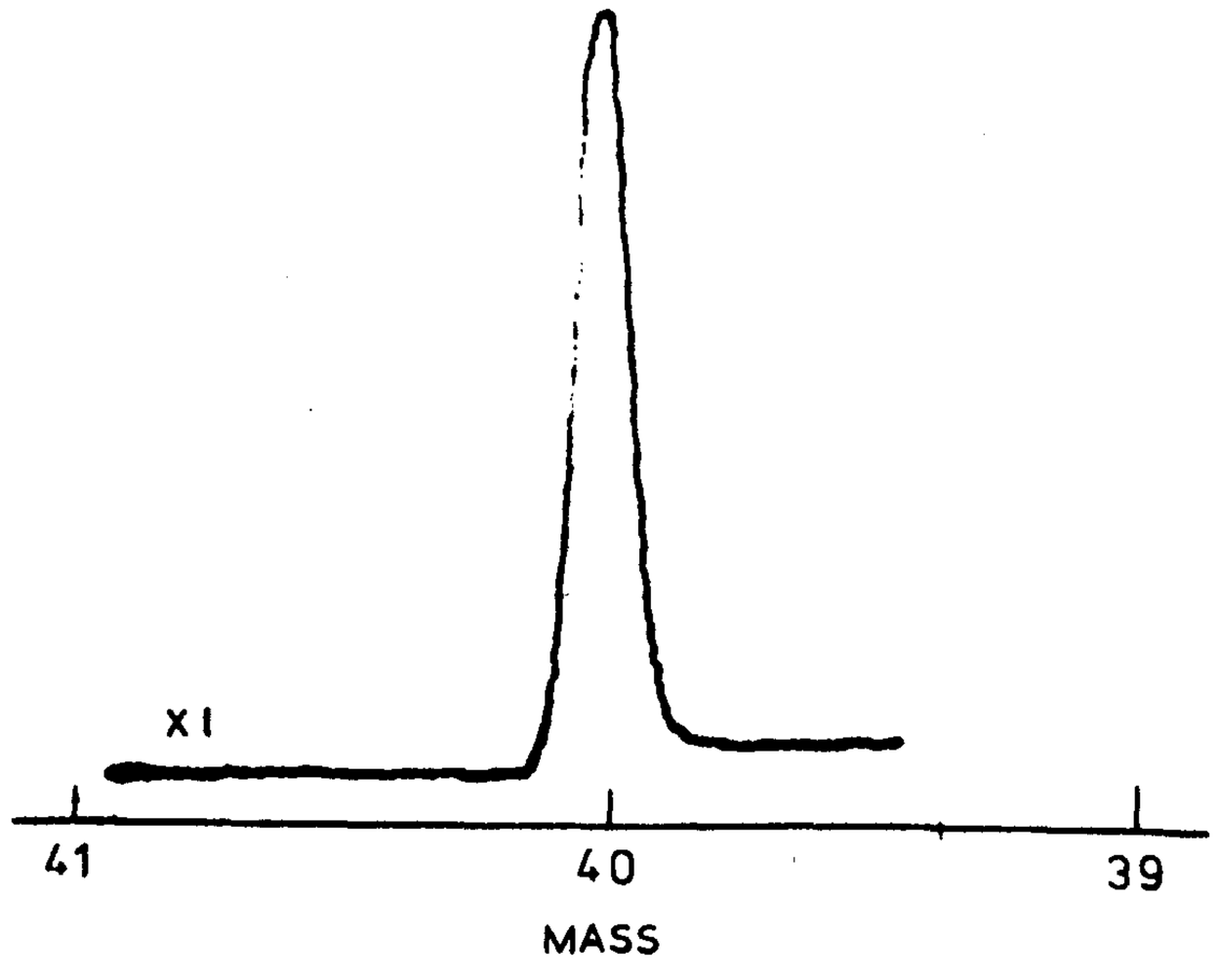

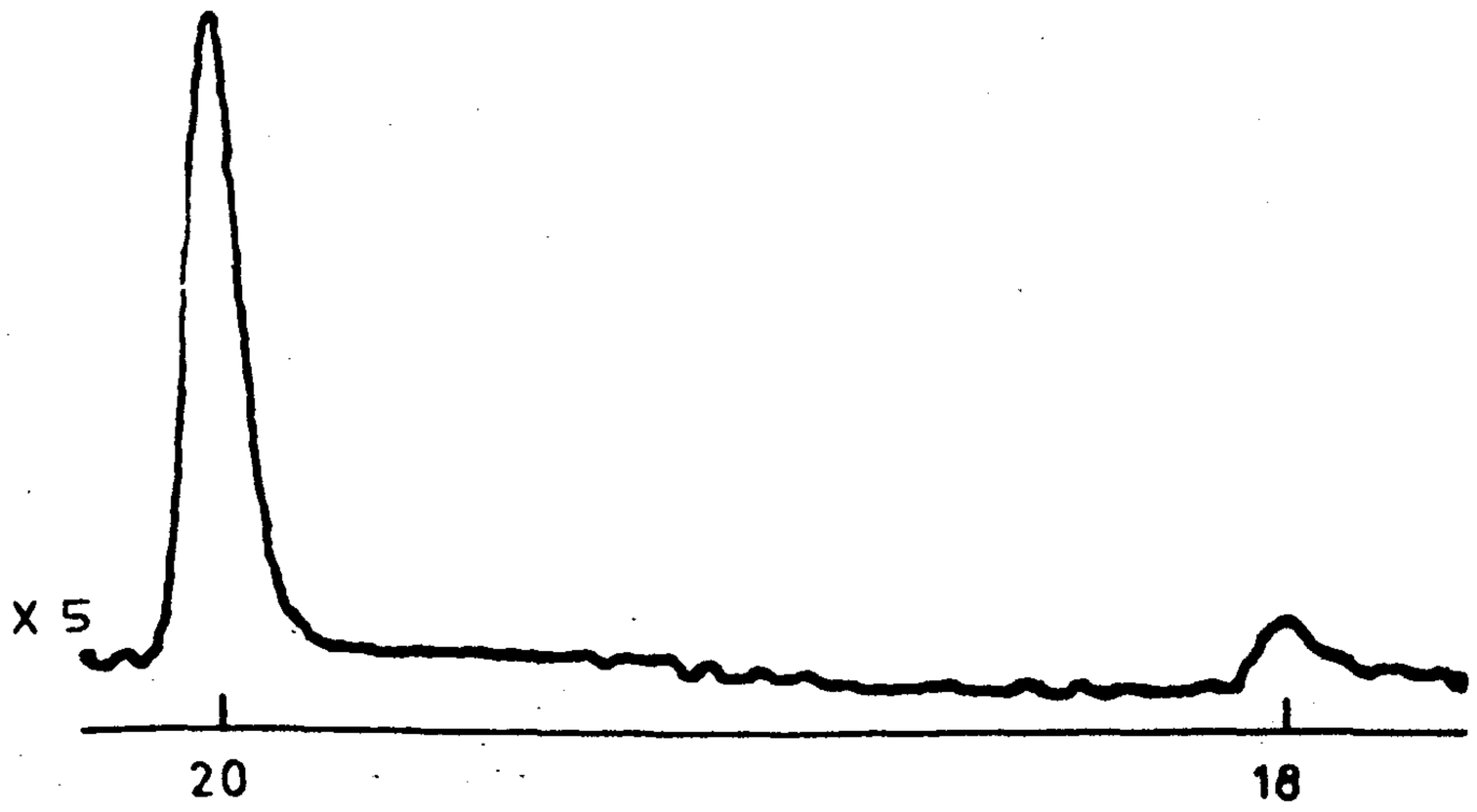

FIG. 4.8.8. RELEVANT PORTIONS OF ARGON SPECTRUM.
F=4MHZ, U_B=3V.

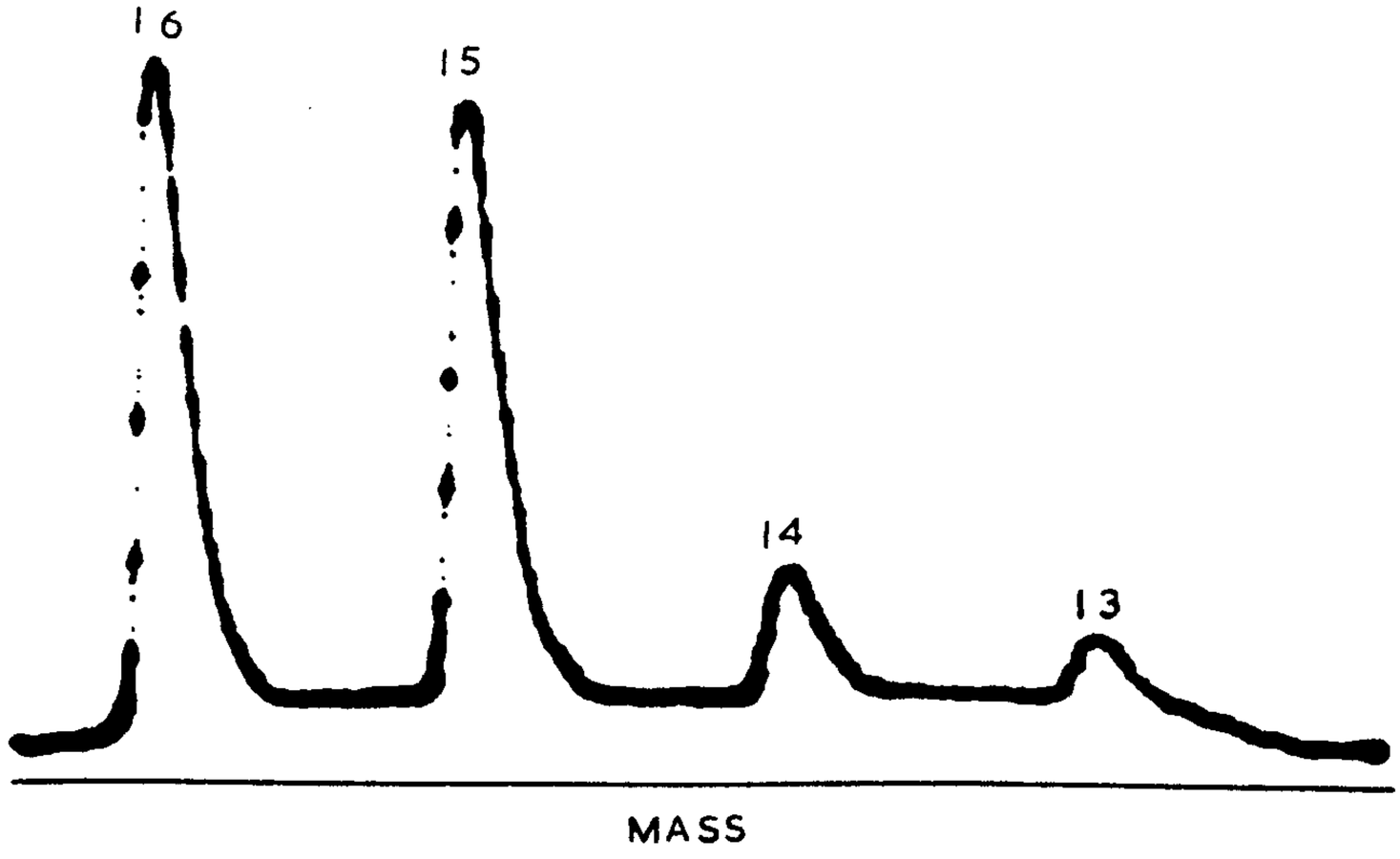

FIG. 4.8.9. A TYPICAL SPECTRUM OF METHANE. F=3MHZ, U_B=3V.

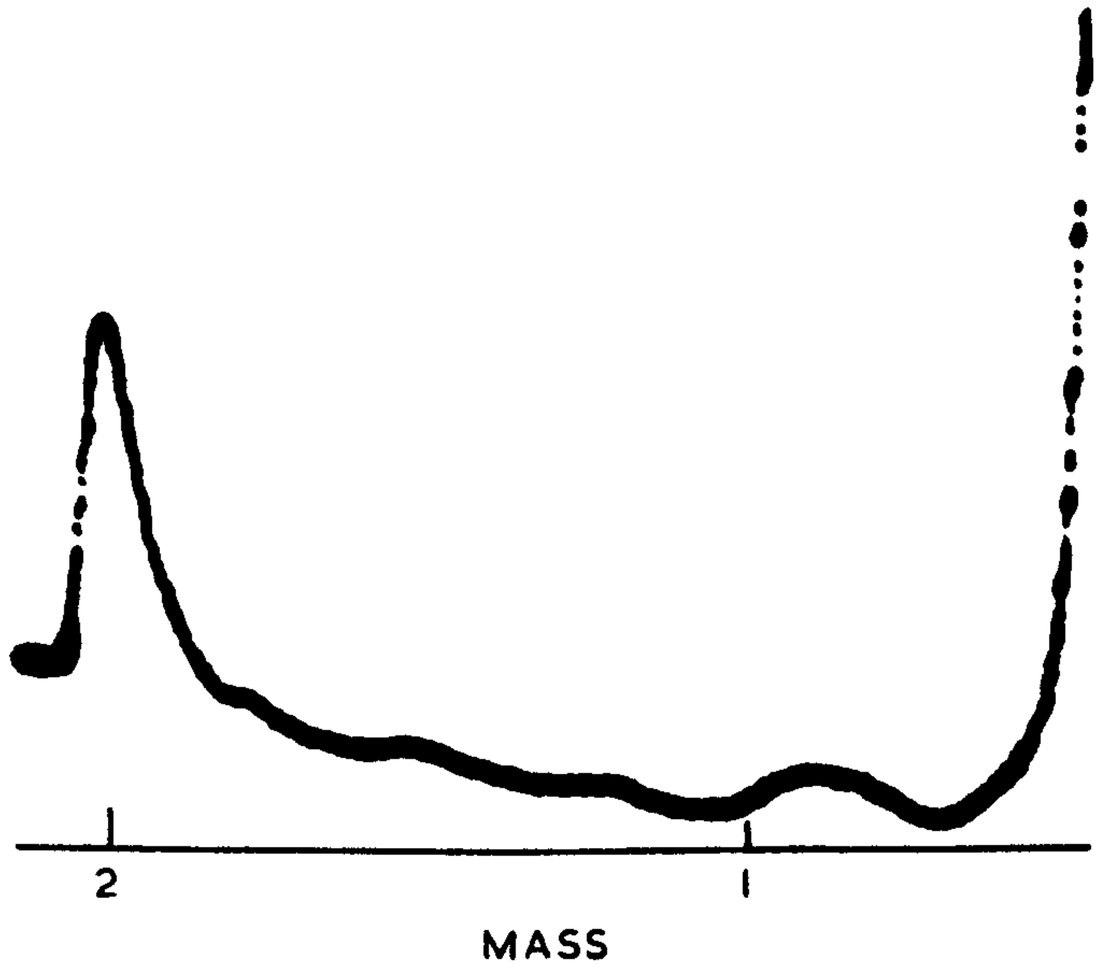

FIG. 4.8.10. A H_2 PEAK OBTAINED BY THE 50MM QUADRUPOLE MASS ANALYSER WITH THE NIER SOURCE IN THE A.C. MODE. F=3MHZ, U_B =2.4 V.

Table 4.8.1. The sensitivity and resolution of the 50 mm quadrupole filter with the Nier source for different gases.

Gases	Krypton	Argon	Methane	Hydrogen
M/e	84	40	16	2
S(A/ma.mbar)	$3x10^{-5}$	$2x10^{-5}$	$2x10^{-5}$	$6x10^{-6}$
ΔM(a.m.u.)	0.18	0.12	0.18	0.10

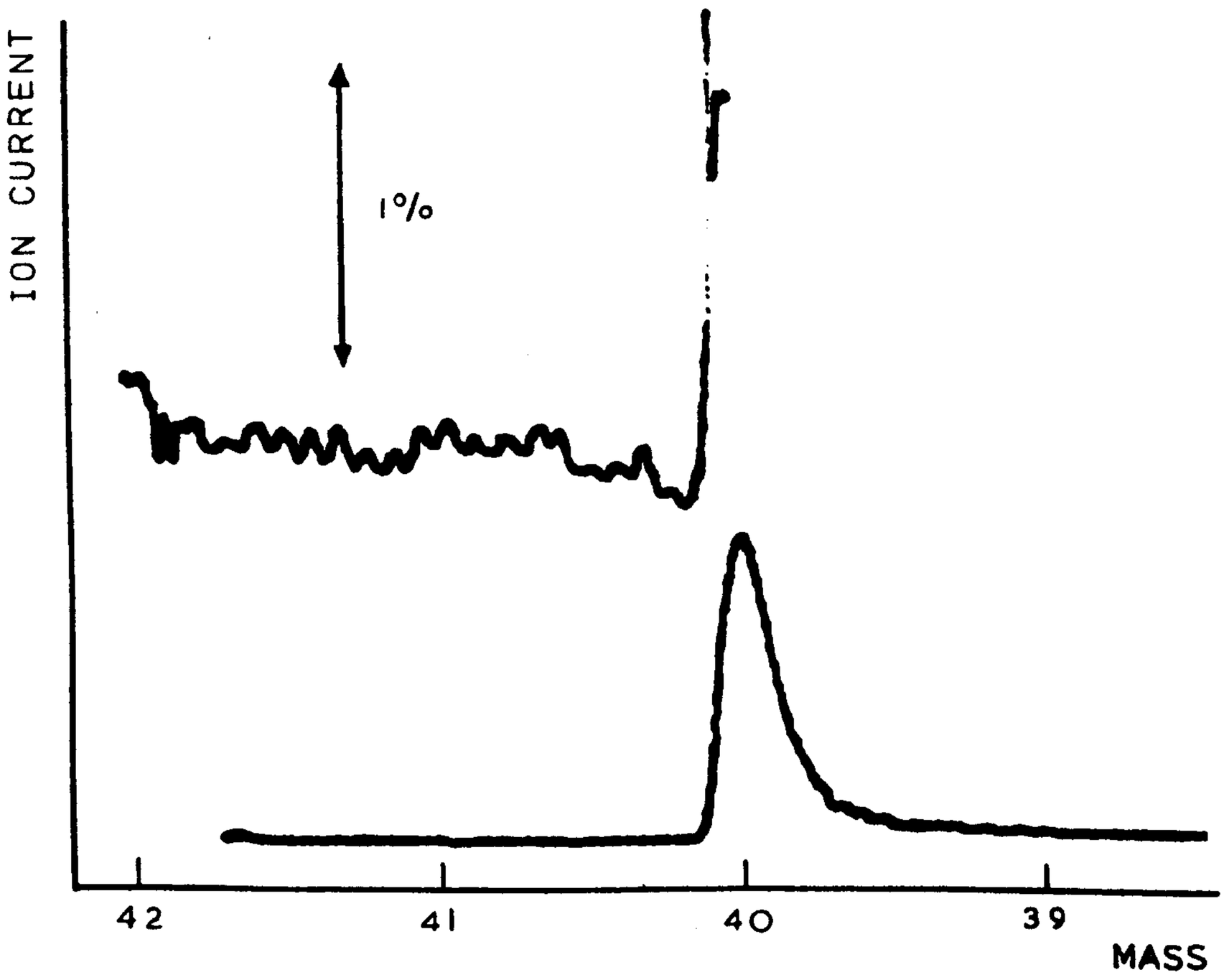

FIG. 4.8.11. DIAGRAM SHOWING THE INTERFERENCE ON THE HIGH MASS SIDE OF THE ARGON PEAK.

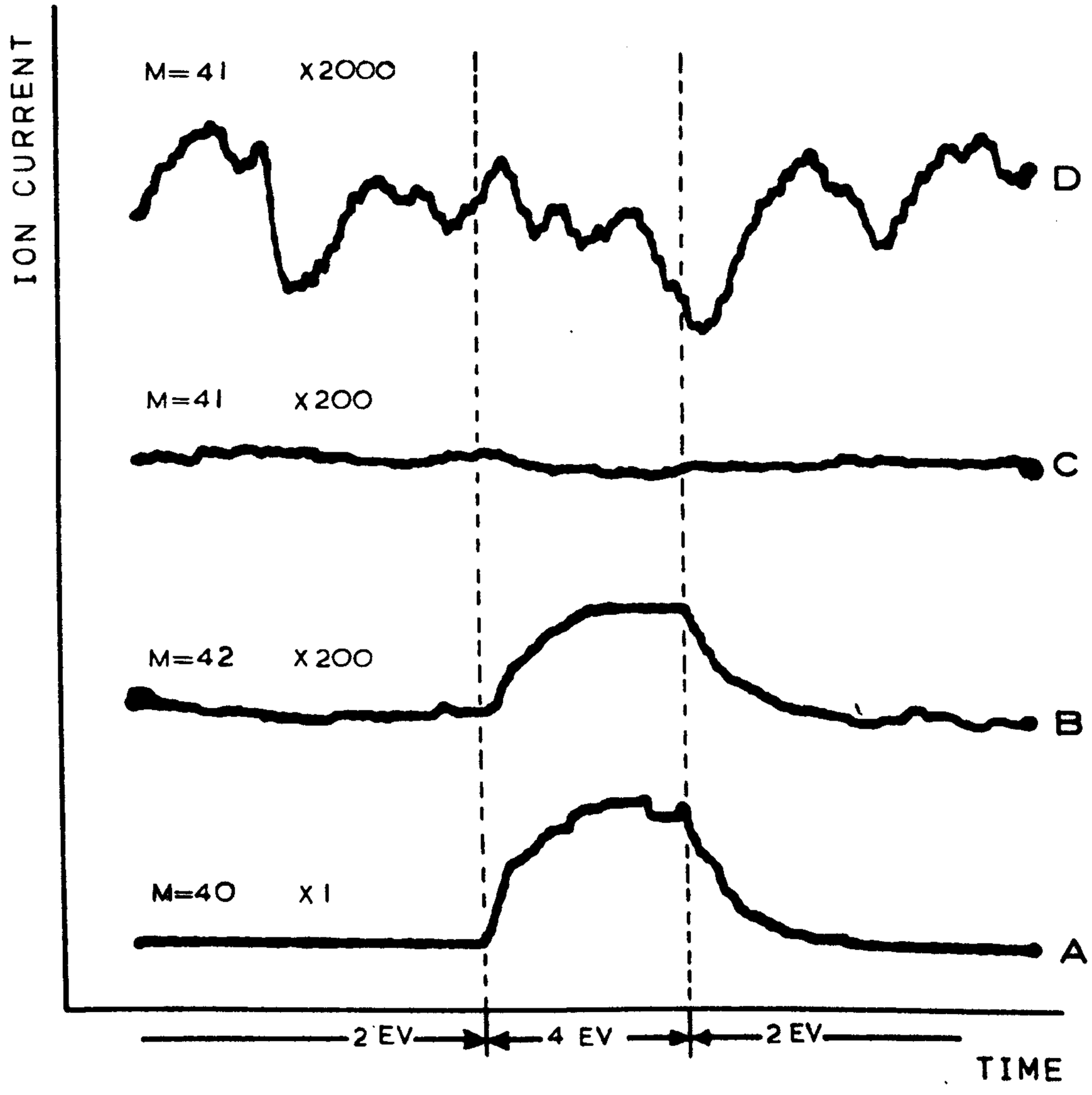

FIG. 4.8.12. DIAGRAM SHOWING THE INTERFERENCE AT M/E=41 BY THE ARGON PEAK.

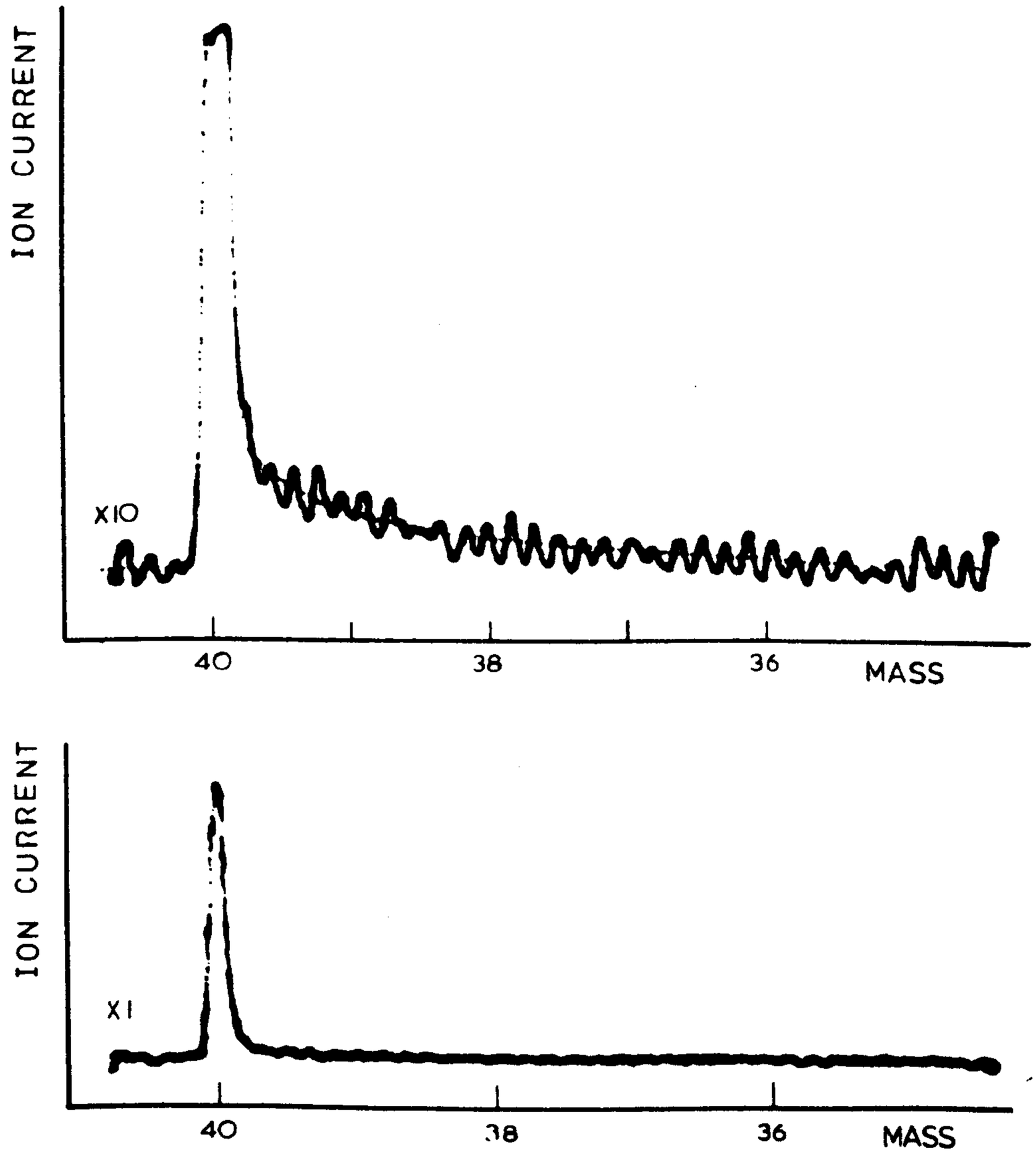

FIG. 4.8.13. DIAGRAM SHOWING THE INTERFERENCE ON THE LOW MASS SIDE OF THE ARGON PEAK AT F=3 MHZ.

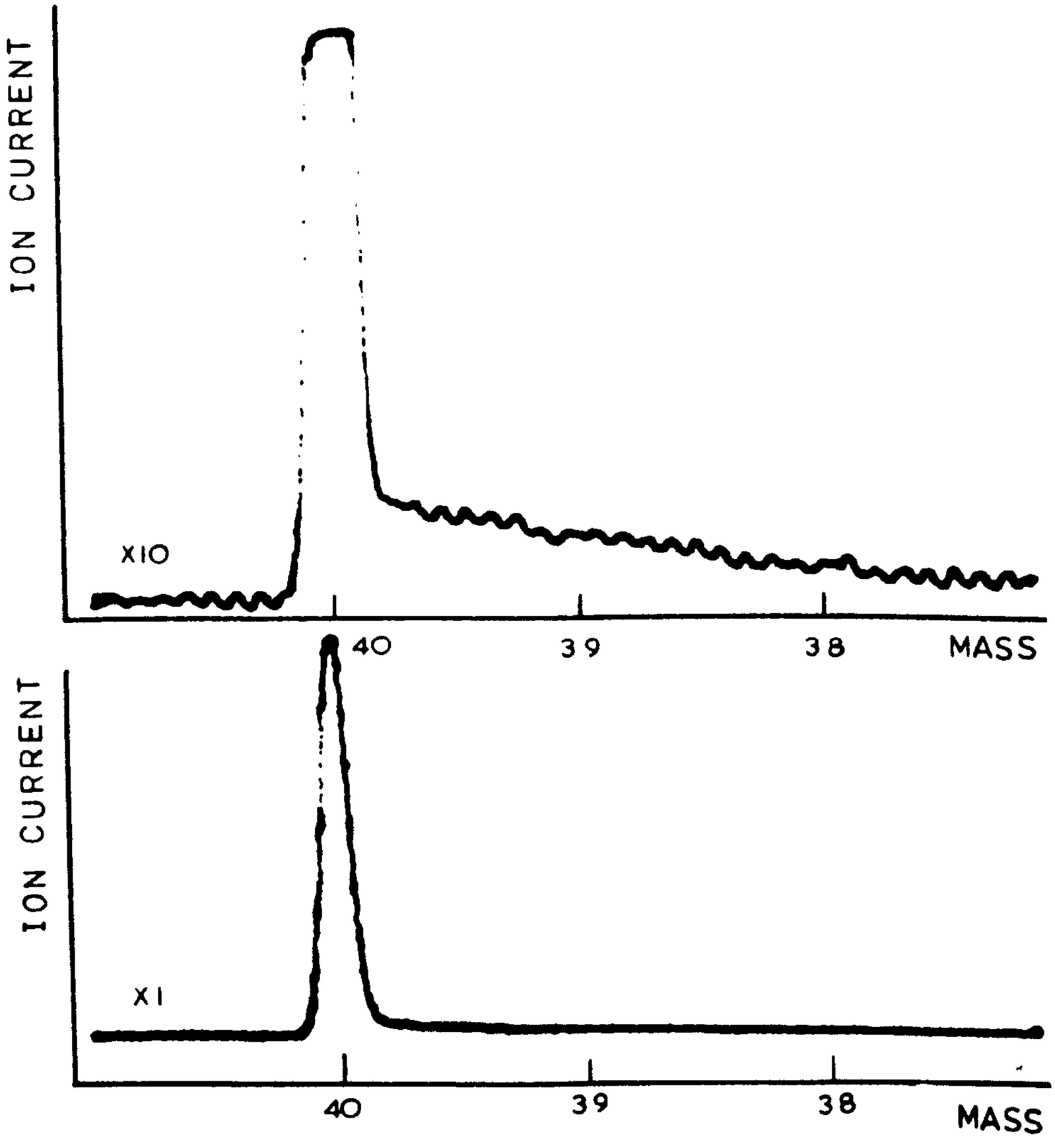

FIG. 4.8.14. DIAGRAM SHOWING THE INTERFERENCE ON THE LOW MASS SIDE OF THE ARGON PEAK AT F=4 MHZ.

TABLE 4.8.2. Interference at the low mass side of the argon peak for different operating frequencies. The data were obtained with the 50 mm filter using the Nier source at the ion energy of 4 eV. The reference argon peak was regarded as 100%.

Mass	Interference (%)	
	3 MHz	4 MHz
39	2.5	1.8
38	2.0	0.8
37	1.0	0.3
36	1.0	

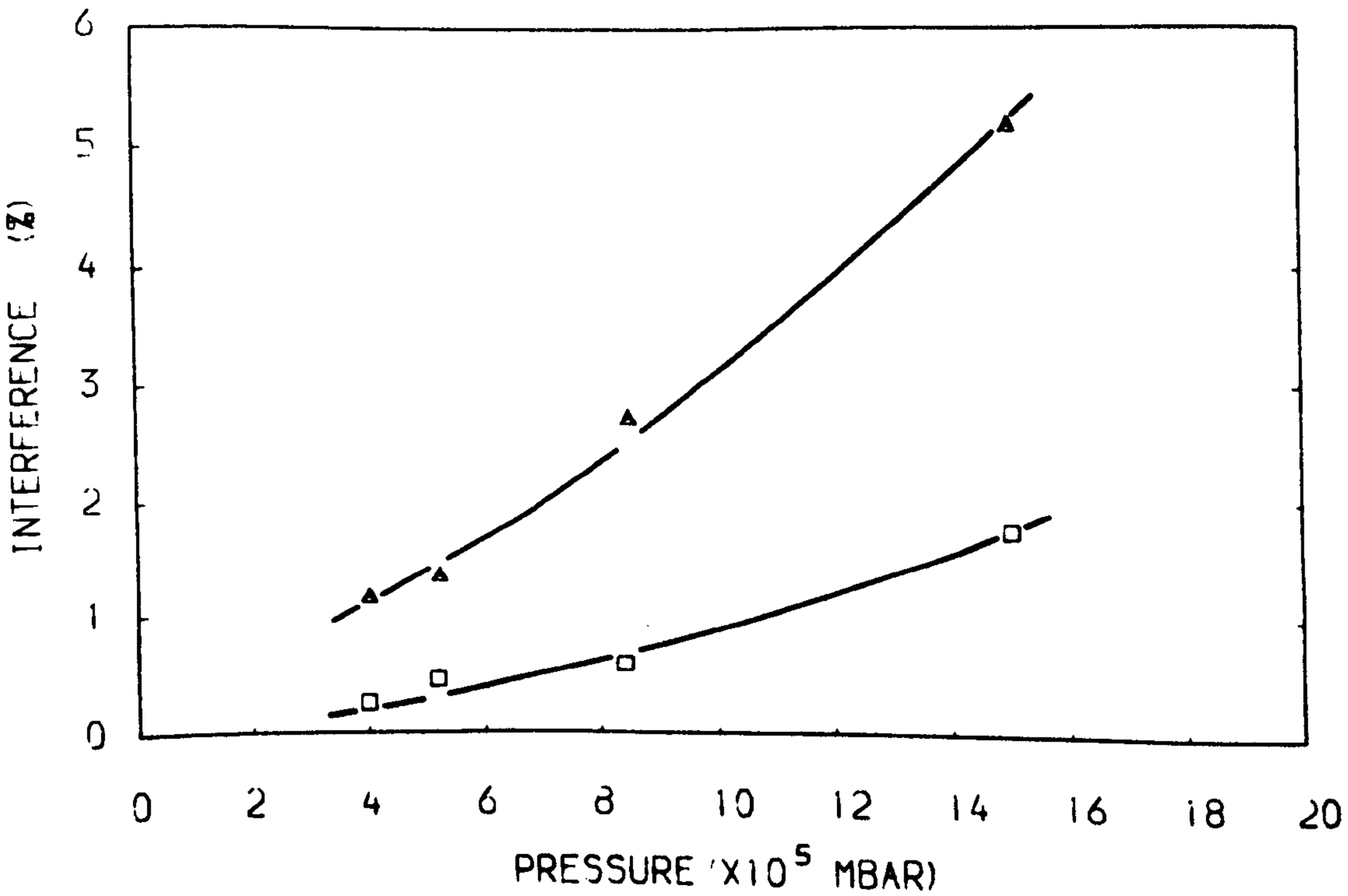

FIG. 4.8.15. THE INTERFERENCE ON THE LOW MASS SIDE OF THE ARGON PEAK AS A FUNCTION OF PRESSURE. F=4 MHZ, U_B=3 V.

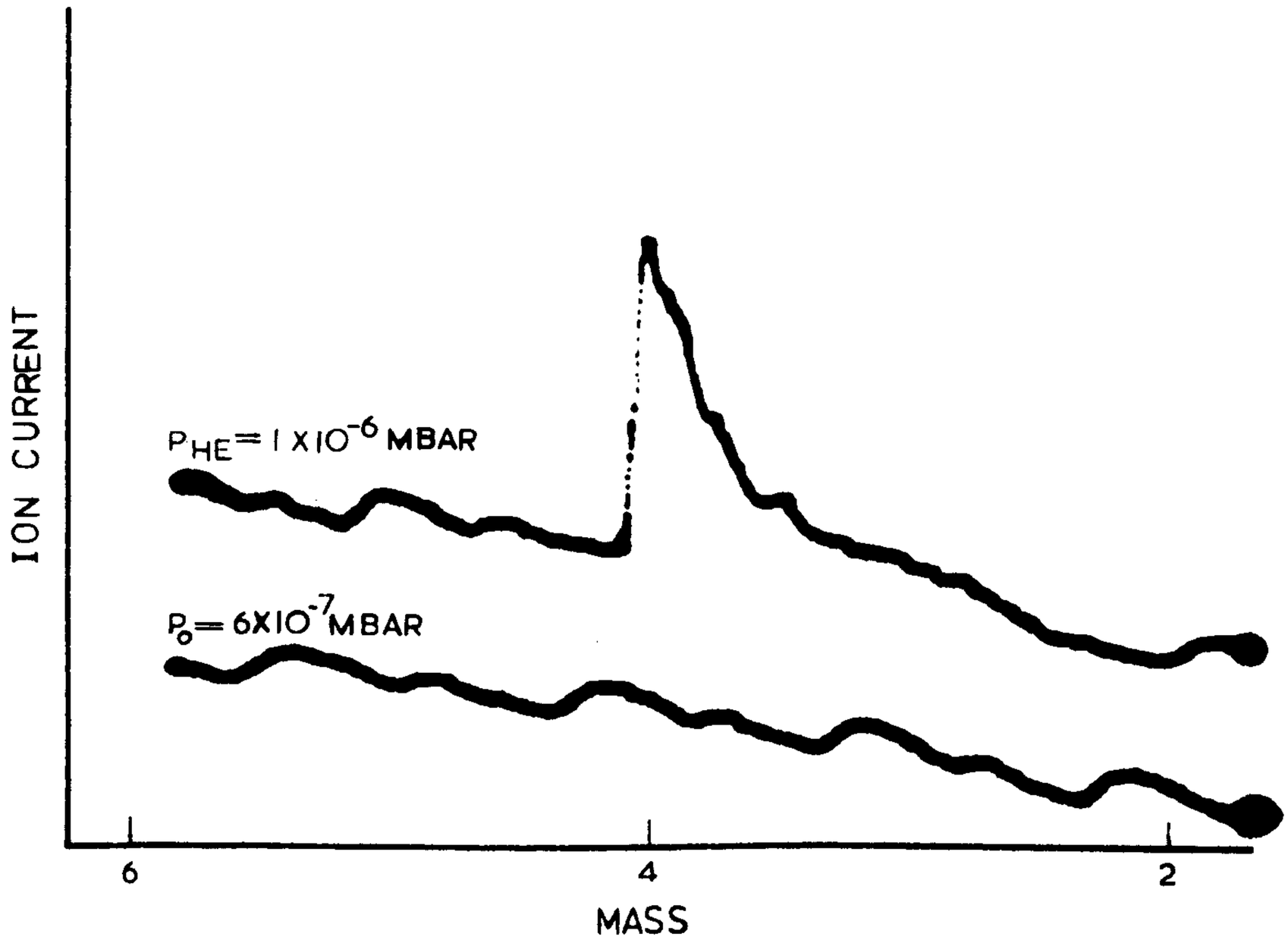

FIG. 4.8.16.A. DIAGRAM SHOWING A HELIUM PEAK AS A REFERENCE. P_o IS THE PRESSURE OF RESIDUAL GASES.

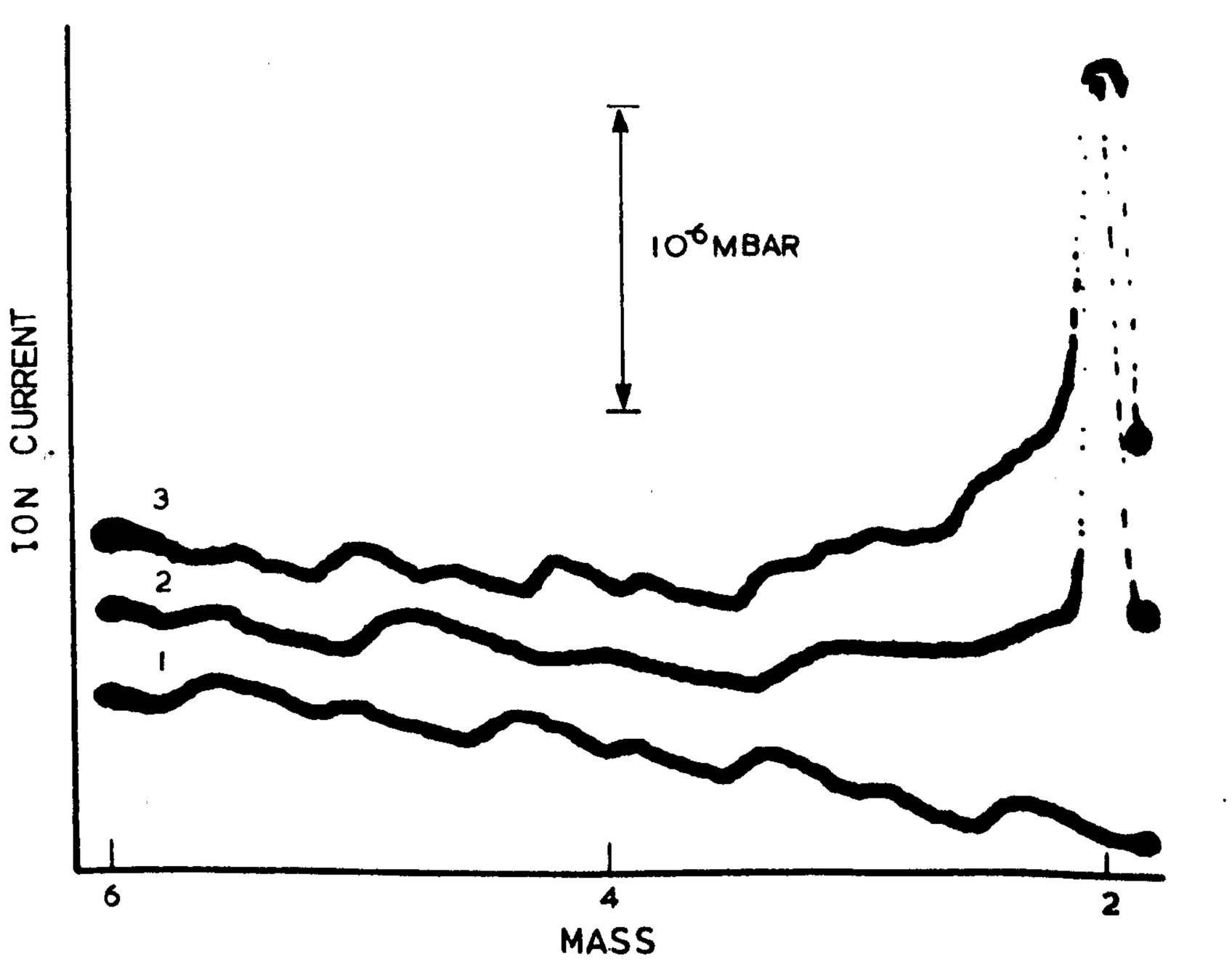

FIG. 4.8.16.B DIAGRAM SHOWING SPECTRA OVER M=2-6A.M.U. IN THE PRESENCE OF THE HYDROGEN PEAK.

1 SHOWING THE RESIDUAL GASES

2 SHOWING A SPECTRUM OF $P_{H_2}=1\times10^{-5}$ MBAR

3 SHOWING A SPECTRUM OF $P_{H_2}=2\times10^{-5}$ MBAR

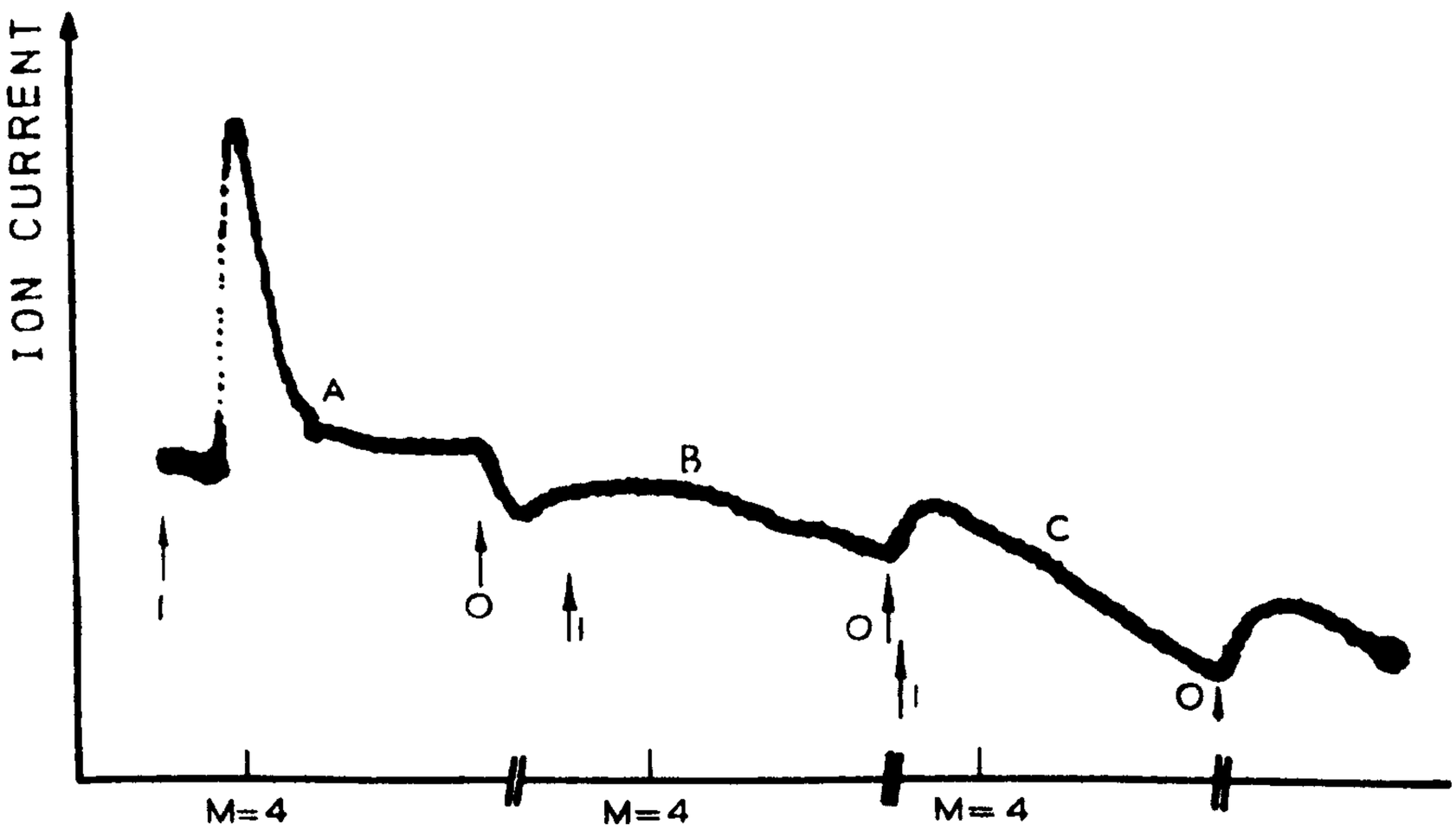

FIG. 4.8.17. DIAGRAM SHOWING SPECTRA NEAR M=4 IN DIFFERENT CIRCUMSTANCES.

1—— START OF A SCAN, 0—— STOP OF A SCAN

SECTION A —— $P_{HE}=1X10^{-6}$ MBAR, $P_{H_2}=0$

SECTION B —— $P_{HE}=0$ MBAR, $P_{H_2}=2X10^{-5}$ MBAR

SECTION C —— $P_{HE}=0$ MBAR,

P_{H_2} FALLS FROM $1X10^{-5}$ MBAR TO 0.

CHAPTER 5. Discussion

5.1. General Performance

The general performance of a mass filter in the a.c. mode, i.e. its sensitivity and resolution, is a function of the number of cycles of the r.f. field experienced by ions.

The number of cycles an ion spends in a quadrupole field is derived as follows. The kinetic energy of the ion of mass (M) is equal to the ion energy (eU_z), i.e.

$$Mv^2/2 = eU_z$$

where v is the velocity of the ion traversing the filter. Therefore

$$v = (2eU_z/M)^{1/2}$$

The transit time (T) of the ion required for passing through the filter is determined by

$$T = L/v$$

$$= L(M/2eU_z)^{1/2} \qquad (5\text{-}1)$$

Thus the number of cycles (N) is given by

$$N = fT$$

$$= 7x10^5 fL(M/eU_z)^{1/2} \qquad (5\text{-}2)$$

where f is in MHz, L in metres, (M/e) in kg/coulomb, and U_z in volts. For instance, the number of cycles experienced by a singly charged argon ion is

$$N = 456fL/(U_z)^{1/2} \qquad (5\text{-}3)$$

If f=4 MHz, L=50 mm, then the numbers of cycles of a singly charged argon ion for different values of ion energy are as follows

U_z (V)	2	4	6	8	10	12
N	65	46	37	32	29	26

From equation (5-2) it can be seen that the number of cycles, and consequently the performance of the filter, depends upon the mass and energy of the ions.

1/ Effect of ion energy

Obviously the energy of the ions as they enter the filter determines the velocity and hence the time the ions spend under the influence of the quadrupole field.

The relationship of sensitivity to ion energy in the a.c. mode follows a very similar pattern to that of the normal mode. This is shown in Fig. 4.1.1. The sensitivity passes through a maximum at an ion energy of the order of 12 eV. The fall-off in the sensitivity is rapid

for decreasing ion energy.

The general characteristics can be explained as follows. When the ion energy is high, the ions have not sufficient time to establish their equilibrium paths. Only a small portion of the ion beam is collected at a time. Hence the sensitivity is low. When the ion energy is low, the ions experience excessive filtering. Thus more ions are lost and the transmission is low. Consequently the sensitivity is low.

2/ Effect of mass

Over a wide mass range, Fig. 4.3.1 shows that the maximum sensitivity shifts towards higher ion energy at high mass. This is to be expected because the greater the mass of the ions, the more the r.f. cycles spent in the quadrupole field.

From equation (5-2) it can be seen that the number of cycles is proportional to the square root of the mass. To compensate for the reduced number of cycles for low mass there must be a corresponding decrease in ion energy.

It was found experimentally that the effect of varying mass could be countered by increasing the ion energy from 6 to 16 eV over the mass range 0-600 a.m.u. (see Fig.4.3.2). The success of this practice is verified by the results listed in Table 4.3.1. This idea produced a practical instrument particularly useful for this mass range as reported in reference (5/1).

5.2. Ion Source

A good alignment of the various elements in an ion source is very important. For reproducibility of experimental results the eccentricity of the source plates must be kept within 0.1 mm. In this work this was ensured by assembling the source using the jig described in section 3.1. The alignments were checked during assembly with a travelling microscope able to measure down to 0.01 mm. Apart from the reproducibility of the results, the benefit of using the jig is evident in Fig. 4.8.4.A. The sensitivity is improved, even when compared with the best results ever obtained with the source not assembled with the jig. The curves B and C in both Fig.4.8.4.A and Fig. 4.8.4.B show that a good ion focussing system is necessary for the operation of an ion source.

The two curves in Fig. 4.1.2 (with sensitivity plotted as a function of cage voltage) are displaced on the horizontal axis by about 1.4 volts. This indicates that an increase in emission current from 0.1 to 1 mA reduces the potential inside the cage by approximately 1.4 V. It suggests that the space charge inside the cage affects significantly the energy of the emitted ions. To obtain the same performance, that is to compensate for the potential change due to space charge, a higher cage voltage is required at high emission currents. At very high emission currents, $I_e > 3$ mA, the effects of the high space charge were found to be complex for the present conventional source. In fact a good performance of the mass filter could not be achieved with an emission cur-

rent in excess of 3 mA.

The results in Figs. 4.4.2 and 3 indicate that the effect of an a.c. potential applied to lens 2 is similar to that caused by making the cage voltage more positive. This means that the ions gain energy from the special fringing fields in the region of lens 2. From the results in Figs. 4.4.5 it is easy to see that the axial component of the fields can give some ions an increased energy when the phase is near 90°. The most likely explanation is that the a.c. fields are acting as a form of linear accelerator increasing the ion injection energy. Thus this is just an alternative technique for increasing ion injection energy which has no practical significance because Fig. 4.4.7 shows that any increase in sensitivity has a corresponding decrease in resolution. This is exactly the behaviour when sensitivity is increased by increasing the cage voltage.

5.3. Collection System

Observations confirmed Ross' conclusion (5/2) that the potential on the inner collector does not affect significantly either the sensitivity or the resolution of the mass filter. This is true for U_{ic}>50 V and certainly over the whole of the mass range of 12-600 a.m.u. There is, however, the effect that as U_{ic} increases above 200 volts, the small step on the low mass side of a peak can be suppressed. This has been observed many times but not recorded because the effect is extremely small.

The photograph of the deposit on the inner collector shown in Fig.4.7.1 indicates that the distribution of the ion beam at the exit of the quadrupole structure is not uniform. The results (figures 4.7.4. to 4.7.6.) from the experiments with different shapes and/or positions of inner collector suggest:

(a) For circular collectors; the larger the area, the lower the sensitivity and the higher the resolution. (Refer to curves A and B in Figs. 4.7.4.A and B).

(b) For a circular collector and a square collector with the same area; if the sides of the square collector face the rods, then the mass filter has a higher sensitivity for the square collector. The peak width is approximately the same. (Refer to curves B and C in Figs. 4.7.4.A and B).

(c) With a square collector rotated through 90^{o}; the sensitivity is the greatest when the sides face the rods. The resolution is slightly worse for the higher sensitivity. (Refer to figures 4.7.5-4.7.6) For instance, at an ion energy = 7 eV, the sensitivity increases by a factor of 2.4 for M/e=40, 1.7 for M/e=84, whilst the peak width increases by a factor of 1.2 for both peaks.

These results indicate that the ions strike the collectors in a form of a square whose corners face the rods. This is also confirmed by the diagram in Fig. 4.7.2, where the areas mid-way between adjacent rods are shown not to be heavily contaminated.

Weavier (5/3) calculated the ion trajectories in

the x-y plane. He recorded the nature of the ion beam at the exit of a quadrupole structure by photographing the phosphor of a position-sensitive detector. The results in this work confirm his conclusions and records. From these limited experiments, however, it is still too early to confirm the advantage of the square over the circular inner collector.

5.4. Performance of the Rod System

The a.c. mode does not give "peak splitting", in the sense that this term is conventionally used, because there are no resonance lines passing through the operating point. (see Fig. 2.7 of section 2.6) These so called resonance lines due mainly to the third and fourth order distortions in the quadrupole field cause instabilities in the paths of the ion near the normal operating point and consequently poor peak shapes. Since the distortions are due mainly to contamination, the shapes of the peaks in the normal mode are often unpredictable. However, in spite of the absence of the conventional peak splitting, "multi-peaks" have been observed in these experiments with the a.c. mode. Both Dawson and Leck give qualitative explanations of the formation of the multi-peaks. From Dawson's calculation (5/4) the shadow of the inner collector is periodic with respect to the parameter q (q is proportional to the amplitude of the r.f. voltage). Therefore a dip in the ion transmission appears periodically with respect to the mass scale. From Leck's

calculation (5/6) the change of the critical stability path from one pattern to another, i.e. from half beat to multi beats, corresponds to the emergence of a spike from one to another (see Fig.5.4.1). The investigation in this work has confirmed the above explanations.

Fig. 4.5.1. shows that when the ion energy is high multi-peaks appear. For comparison purposes, the distance between the first peak and the second was monitored. The values ranged from 0.05 to 0.1 a.m.u. in the experiments reported above depending upon the individual operation. The calculated values were approximately 0.1 a.m.u. by Leck and 0.07 a.m.u. by Dawson. These are in good agreement. From Fig. 4.5.3 and Fig. 4.5.4 it can be seen that the distance between the "sister peaks", i.e. the width of the multi-peaks, is dependent on ion energy. When this energy is small, the sister peaks merge together into a single peak. When the energy is high, they are well separated. The distance is also dependent on the rod length and operating frequency. Short rods or low operating frequency spreads out the multi-peak structure.

The width of the multi-peaks is dependent on the number of cycles of the r.f. field experienced by the ions, as shown in Fig. 4.5.5. The larger the number of cycles, the closer together are the multi-peaks. For the 85 mm filter (No.4) the results are clear-cut. For the 50 mm instrument, however, there are some anomalies. At a given number of cycles, the width of the multi-peaks is found to be larger when operating at high frequency.

This is probably due to the fact that the fringing fields are comparable in importance with the quadrupole field in the shorter instrument.

The multi-peaks are independent of the potential of the inner collector and other parameters of the ion source, such as the potentials of lens 1 and 2 (figures 4.5.2.A to C). This of course is to be expected.

5.5. High Pressure Limitation

As shown in Fig.4.2.1, the relationship between ion current and pressure is the same for both the a.c. and the normal mode. There is a linear relation between P and I^+ up to approximately 10^{-4} mbar. A maximum ion current is obtained at a pressure of about $2x10^{-4}$ mbar. (Note:the discussion here refers specifically to singly charged argon ions.) It can be seen from Figs. 4.2.2 and 3 that the linear limitation depends strongly upon the length of the rods and the operating frequency. The pressure at which a maximum output is obtained is inversely proportional to both length and frequency. This indicates that the number of cycles the ions spend in a quadrupole field is a determining factor for the high pressure performance.

The ion energy determines the number of cycles of the r.f. field experienced by the ions. Over the useful practical range, however, the change of the number of cycles is small. For instance,if the ion energy increases from 6 to 12 eV the number of cycles decreases only by 30% ($=1-(1/2)^{1/2}$). Thus as shown in Fig. 4.2.4 the change

in performance at high pressure is within limits of measurement error.

The step on the low mass side of a peak has been observed carefully with relation to the operating pressure. The observations confirm Dawson's (5/4) initial result that the height of the step relative to the total peak height is proportional to the pressure. Also the cause of the step is mainly due to gas scattering. Usually the step becomes insignificantly small at a partial pressure below 10^{-6} mbar.

The ion motion in a quadrupole field is helical. For an ion in resonance the helical motion is synchronized with the r.f. field. The number of pitches is the same as the number of cycles the ion undergoes in this field. The path taken by the ion depends mainly upon the inscribed radius of the rods (r_o) and the number of cycles experienced by the ion in the r.f. field. For all the filters used in this work r_o is fixed at 2.77 mm, so that only the number of cycles is variable. The greater the number of cycles, the greater the path length. When the path length is equal to the mean free path of the ion, a collision between the ion and molecules or other ions becomes probable. This therefore results in a pressure limitation for the mass filter.

A detailed theoretical calculation of the relationship between ion current and operating pressure for the normal mode has been published by Kubicek (5/6). For the a.c. mode, a simplified but practical estimation is made

of the pressure at which the path length is equal to the mean free path. If $r_o/2$ is assumed to be the average radius of the trajectories of the helices, then the path length (L_p) is

$$L_p = \pi r_o N \qquad (5\text{-}4)$$

The pressure (P) at which L_p is equal to the mean free path is obtained by

$$P = L_r P_r / L_p \qquad (5\text{-}5)$$

where P_r is a reference pressure, L_r is the mean free path at the reference pressure for a specific gas at temperature of 25°C. Substituting for L_p and N from equations (5-4) and (5-2) the limiting pressure is derived from equation (5-5) as

$$P = 4.5\text{x}10^{-7}(eU_z/M)^{1/2} L_r P_r / fLr_o \qquad (5\text{-}6)$$

where r_o is in metres, P is in mbar, the other dimensions are the same as in equation (5-2). For argon if P_r=1 mbar, then L_r=1x10^{-4} metres (5/7), thus

$$P = 7\text{x}10^{-8} U_z^{1/2} / fLr_o \qquad (5\text{-}7)$$

As an example, for U_z=5.3 V, f=4 MHz, L=50 mm, and r_o=2.7 mm, then P= 3x10^{-4} mbar. This indicates a saturation

which is consistent with the result shown in Fig. 4.2.2.

5.6. Contamination

1/ Short Term

From the experiments to observe short term contamination it was found that an improvement in resolution always corresponded to a lower sensitivity and vice versa. Moreover the changes of performance were reversible, the original sensitivity and resolution being restored when the gas was removed from the system.

The results in Table 4.6.1 show that the effect on the performance for short term contamination depends upon the cage voltage. The lower the cage voltage (i.e. the ion energy), the greater the effect of contamination.

The results in Table 4.6.2 show that the behaviour pattern is determined by gas composition. For example the introduction of oxygen or water vapour always reduces the sensitivity, whereas hydrogen and acetone increase the sensitivity. This can be explained by assuming a change of contact potential between the molybdenum cage and the stainless steel rods due to gas adsorption. The adsorption of oxygen and water introduces a small negative offset potential on the cage. This decreases the ion energy, thereby decreasing the sensitivity and increasing the resolution of the mass filter. The adsorption of hydrogen and acetone, however, introduces a small positive offset, thereby resulting in an increase in sensitivity and a decrease in resolution. When a gas

contaminant is removed from the system, the performance of the mass filter is restored to the original because the surfaces return to their previous equilibrium. Since the cage is in the ionization region, it is to be expected that its surface will dominate the contamination effect. Curves showing sensitivity plotted as a function of cage voltage (ion energy) indicate the importance of this voltage (for example Fig. 4.3.1). The rate of change of sensitivity with cage voltage is dependent very critically upon the cage voltage as can be seen from the following data derived from curve A of Fig.4.6.4.A.

U_c(V)	S (10^5 A/mA.mbar)	dS/dU_c (10^5A/mA.mber.V)
4	1.3	
6	5.5	2.3
8	10	2.0
10	13	1.2
12	14	0.2
14	13	-0.7
16	12	-1.2

Clearly the effect of changes in U_c is much more important at 6 volts than at 12 volts. This was indeed confirmed beyond doubt in the experimental work. Therefore choosing a high cage voltage is necessary to obtain stable performance in a practical instrument.

All the observations made indicated that the instabilities due to contamination were reduced if the

cage operated at high temperature. Presumably at the higher temperature the rate of contamination is reduced in a given environment. Thus to set up a practical instrument the cage should be operated at a high voltage and a temperature in excess of 200°C.

2/ Long term

In the investigation of the long term effect of hostile vapours metallic samples were deliberately chosen to degas a full range of hydrocarbons. The hydrocarbons can be seen from the spectrum shown in Fig. 4.6.3, which recorded the residual gases of plant No.2 during a baking cycle. Viton samples were chosen because of the very reactive vapours (fluorocarbons) given off under extreme baking conditions. From the spectrum in Fig.4.6.2 it can be seen that the decomposed fluorides consist of ion species: HF, CF, CF_2, CF_3, C_2F_2, C_2F_3, etc. The spectrum in Fig.4.6.2 was taken after the viton rings had been heated to the point of total decomposition. All the samples provided the desired extremely hostile atmosphere. The mass filter was operated in this hostile atmosphere for 100 hours.

(A) The effect on the construction

Under the heavy contaminations three effects on the construction of the mass filter were observed:

(1) The insulation of some parts of the filter were damaged by the deposition of contaminants. For example, the deposit on the ceramic support of the filament caused a short circuit between the filament and the cage. The

deposit on the surface of the ruby balls led to a break down of the r.f. voltage. Consequently various insulators had to be replaced during the investigation.

(2) The collectors were covered by contaminant films. Eventually the collector assembly had to be cleaned because it became covered with an insulating layer.

(3) The lifetime of the tungsten filament was reduced to about 15 hours. Obviously a new filament had to be fitted at fairly frequent intervals.

(B) The effect on the maximum sensitivity

During the investigation of contamination the sensitivity was always found to decrease slowly. Ion source contamination was established to be the main cause of loss of sensitivity. The sensitivity could be recovered by electron bombardment heating of 5 W for one hour. The temperature of the cage during bombardment was about 200°C. The values of maximum sensitivity shown in Table 4.6.3 indicate it to fall gradually and steadily to 64% of its original value over 100 hours of the heavy contamination. For the normal mode, the sensitivity was much less stable. A drop in the maximum sensitivity of the filter by a factor of 2 or more after 20 hours contamination was usually observed. Sometimes a fall by a factor of 10 was found.

(C) Comparison of the stability for the a.c. mode with that of the normal mode

The stability measurements for operation in the

a.c. mode are shown in Table 4.6.3. which gives the time of operation as well as the differing conditions of contamination. By way of contrast, the instability for the normal mode is shown in Fig.4.6.5. The peaks were recorded for U_c=12V. At this cage voltage the sensitivity of the filter was at its maximum and did not change rapidly with U_c. Therefore the instability of the normal mode was almost certainly due to the unstable d.c. potentials on the quadrupole filter. This was no doubt due to the build up of charge on the contaminated rods which could not disperse quickly. The variation of the charge with time resulted in a change of the d.c. potential. Consequently the "operating line" for the normal mode moved up and down. Thus the performance of the filter as seen in Fig. 4.6.5 was unstable.

(D) The relative sensitivity of the a.c. and normal modes

This was monitored by observing the two peaks, the singly and doubly charged ions at mass 40 and 20 in the argon spectrum. For the a.c. mode the ratio of these peaks I_{40}/I_{20} was always found to be within the range 5.8 to 6.2, no matter what the history of contamination of the mass spectrometer. This is in complete contrast to the normal mode, where more than one series of experiments showed the relative sensitivity to depend very much upon the precise position of the operating line after contamination. Figs. 4.6.6.A, B, C, and D are reproduced from measurements made with a heavily contaminated ins-

trument (50 mm quadrupole No.1). A small change in the operating line to improve resolution makes an enormous difference to the relative peak heights at mass 40 and 20. Indeed it alters the spectrum completely.

A comparison of the performances of the two modes shown in figures 4.6.6.A to E can be made as follows. In the normal mode the ratio of I_{40} to I_{20} decreases from 2.7 to 0 for a change of d.c. voltage on the rods of 2 volts (r.f. voltage is 800 V for mass 40). This differs from its original performance in which the ratio of I_{40}/I_{20} is not critically dependent on resolution setting. It suggests that a small change of d.c. potential on the contaminated rods, whether by deliberate adjustment or by spurious fluctuation of the surface charge, will change the relative sensitivity unpredictably. In the a.c. mode, however, the ratio of I_{40}/I_{20} remains constant at 6.0.

Table 4.6.4 presents the data obtained with an 85 mm quadrupole mass filter No.4 after contamination for 50 hours. The ratio of the singly charged ion current to the doubly charged ion current was specially observed. Within the normal range of cage voltage the ratio reduced by not greater than 15% during the 50 hours contamination.

All these distinct differences demonstrate the different behaviours of the two modes during contamination. This different behaviour is due to the different operating conditions on the stability diagram for the two modes. In hostile environments the surfaces of the

rods become covered by an insulating layer. During operation, ions, and sometimes even electrons, strike the rods. They change the d.c. potential of the rod surfaces. The distribution of ions striking the rods is non-uniform. Therefore the disturbance of the surface potentials is very complex. Nevertheless the changes in the surface potential result in:

(a) A change in the difference of the d.c. potential between the ionization region and the central axis of the quadrupole structure. This changes significantly the energy of the ions as they enter the filter.

(b) A change in the slope of the operating line. The operating point consequently changes.

(c) The distortion of the quadrupole field.

In the a.c. mode the surface contact potential merely reduces the ion energy as shown in figures 4.6.4.A and B. It does not distort the quadrupole field laterally. Therefore the filter performance is independent of the surface potential.

In contrast, in the normal mode, the surface potential on the rods plays an important role in determining the filter performance. Even small changes of the surface potential can shift the operating line (see Fig. 2.5) quite significantly making quite large changes in performance. This is demonstrated in the results presented in Figs. 4.6.7 and 4.6.8. The different responses of the two modes to the balanced and the unbalanced d.c. bias vol-

tages suggest that, not surprisingly, their behaviours in hostile envionments are so completely different. This adds weight to the results presented in figures 4.6.6.A to E.

5.7. Nier Source

1/ General Performance

Variation of the position of the magnet changes the proportion of the trap to the emission current which indicates the focussing effect of the magnet. In its optimum position, a maximum number of electrons are focussed to reach the trap. This is clearly the condition for maximum ion production in the ionization region. With the magnet in the optimum position the trap current is approximately 10% of the total emission current.

Fig. 4.8.2.A indicates that the sensitivity increases linearly with electron current until the electron current reaches 100 uA. Beyond 100 μA saturation is fairly rapid, the sensitivity reaching a maximum for an electron current of 200 μA. This saturation is to be expected because of electron space charge effects in the ionization region.

The potentials on the gate, trap, and lens are not critical to the performance of the mass filter. This can be seen from the figures 4.8.3.A, B and 4.8.5.A, B. However the potential on the ionization chamber is important because it determines the energy with which the ions enter the mass filter. Fig. 4.8.4.A shows that the relationship

between sensitivity and ion energy is similar to that obtained with the conventional ion source.

2/ Main differences between the Nier and the conventional source

There are two significant differences in the geometry of the sources.

(A) There is a narrow channel exit from source to the quadrupole filter with the Nier source. (The circular emittance orifice of the Nier source is 3.0 mm diameter and that of the conventional source is 5.2 mm diameter) Therefore the initial displacements and the spread of the transverse velocities of ions at the entrance of the quadrupole lens are smaller for the Nier source than for the conventional source.

(B) The comparatively weak penetration of electric fields into the ionization region of the Nier source leads to a very low spread of ion energies and small transverse velocities for the Nier source.

In the conventional source, the opening in the cage is 6.2 mm in diameter. This is relatively large compared with the other dimensions. Thus the electric field set up by lens 1 penetrates into the ionization region inside the cage. Therefore there will always be a gradient of axial potential and a significant transverse field component in the ionization region. These give ions a spread axial energy and a considerable transverse momentum.

In the Nier source (see Fig. 3.3.A) there is an isolation chamber with entrance and exit orifices only 3

mm diameter. Thus the field set up by the lens has a very low penetration into the ionization region. The ions produced in the ionization region therefore have a more uniform axial energy and a much weaker transverse component of velocity than those produced in the conventional source.

3/ The performance of the mass filter with the Nier source

The above differences of the Nier from the conventional source give certain distinct improvement in instrument performance for the Nier source. These are as follows.

(A) Resolution of peaks down to mass 2

With the conventional source there is a "blind region" in the mass spectrum below 10 a.m.u., where peaks are not resolved with the a.c. mode. On the other hand, with the Nier source the useful range extends down to mass 2. A peak of H_2 in Fig. 4.8.10 shows sensitivity and resolution at 2.4 eV ion energy to be $6x10^{-6}$ A/mA.mbar and 20 respectively. The probable explanation of the improvement in performance is as follows.

For the conventional ion source, when the amplitude of the r.f. voltage is small, the weak focussing effects at low mass do not overcome the effect of large transverse displacements and velocities. As the mass filter scans downwards below mass 10, a continuously rising background ion current is observed. This is almost certainly due to the large transverse displacements and velocities of the heavy ions. In detail its magnitude depends upon individual instrument and operation. It masks the low mass

peaks.

(B) Good resolution obtained by reducing the ion energy

From figures 4.8.7 to 4.8.10 it can be seen that a very good resolving power for the mass filter with the Nier source was obtained at low ion energy. This good resolution could not be achieved with the conventional source. With the limited evidence it appears in these experiments that the resolution does not increase as the ion energy decreases below about 4 eV for the conventional source. This is probably due to the effect of the large transverse velocities and displacements of the ions as they enter the quadrupole field.

(C) Significantly improved peak shape

By examining the interference from Fig. 4.8.12 it can be seen that the interference of an Ar^+ peak at M=41 is less than 0.05%. The interference of the same peak at M=39 depends upon pressure, frequency and also ion energy. Fig.4.8.15 shows the relationship between the interference and the pressure. When the gas scattering effects are negligible, for instance at the pressure 10^{-6} mbar, the interference is very low.

4/ Comparison of the performance of two sources and comparison with previous work

Fig. 5.7.1 shows that the sensitivity for the Nier source is greater than that for the conventional source by a factor of about 10. Fig. 5.7.2 shows comparable resolutions for the two sources. The main point to note is that

the Nier source can be operated satisfactorily at low ion energy, whereas the conventional source gives poor performance due to the large transverse displacements and velocities. The slope of the straight line in Fig. 5.7.2 is 2.3, suggesting that the resolution $R \alpha N^{2.3}$, where N is the number of cycles the ions spend in the r.f. field. This is in a good agreement with Ross' (5/2) results with a 50 mm quadrupole filter. Also it is close to $R \alpha N^2$ which was postulated by Paul (5/8) and confirmed by Holme (5/9).

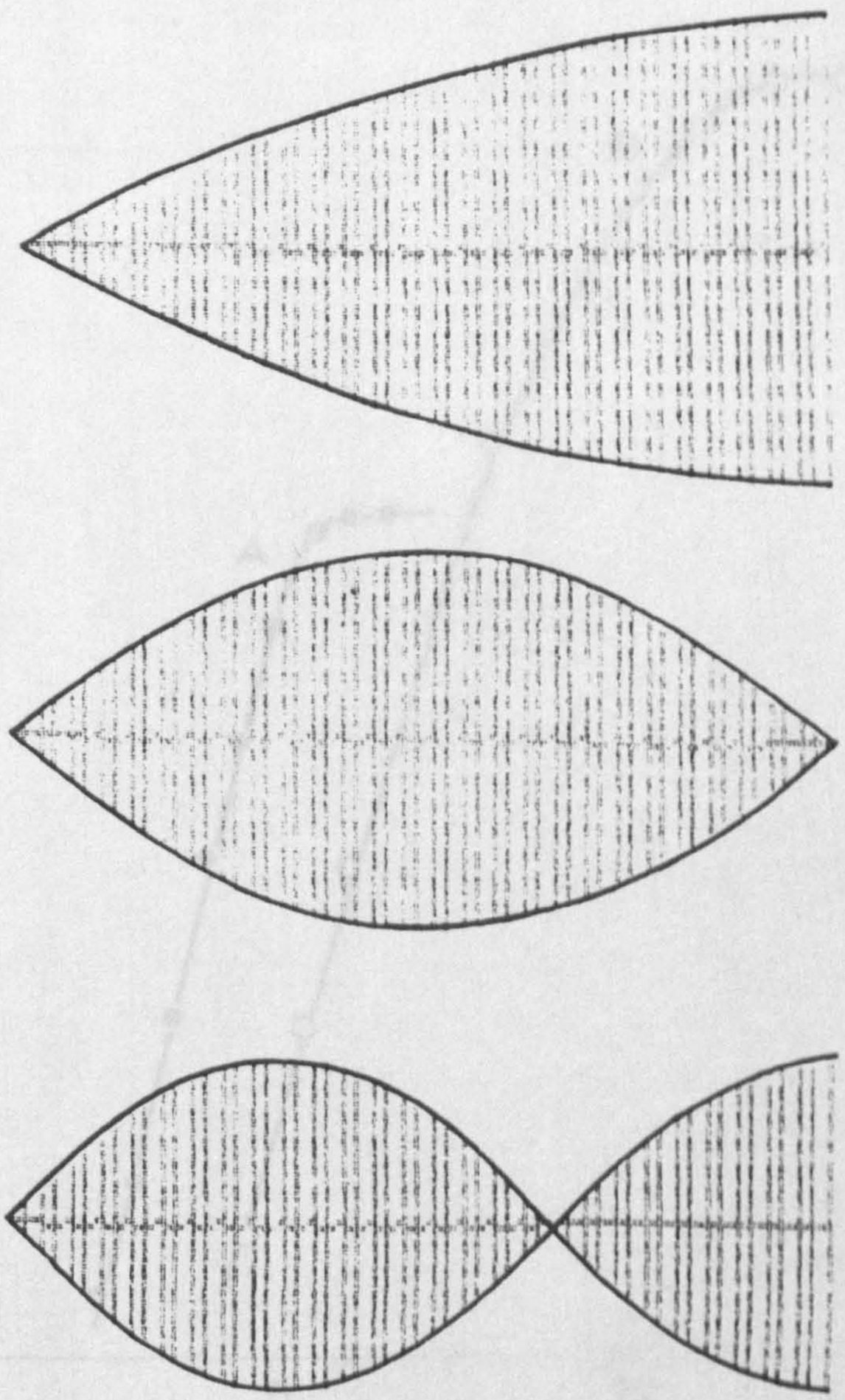

FIG. 5.4.1. DIAGRAM SHOWING THE CONTOUR OF ION TRAJECTORIES CHANGES FORMING THE FIRST AND THE SECOND SPIKES.

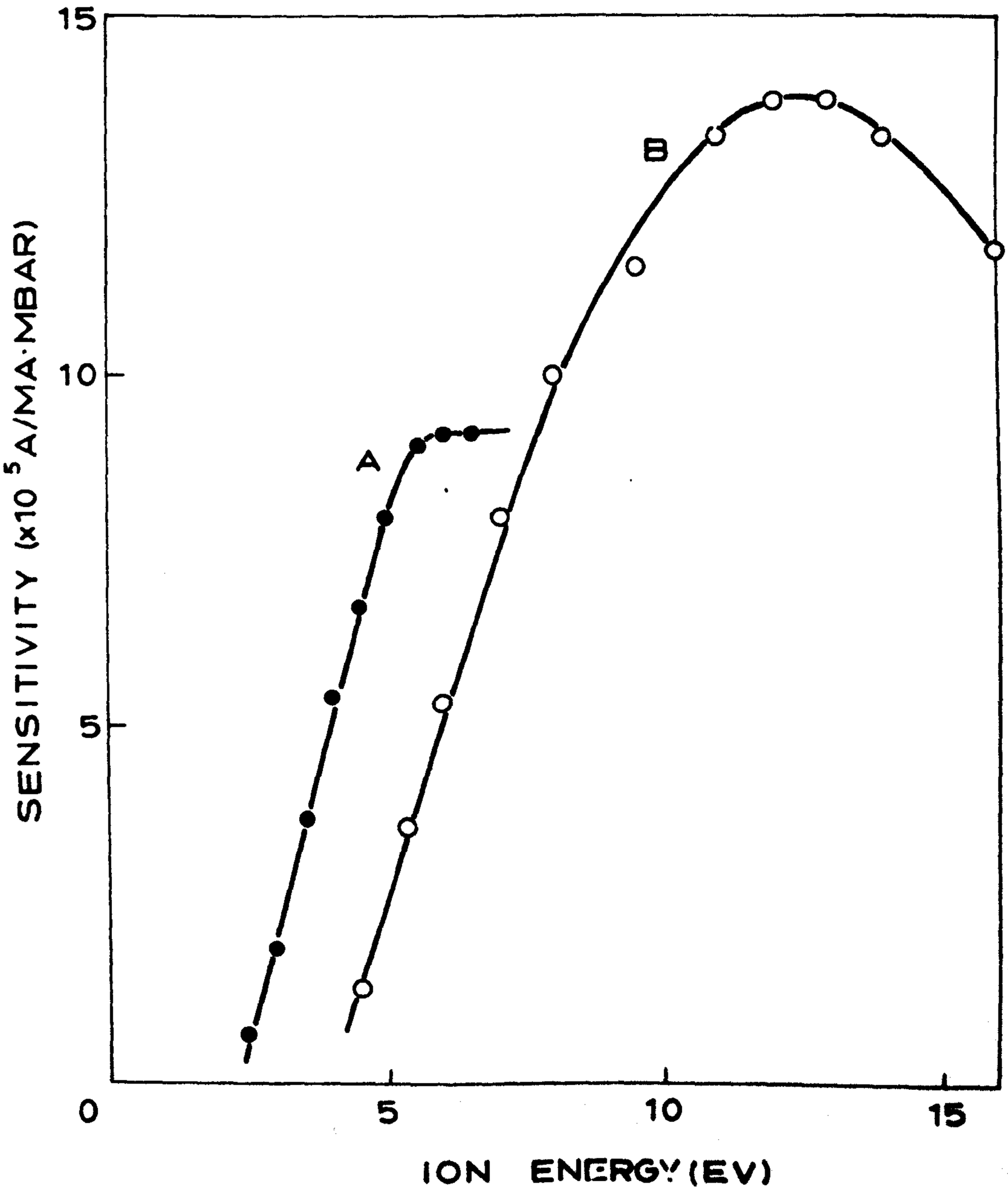

FIG. 5.7.1. COMPARISON OF SENSITIVITY FOR THE NIER SOURCE WITH THAT OF THE CONVENTIONAL SOURCE.

A-NIER SOURCE B-CONVENTIONAL SOURCE

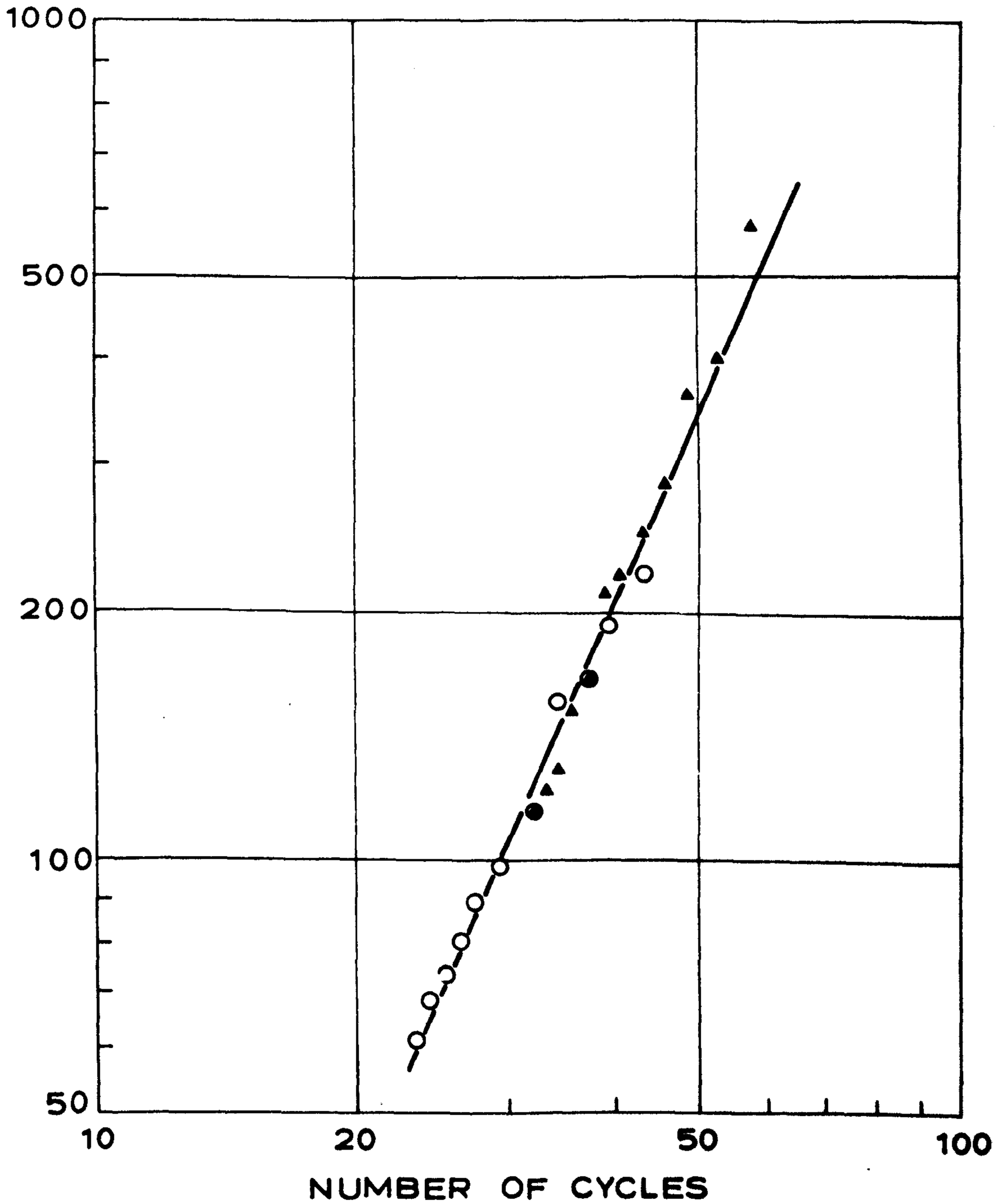

FIG. 5.7.2. RESOLUTION AS A FUNCTION OF NUMBER OF CYCLES.

▲ NIER SOURCE ○ CONVENTIONAL SOURCE

CHAPTER 6 Conclusions

This work has established quite conclusively that the a.c. has a distinct advantage over the normal mode for QMF operation in hostile environments. The advantage is the stability of the relative and maximum sensitivity over a long period of time. The relative sensitivity of the a.c. mode does not change significantly over the mass range of 10-100a.m.u. even after heavy contamination, and thus there is no mass discrimination even when working for long periods in hostile environments. The maximum sensitivity of the a.c. mode remains stable after a heavy contamination. In contrast the normal mode for the same instrument has disadvantages, its instability being the most important. Its relative sensitivity and maximum sensitivity both vary with time and with the resolution setting after even a minor contamination. Therefore the sensitivities can not be predicted. The above advantage of the a.c. mode is due to the small effect of d.c. voltage on the rods. It is particularly important when the instrument is operating in hostile environments.

It has been established that the quadrupole mass filter in the a.c. mode meets the requirements of the project with only two minor modifications from standard QMF operation. These are: (a) Operating with a conventional source whose cage is heated to about 250^{o}C. (b) Varying the ion energy over a mass range: low value for

low mass, and high value for high mass.

(a) During contamination the performance of a QMF deteriorates because the surface potentials on the ion source, especially on the cage, reduce the ion energy. Cleaning the cage with electron bombardment has been shown to be effective in stabilizing the performance of the mass filter. Heating the cage with an external heater has a similar effect. In practice it has been found that installing a heater to raise the cage temperature to 250°C stabilizes the performance of the instrument.

(b) The quadrupole mass filter in the a.c. mode has been shown to have constant sensitivity over a wide mass range. This is achieved by decreasing the time the high mass ions spend in the filter (i.e. increasing their axial velocity by increasing the injection energy). In the present work using a 100 mm mass filter it is realised by increasing linearly the cage voltage from 6 V at mass zero to 16 V at mass 600 a.m.u.. As a consequence of this modification the mass filter has constant sensitivity over the mass range of 18 to 600 a.m.u., whilst the relative sensitivity is comparable with that of the more complex mass spectrometer MS9. The resolution ($M/\Delta M$) of the filter is also constant over the mass range of 200 to 600 a.m.u.. In addition, this modification has almost no effect on the other electric parameters of the instrument, such as the emission current and the potential on lens 1 or lens 2, and hence does not require any extra adjustment of the parameters.

Although the performance of the quadrupole mass filter in the a.c. mode inevitably changes under the effects of extremely heavy contaminations, the degradation is gradual and very slow. For example, the maximum sensitivity of the 50 mm quadrupole at 4 MHz reduces by only 40% even after 100 hours of operation in a hostile atmosphere at 10^{-3} mbar. Under this extreme condition any other analytical mass spectrometer would suffer very serious degradation.

The high pressure operation is limited by "gas-ion" collision. The mean free path is clearly all-important. Because of their helical paths the ions must travel a much longer distance than the simple geometric distance from the source to the collector. From the results of Kubcek's calculation (6/1) for the normal mode, the high pressure limit is dependent on the mass of the ion in the order of 10^{-4} mbar. From the results of the experiments in this project, it can be inferred that the high pressure limit in the a.c. mode is also about 10^{-4} mbar. This limit has been shown to be inversely proportional to both the radius and the length of the rods, and also the operating frequency.

The observations on the importance of the alignment are in good agreement with the conclusions arrived at by Holme (6/2) and Ross (6/3). Holme's conclusion, resulting from the normal mode operation of the instrument, that "accurate angular and axial alignment of the source are necessary if the highest sensitivity and resolving power

are to be achieved" is confirmed. Ross' conclusion, resulting from the a.c. mode operation, that "optimum performance can only be obtained from the r.f. mode if the analyser is accurately aligned." is also confirmed. The experiments in this work show that good performance of a quadrupole mass filter is obtained if the eccentricity between the plates of the ion source is less than 0.1 mm.

The multi-peaks can be a disadvantage for the a.c. mode. They are predicted with Dawson's (6/4) and Leck's (6/5) explanation described in section 5.4. The multi-peaks are not spurious but fundamental effects due to finite length of the rods. With very short rods the multi-peaks are prominent. Increasing the number of cycles the ions spend in the quadrupole field by either increasing the length of the rods or decreasing the ion energy causes the multi-peaks to merge into a single peak. This is completely different from the peak splitting in the normal mode. Peak splitting is due to the contamination and/or misalignment of the rods. Its appearance depends upon a spurious condition and therefore is unpredictable.

A disadvantage of the a.c. mode is that the resolving power is unsatisfactory at very low mass when a normal commercial ion source is used. The investigations using the Nier source indicate that an improvement in the performance of the a.c. mode is achieved with a well aligned and intense source having a small exit orifice.

In summary, the quadrupole mass filter in the a.c. mode covers the mass range of 10 to 100 a.m.u. with an

r.f. voltage of 1.5 KV at 3 MHz. By improving the initial conditions of the ion beam the range can be extended down to 2 a.m.u.. The instrument has constant sensitivity over the above mass range and maintains the relative sensitivity even with hostile environments, making it particularily good for applications in these conditions. In addition the instrument is easy to operate and should be simple to produce especially by a manufacturer who has produced a similar instrument for operation in the normal mode.

References

Chapter 1

(1/1) Dempster, A.J. Phys. Rev. 11 (1918) 316.

(1/2) Nier, A.O. Rev. Sci. Instr. 11 (1940) 212.

(1/3) Herzog, R. and Mattauch, J. Ann. d. Phys. 19 (1934) 345.

(1/4) Paul, W. and Steinwedel, H. Z. Naturforsch. 8a (1953) 488.

(1/5) Knewstubb, P.F. Mass Spectrometer and Ion-Molecule Reactions, Cambridge University Press, (1969)

(1/6) Zahn, U.von Rev. Sci. Instr. 34 (1963) 1.

(1/7) Stephens, W.E. Phys. Rev. 69 (1946) 691.

(1/8) Hipple, J.A., Sommer, H., and Thomas, H.A. Phys. Rev. 76 (1949) 1877.

Chapter 2

(2/1) Paul, W. and Steinwedel, H. Z. Naturforsch., 8a (1953) 488.

(2/2) Post, R.F. University of California Radiation Laboratory, Report No. UCRL-2209 Berkeley, CA (1953)

(2/3) Paul, W. and Raether, M. Z. Phys. 140 (1955) 262.

(2/4) Paul, W., Reinhard, H.P., and Zahn, U. von Z. Phys. 152 (1958) 143.

(2/5) Paul, W. and Steinwedel, H. German Patent No. 944, 900, June 28 (1956)

(2/6) Brinkmann, U. Int. J. Mass Spectrom. Ion Phys., 9 (1972) 161.

(2/7) Dawson, P.H. (Editor) Quadrupole Mass Spectrometry and its Applications, Elsevier, Amsterdam (1976)

(2/8) Todd, J.F.J. in D. Price and J.F.J. Todd (Eds.), Dynamic Mass Spectrometry, Vol. 4, Heyden & Son, London, 1975, P. 11.

(2/9) Todd, J.F.J. — in D. Price and J.F.J. Todd (Eds.), Dynamic Mass Spectrometry, Vol. 5, Heyden & Son, London, 1978, P. 3.

(2/10) Todd, J.F.J. — in D. Price and J.F.J. Todd (Eds.), Dynamic Mass Spectrometry, Vol. 6, Heyden & Son, London, 1980, P. 3.

(2/11) Todd, J.F.J. — Int. J. Mass Spectrom. Ion Proces., 60 (1984) 3.

(2/12) McLachlan, N.W. — Theory and application of Mathieu functions, Oxford University Press, 1947.

(2/13) Dawson, P.H. — Int. J. Mass Spectrom. Ion Phys., 17 (1975) 423.

(2/14) Holme, A.E., Thatcher, W.J., and Leck, J.H. — Vacuum, 24 (1974) 7.

(2/15) Austin, W.E., Holme, A.E. and Leck, J.H. — In P.H. Dawson (Ed.), Quadrupole Mass Spectrometry and its Applications, Ch. 6, Elsevier, Amsterdam (1976)

(2/16) Busch, F.v. and Paul, W. — Z. Phys. 164 (1961) 588.

(2/17) Dawson, P.H. and Whetten, N.R. — Int. J. Mass Spectrom. Ion Phys., 2 (1969) 45.

(2/18) Dawson, P.H. and Whetten, N.R. — Int. J. Mass Spectrom. Ion Phys., 3 (1969) 1.

(2/19) Holme, A.E., Sayyid, S., and Leck, J.H. — Int. J. Mass Spectrom. Ion Phys., 26 (1978) 191.

(2/20) Denison, D.R. — J. Vac. Sci. Technol. 8 (1971) 266.

(2/21) Dawson, P.H. and Meunier, M. — Int. J. Mass Spectrom. Ion Phys. 29 (1979) 269.

(2/22) Holme, A.E. — Int. J. Mass Spectrom. Ion Phys., 22 (1976) 1.

(2/23) Leck, J.H. — British Patent Specification, 1539607, 31st January (1979)

(2/24) Ross, D.N. and Leck, J.H. — Int. J. Mass Spectrom. Ion Phys., 49 (1983) 1.

(2/25) Ross, D.H. — Ph.D. Thesis of Liverpool University (1983)

(2/26) Dawson, P.H., Meunier, M., and Wing-Cheung Tam — Advan. Mass Spectrom. 8a (1980) 1629.

(2/27) Yang, J. and Leck, J.H. — Int. J. Mass Spectrom. Ion Proces., 60 (1984) 127.

Chapter 5

(5/1) Yang, J. and Leck, J.H. — Vacuum, 32 (1982) 691.

(5/2) Ross, D.N. and Leck, J.H. — Int. J. Mass Spectrom. Ion Phys., 49 (1983) 1.

(5/3) Weavier, H.E. and Mathers, G.E. — IN D. Price and J.F.J. Todd (Eds.) Dynamic Mass Spectrometry, Vol. 5, Ch. 3.

(5/4) Dawson, P.H., Meunier, M., and Wing-Cheung Tam — Advan. Mass Spectrom. 8a (1980) 1629.

(5/5) Yang, J and Leck, J.H. — Int. J. Mass Spectrom. Ion Proces., 60 (1984) 127.

(5/6) Kubicek, P. and Mrazek, L. — Ann. Phys. (Leipzig), 24 (1970) 289

(5/7) Dushman, S. and Lafferty, J.M. — Scientific Foundations of Vacuum Technique, Sec. Ed., John Wiley & Sons. (1966)

(5/8) Paul, W. and Reinhard, H.P. — Z. Phys. 152 (1958) 143.

(5/9) Holme, A.E., Sayyid, S. and Leck, J.H. — Int. J. Mass Spectrom. Ion Phys., 26 (1978) 191.

Chapter 6

(6/1) Kubicek, P. and Mrazek, L. — Ann. Phys. (Leipzig), 24 (1970) 289

(6/2) Holme, A.E. — Ph.D. Thesis of Liverpool University (1972)

(6/3) Ross, D.N. — Ph.D. Thesis of Liverpool University (1983)

(6/4) Dawson, P.H., Meunier, M. and Wing-Cheung Tam — Advan. Mass Spectrom. 8a (1980) 1629.

(6/5) Yang, J. and Leck, J.H. — Int. J. Mass Spectrom. Ion Proces., 60 (1984) 127.

International Journal of Mass Spectrometry and Ion Processes, 60 (1984) 127—136
Elsevier Science Publishers B.V., Amsterdam — Printed in The Netherlands

THE OPERATION OF A NOVEL QUADRUPOLE MASS SPECTROMETER IN HOSTILE ATMOSPHERES

J. YANG and J.H. LECK
Department of Electrical Engineering & Electronics, The University, P.O. Box 147, Liverpool, L69 3BX.

ABSTRACT

Measurements are presented showing how the novel method of operating the quadrupole mass spectrometer with only alternnating electric fields (without the normal steady state component) can have advantages in practical operation. In particular it is shown that the behaviour of the new instrument is only slightly affected by small spurious potentials applied to the rod electrodes in the analyser. This relative independence of d.c. fields improves the stability of the instrument which may be of critical importance especially when operating in hostile environments.

INTRODUCTION

This paper reports some recent work on the novel method of operating the quadrupole mass spectrometer where only a.c. voltages are applied to the rods in the filter. In this mode of operation mass separation of the ions is achieved partly in the main hyperbolic field and partly in the fringing fields at the exit from the filter. The original suggestion for this alternative operating technique was made by Brinkmann (ref. 1) and followed up subsequently at Liverpool (ref. 2,3,4). This a.c. mode has been shown to have practical advantages of sufficient importance in a number of applications to offset the disadvantage of the operator being unable to exchange sensitivity for resolution by the simple change of slope of the "scan" line. The work at Liverpool has shown the following to be the main advantages of the new mode,

a) Relative sensitivity can easily be made constant over the whole operating mass range of the instrument (certainly up to mass m/z = 600) (ref. 4) and cannot be upset by changes in resolution setting.

b) Performance in terms of sensitivity or resolution under given operating conditions is less likely to be affected by errors in the mechanical construction or assembly of the instrument. This means that at a given sensitivity resolution is almost always greater than in the normal mode.

0168-1176/84/$03.00

c) By operating away from the apex of the quadrupole stability regime (in the V_{ac}, V_{dc} diagram Fig. 1) the peaks in the output spectrum are unlikely to suffer splitting or other distortions due to third, fourth or higher order disturbances in the quadrupole field.

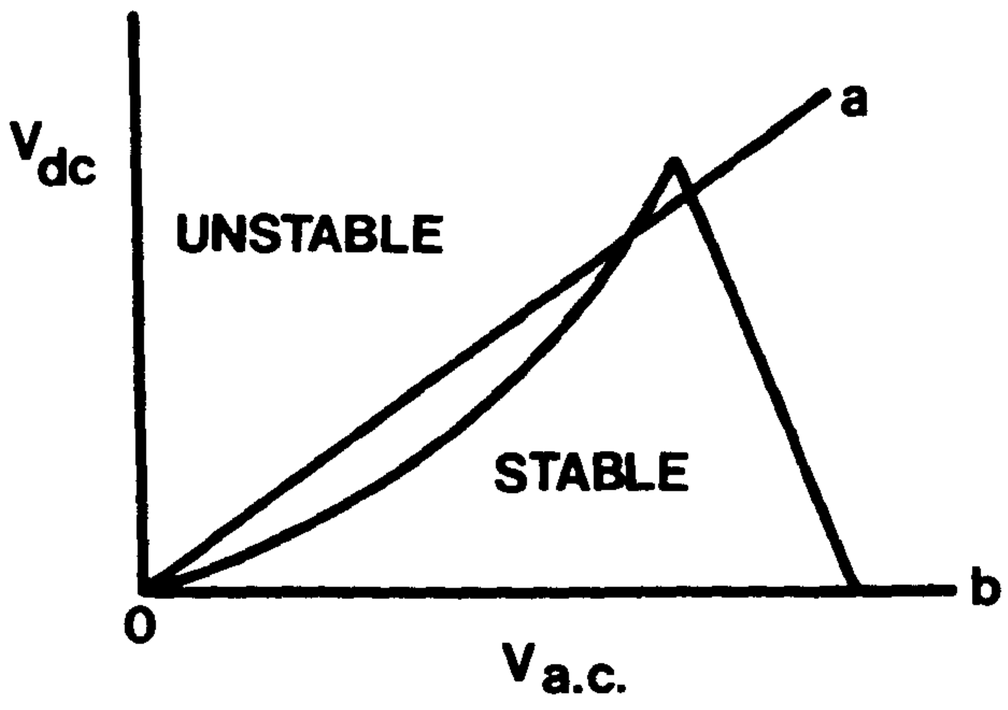

Fig. 1. Stability diagram for the quadrupole mass filter showing the stable and unstable regions for one particular value of m/z. oa and ob are the scan lines for normal and a.c. operation respectively.

In addition to the advantages described above, there is the strong possibility that the long term stability of the operating characteristics should be better than those of the normal instrument because the characteristics do not depend upon any d.c. fields in the filter. The simple experiments described below show that small changes in the d.c. potentials of the rods in the mass filter have much less effect on the performance of the quadrupole in the a.c. than in the normal mode. From one fairly extensive series of experiments there is strong evidence that the a.c. mode does provide a stable operation over a long period even when operated in a very hostile environment. Other results presented below show that the complex peak shapes observed with the new mode when operated outside its optimum range can be explained in qualitative terms from basic theory.

Experimental results

A standard quadrupole lens assembly with circular rods 6.25 mm diameter and 50 mm long was used throughout these experiments. It was fitted with the conventional electron bombardment ion source shown schematically in Fig. 2.

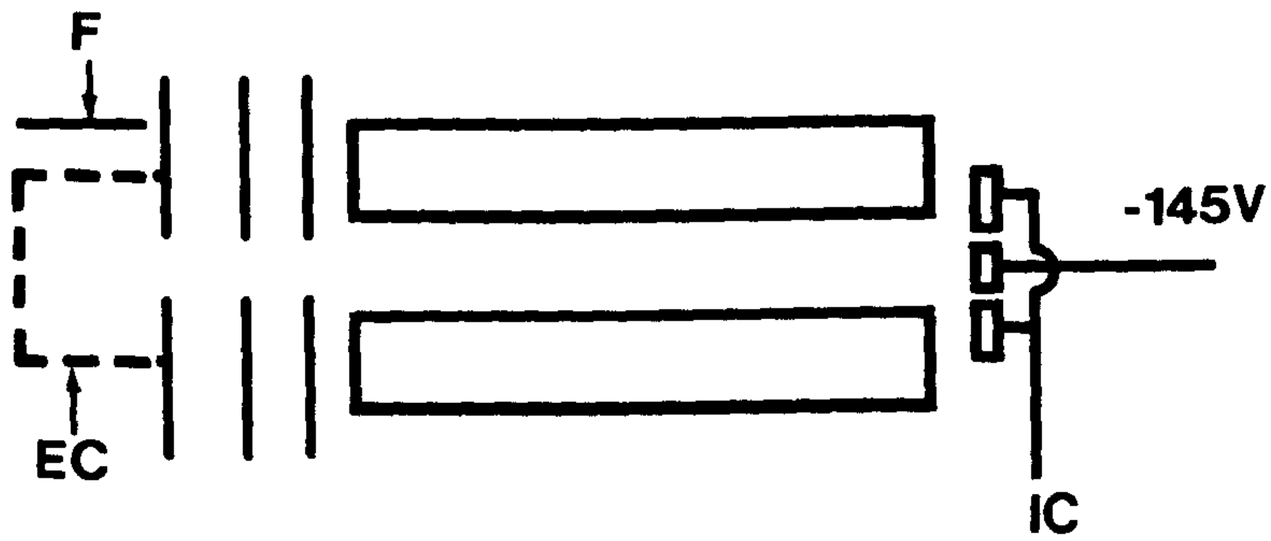

Fig. 2. Schematic diagram of the quadrupole mass spectrometer showing ion source, quadrupole filter and collector assembly. F represents the electron emitting filament, EC the electron collector and IC the ion collector.

The positive ions, formed by electron impact inside the cylindrical ionization chamber approximately 5 mm long x 5 mm diameter, were focussed and injected axially into the quadrupole filter in an approximately parallel beam. The ion injection energy into the filter was defined by the difference between the potentials inside the ionization chamber and along the central axis of the quadrupole filter which could be varied over the range 2 to 20 eV. For the a.c. mode the collector assembly was used exactly as shown in Fig. 2, the outer ring forming the ion collector with the central electrode biassed at -145 volts to attract unwanted ions. To operate in the normal mode the inner and outer ring electrodes were connected together to form a single plate collector held at ground potential. The whole instrument was connected to a simple stainless steel vacuum manifold evacuated by an oil diffusion pump and conventional traps. For this work it was not considered necessary to achieve U.H.V. conditions, background pressures in the range 1 to 5 x 10^{-7} m bar being adequate. Sample gases were introduced to the system in the range 0.5 to 5 x 10^{-5} m bar. All measurements of pressure and hence sensitivity were made with reference to two conventional ionization gauges. Although this in no way provided any absolute reference standard it was perfectly adequate for these experiments giving a stability of the reference to better than $\pm$ 5%.

As in normal operation sensitivity is critically dependent upon the energy with which the ions are injected into the filter. The characteristics are found to be identical for both modes of operation at low energies. At high energy however (very much above the normal operating level) sensitivity falls with increasing energy for the a.c. mode whilst it remains constant, or even increases slowly for the normal mode. In both modes sensitivity changes only slowly with change in ion energy at the operating level of around 7 or 8 eV.

Considering now the effect of small changes in the d.c. potentials of the four rods in the filter assembly. There is now a complete difference between the two modes of operation no matter whether d.c. potentials are applied in a symmetrical

or asymmetrical manner. The symmetrical change in potential, where one pair of rods is incremented by a small voltage + V and the other pair by - V, can be achieved merely by altering the slope of the so called "scan line" (Fig. 1). The difference between the normal and a.c. modes is clearly evident from the results plotted in Fig. 3. Here change in sensitivity is expressed as a function of the change in voltage from the standard operating level. For the a.c. mode the operating d.c. level is obviously zero. The reference level (i.e. slope of the scan line) for the normal mode is taken as that which gives the two instruments approximately the same sensitivity.

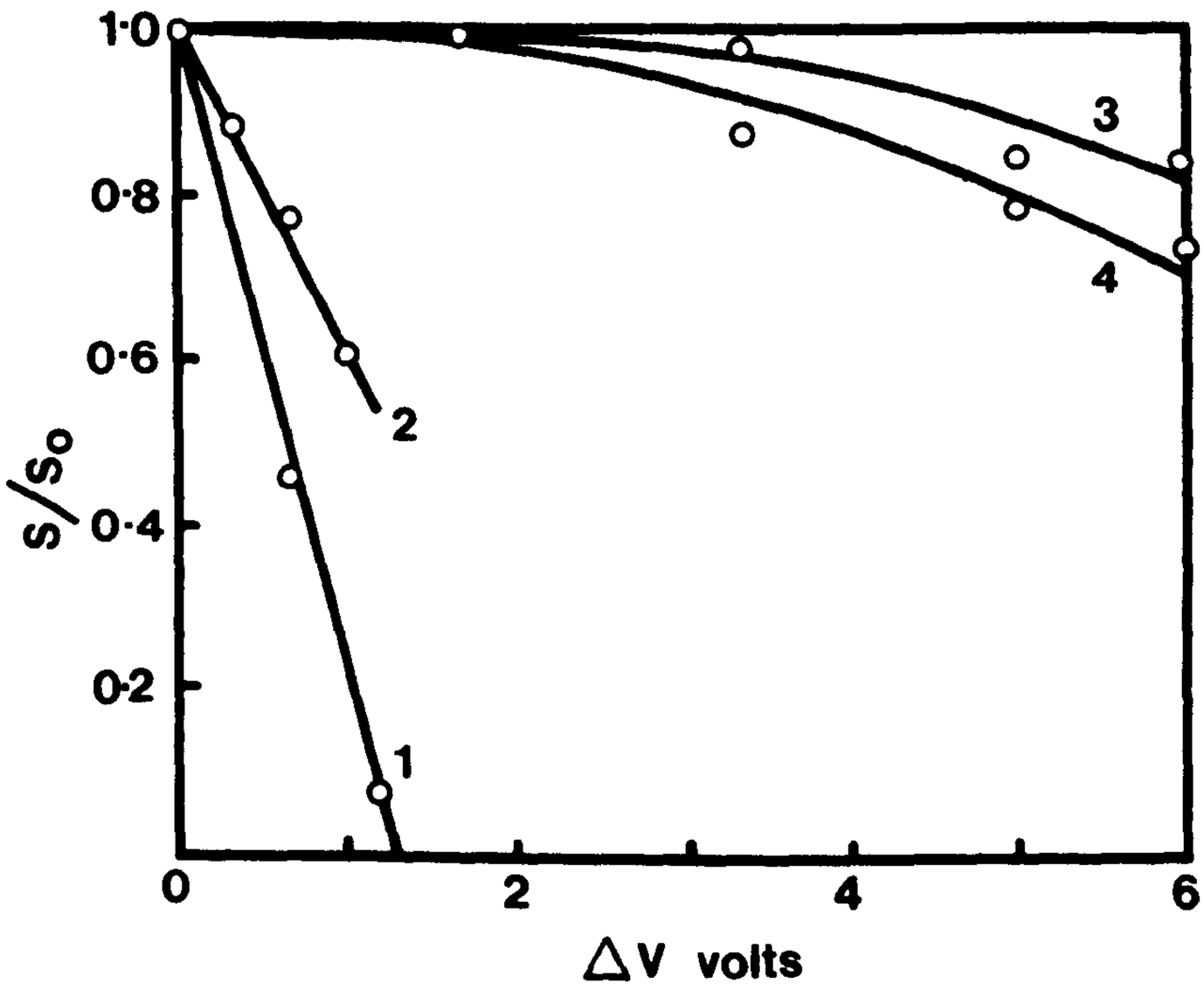

Fig. 3. Curves showing the fractional changes in sensitivity (s/s) resulting from changes in the d.c. potentials applied to the rods. The small increments in d.c. voltage were effected by altering the slopes of the scan lines oa and ob.

Curves 1 and 2 for the normal mode
Curves 3 and 4 for the a.c. mode
Curves 1 and 3 for m/z = 40
Curves 2 and 4 for m/z = 20

The effect of applying an unbalanced d.c. disturbance to the rods is shown in Fig. 4. To obtain these results the procedure was the same as that described above except that a d.c. bias was applied to only one pair of rods, in this case from a small auxiliary battery. Again the normal is affected much more than the a.c. mode. It is easy to present the data for the a.c. mode as the small changes in sensitivity induced by the spurious d.c. potentials are not critically dependent upon the

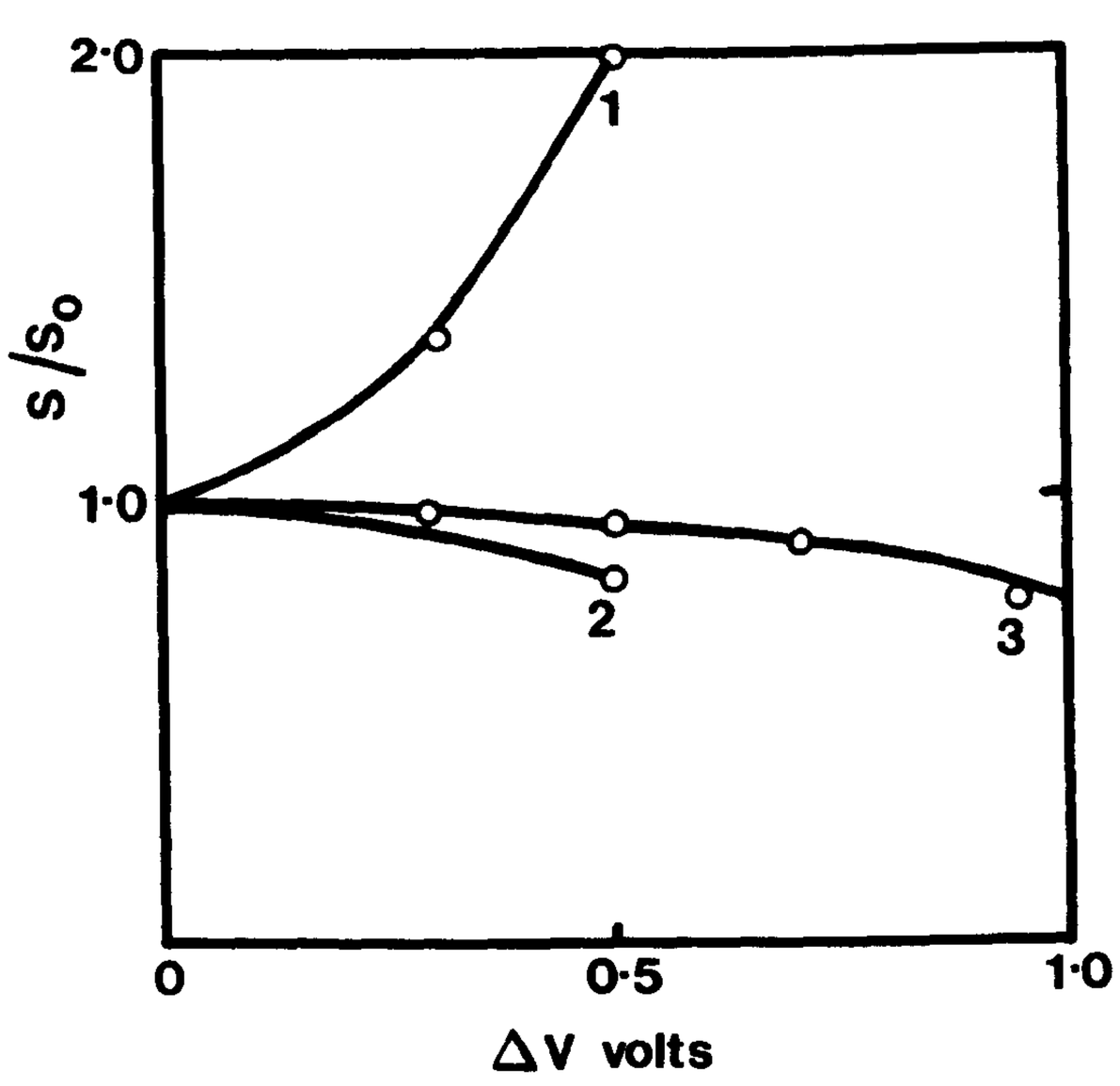

Fig. 4. Fractional changes in sensitivity s/s_o caused by a small inbalance in the d.c. potentials applied to the rods

Curves 1 and 2 for the normal mode
Curve 3 for the a.c. mode
Curve 1 for m/z = 40
Curve 2 for m/z = 20
Curve 3 for m/z = 20 and 40

operating parameters. They are fairly independent for example on the sign of the d.c. voltage, the mass of the ion and the injection energy. For the normal mode the behaviour is much more complex. The disturbance can either increase or decrease sensitivity depending in particular upon the ion mass and the resolution setting of the instrument. The results presented in Fig. 4 are fairly typical showing an increase at one mass and a decrease at another. Certainly it is easy to choose operating conditions which show considerably greater variations than those illustrated here.

Whilst casual observation over a considerable period indicated a relatively stable operation with the a.c. mode a quantitative measurement has been carried out only recently. To obtain confirmation of the stability the small 50 mm quadrupole was operated for a long period on a small auxiliary vacuum system which was deliberately kept very dirty. The pumping of the system was severely restricted by baffles and a high background pressure maintained by baking materials such as "workshop swarf" and samples of viton rubber. The mass spectrometer operated for many hours, at

the normal electron emission and sweeping continuously over the mass range, at a pressure of 10^{-3} m bar. The atmosphere consisted mostly of water and hydrocarbon vapours and, in the later stages, fluorinated compounds. From time to time the quadrupole was returned to the main vacuum system for re-calibration. The measured calibration during the test is shown in Table I.

TABLE 1

Sensitivity variation of the quadrupole during 100 hours operation in a hostile environment. Sensitivity is quoted in terms of the current to the ion collector in amperes for 1 mA electron current at a pressure of 1 mb. In the first half of the experiment the major contaminents were hydrocarbon vapours, in the second half fluorinated compounds arising from heating viton "O" rings in the vacuum system. The ion source was changed after 16 hours operation. The second ion source was cleaned repeatedly by ion bombardment.

Date	Total line (hours)	Sensitivity $\times 10^4$ A/mA/mb	Main Contamination
9.9.82	0	1.4	hydrocarbons
28.9.82	18	1.0	"
11.10.82	18	1.4	"
12.11.82	32	1.6	"
26.1.83	51	1.2	viton
17.2.83	78	0.9	"
10.5.83	96	0.9	"

During this test the performance of the ion source deteriorated considerably and was from time to time cleaned by electron bombardment. After a long period a visible insulating film formed on the central electrode (-145 volts, Fig. 1) of the collector assembly. This was cleaned with a simple abrasive. Thus although the effects of contamination were observed in both source and collector assemblies there was no evidence of any deterioration of the filter itself. Although some blackening could be seen at the source ends of the four rods they were left completely untouched through the whole period covered by Table I.

Whilst extremely good "peak shapes" are usually obtained in the a.c. operating mode there is a rapid deterioration with severe peak splitting when the ion injection energy is taken to excessively high levels. This is most noticeable at low mass. To illustrate the effect two traces are reproduced in Fig. 5, one taken at just a little in excess of the normal operating ion energy, the other at a very high ion energy. Even at the lower energy the first signs of peak splitting can be seen.

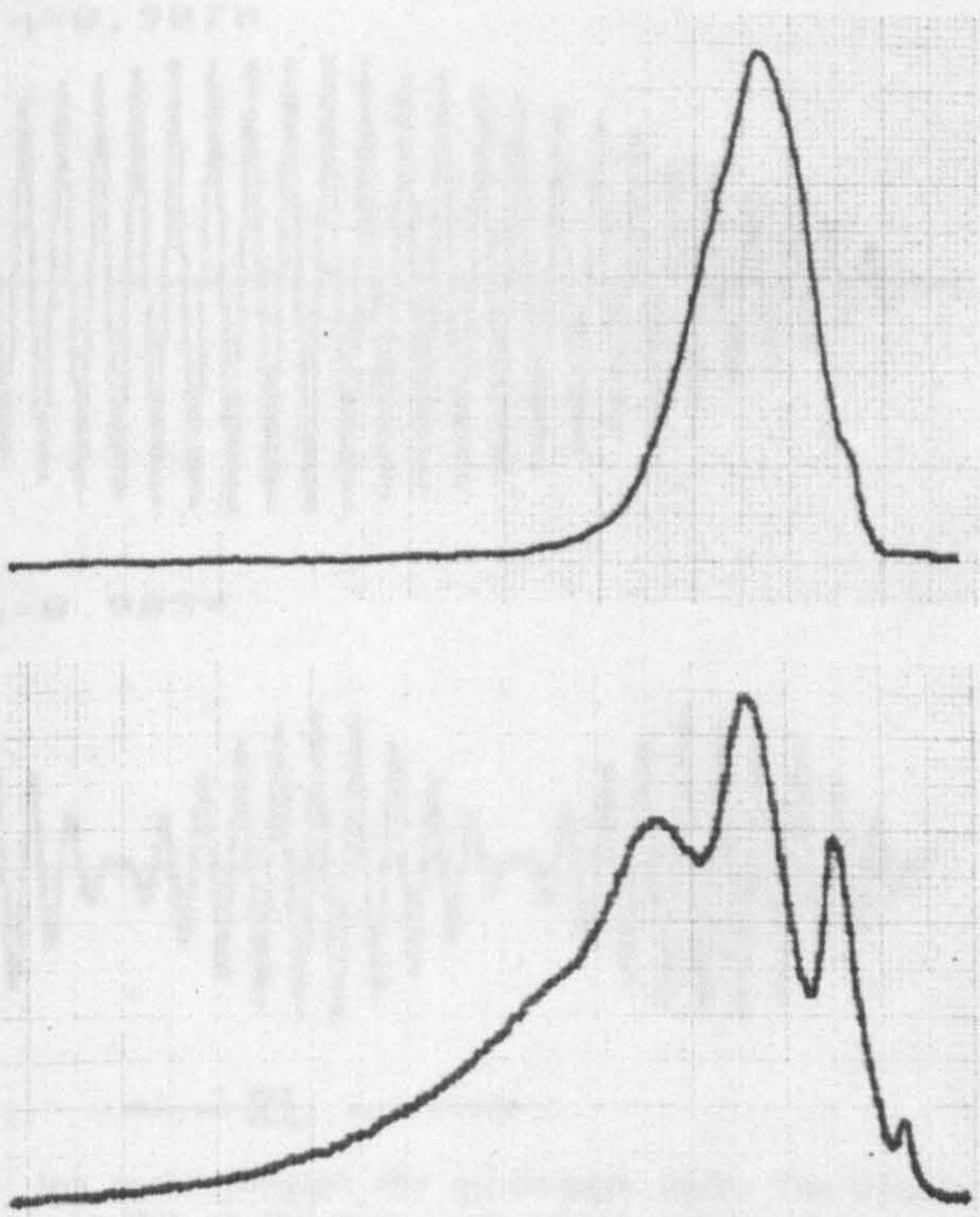

Fig. 5. Single peaks in the mass spectrum for m/z = 40

The upper spectrum was obtained at a near normal ion energy of 7 eV. The lower spectrum at an excessively high energy of 12 eV.

In each curve the trace extends over exactly one mass unit.

Reference to the basic theory indicates that this peak splitting is a fundamental property of the filter and not a spurious effect. It was in fact predicted by Dawson who showed by mathematical analysis that the mass discrimination of the special collector could be explained by considering the central electrode (-145 volts, Fig. 1) to "cast a shadow" over the collector. Dawson (ref. 5) showed that this shadow would fluctuate in size as the a.c. voltage changed. This rather unusual oscillating effect can be visualised by tracing the paths of the positive ions as they move through the field of the quadrupole. Typical paths are shown in Fig. 6. These are taken directly from computer plots (using a double Euler algorithm) which have been calculated for ions injected into the hyperbolic field parallel to the main axis and offset by a finite amount.

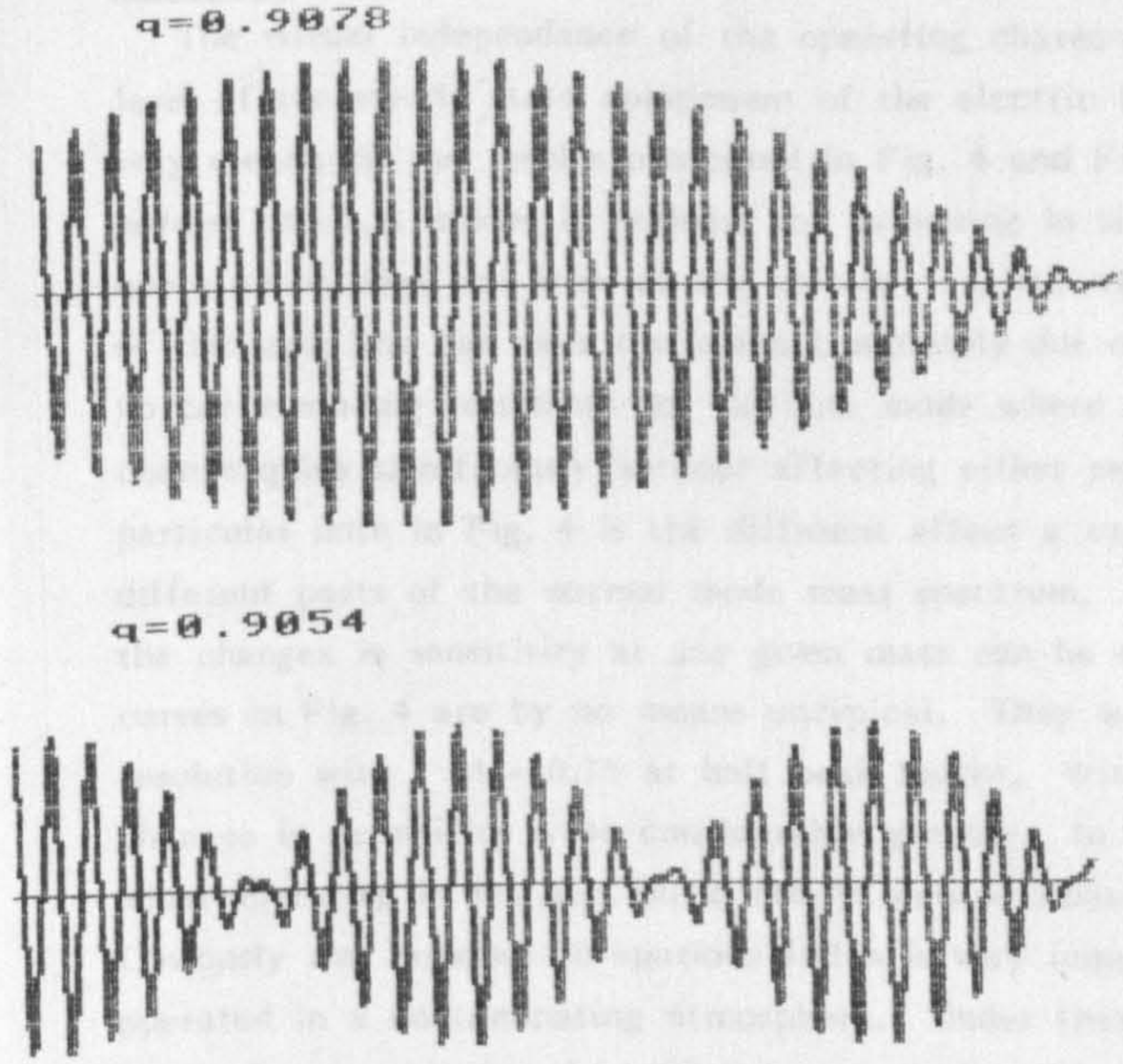

Fig. 6. Ion paths through the quadrupole under the idealized conditions of ion injection parallel to the main axis at the instant in time when the a.c. field was zero. 2L represents the distance between two nodes. The change in q between the two curves represents an effective change in mass of 0.3 units when referred to m/z = 40.

Two values of a.c. voltage were chosen for the calculations, both just below the value v_o which defines the transition between the stable and unstable regimes of the quadrupole. A slight increase of the a.c. voltage would take the filter right outside the stable zone, making the ion paths completely unstable. It requires only a small change in the a.c. voltage to sweep through the oscillating shadow region from complete instability to total shadow. The range is in fact of the order of 1 mass unit if the scale is translated into those units. Also it is not difficult to show that this range gets less, the slower the ions travel through the lens (the lower the ion energy the greater the number of oscillations of the a.c. field experienced by the ions in going through the lens). Thus for ions injected with low energy the individual sub-peaks merge together to form a single relatively broad peak as in Fig. 5a. That is why in normal operating conditions the peak splitting is not observed except possibly at the very low end of the mass spectrum where the ions move very rapidly through the quadrupole field.

Discussion

The virtual independance of the operating characteristics for the a.c mode on the level of the steady state component of the electric field in the analyser is shown very clearly in the results presented in Fig. 4 and Fig. 5. The contrast between the normal and a.c. modes is perhaps not surprising in view of the fact that normal operation is near the apex of the stability regime where a small change in the slope of the scan line can take operation completely out of the stable regime. There are no corresponding restraints for the a.c. mode where the scan line (ob in Fig. 1) can change quite significantly without affecting either resolution or sensitivity. Of particular note in Fig. 4 is the different effect a small applied potential can have on different parts of the normal mode mass spectrum. There is in fact no consistency, the changes in sensitivity at any given mass can be either positive or negative. The curves in Fig. 4 are by no means untypical. They were obtained at a relatively low resolution with M = 0.75 at half peak height. With higher resolution settings the changes in sensitivity were considerably greater. In contrast d.c. potentials applied when operating in the a.c. mode always caused relatively small changes in sensitivity. Obviously the response to spurious fields is very important when the analyser is to be operated in a contaminating atmosphere. Under these conditions surface insulating layers forming on the electrodes can easily become electrically charged positive or negative giving potential changes of the order of 1 volt. The highly stable operating characteristics listed in Table 1 are only possible because of the relative insensitivity of the a.c. operating mode to spurious d.c. fields in the analyser. The systematic measurements in the hostile environment reinforce the general observation over many months which indicated a highly stable operation. This together with the fixed scan line also accounts for the very useful property of the new mode of having a fixed mass discrimination over the whole mass range. This is a particularly useful property for any application and has been checked experimentally for the 50 mm analyser up to m/z = 600.

When the mass spectrum is scanned in the usual manner the a.c. mode gives symmetrical peaks without any splitting. This is ideal when automatic peak selection techniques are used. The multi-peak structure depicted in Fig. 5b can be explained in qualitative terms from the simplified analysis of the ion paths depicted in Fig. 6. As the wave-length (2L) of the envelope changes the ion collector will come in and out of shadow. Equation (1) gives the simple relation between (L) and the length of the quadrupole lens (2) for perfect shadowing,

$$2/L = 2n + 1 \qquad (1)$$

where n is an integer.

The theoretical traces in Fig. 6 predict that at mass 40 the spectrum goes from the first to the third shadow over a distance of 0.3 mass units. In Fig. 5b the distance between adjacent "troughs" is about 0.1 mass units. Given the simplicity of the

model this is as good an agreement as can be expected.

ACKNOWLEDGEMENTS

This work has been carried out with the help of a contract from the U.K.A.E.A. It is a pleasure also to acknowledge the help we have received from Mr. H.H.H. Watson and his colleagues at the U.K.A.E.A. Culham Laboratories.

REFERENCES

1 U. Brinkmann, Int. J. Mass Spectrom Ion Phys., 9 (1972) 161.
2 A.E. Holme, S. Sayyid and J.H. Leck, Int. J. Mass Spectrom Ion Phys., 26 (1978) 191.
3 D.N. Ross and J.H. Leck, Int. J. Mass Spectrom Ion Phys., 49 (1983) 1.
4 J. Yang and J.H. Leck, Vacuum, 32 (1982) 691.
5 P.H. Dawson, M. Meunier and Wing-Cheung Tam, Advances in Mass Spectrometry, 8B (1980) 1629.

Synopsis.

This thesis describes a series of experiments designed to investigate various factors which limit the performance of conventional quadrupole mass filters. The effect of imperfect mechanical construction of both the analyser and ion source and also of imperfect electrical supplies were investigated. In addition the importance of maintaining the spectrometer free from contamination was demonstrated. Provided that both the mechanical and electrical constructions were sufficiently accurate the maximum resolving power attainable, R_{max}, was found to depend only on the number of r.f. oscillations, N, performed by the ions. The simple relationship R_{max} = constant x $N^{1.7}$ applied for ions in the mass range H_2 to Xe when injected into the analyser with energies of 2 to 32eV. The resolving power of the spectrometer described here was finally limited to about 800 because of imperfections in the analysing field produced by the mechanical misalignment of the electrodes.

The problems of ion injection through the fringing fields at the entrance to the analyser have also been considered in detail. The alignment of the ion source with respect to the analyser was shown to be of critical importance if optimum performance was to be achieved. The effect on performance of the length of the fringing fields, expressed in r.f. cycles, has been considered and the results have been compared with a corresponding theoretical investigation. Similarly the effect on sensitivity of the phase at which the ion is injected into the analyser has been investigated and shown to be of less importance than was predicted by the theory.

Finally the data obtained from experiments with the conventional 6" analyser have been used in the design of a spectrometer intended primarily for use in residual gas analysis.